TESTING AND RESEARCH SECTION
CONSTRUCTION AND TECHNOLOGY DIVISION
RESEARCH REPORT NO. RC-1430

UMCEE 03-09

LAST COPY
DO NOT REMOVE FROM LIBRARY

ANALYTICAL DESIGN PROCEDURES AND LOAD RATING FOR ISOTROPIC BRIDGE DECKS

Report submitted to
The Michigan Department of Transportation

Andrzej S. Nowak, Maria M. Szerszen and David Ferrand

Department of Civil and Environmental Engineering
University of Michigan
Ann Arbor, Michigan 48109-2125

1. Report No. Research Report RC-1430	2. Government Accession No.	3. MDOT Project Manager: Roger Till
4. Title and Subtitle Analytical Design Procedures and Load Rating for Isotropic Bridge Decks		5. Report Date May 14, 2003
7. Author(s) Andrzej S. Nowak, Maria M. Szerszen and David Ferrand		6. Performing Organization Code
9. Performing Organization Name and Address University of Michigan 2340 G.G. Brown Ann Arbor, MI 48109-2125		8. Performing Org Report No. UMCEE 03-09
12. Sponsoring Agency Name and Address Michigan Department of Transportation Construction and Technology Division P.O. Box 30049 Lansing, MI 48909		10. Work Unit No. (TRAIS) 11. Contract Number: 01-0367 11(a). Authorization Number:
15. Supplementary Notes		13. Type of Report & Period Covered Final Report, 3/19/01-2/28/03 14. Sponsoring Agency Code

16. Abstract

In this project, the behavior of reinforced concrete isotropic decks with empirical reinforcement supported on girders spaced up to 10 ft is considered. Stress/strain analysis was performed based on finite element models of the bridge superstructure. Two types of decks were investigated, one supported on steel girders, and the other on prestressed concrete girders. The study involved field testing and analysis. The bridge superstructures were modeled using the finite element method (FEM) and the ABAQUS program. The analytical models were calibrated using the field test data. The computations were performed to determine stress values in the deck under a service load represented by 11-axle trucks. Stress distribution was investigated at the top and bottom of the deck, and transversally through the thickness of the deck. The possibility of cracking was analyzed for various load combinations. It turned out that the stress due to the dead load and live load is less than the cracking limit, and that the empirical deck design method provides an adequate amount of reinforcement in the deck. However, the restrained shrinkage analysis, based on the finite element model, and the analytical model developed to calculate shrinkage stress in composite sections, revealed that the tension stress can exceed the modulus of rupture for concrete. It was found that the restrained shrinkage stress in concrete decks can be affected by the geometry of a composite section, the girder stiffness, and girder spacing. The transversal shrinkage cracks first develop along the longitudinal edges of the deck and then propagate towards the middle sections. Isotropic concrete decks, supported on deeper steel girders (48 in or more), or on Type IV (depth of 54 in.) prestressed concrete girders, may require additional reinforcement to resist restrained shrinkage stress. The recommendations for changes in the design requirements for reinforcement are included.

17. Key Words: isotropic bridge deck, stress analysis, restrained shrinkage	18. Distribution Statement No restrictions. This document is available to the public through the Michigan Department of Transportation.		
19. Security Classification (report) Unclassified	20. Security Classification (Page) Unclassified	21. No of Pages	22. Price

UMCEE 03-09 October 2003

ANALYTICAL DESIGN PROCEDURES AND LOAD RATING FOR ISOTROPIC BRIDGE DECKS

Report submitted to
The Michigan Department of Transportation

Andrzej S. Nowak, Maria M. Szerszen and David Ferrand

Department of Civil and Environmental Engineering
University of Michigan
Ann Arbor, Michigan 48109-2125

DISCLAIMER

The contents of this report reflect the views of the authors, who are responsible for the facts and accuracy of the information presented herein. This document is disseminated under the sponsorship of the Michigan Department of Transportation in the interest of an exchange of information. The Michigan Department of Transportation assumes no liability for the contents or use thereof.

EXECUTIVE SUMMARY

The project objective was to analyze the behavior of isotropic decks with empirical reinforcement supported on girders with larger spacing. There is a need for verification of the current design specifications to determine if the deck slabs are sufficiently protected against premature deterioration. Therefore, a stress/strain analysis of reinforced concrete isotropic decks supported on girders spaced up to 10 ft was performed based on the finite element models of the bridge superstructure.

Two types of decks were investigated, one supported on steel girders and the other on prestressed concrete girders. Accordingly, a steel girder bridge and a prestressed concrete girder bridge were selected for field testing and analysis. The bridge superstructures were modeled using the finite element method (FEM) and the ABAQUS program. The analytical models were calibrated using the field test data. The computations were performed to calculate the stress distribution in the deck under a service load represented by 11-axle trucks.

In the FEM analysis, truck axle loads and axle configurations were the same as in the field tests. The transversal and longitudinal positions of the trucks in the FEM model were selected to obtain the extreme stress at the midspan and close to supports. Stress distribution was investigated at the top and bottom of the deck, and transversally through the thickness of the deck.

The possibility of cracking was analyzed for various load combinations. It turned out that the stress due to the dead load and live load is less than the cracking limit, and the empirical deck design method provides an adequate amount of reinforcement in the deck. However, the restrained shrinkage analysis based on the finite element model, and the analytical model developed to calculate shrinkage stress in a composite section, revealed that the tension stress can exceed the modulus of rupture for concrete. It was found that the restrained shrinkage stress in concrete decks can be affected by the geometry of a composite section, the girder stiffness, and girder spacing.

The transversal shrinkage cracks first develop along the longitudinal edges of the deck and then propagate towards the middle sections. Isotropic concrete decks, supported on deeper steel girders (48 in or more), or on Type IV (depth of 54 in) prestressed concrete girders, may require additional reinforcement to resist restrained shrinkage stress. The recommendations for changes in the requirements for reinforcement are included.

ACKNOWLEDGMENTS

The presented study was sponsored by the Michigan Department of Transportation, which is gratefully acknowledged. The authors thank the technical staff of the Michigan DOT, in particular Roger Till, David Juntunen, Steve Beck, and Amir Gilani, as well as Jon Nekritz (FHWA) for their useful comments, discussions and support.

The Project Team received help from other researchers, current students and staff of the University of Michigan. In particular, thanks are due to Aleksander Szwed, who was involved in the finite element modeling and shrinkage analysis of bridge superstructures, and Junsik Eom, Pascal Laumet, and Tejun Cho who were involved in field instrumentation and measurements.

Thanks are due to the Michigan State Police for their cooperation during the field tests.

The realization of the research program would not be possible without the in-kind support of the Michigan Department of Transportation and the University of Michigan.

TABLE OF CONTENTS

1. INTRODUCTION

The reinforced concrete deck slab design is carried out by the Michigan Department of Transportation using two design procedures: the Standard Bridge Slab Empirical Design, and the Standard Bridge Slab Load Factor Design. The maximum girder spacing covered by these design procedures is 10 ft for the Empirical Design, and 10.5 ft for the Load Factor Design. Using the empirical design method (AASHTO 9.7.2), the percentage of reinforcement is less than the percentage with the load factor design method (AASHTO 9.7.3). In the empirical design method, reinforcement is not adjusted for different girder spacing. The flexural and punching shear capacities of the deck depend on the percentage and distribution of the reinforcement. The main goal of the project is to determine whether isotropic decks designed using the empirical method can be used for the maximum allowed girder spacing (10 ft). The proposed design procedure for this type of deck is based on the analysis of stress and strain distribution in the deck. The calculations are performed using the Finite Element Method (FEM).

Two finite element models of the bridge superstructure are developed for a slab on steel girders, and the other one for prestressed concrete girders in order to investigate the bridge deck behavior, regarding to different supporting beams (with different stiffness). The performance of the supporting beams is critical for behavior of the deck, and it is affected by the stiffness and support conditions of the girders. Because of this fact, it was necessary to adjust boundary conditions for beams in the finite element models, in order to model the actual behavior of the girders. The FEM parameters were calibrated using the field test data.

Increased girder spacing of up to 10 ft requires the development of a design procedure that takes into consideration the requirements for adequate load carrying capacity and long-term performance, including resistance to deterioration. Previous studies on forms of deck deterioration identified major parameters that influence the structural and functional performance of a concrete deck. One of the major factors that affect the lifetime performance is shrinkage of concrete, because it initiates cracks that grow with freeze and thaw cycles, and truck load cycles.

Calibrated finite element models of reinforced concrete decks supported on steel and prestressed concrete girders are used to find the stress/strain range in the deck slab. The distribution of stress and strain values is investigated for the dead load and live load. A special analysis is performed to find the extreme positions of the live load (two 11-axle trucks), producing maximum stresses at the midspan and close to supports.

The study of shrinkage in the deck is performed using two different approaches. In the first one, shrinkage is investigated as a uniform decrease of temperature in deck causing strain equivalent to shrinkage, applied to a composite section using a finite element method. In the second approach, the analysis is performed based on strain compatibility of the cross section.

The maximum stresses obtained due to dead load and live load, in addition to shrinkage, are used to check the flexural capacity of empirically designed decks. For composite sections with deep beams (with large stiffness compared to the deck slab stiffness), empirical reinforcement is not sufficient to resist stress caused by the restrained shrinkage. The same observation applies to the edge sections of the deck, because the overhang is smaller than 0.5 of the girder spacing. As a result of this study some recommendations for the empirical design procedures are proposed.

1.1. Current design

A current Standard Bridge Slab Empirical Design used by the Michigan Department of Transportation follows provisions presented in Figure 1-1. This empirical design can be only used for isotropic decks supported on longitudinal components. The method is based on extensive research on behavior of concrete deck slabs, that discovered that the primary structural action by which these slabs resist concentrated wheel loads is not as traditionally believed, but a complex internal membrane stress referred as an internal arching.

Requirements for empirical method of designing according to the AASHTO LRFD Code (A.9.7.2) are as follows:

- Cross-frames or diaphragms are used throughout the cross section at lines of support.

- Intermediate diaphragms for torsionally stiff cross sections (box beams) should be spaced not more than 25 ft, or supplemental reinforcement over webs is needed.
- The supporting components (girders) are made of steel and/or reinforced or prestressed concrete.
- The deck is fully cast-in-place and water cured.
- The deck has uniform depth, except for haunches at girder flanges and other local thickening.
- The ratio of effective length to design depth does not exceed 18 and is not less than 6.
- Core depth of the slab is not less than 4 in.
- The effective length does not exceed 13.5 ft.
- The minimum depth of the slab is not less than 7 in., excluding the wearing surface.
- There is an overhang beyond the centerline of the outside girder of at least 5 times the depth of the slab.
- The specified 28-day strength of the deck concrete is not less than 4 ksi.
- The deck is made composite with the supporting structural components.

AASHTO LRFD Code requires that four layers of isotropic reinforcement shall be provided in empirically designed slabs. Reinforcement shall be provided at each face of the slab with the outermost layers placed in the direction of the effective length, as close to the outside surfaces as permitted by cover requirements. The minimum amount of reinforcement shall be 0.27 in^2/ft of steel for each bottom layer, and 0.18 in^2/ft of steel for each top layer. Spacing of steel should not exceed 18 in.

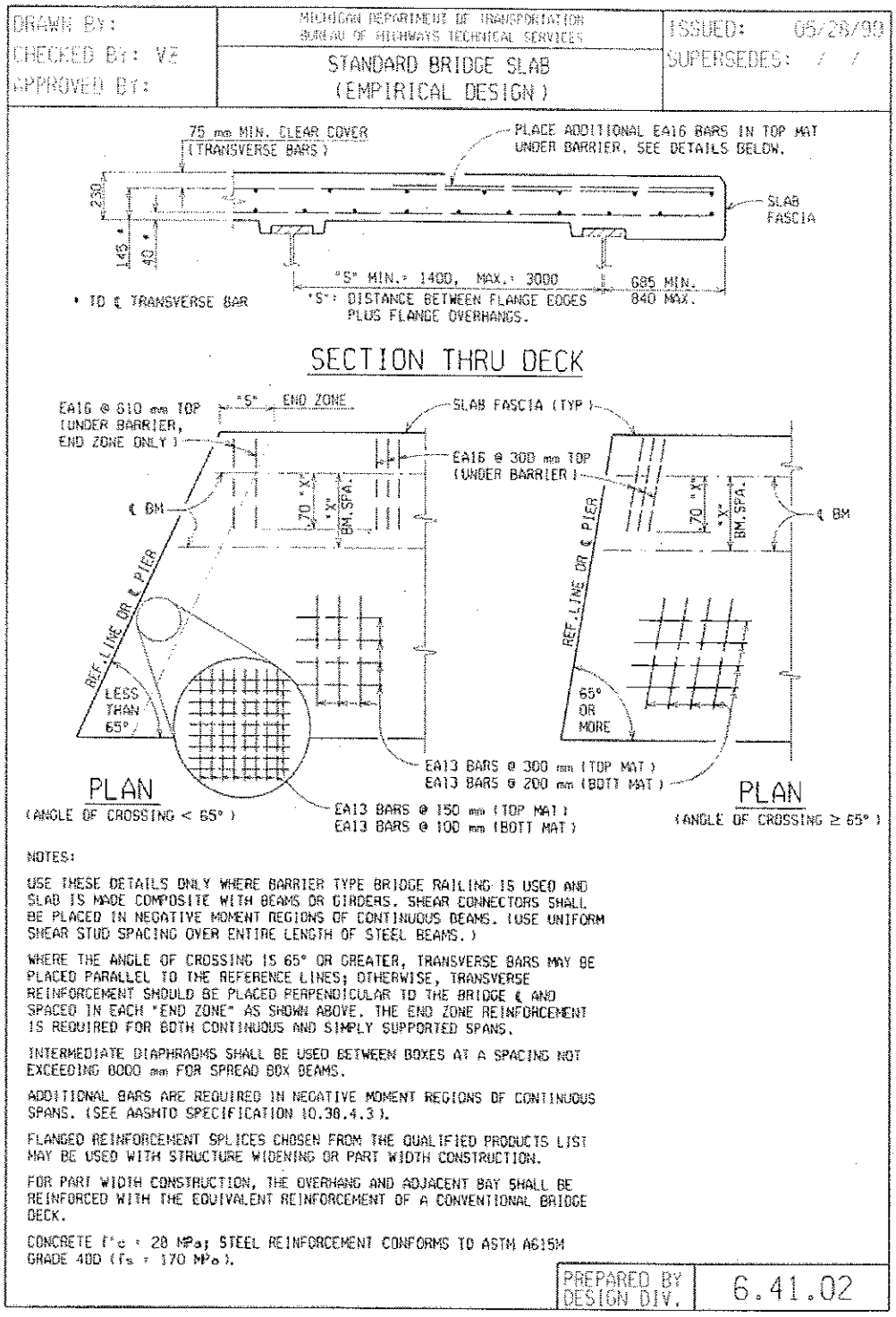

Figure 1-1. Standard Bridge Slab Empirical Design according to MDOT Bridge Guides

1.2. Literature review

The available literature is reviewed covering bridge deck behavior and finite element modeling.

A reinforced concrete slab placed over steel girders is the most common highway bridge superstructure. Many field tests have been performed for such bridges; however, the test results apply mostly to the lateral load distribution.

In the FEM analysis, the geometry of the bridge superstructure can be idealized in many different ways. The following types of models are used:

- plane grillage model,
- 3-dimensional grillage model
- 2-dimensional model with shell elements for slab and beam elements for girders,
- 3-dimensional model with shell elements for slab and beam elements for girders,
- 3-dimensional model with shell elements for slab and girders,
- 3-dimensional model with solid elements for slab and shell elements for girders.

The plane grillage models (Cussens 1975 and Bhatt (1986) are the most commonly used, particularly in design practice. The bridge deck slab is divided into a number of longitudinal and transverse beams lying in the same plane. Each longitudinal beam represents a girder and part of the slab. The properties of such beams are determined by the position of the neutral axis, which is dependent on the composite or non-composite behavior of the bridge. A transverse grillage beam represents a strip of slab and makes the connection between longitudinal elements. Detailed recommendations on the implementation of a grillage analysis for slab bridges can be found in West (1973), Hambly (1991), and Zhang and Aktan (1997). Such simple FEM models allow only for a global evaluation of bridge behavior. This accuracy of calculations depends on the assumed location of the neutral axis in bending elements (O'Brien and Keogh 1998). The determination of this location is difficult, especially in bridges where wide cantilevers, barriers, or sidewalks cause the neutral axis to change position across

the bridge width. In such cases, a more complex, 3-dimensional grillage model can be used (O'Brien and Keogh 1998 and Zhang and Aktan 1997). In these models, grid beams placed on two levels are connected using rigid vertical links. Although both grillage analyses represent a simple geometry that is easy to model, they require an elaborate determination of beam properties, often based on questionable assumptions.

In the next group of models the slab is divided using shell elements and girders are represented using beam elements (Mabsout et al. 1999 and Hays et al. 1997). Diaphragms (if considered) are also represented by beam elements. In such plane models (Mabsout et al. 1999), centroids of beams coincide with the centroid of the slab. To determine the cross-section properties of the beam, the actual distance between its neutral axis and the middle plane of the slab must be taken into account. In 3-dimensional models, space frame elements are connected with shell elements using rigid links that account for the eccentricity of the girders. It is still difficult to include a precise composite action when determining beam stiffness.

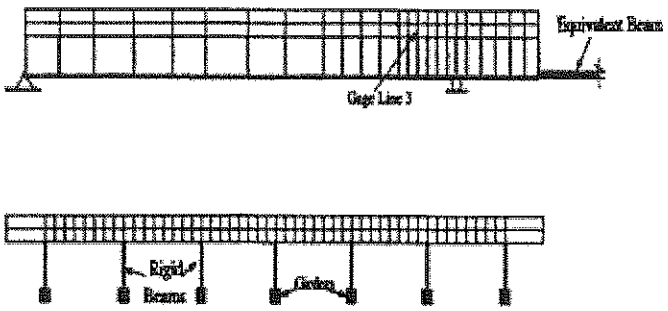

Figure 1-2. Finite element meshes with beam elements.

To overcome this problem, shell elements can be used to model the girders (Alayhoglu 1997 and Tarhini and Frederic 1992). This seems to be a better solution, especially for elements such as steel girders consisting of thin parts. Sometimes, the bridge behavior can be strongly affected by the structural components such as sidewalks, curbs, and barriers. In such cases, it can be incorrect to model them only by changing the thickness of shell elements.

Tarhini and Frederic (1992) showed that it is more realistic to use the solid elements for slabs, sidewalks, and barriers.

The application of solid elements also allows for a more detailed investigation of the local stress and strain distribution. Modeling the slab with solid elements, and the girders and diaphragms with shell elements, seems to describe most adequately the bridge geometry and physical properties.

The evaluation of FEM models for bridges shows a tendency towards more complex model geometries with a larger number of elements. At the same time, the determination of element properties is clearer and stands closer to reality.

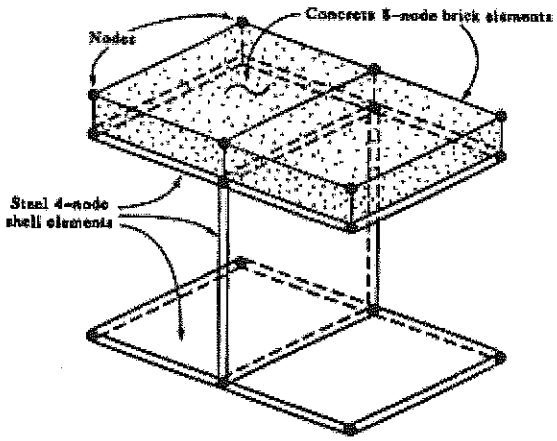

Figure 1-3. Typical Section through Part of the Finite Element Model by Tarhini and Frederic.

Therefore, in this study, the model developed by Tarhini and Frederic (1992) is used, in addition to the practical experience of the University of Michigan team in bridge testing and modeling of material behavior.

The second part of the literature review is focused on designing, durability, and performance of the bridge decks.

In the most of the available literature, the analytical models do not take into account the deflection of the girders and the transverse deck slab behavior is analyzed using a classical

beam theory, assuming that the girders provide a rigid support. But because of the girder flexibility, the maximum stresses in a bridge deck can vary significantly from the design values. Fang et al. (1988) showed that the negative bending moment in bridge decks and the resulting top tensile stresses are very low, much less than the positive bending moments and the bottom tensile stress. Their work indicates that, in general, the tensile strength of a concrete deck considerably exceeds the top tensile stress induced by traffic loads due to the deflection of girders.

Cao et al. (1996 and 1999) developed a simplified analytical method for the slab-on-girder bridge deck, and analyzed the behavior of a reinforced concrete bridge deck with flexible girders.

The analysis was based on the plate theory and was validated using the results of the finite-element computations conducted on two different bridge decks. They concluded that the design formula in the AASHTO specification overestimates the negative bending moments in a slab-on-girder deck. They developed an analytical procedure for the evaluation of the maximum negative bending moments in a bridge deck by the superposition of the negative bending moment in a deck slab on rigid girders and the positive bending moment in a deck slab induced by girder deflection. They found that the reduction of the maximum negative bending moment in a deck slab due to girder deflection depends on the stiffness ratio of the deck and girder, and the ratio of the girder spacing and the span length of the bridge. The maximum negative moment decreases with an increasing span length and stiffness of the supporting girders.

Cao et al. (1996) suggested eliminating most of the top reinforcing bars in a deck. They conducted a test to assess the maximum tensile stress, as well as the durability of the deck slab in the absence of a top reinforcement. For all considered truck-load positions, the transverse tensile strains at the top of the deck were less than 30% of the expected cracking strain of the concrete. However, even though top transverse reinforcement is not required to carry traffic loads, they recommended further research on the control of temperature and shrinkage cracks.

In general, the top reinforcing bars are most susceptible to corrosion. Therefore, the reduction of the amount of top reinforcement can slow down the deck deterioration. Mufti et al. (1999) suggested to simply eliminating the reinforcement in concrete bridge decks as one solution for corrosion. A number of tests were conducted to show that the behavior of such a deck slab is

acceptable, providing a number of ties are installed to connect top flanges of adjacent girders. Extra shear studs are necessary in order to insure arching action without reinforcement. So far, several bridge decks without reinforcement were built. However, an extensive longitudinal cracking was observed between the girders.

The performance of bridge decks is often attributed to serviceability limit state. Deck deterioration starts with corrosion of reinforcement when deck is subjected to sodium chloride deicers. The process speeds up in a presence of shrinkage cracks. The limitation or elimination of these cracks at early stages of deck construction significantly increases deck durability. The deck performance can be improved by a better design. The story of the construction of the New Jersey Turnpike (O. Riley 1993) is a good example of such improvement. Originally, bridges were opened to traffic in 1951 and after 8 years about 10 percent of slabs had to be replaced, and so far about 38 percent of the slabs were replaced. Originally designed deck slabs were 6 ½ in. thick reinforced with bars #5 @ 7-1/2 in. at the top and bottom in transversal direction and bars #4 @ 12in. at the top and #5 @ 10 in. at the bottom in the longitudinal direction. After design revision in 1960's, the replaced new decks have thickness close to 1 ft (with latex modified concrete wearing surface) and they are reinforced with bars #6 @ 6 in. at the top and bottom in transversal direction, and bars #5 @ 6 in. at the top and the bottom in the longitudinal direction. These new deck slabs with an increased thickness and area of reinforcement do not show any deterioration signs after 25 years in service. The increased deck stiffness helps to limit restrained shrinkage cracking, and increased percentage of reinforcement can even eliminate these cracks.

The other way to improve the durability of bridge decks can be by using better materials, for example higher strength concrete. However, greater compressive strength is not always better or necessary. Mistakes and misconceptions concerning structural concrete are discussed by E.K. Schrader (1993) in articles presented at the ACI seminars on "Repairing Concrete Bridges". If extra strength is gained by adding cement, the cost will increase with only a negligible increase in load-carrying capacity for reinforced concrete flexural designs. More importantly, there will be more shrinkage, especially if there also is as increase in water (even when water/cement ratio is kept constant). Higher strength mixes generally become more brittle because they have higher modulus of elasticity and they produce more internal heat.

More cracking and internally developed stress will result. Such characteristics as flexural, thermal shock, impact, or fatigue will be worse for high strength concrete than for ordinary one. From that, it is clear that idea to increase slab stiffness by using higher strength concrete with higher modulus of elasticity is not a good one.

2. ANALYSIS OF CONCRETE DECK SUPPORTED ON STEEL GIRDERS

A reinforced concrete bridge deck supported on steel girders is analyzed to find the distribution and values of stress and strain in the deck under the dead load and live load. The analysis is focused on isotropic decks supported on girders spaced at 10 ft. The finite element model is developed for such a bridge superstructure. The behavior of the deck is strongly affected by the stiffness and supporting conditions of the girders. The experience from previous field tests shows that simply supported bridge beams, have some partial fixity at supports in reality. This fact requires special adjustments to girder supports in the finite element model. The best way to control boundary conditions in the FEM model is to calibrate the model using field test data. This procedure was used in the presented analysis.

Based on a list of bridges with steel girders spaced at close to 10 ft, provided by MDOT, a bridge suitable for field testing was selected. This bridge was modeled using the finite element method, and then load tested. The data from field measurements were used to calibrate the finite element model of the bridge superstructure. The calibrated finite element model served to find the stress/strain range and distribution in the deck due to dead load and live load. A restrained shrinkage analysis of the deck was also performed using this model.

2.1. Description of the tested bridge

The selected bridge (see Figure 2-2), S06 of 82291, was built in 1974 and it is located on Pennsylvania Road over I-275, near New Boston, Michigan. It is a two span structure with a span length of 144 ft, and a cantilever of 12 ft. The total bridge length is 288 ft, without any skew. The bridge has five steel girders spaced at 10 ft 3 in, and the deck is 9 ½ in thick (see Figure 2-1a and 2-1b). The depth of the steel girders is 60 in. The reinforced concrete deck carries one lane in each direction. The selected bridge was tested using an 11-axle truck as a live load (the largest live load legally permitted in the State of Michigan).

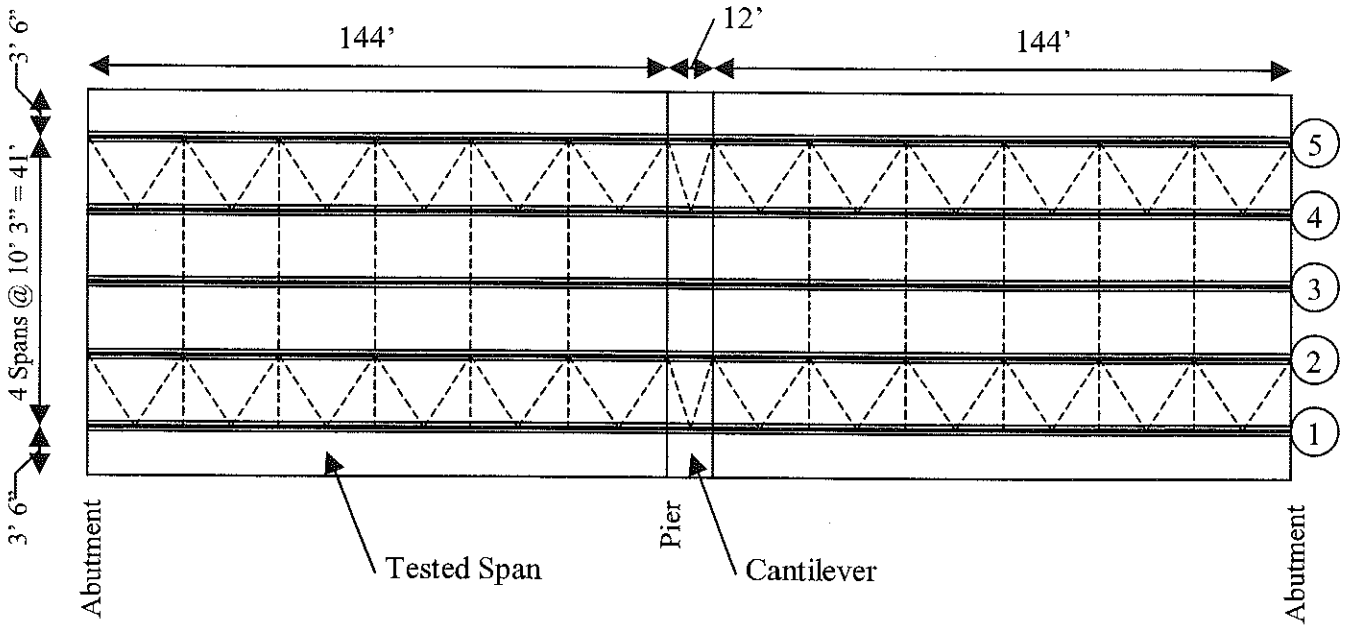

Figure 2-1a. Diaphragm – Cross frames

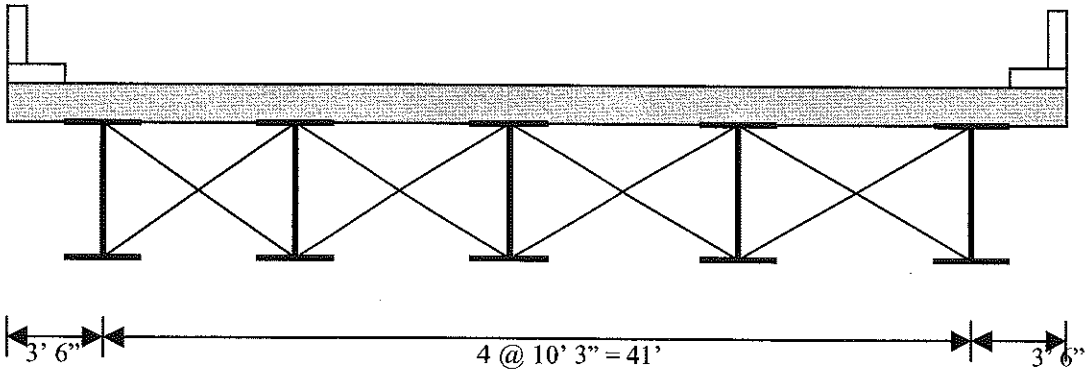

Figure 2-1b. Cross - section of tested span.

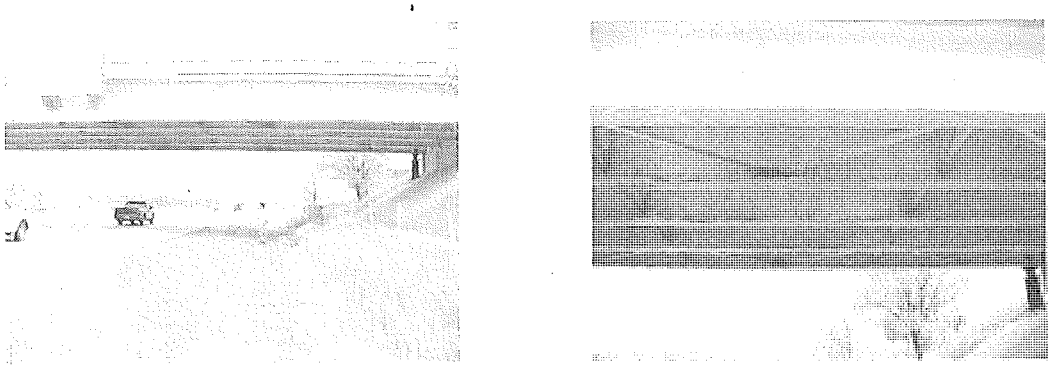

Figure 2-2. Pennsylvania Road Bridge.

2.2. Testing procedure

The following tests were performed on the bridge:

- Visual inspection of the bridge.
- Strain measurements on the west span (steel girders).

2.2.1. Instrumentation and Data Acquisition System

The strain transducers were attached to the following parts of the bridge

- Close to support (2 ft from the support, Figure 2-3).
- 26 ft from the support (it was not possible to install them closer to the mid-span because it would require closure of a traffic lane on I-275, Figure 2-4).

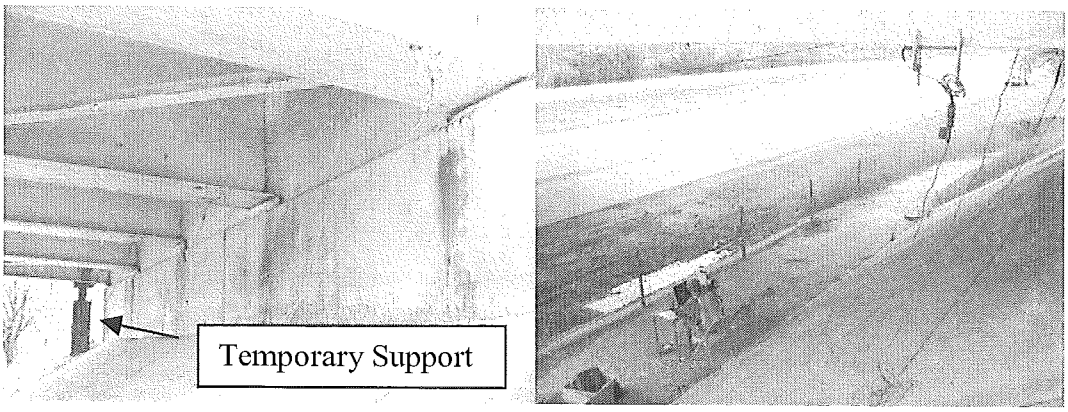

Figure 2-3. Location of the strain transducers close to support –View of the temporary support.

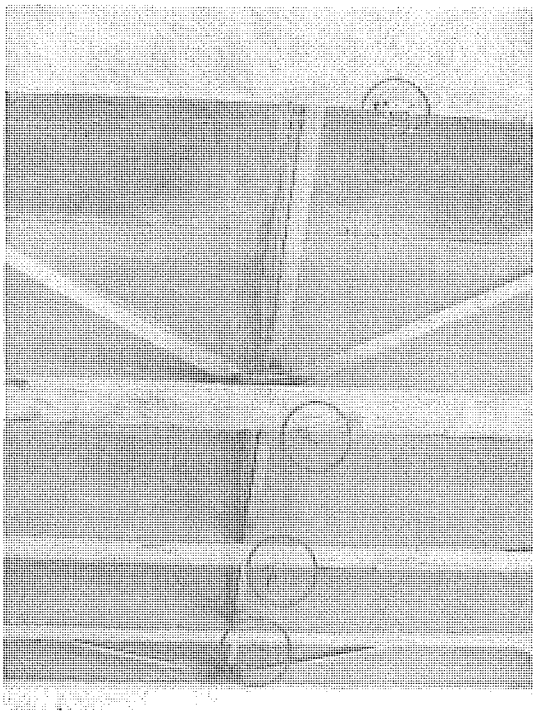

Figure 2-4. Location of strain transducers at 26 ft from support.

Strain transducers were connected to the SCXI data acquisition system (National Instruments). The data acquisition mode is controlled from the external PC notebook computer, and acquired data is processed and directly saved in the PC's hard drive (Figure 2-5).

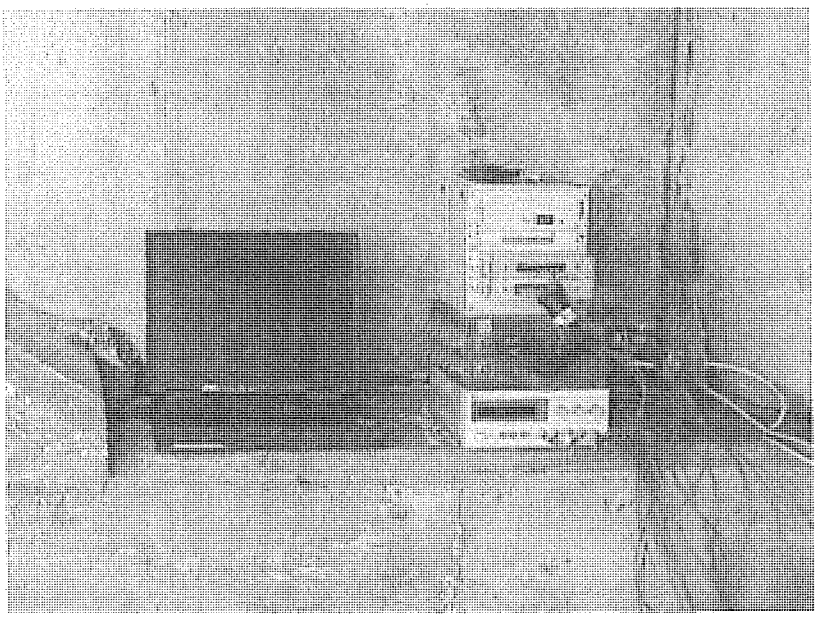

Figure 2-5. Connection box and computer.

The data acquisition system consists of a four slot SCXI-1000 chassis, one SCXI-1200 data acquisition module, and two SCXI-1100 multiplexers. Each multiplexer can handle up to 32 channels of input data. The current system is capable of handling 64 channels of strain or deflection inputs. A portable field computer is used to store, process and display the data on site. A typical data acquisition setup is shown in Figure 2-6. The data from all of the instruments is collected after placing the trucks in the desired positions or while trucks are crossing over the bridge. For the normal truck speed tests, a sampling rate of 300 per second was used for the calculation of the dynamic effects. This is equivalent to 11.4 samples per meter for the truck speed of 60 mph. The real time responses of all transducers are displayed on the monitor during all stages of testing.

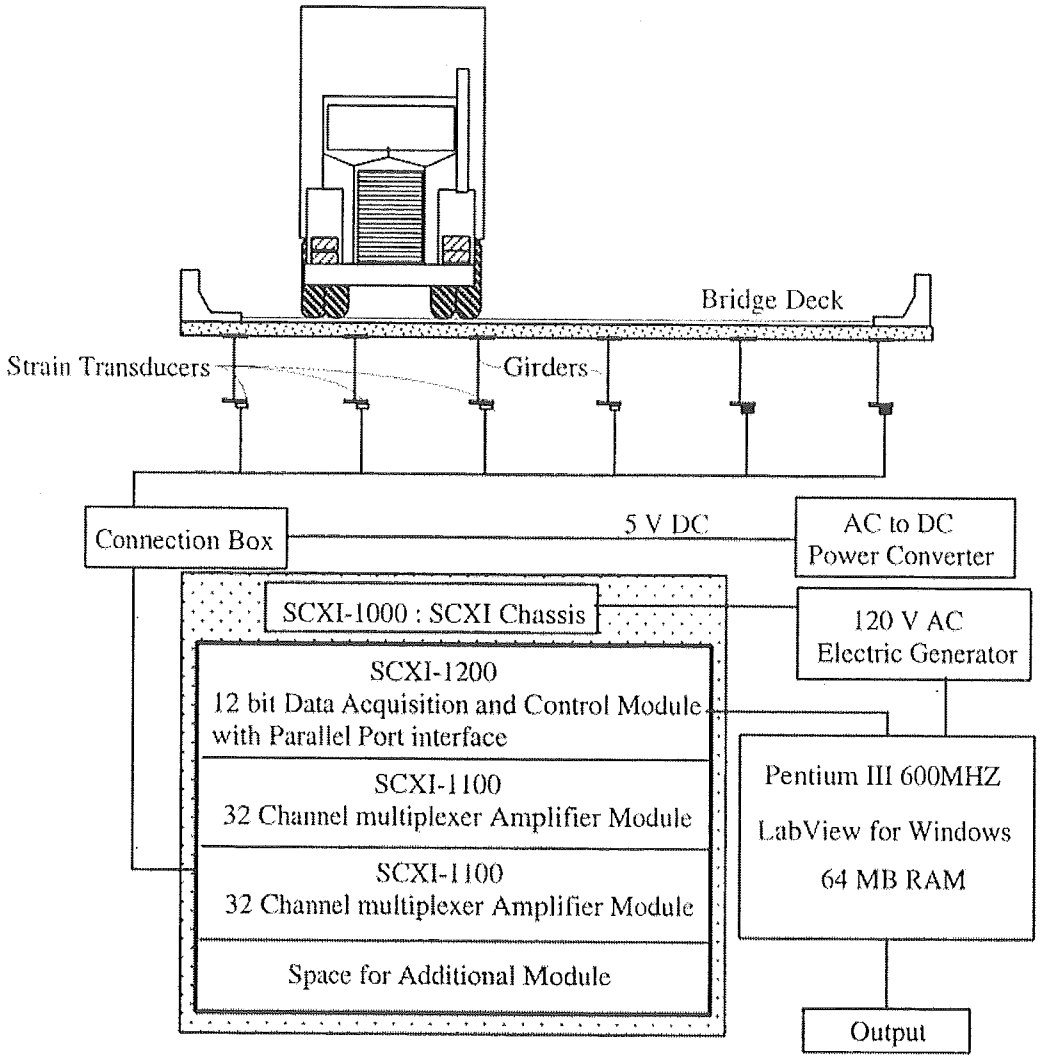

Figure 2-6. SCXI Data Acquisition System Setup.

2.2.2. Live Load

The live load was applied in the form of an 11-axle truck, shown in Figure 2-7. The measurements were taken under each passage of the test truck. The actual axle weights of the test truck were measured prior to the test using the State Truck Weigh Station scales in Cambridge Junction, MI. The truck was driven over the bridge at a crawling speed and was stopped at fixed positions.

The truck has a gross vehicle weight of 143.42 kips, with a wheelbase of 58'-7". The truck configuration is shown in Figure 2-7.

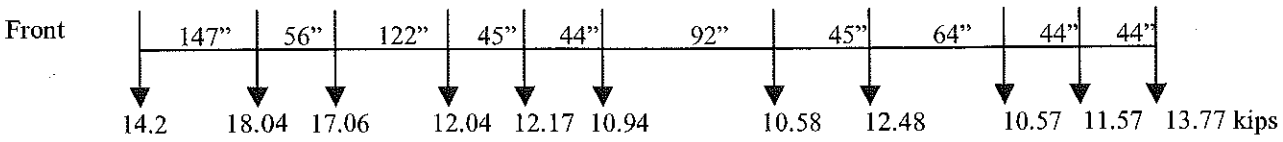

Figure 2-7. Truck configuration

2.2.3. Location of strain transducers

The strain transducers were installed on the bottom flanges of girders close to the support and at 26 feet from the support in the West span. Figure 2-1a shows the cross-section of the tested span and Figure 2-8 shows the location of strain transducers. Overall, 10 locations in the tested span were selected for the strain measurement. Gages No.1 to 5 were installed close to the support (S1 to S5). Gages No.6 to 10 were installed 26 feet away from the support.

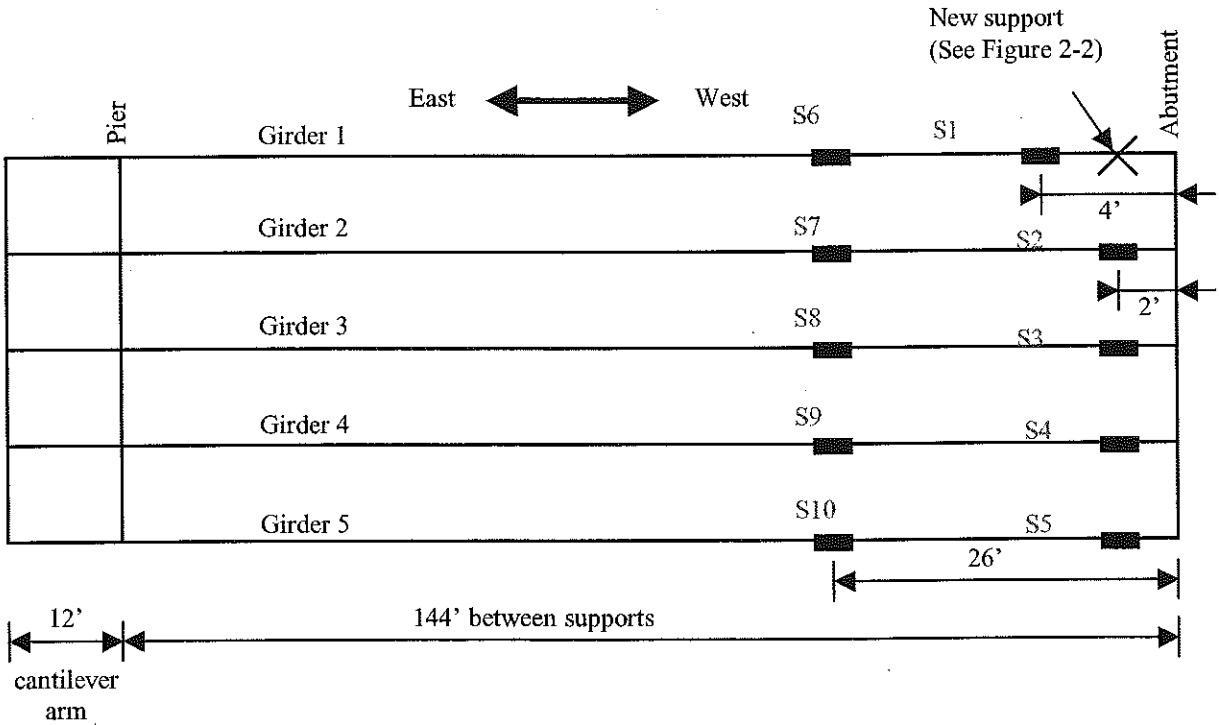

Figure 2-8. Location of measuring points.

The main purpose for the strain transducer instrumentation was to measure the strain level in the support area. These values were used to calibrate the finite element model of the bridge.

2.2.4. Loading cases

The bridge was loaded with the 11-axle truck (Figure 2-6). A total of 9 loading cases were considered, as shown in Table 2-1. For the first five runs, the truck was driven at a crawling speed over the bridge (from West to East) in different transversal positions. For runs 6 to 8, the measurements were taken at fixed positions of the truck (three transversal positions), producing the maximum moment at the midspan. Finally, run 9 was at a fixed position with the rear axle of the truck placed directly over the support.

Table 2-1. Loading runs.

Run #	Loaded Lane	Truck Position	Truck speed
1	North	Center	Crawling
2	South	Center	Crawling
3	North	Curb	Crawling
4	South	Curb	Crawling
5	Center	Center	Crawling
6	North	Center	Stop at fixed position (Rear axle at 1/3 span)
7	South	Center	Stop at fixed position (Rear axle at 1/3 span)
8	Center	Center	Stop at fixed position (Rear axle at 1/3 span)
9	North	Center	Stop at fixed position (Rear axle at support)

2.2.5. Test results

The strain values measured at the bottom flange of girders were registered at 10 measuring points for all 9 truck runs. These values were used to a calibrate finite element model of the tested bridge superstructure.

2.3. Finite element model

The FEM model of the bridge superstructure is presented in Figures 2-10 through Figure 2-16. A temporary support was included in the model and was used to replace the original support (observations on the bridge show that the old support was not active anymore). The longitudinal gradient of the deck, which is less than 0.5 % was neglected. The model was built using eight-nodes solid elements for the deck slab, four-nodes three dimensional shell elements for girders, and two-nodes three dimensional beam elements for cross frames and cross bracing. All these elements have six degrees of freedom at each node – translations and rotations in the nodal x, y, and z directions. The application of solid elements in the deck allowed for a more detailed investigation of local stress and strain distribution. In addition, the steel reinforcement was added into the solid elements of the deck as 4 layers of steel (one for each direction at the top and at the bottom), with a thickness determined in such a way to obtain the same total steel area in the cross section. Reinforcement was modeled as layers of bars treated as a smeared layer with a constant thickness equal to the area of each reinforcing bar divided by the reinforcing bar spacing. The geometry and node locations for these element types are shown in Figure 2-9.

The finite element model was loaded with an 11-axle truck, the same as in field test. Two different support conditions were considered in the model: a hinge–roller support, and a hinge–hinge support. These two conditions represent the two extreme cases in terms of boundary conditions for a simply supported beam. For runs 1 to 5, two models (with two different support conditions) were considered in each loading case (two longitudinal positions for each run) to analyze the results at the support and 26 ft from the support. For runs 6 to 9, because the measurements were taken at the fixed positions of the truck, two models for each run were investigated (with two different support conditions). A total of 28 different models were analyzed.

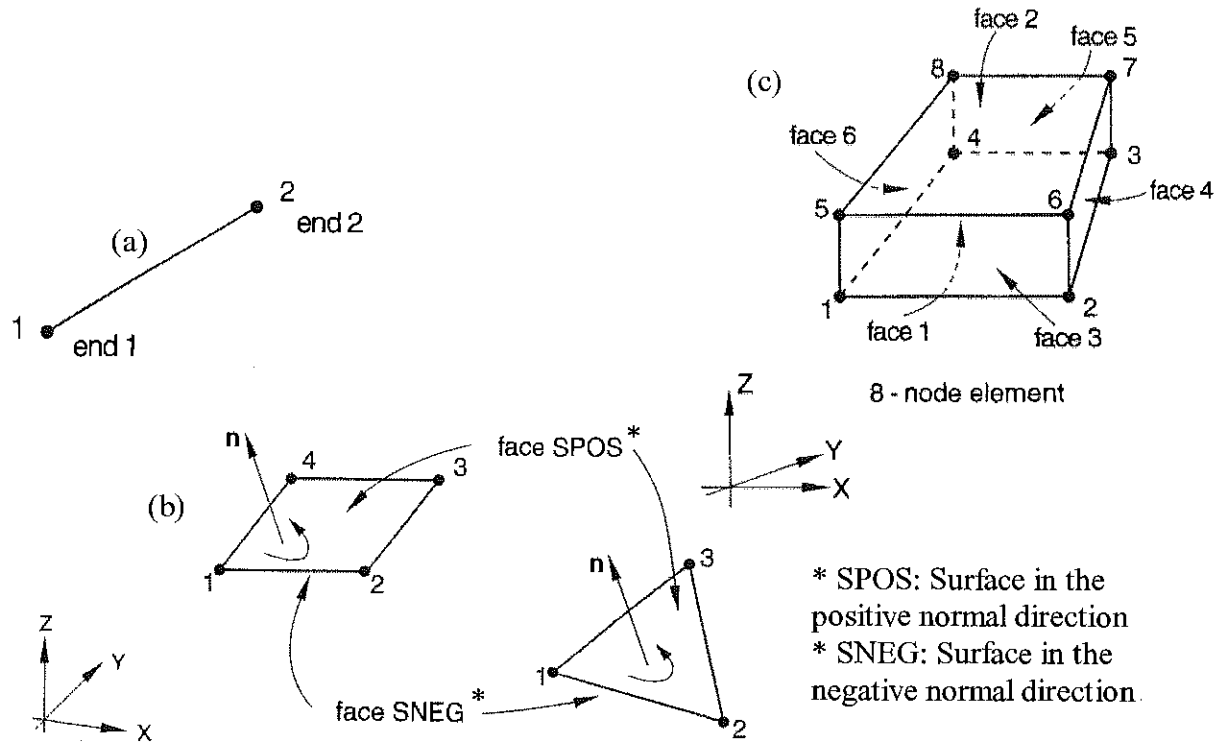

Figure 2-9. Node numbering for three-dimensional element, (a) three-dimensional beam element, (b) three-dimensional shell element, (c) three-dimensional solid element

Figure 2-15 and Figure 2-16 show the detail of the hinge support. Because the model is in 3 dimensions, it is necessary to define a boundary condition in the horizontal transverse direction (direction 1 in Figure 2-16) in order to avoid an unstable structure. This boundary condition (shown in figure 2-16 for the hinge support) is present only on the north side, in order to avoid transversal hyper static behavior, which could create some transverse stresses in the structure. This boundary condition is also present for the roller support.

Geometry of the bridge

The first step of the modeling process is to divide the model into a number of small elements so that we obtain a good accuracy in the results in term of strain and stress at each node. On the other hand, a very large number of nodes and elements make the computation too complicate. A general view of the model is shown in Figure 2-10.

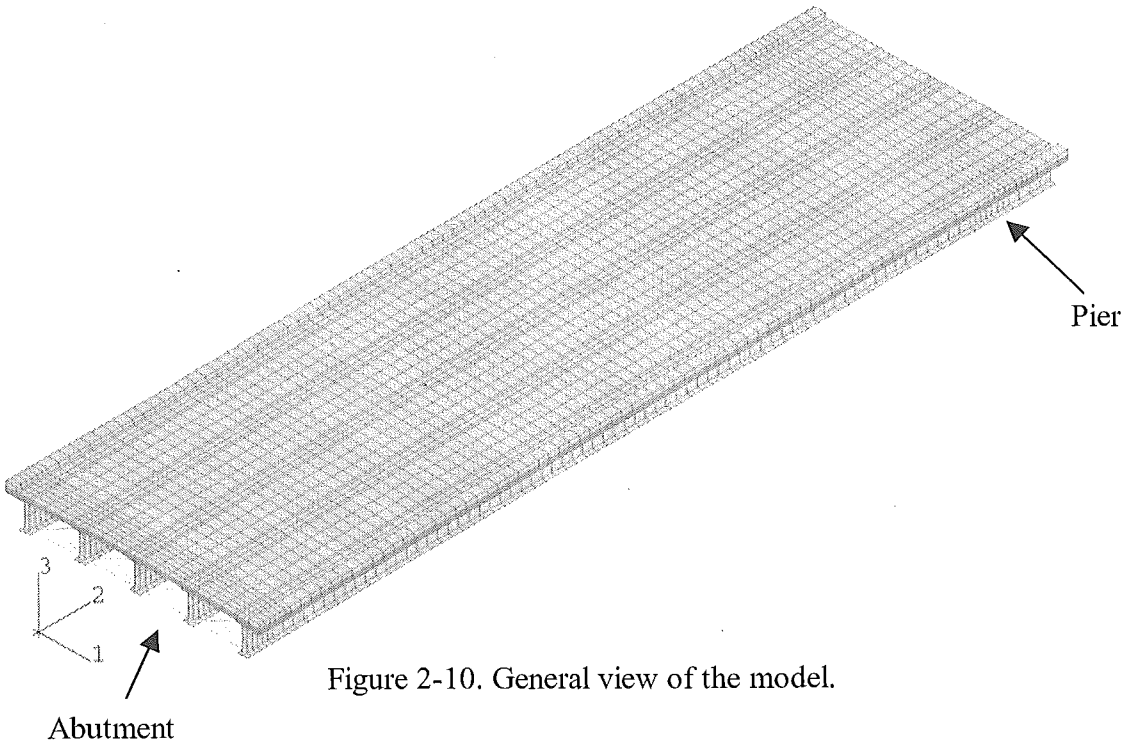

Figure 2-10. General view of the model.

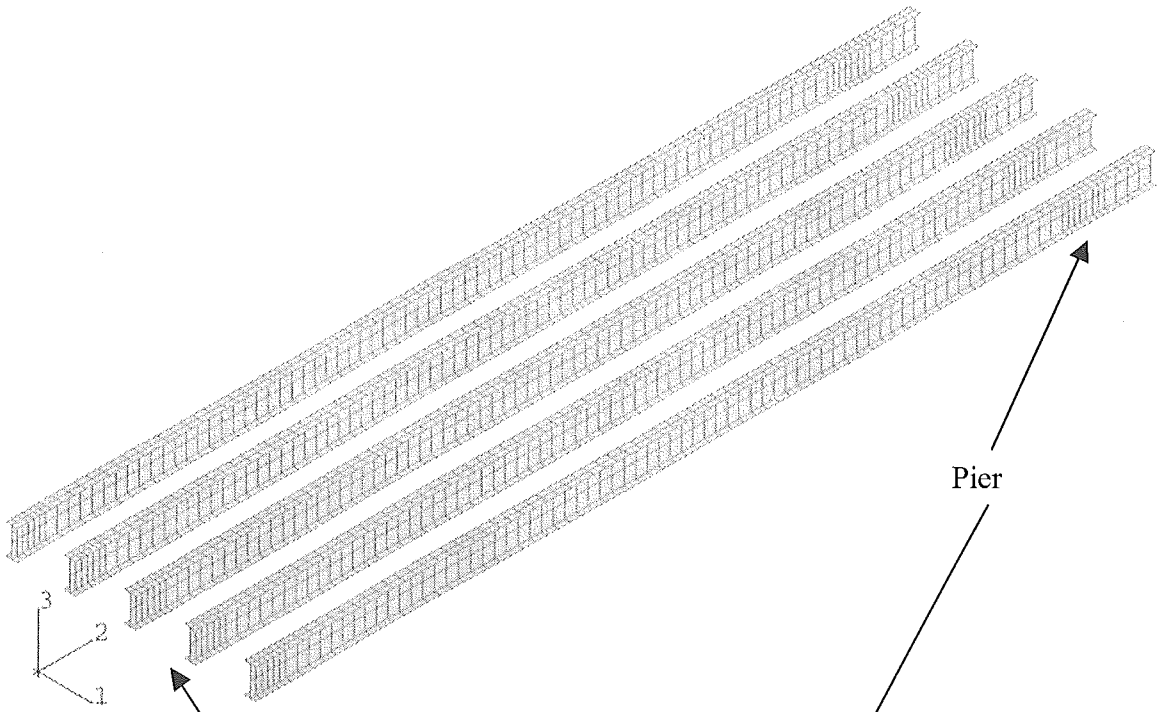

Figure 2-11. Model of the girders.

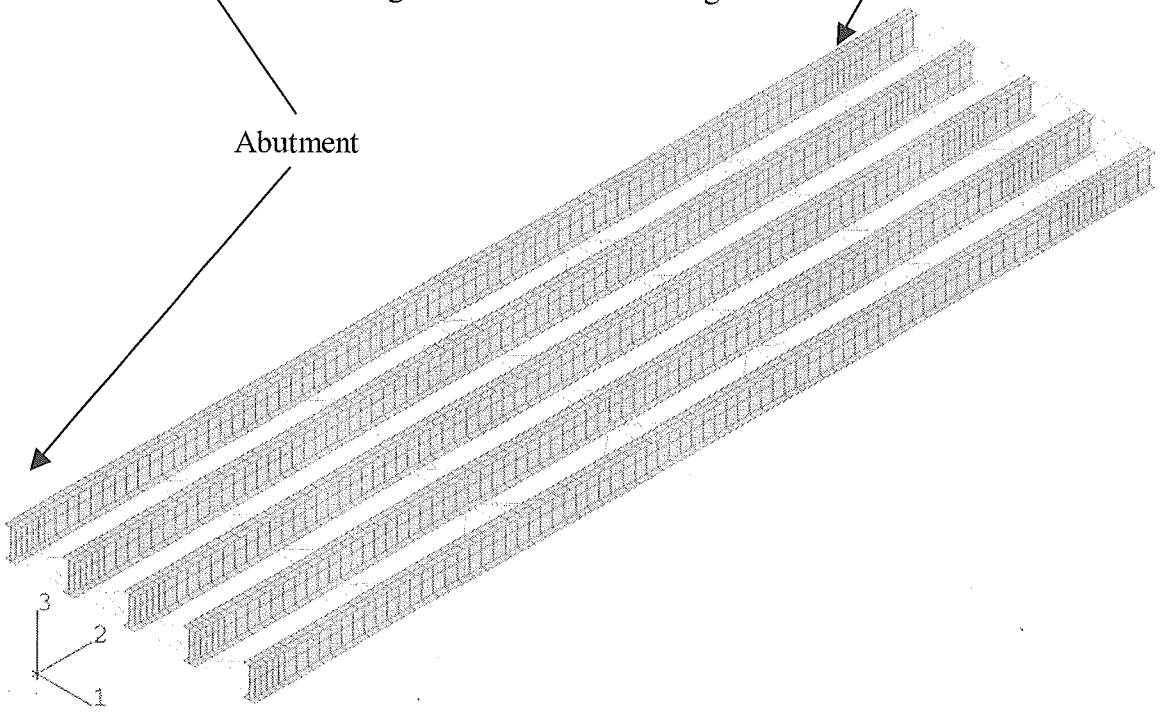

Figure 2-12. View of the girders with cross frames and cross bracing.

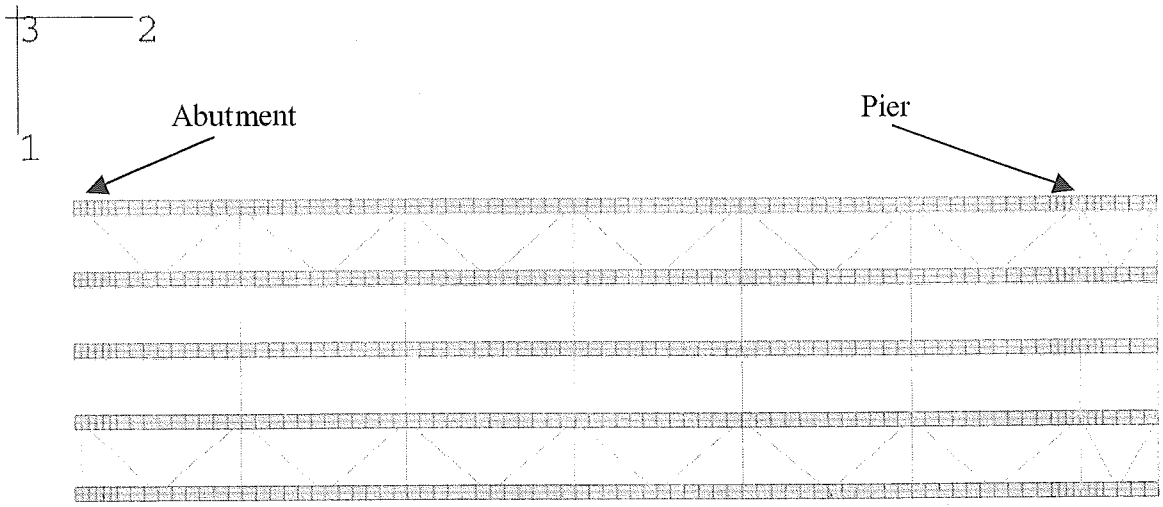

Figure 2-13. Top view of the girders with cross frames and cross bracing.

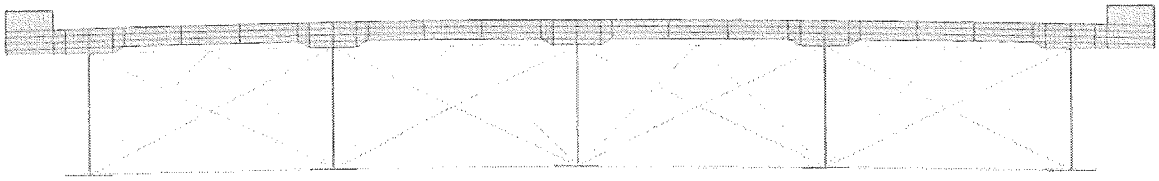

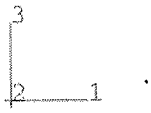

Figure 2-14. Cross section of the model.

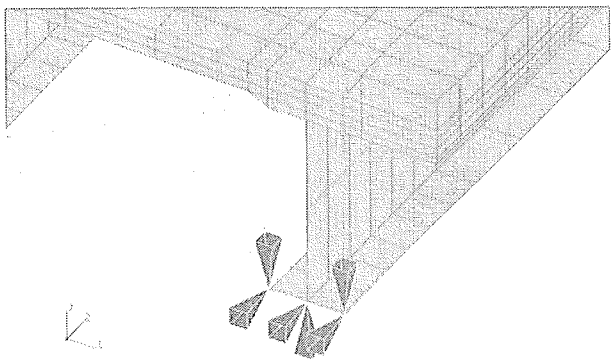

Figure 2-15. Detail of the hinge support (South Side).

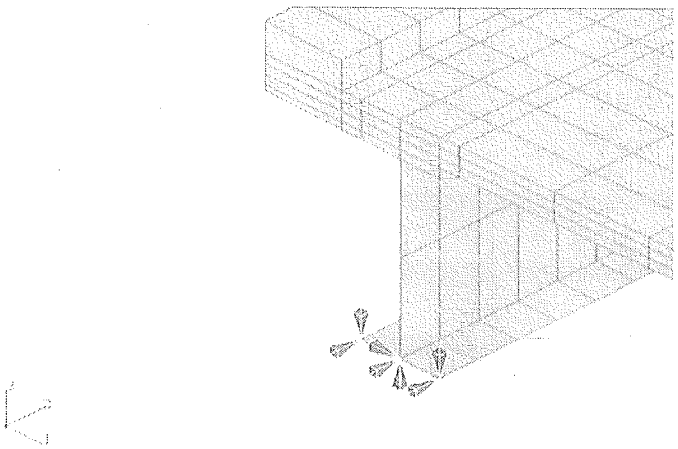

Figure 2-16. Detail of the hinge support (North Side).

The positions of the live load used in the finite element models calculations are explained in Figures 2-17, 2-19, 2-21, 2-23, 2-25, 2-27, 2-29, 2-31, 2-33, 2-35, 2-37, 2-40, 2-43 and 2-46. These positions are the same as those used during the field test, as explained above in Table 2-1. Strains that were calculated using the finite element models, with two options of supporting conditions (hinge-roller and hinge-hinge), are compared with test results for all 9 runs, shown in Figures 2-18, 2-20, 2-22, 2-24, 2-26, 2-28, 2-30, 2-32, 2-34, 2-36, 2-38, 2-39, 2-41, 2-42, 2-44, 2-45, 2-47 and 2-48.

Position 1: Center of North Lane – crawling speed

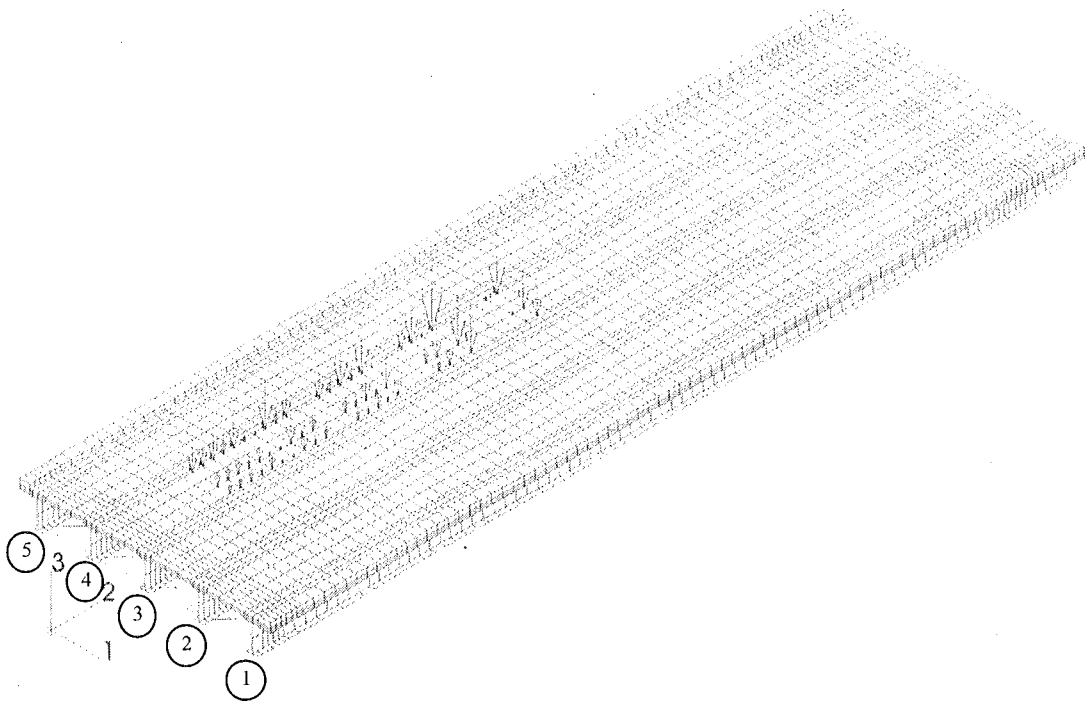

Figure 2-17. Load Position for the maximum moment at 26 ft from the support.

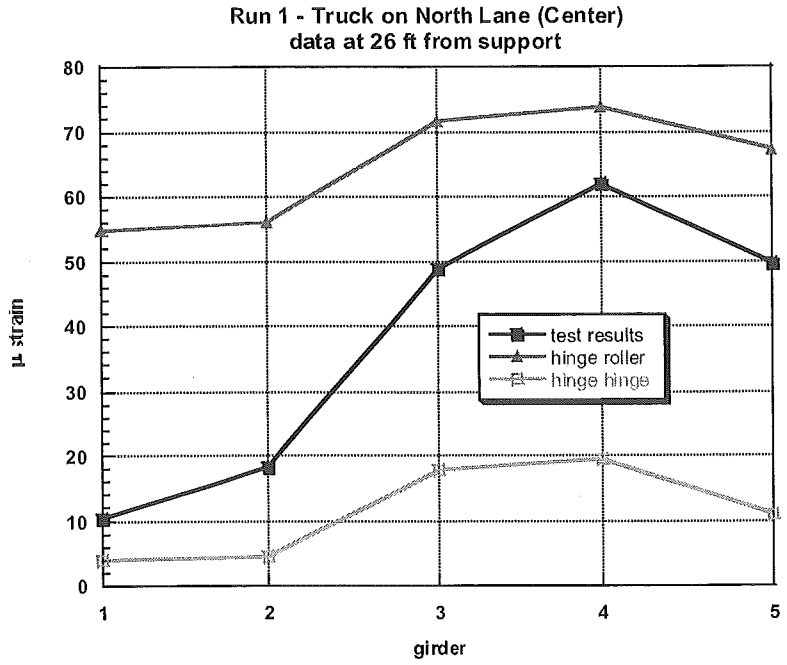

Figure 2-18. Comparison of analytical model and test results at 26 feet from the support.

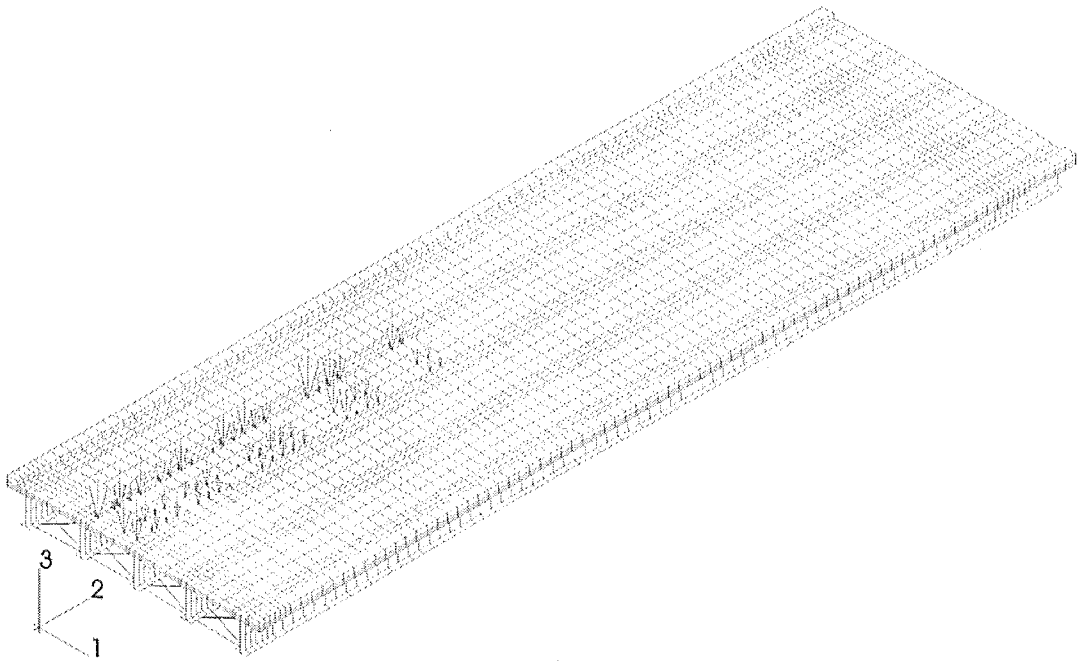

Figure 2-19. Load Position for the maximum moment at 2 ft from the support.

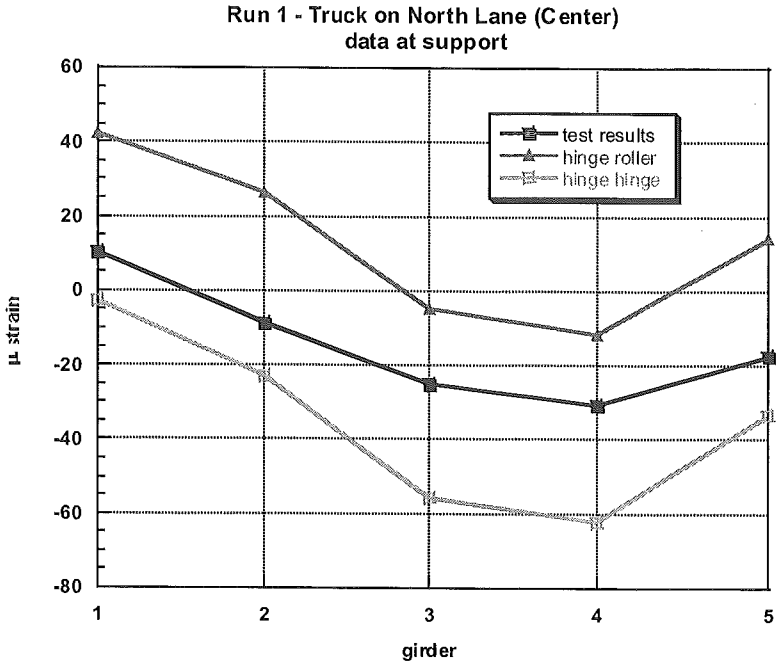

Figure 2-20. Comparison of analytical model and test results at 2 feet from the support.

Position 2: Center of South Lane – crawling speed

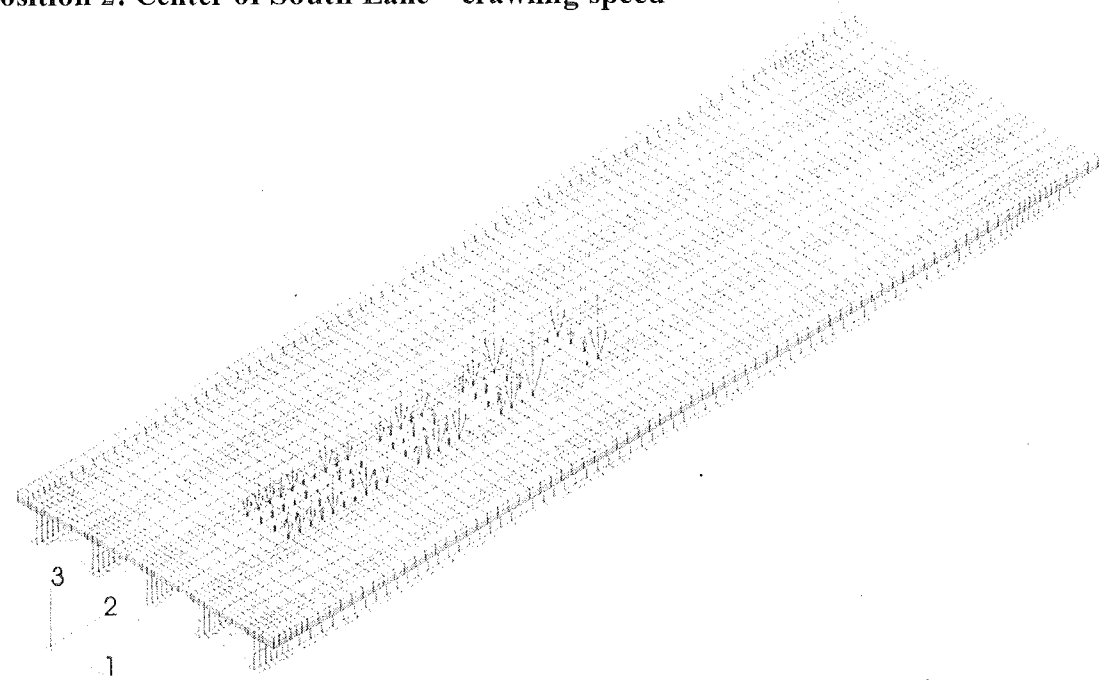

Figure 2-21. Load Position for the maximum moment at 26 ft from the support.

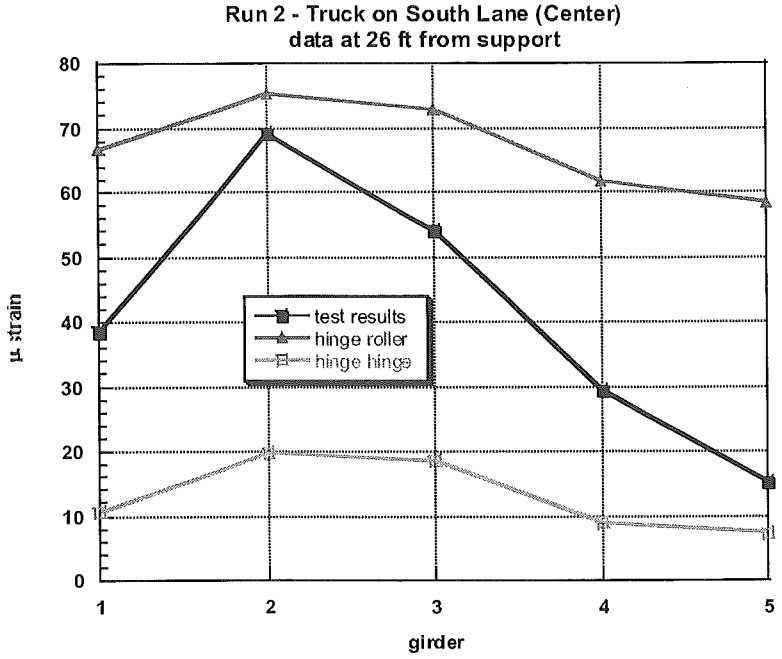

Figure 2-22. Comparison of analytical model and test results at 26 feet from the support.

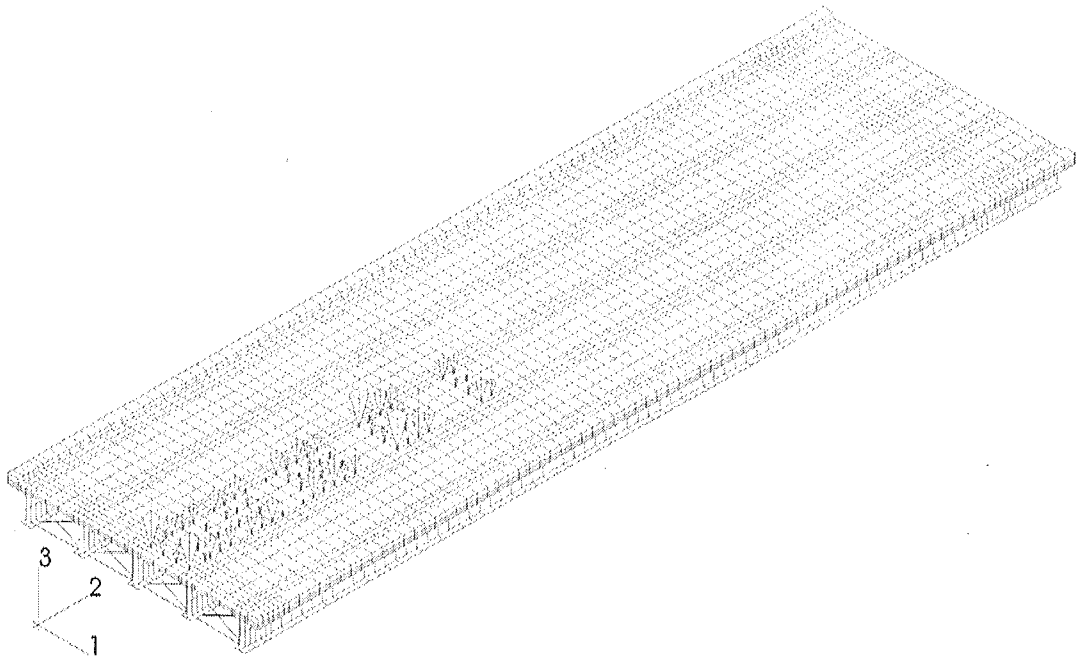

Figure 2-23. Load Position for the maximum moment at 2 ft from the support.

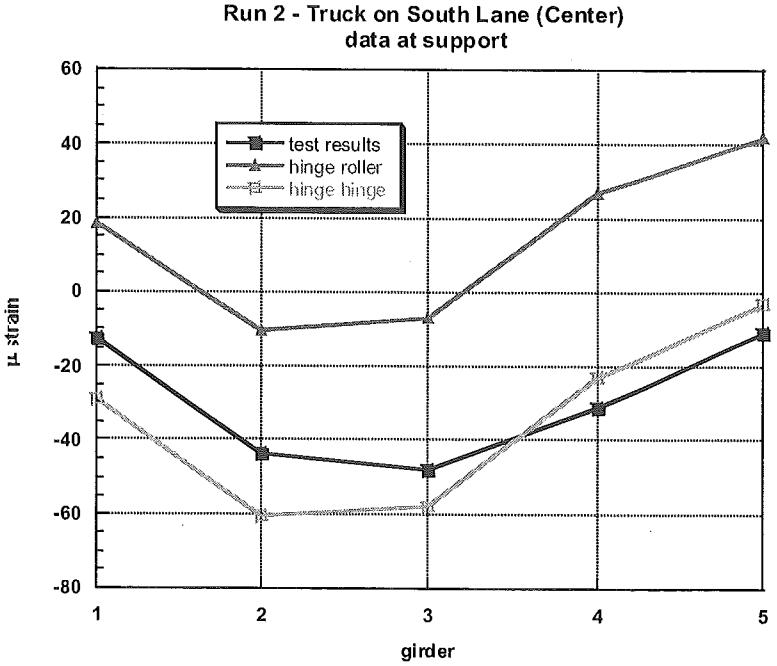

Figure 2-24. Comparison of analytical model and test results at 2 feet from the support.

Position 3: close to curb of North Lane – crawling speed

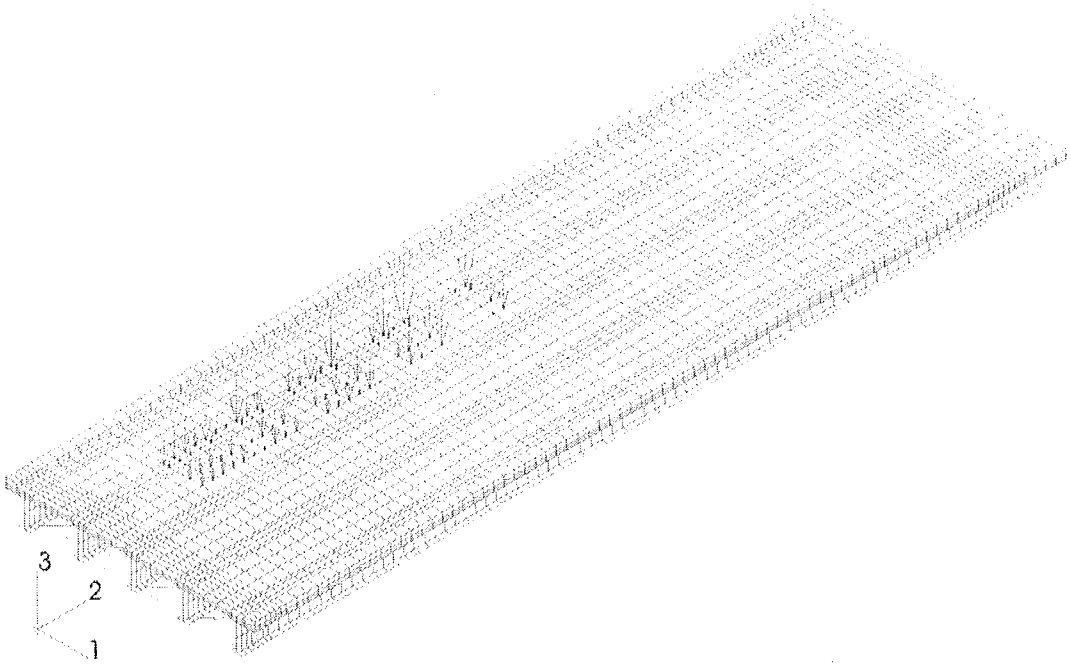

Figure 2-25. Load Position for the maximum moment at 26 ft from the support.

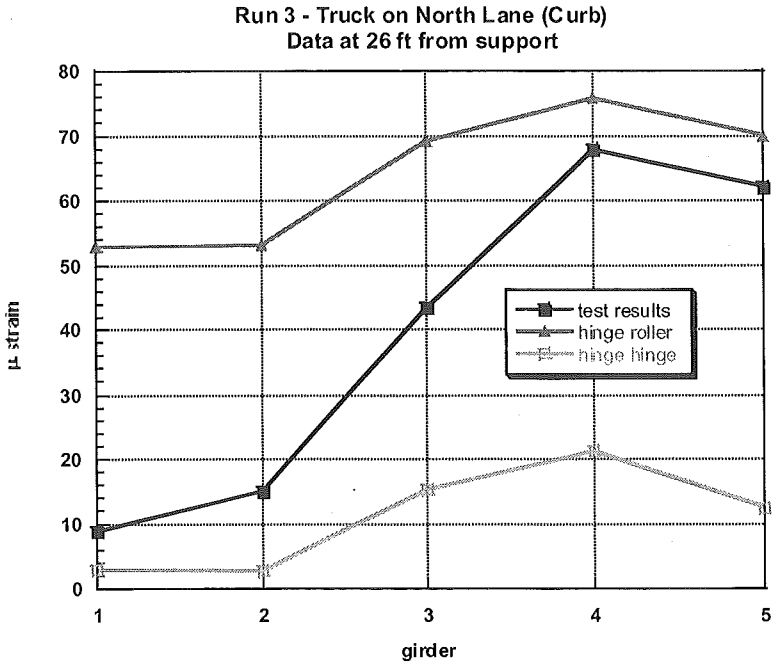

Figure 2-26. Comparison of analytical model and test results at 26 feet from the support.

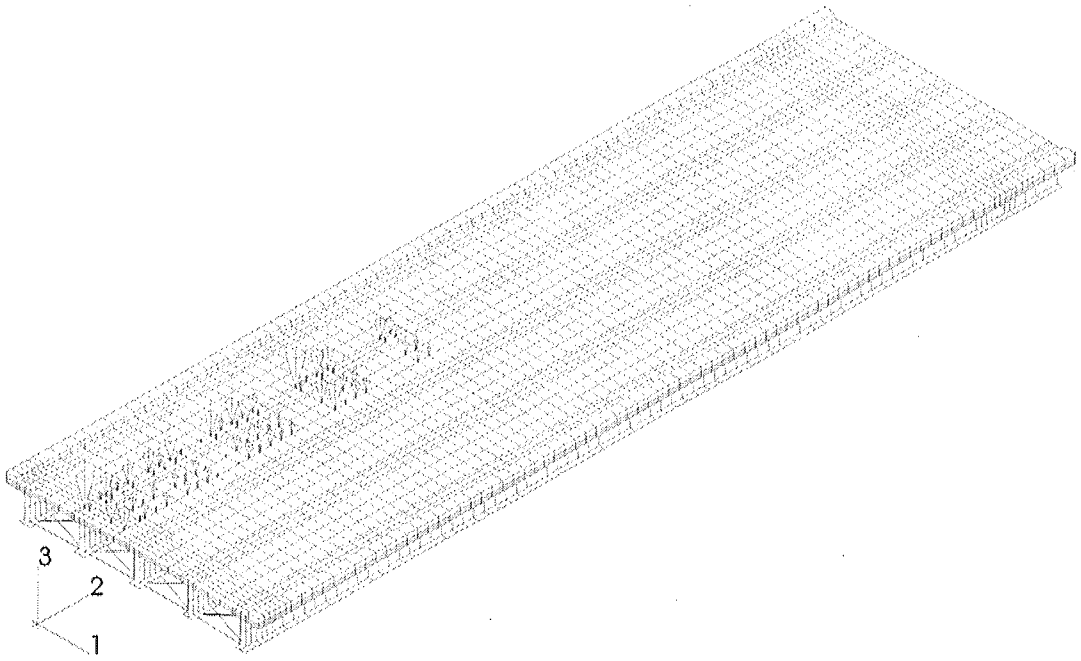

Figure 2-27. Load Position for the maximum moment at 2 ft from the support.

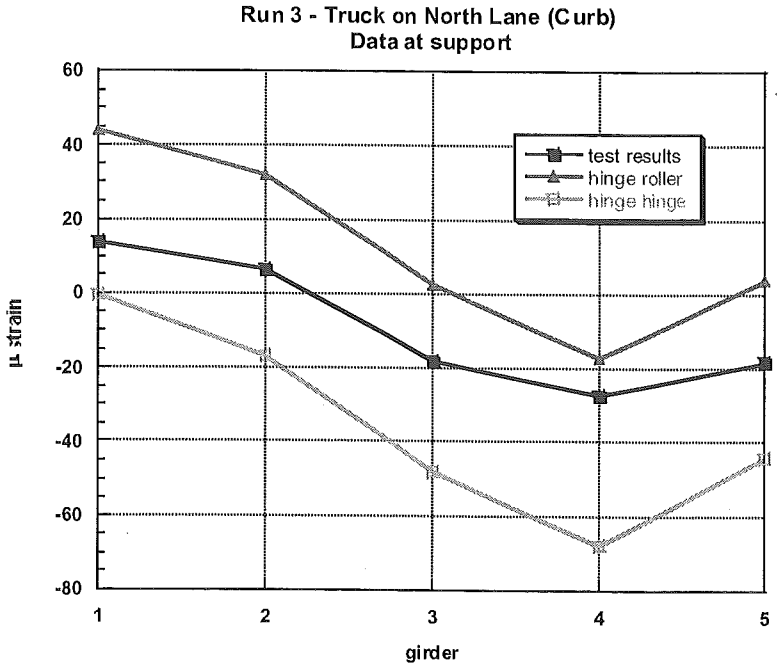

Figure 2-28. Comparison of analytical model and test results at 2 feet from the support.

Position 4: close to curb of South Lane – crawling speed

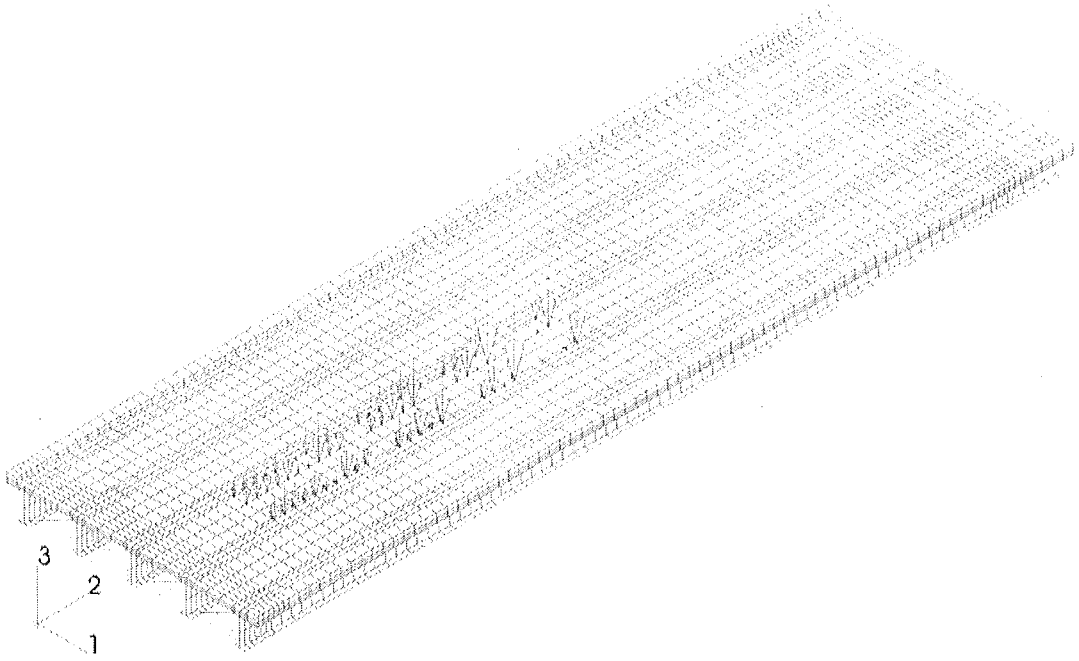

Figure 2-29. Load Position for the maximum moment at 26 ft from the support.

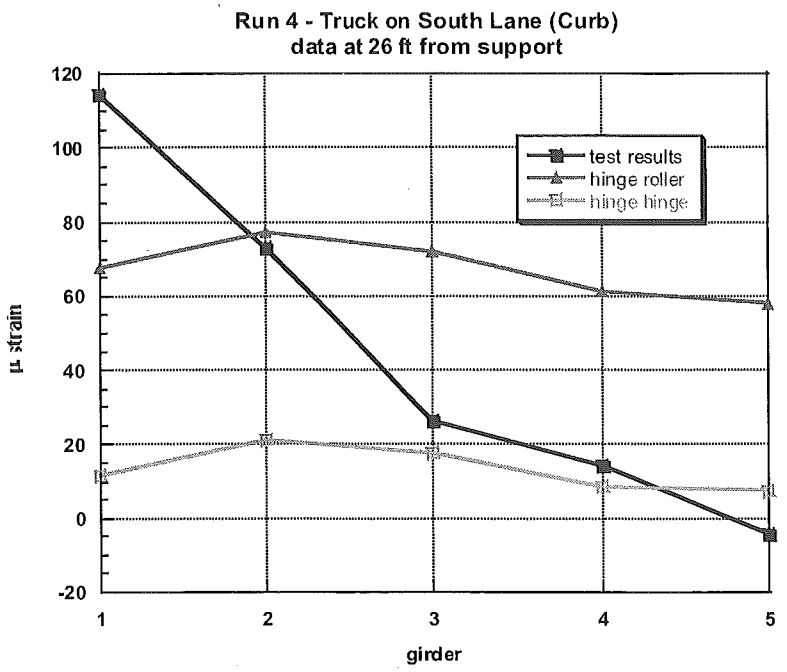

Figure 2-30. Comparison of analytical model and test results at 26 feet from the support.

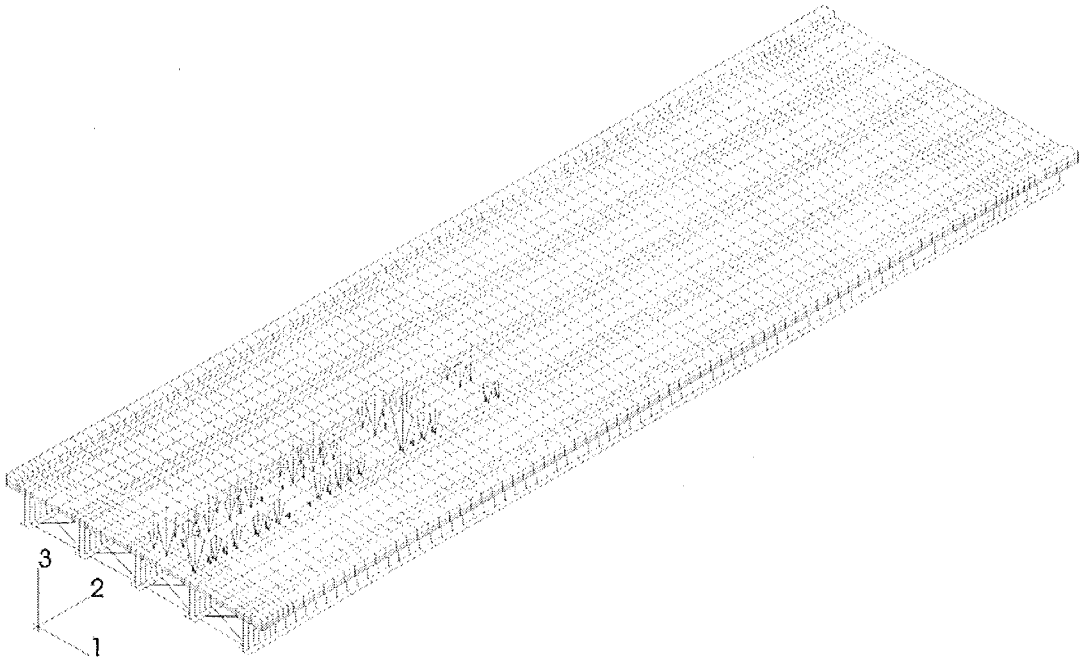

Figure 2-31. Load Position for the maximum moment at 2 ft from the support.

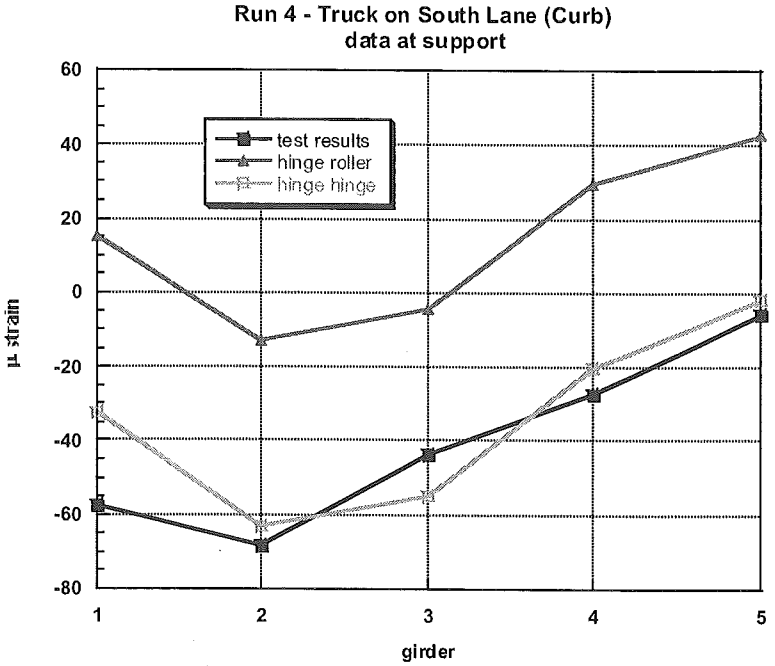

Figure 2-32. Comparison of analytical model and test results at 2 feet from the support.

Position 5: Center of bridge – crawling speed

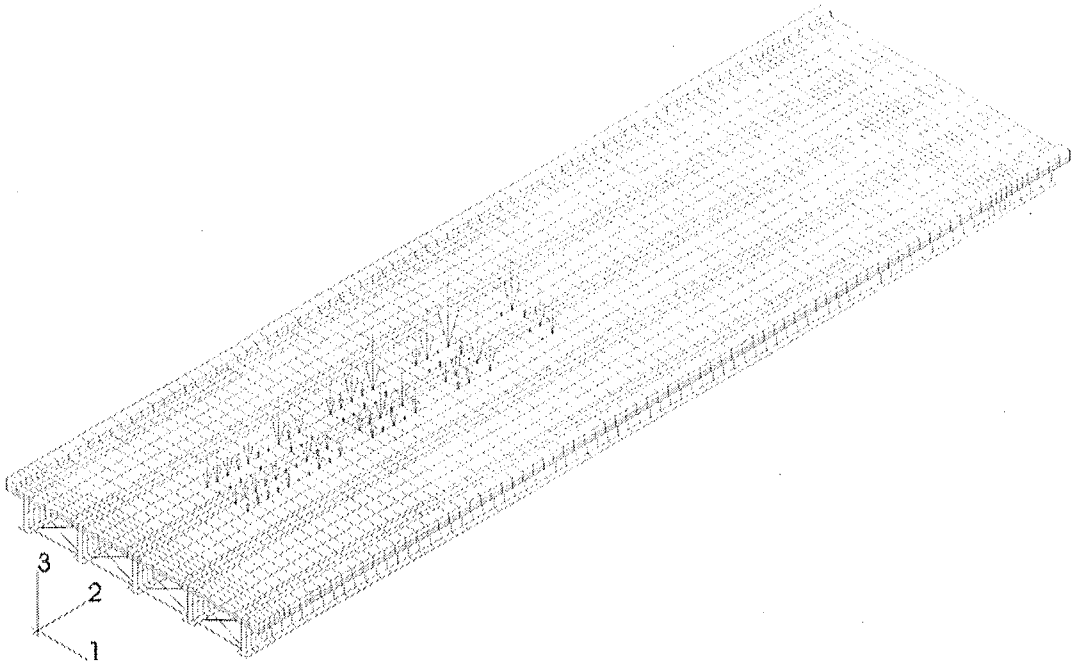

Figure 2-33. Load Position for the maximum moment at 26 ft from the support.

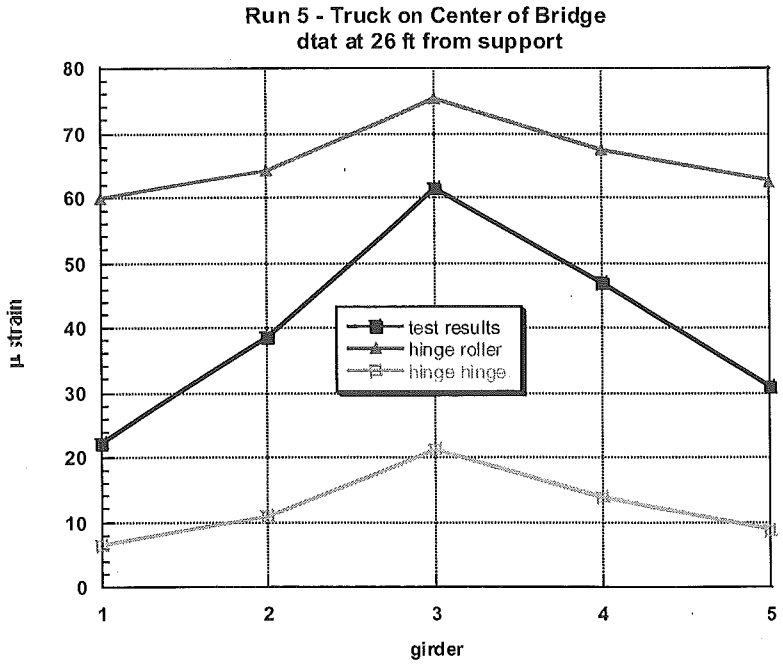

Figure 2-34. Comparison of analytical model and test results at 26 feet from the support.

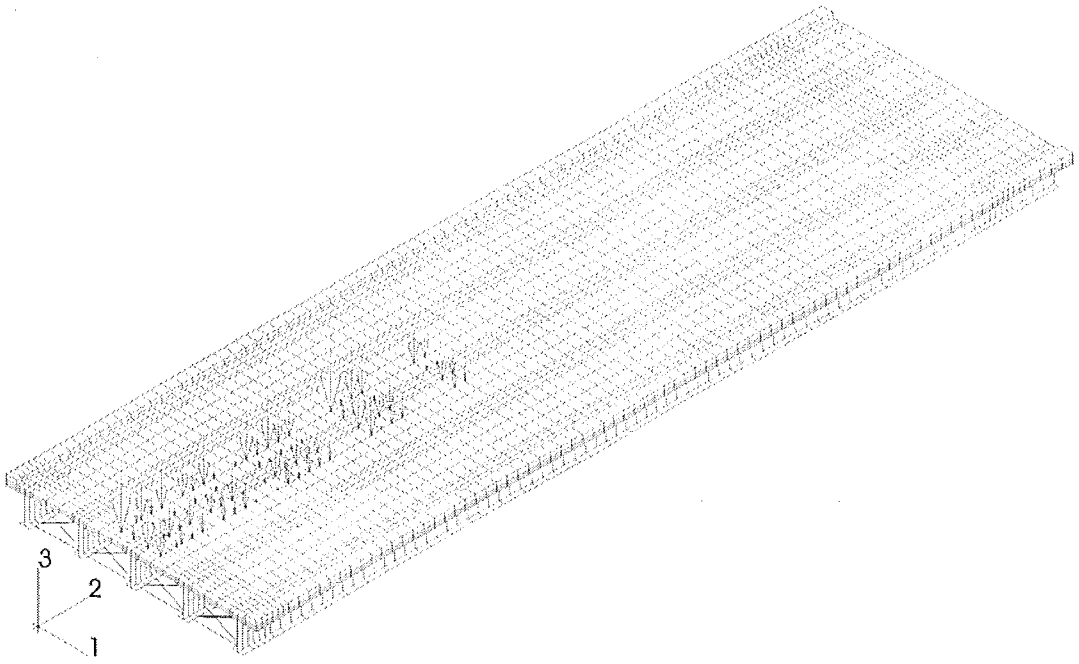

Figure 2-35. Load Position for the maximum moment at 2 ft from the support.

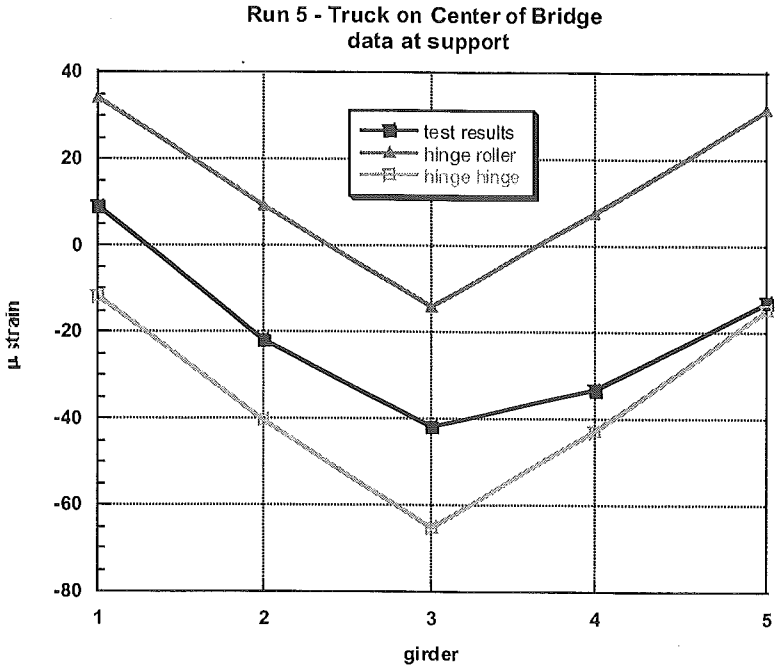

Figure 2-36. Comparison of analytical model and test results at 2 feet from the support.

Position 6: Center of North lane – fixed position

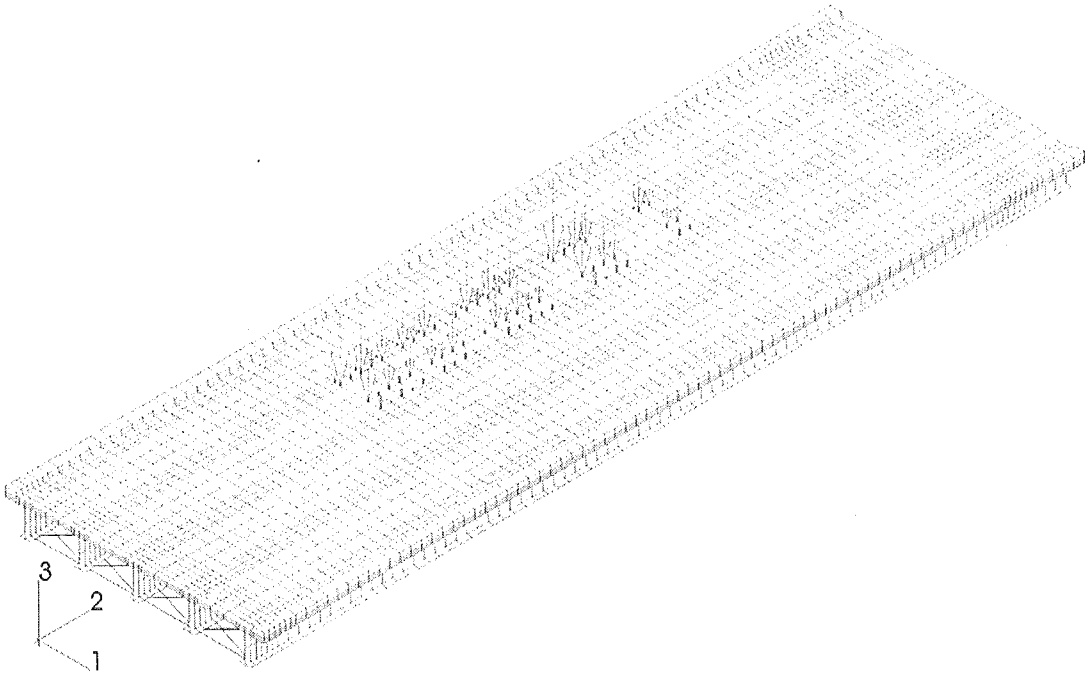

Figure 2-37. Fixed load position with the rear axle at 1/3 of the span.

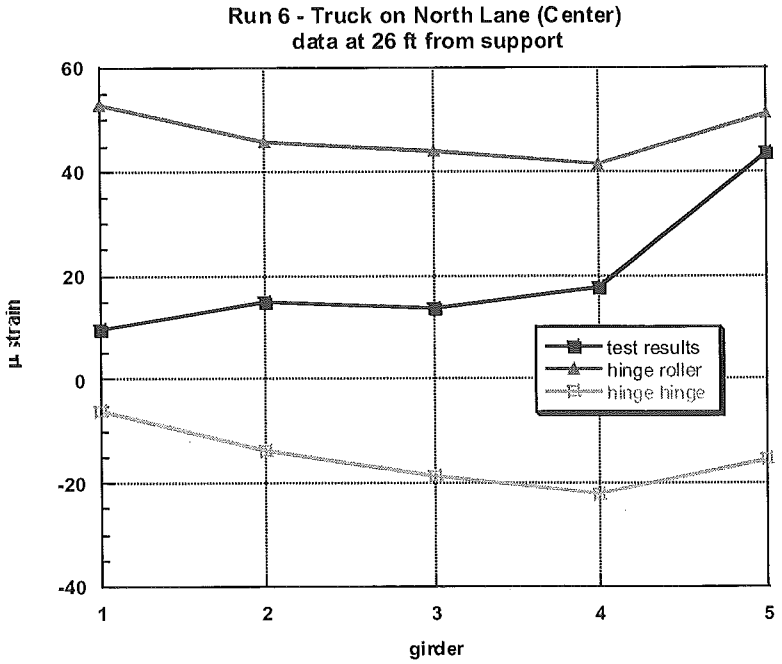

Figure 2-38. Comparison of analytical model and test results at 26 feet from the support.

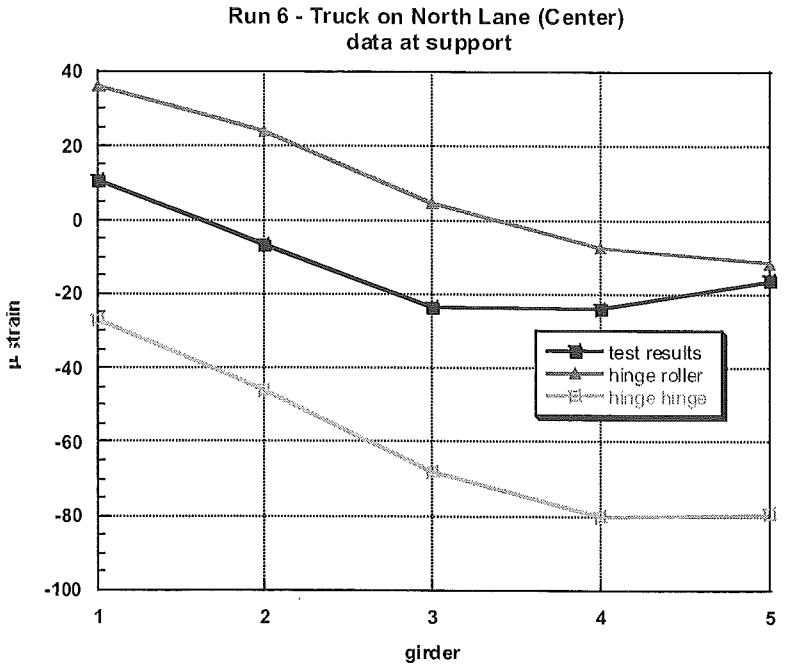

Figure 2-39. Comparison of analytical model and test results at 2 feet from the support.

Position 7: Center of South lane – fixed position

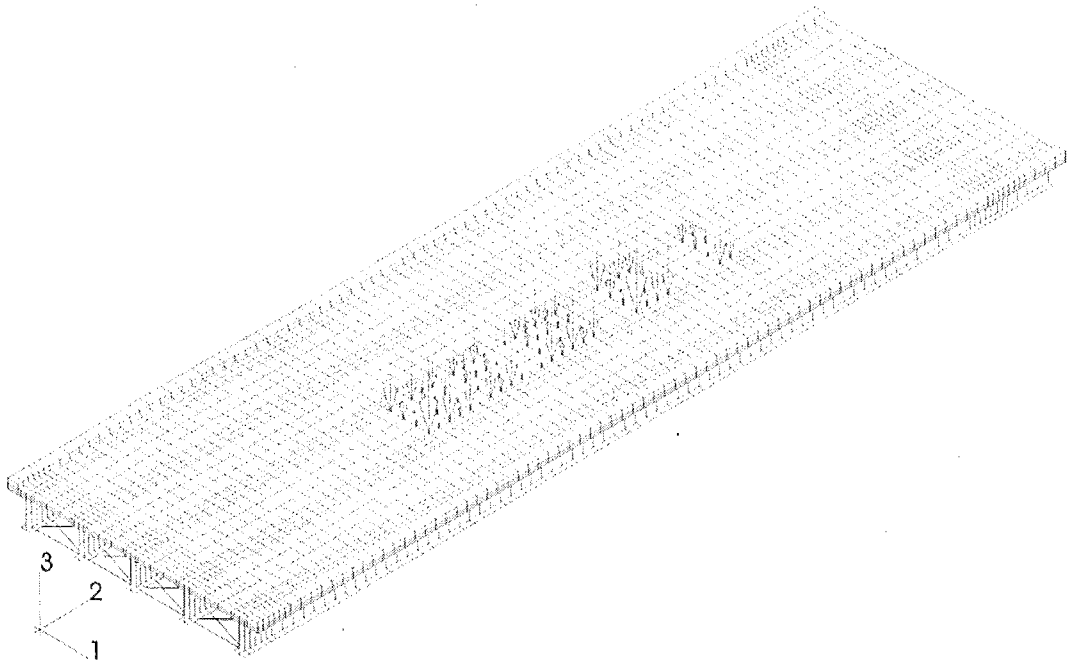

Figure 2-40. Fixed load position with rear axle at 1/3 of the span.

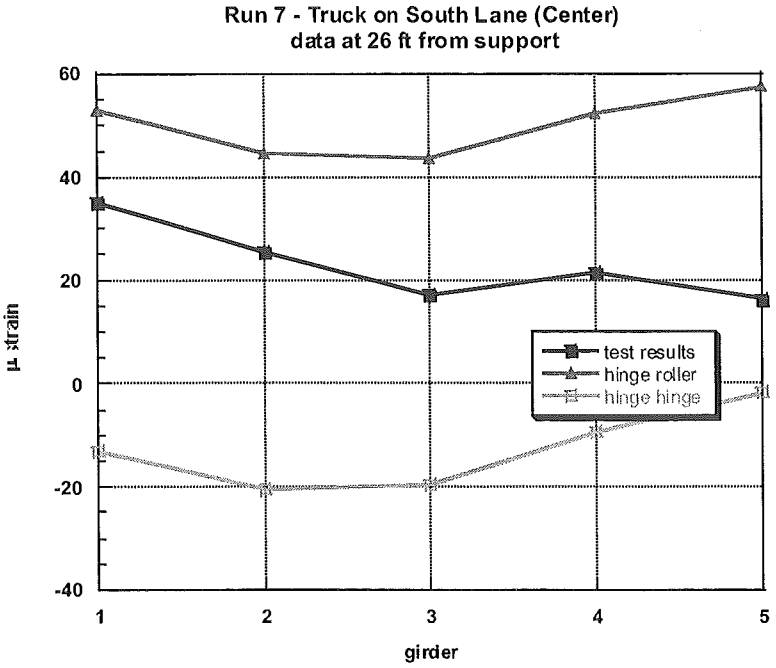

Figure 2-41. Comparison of analytical model and test results at 26 feet from the support.

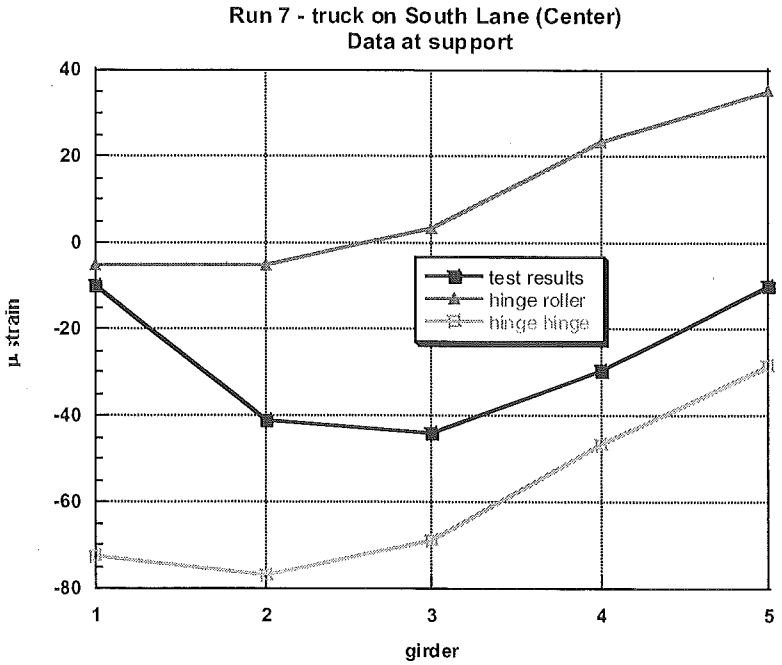

Figure 2-42. Comparison of analytical model and test results at 2 feet from the support.

Position 8: Center of the bridge – fixed position

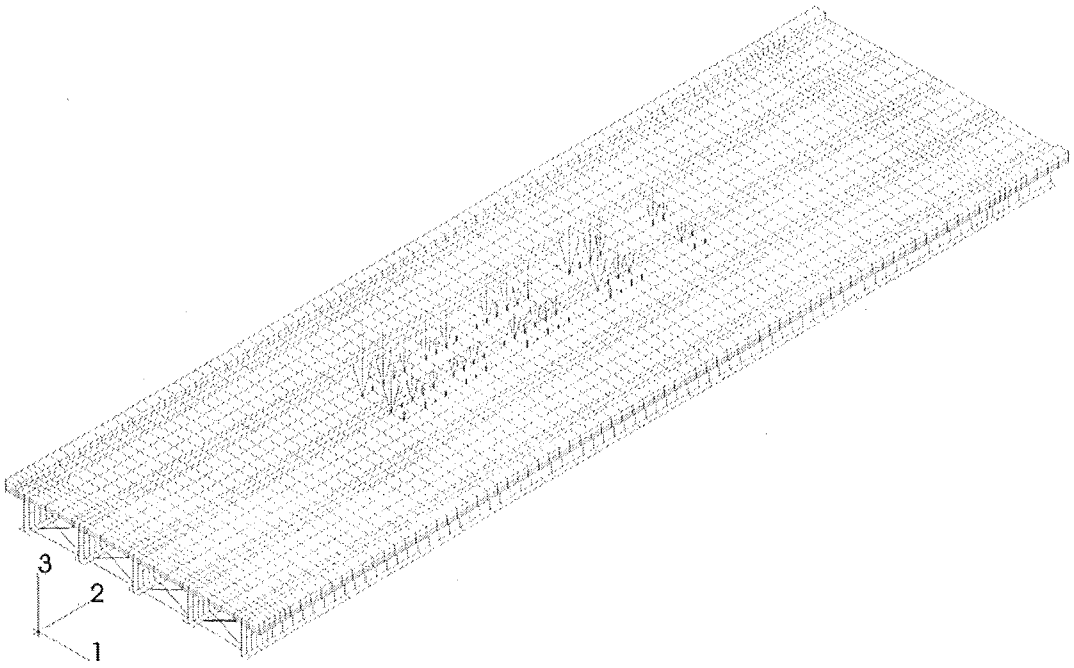

Figure 2-43. Fixed load position with rear axle at 1/3 of the span.

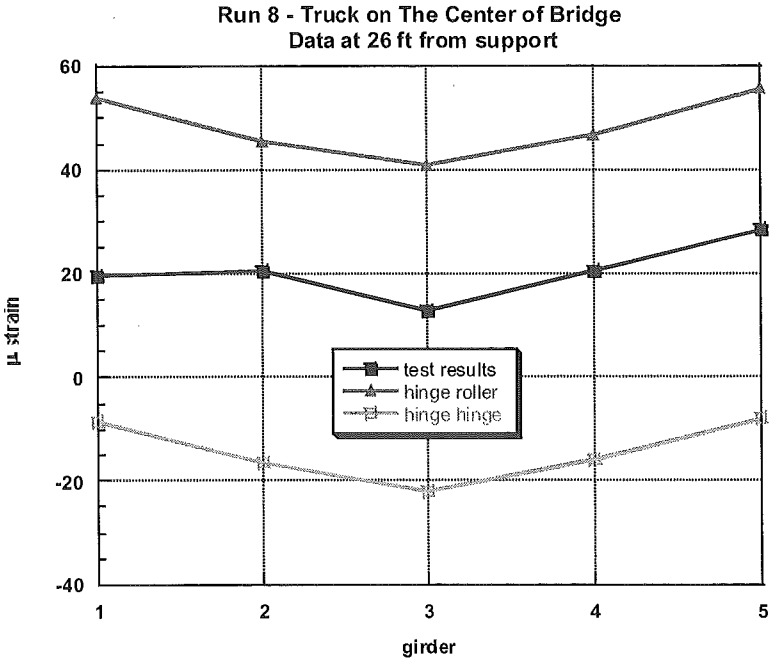

Figure 2-44. Comparison of analytical model and test results at 26 feet from the support.

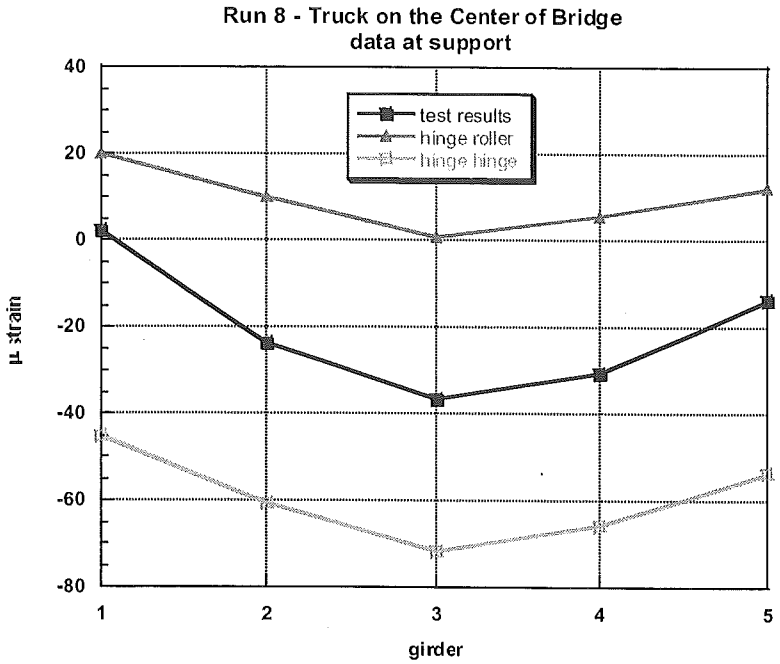

Figure 2-45. Comparison of analytical model and test results at 2 feet from the support.

Position 9: Center of North lane – fixed position

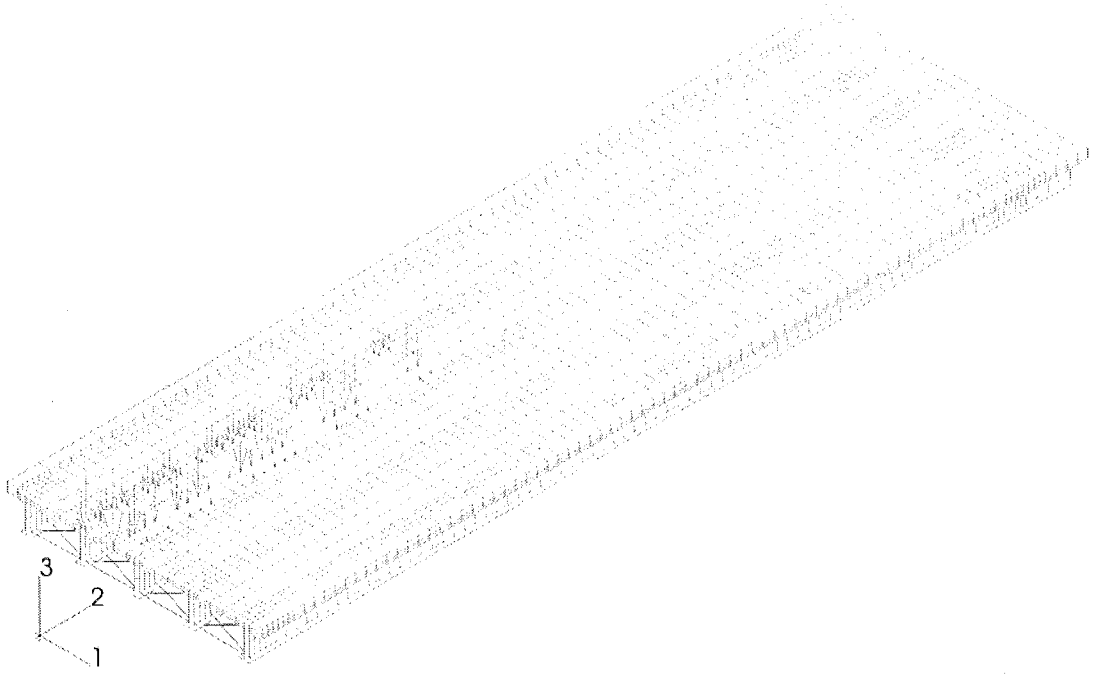

Figure 2-46. Fixed load position with rear axle at the support.

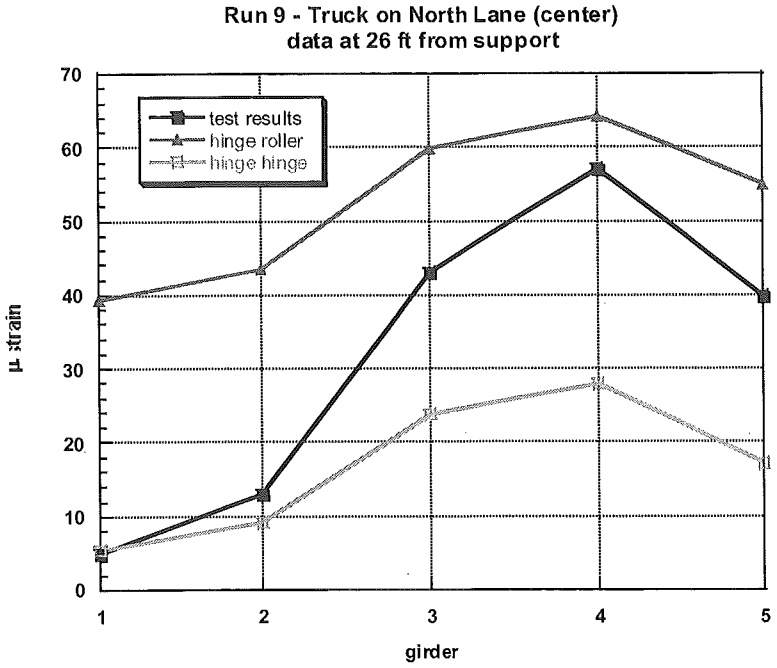

Figure 2-47. Comparison of analytical model and test results at 26 feet from the support.

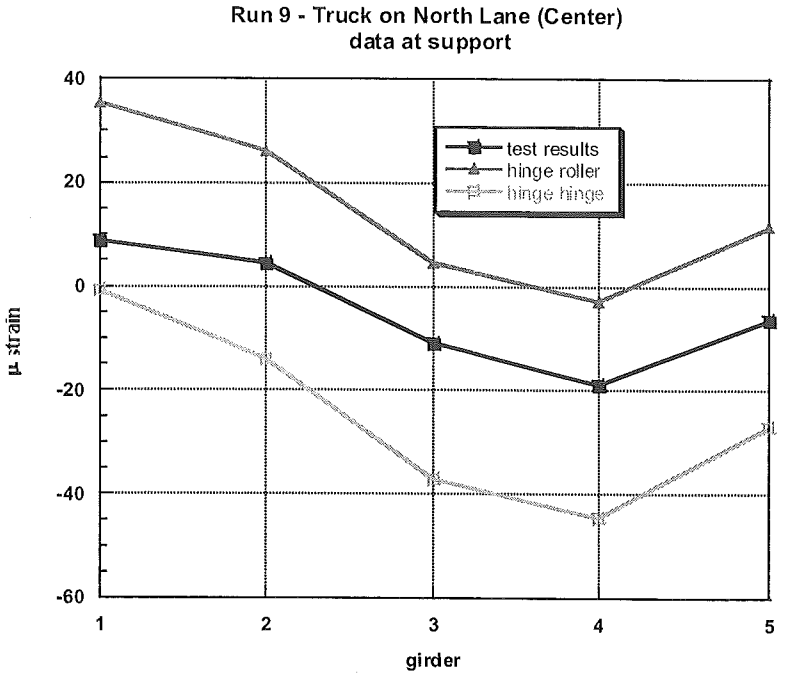

Figure 2-48. Comparison of analytical model and test results at 2 feet from the support.

The bridge test was carried out to measure strain values in the girders close to the support. The obtained data was used to determine the actual support conditions. For flexural members used in the finite element model, two types of support were considered: hinge-roller support or hinge- hinge support. In real structures, the actual support conditions are somewhere between these two theoretical boundaries. The solution in the case of the hinge-roller support can be treated as the upper bound for the measured values. The hinge-hinge solution can be treated as the lower bound.

The measured strains at the distance of 26 feet from the support and 2 ft from the support are between the strain values obtained from the finite element analysis. In each loading case, with the most loaded girder, it can be seen that the strain value measured at 26 ft from the support is closer to the hinge-roller support than to the hinge-hinge support. The strain values measured at 2 ft from the support, with the same girder and load position, are in the middle between the two theoretical values. This tendency can be seen in all considered load cases. The reason for this behavior is a non-uniform load distribution through the deck to the girders, especially for larger girder spacing (123 inches or about

10 feet). The load distribution seems to be more uniform for the cross sections closer to the support. This can be attributed to the influence of a stiff concrete backwall (diaphragm) placed at the end of the girders.

Based on the test results, the support conditions were modeled using spring elements that represent partial fixity. A spring element with a certain stiffness (coupling a force to a relative displacement) was added longitudinally to the nodes located at the upper and lower flange of the girder ends (see Figure 2-49), as well as transversally at both bottom ends of the girder. This model better reflects the real behavior of the bridge superstructure, and it can be used in the FEM analysis. Based on all considered load cases, with nine positions of the truck moving at a crawling speed or at fixed positions, the average values of the spring stiffness were used to calibrate the finite element model.

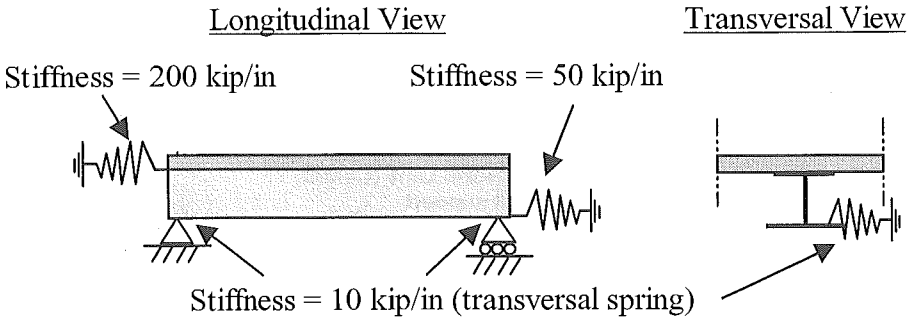

Figure 2-49. Modeling of partially fixed support using springs

After adding the springs, the strain values were recalculated for all load cases and compared with measured strain values at 26 feet from the support and at 2 feet from the support. The comparison of calculated and measured values after calibration is shown in Figures 2-50 to 2-59. There is a good agreement between the calculated and measured strain values, and that indicates the validation of the finite element model.

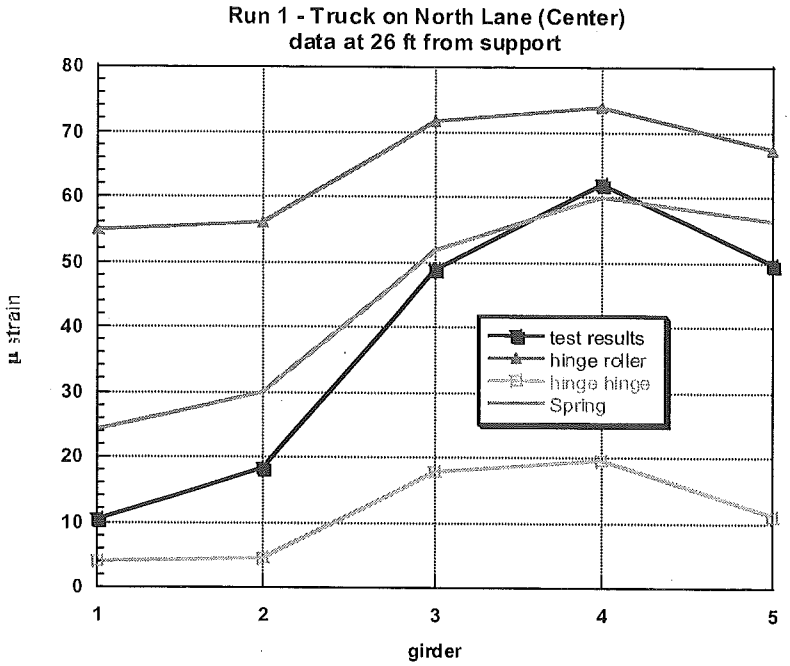

Figure 2-50. Comparison of calibrated finite element model and test results at 26 feet from the support.

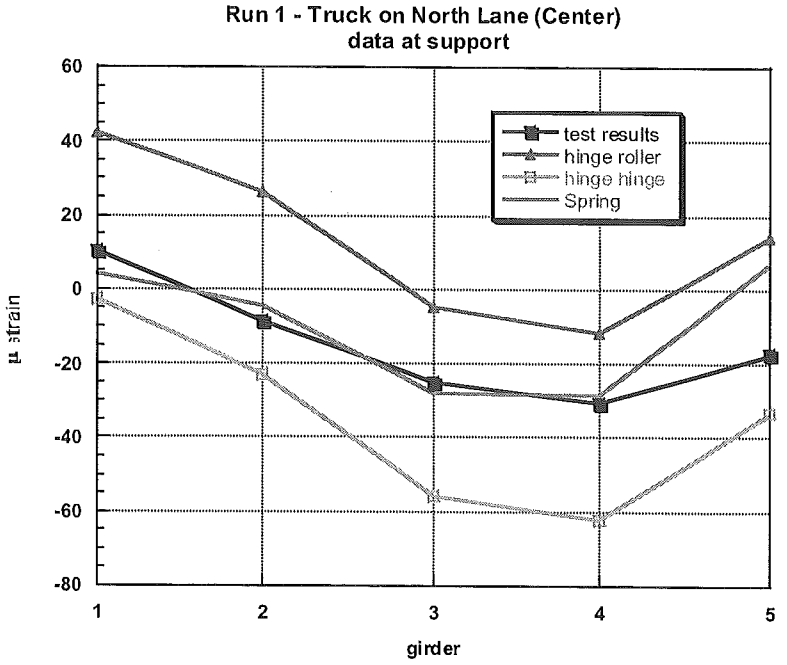

Figure 2-51. Comparison of calibrated finite element model and test results at 2 feet from the support.

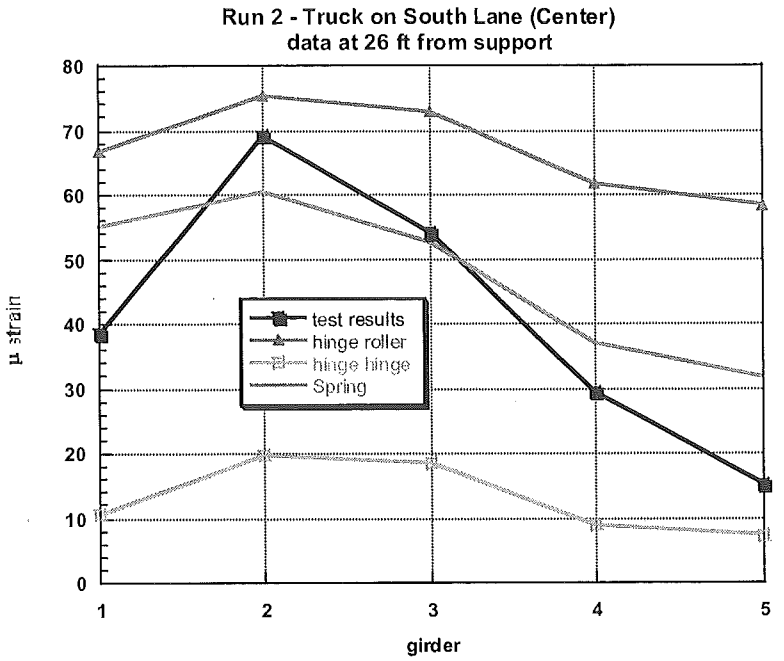

Figure 2-52. Comparison of calibrated finite element model and test results at 26 feet from the support.

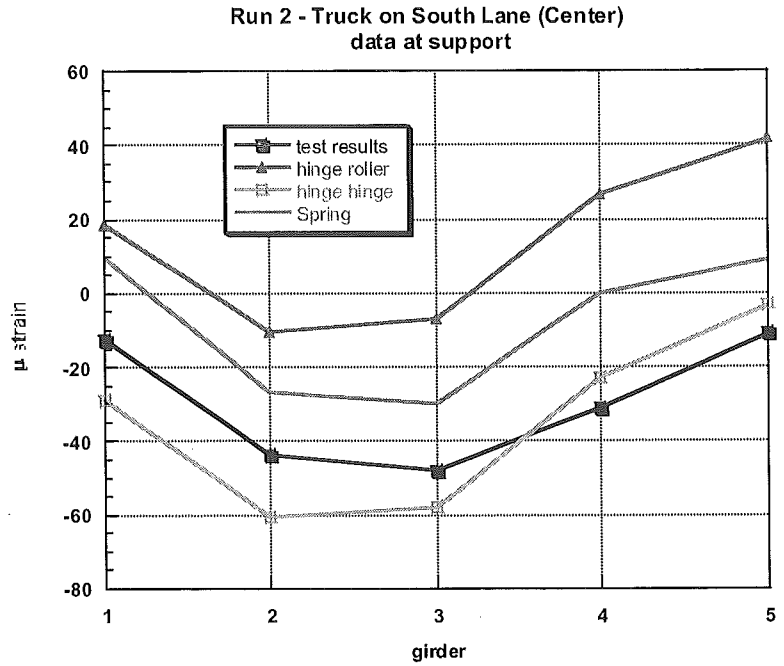

Figure 2-53. Comparison of calibrated finite element model and test results at 2 feet from the support.

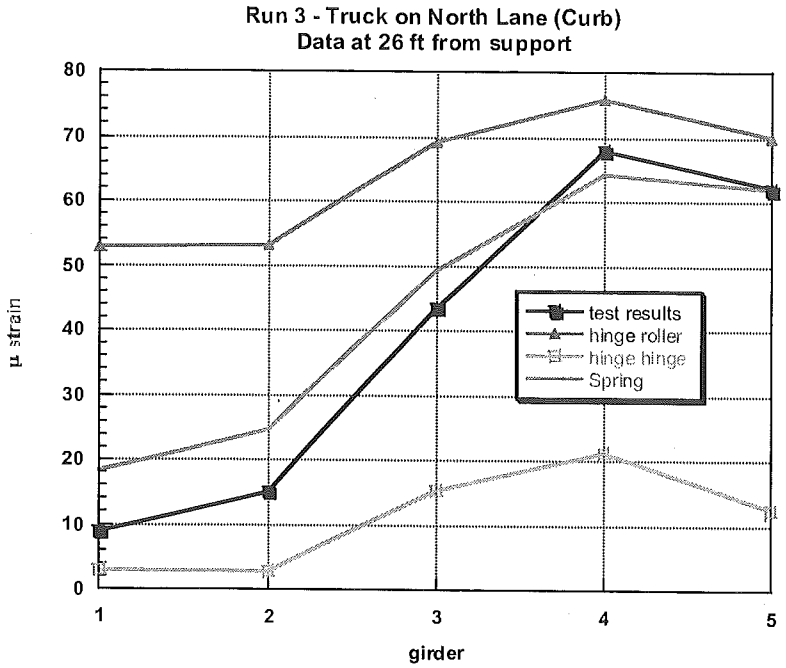

Figure 2-54. Comparison of calibrated finite element model and test results at 26 feet from the support.

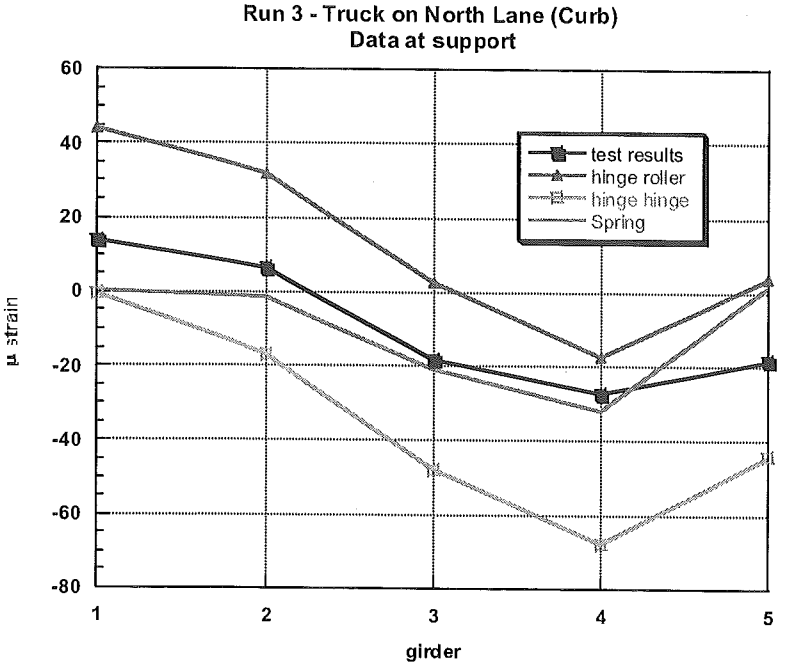

Figure 2-55. Comparison of calibrated finite element model and test results at 2 feet from the support.

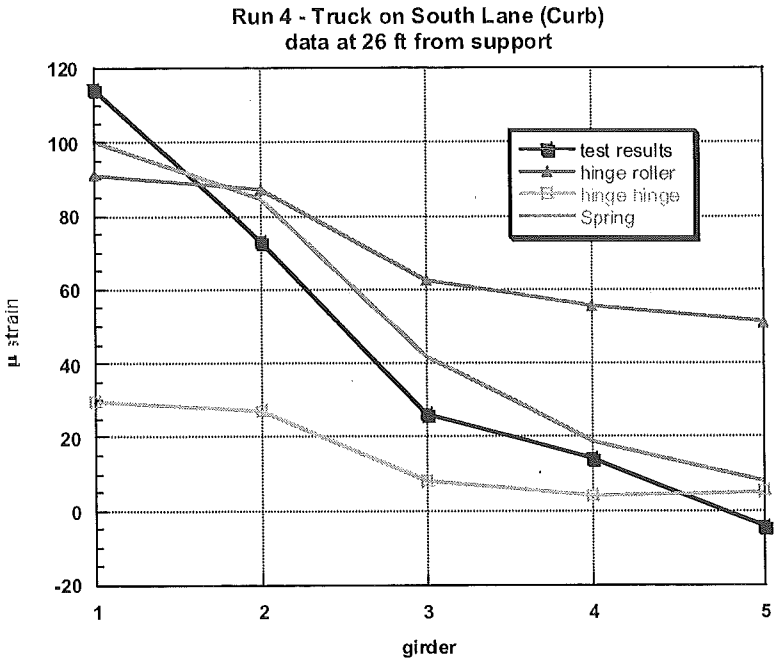

Figure 2-56. Comparison of calibrated finite element model and test results at 26 feet from the support.

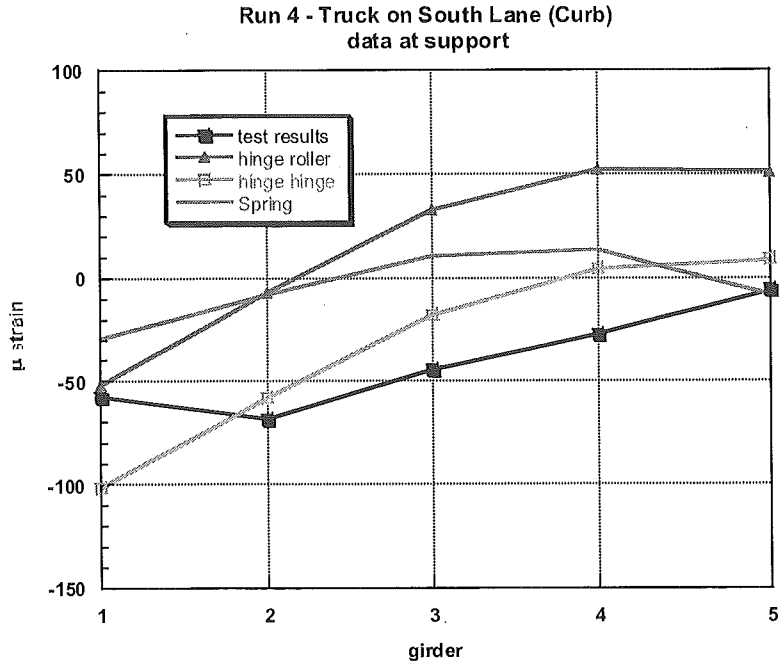

Figure 2-57. Comparison of calibrated finite element model and test results at 2 feet from the support.

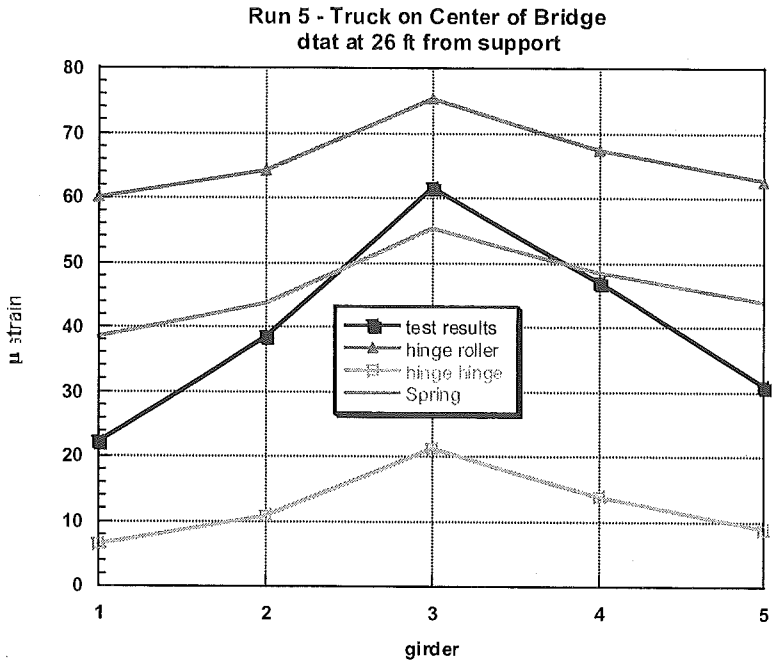

Figure 2-58. Comparison of calibrated finite element model and test results at 26 feet from the support.

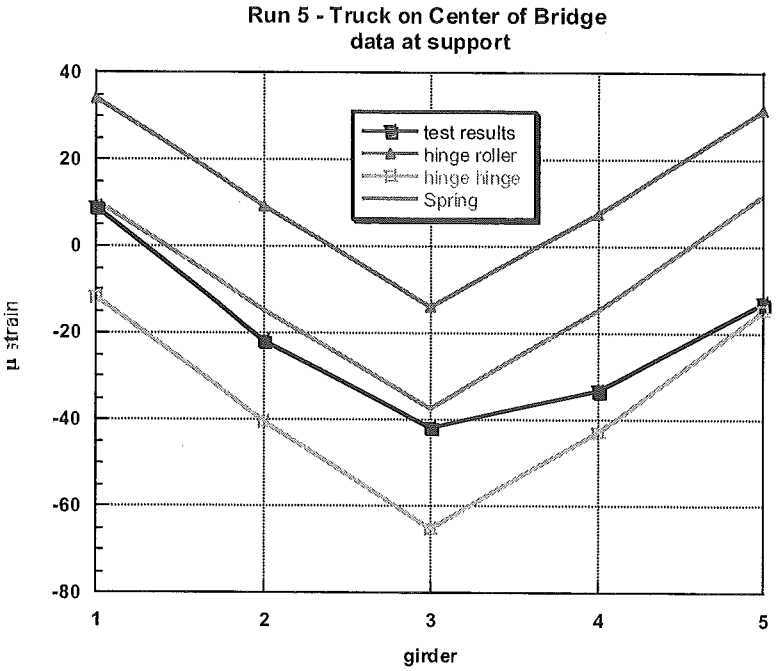

Figure 2-59. Comparison of calibrated finite element model and test results at 2 feet from the support.

Established support conditions were used in the FEM model of the bridge superstructure with a concrete deck supported on steel girders spaced at 10 feet. This model was used for the analysis of concrete deck behavior under the most extreme loading cases.

First, the calibrated ABAQUS bridge model was used to calculate stresses at the top and bottom of the deck for the transversal positions of the truck used during the field test (Positions from 1 to 5 explained in the figures above). Longitudinally, the truck was positioned to obtain the maximum stress at the midspan and close to support. Next, the same calibrated model was used to calculate the maximum possible stresses that can occur in the deck under the live load. For that purpose, two 11-axle trucks were used as a live load. The two identical trucks, with weights and configurations that were the same as the test truck, were positioned on the deck to obtain maximum stress at the midspan and close to the support. The results of all these stress calculations are presented in Appendix A. The positions of the one truck and the two trucks on the bridge, used in the analysis, are also presented in Appendix A. The maximum and minimum stress values obtained from the described analysis are shown in the table at the end of Appendix A.

The extreme cases from the stress analysis for the deck supported on steel girders are presented in Section 4.1. These maximum stress values are used in the ultimate and cracked limit state analysis.

3. ANALYSIS OF CONCRETE DECK SUPPORTED ON PRESTRESSED CONCRETE GIRDERS

A typical bridge superstructure with an isotropic deck supported on prestressed concrete girders was selected to investigate the behavior of the deck under the live load. The concrete deck together with the prestressed concrete girders was modeled using the finite element method (ABAQUS). The structure was modeled according to drawings provided by MDOT. The bridge was scheduled for a load test to obtain the data suitable for the modeling boundary (support) conditions for the girders.

The selected bridge (B05 of 50022) is located on M-59, over the middle branch of the Clinton River near Detroit, Michigan. It is composed of three 45 foot simply supported spans. The cross section consists of seven prestressed concrete Type II girders, spaced at 10 ft 5 in, and a concrete deck that is 9 inches thick, without a wearing surface. The Michigan Department of Transportation provided a set of drawings related to this bridge. Figures 3-1 to 3-4 show different views of the bridge: general view, layout, elevation and cross section.

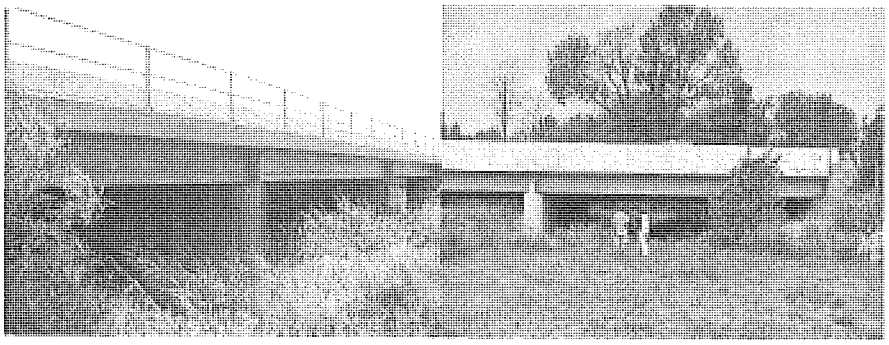

Figure 3-1. General view of the selected bridge.

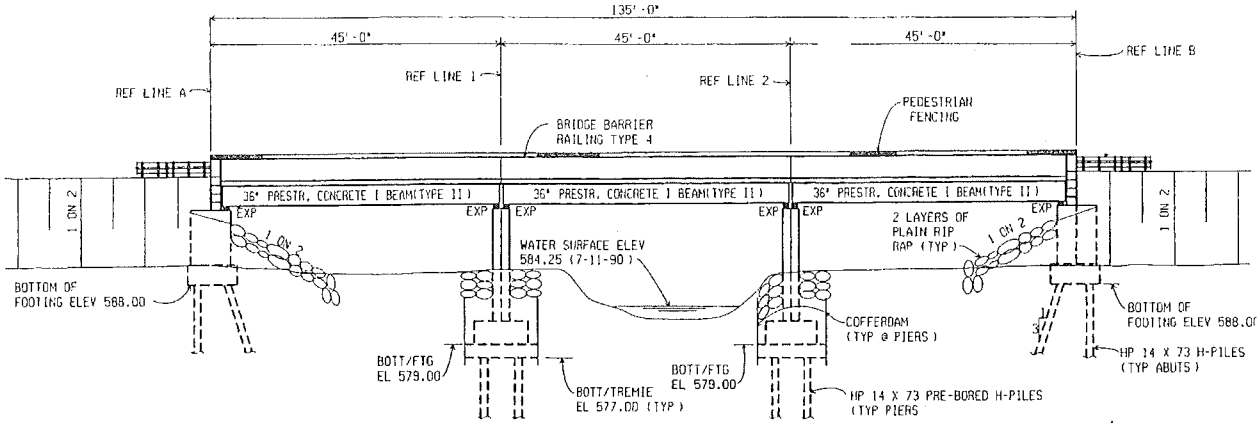

Figure 3-2. Longitudinal elevation of the selected bridge.

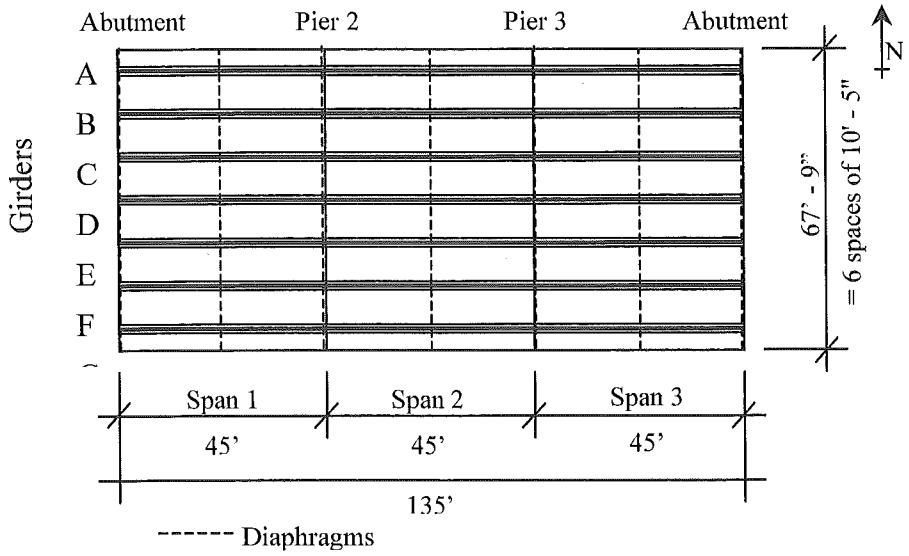

Figure 3-3. Bridge layout.

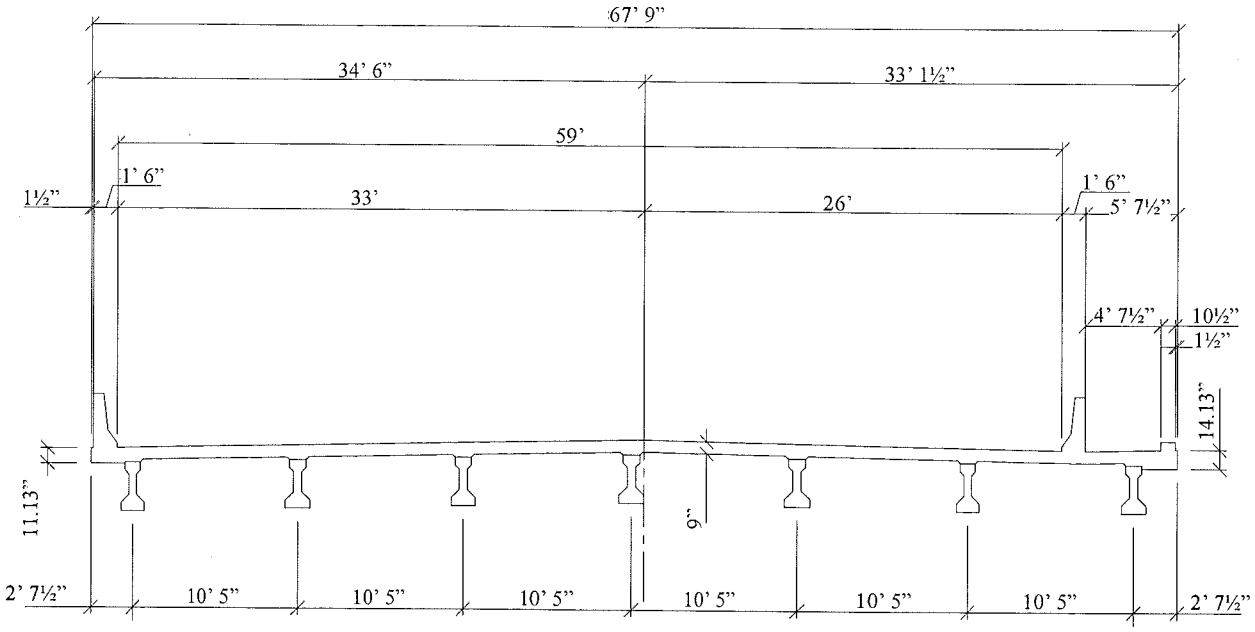

Figure 3-4. Typical deck cross section.

Standard Type II precast prestressed concrete I-girders are used for this bridge. The section dimensions for such a beam are shown in Figure 3-5.

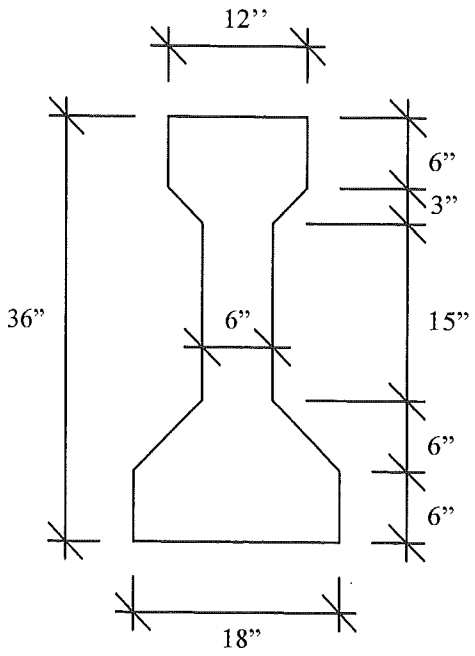

Figure 3-5. Type II prestressed concrete girder.

3.1. Finite element model of bridge superstructure

The FEM model of the deck and the girders was prepared for various stages. First, the prestressed concrete girders were modeled with the existing prestressing to find the initial stress/strain state. Then, the concrete deck was added to provide the total dead load acting on the structure. In this stage, the composite section was considered. In the next stage, a live load was applied to the deck. The final stress/strain state is the superposition of prestressing, dead load, and live load. The girders are simply supported and the deck slab is continuous over supports. The support conditions for girders in the FEM model were modeled using the field test results of the bridge. Then, the FEM model of the bridge superstructure was used to investigate the stress/strain pattern and deflection of the deck slab under various positions of live load.

3.1.1. General assumptions

The bridge is composed of simply supported girders, but the reinforced concrete slab is continuous. Over the support, the resistance is provided only by the slab, and it is very small compared to the whole composite section. However, in order to take into account the continuity of the deck and the presence of the diaphragm at the support, rollers were applied, in the FE Model, along the depth of the slab (Figure 3-6), in order to prevent longitudinal movement and produce tension force along the face of the slab.

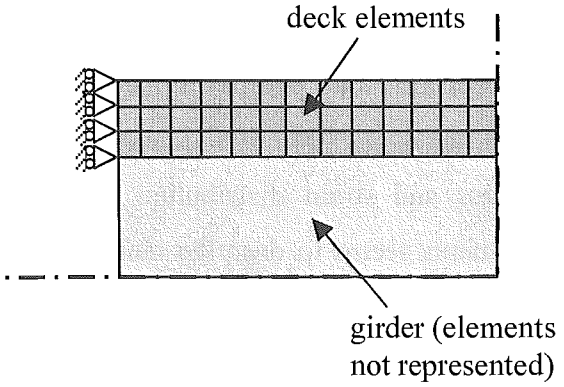

Figure 3-6. Assumption in FEM model for slab.

The assumption of a slab is also supported by the condition of the modeled bridge. Figure 3-7 shows a transversal crack in the deck located over the support. The crack penetrated through the full thickness of the deck. The concrete barrier is also cracked.

With this assumption, the response of each span becomes independent of the other spans and, thus, only one span needs to be modeled. The end span between the abutment and the first pier – referred to as Span 3 – was chosen. This span was the most accessible and the experimental data was obtained for that span.

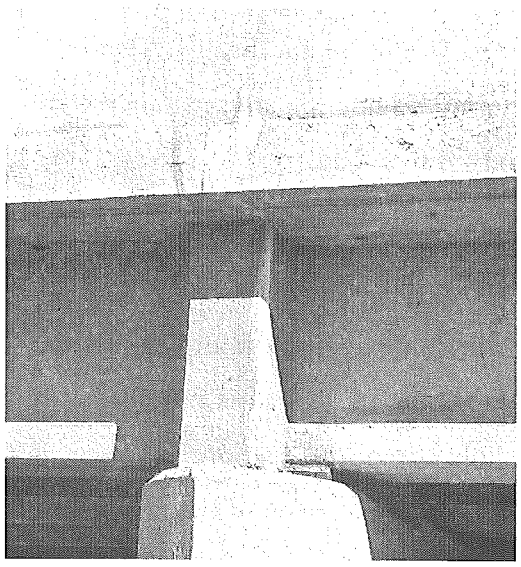

Figure 3-7. Crack in the deck over support.

The longitudinal gradient of the deck, which is less than 0.5 %, was neglected, making the mesh representing the concrete slab parallel to the XY-plane. Regarding the type of elements used in the model, the application of solid elements allowed for a more detailed investigation of local stress and strain distribution. Modeling the slab, girders and diaphragms with solid elements seems to describe most adequately the bridge geometry and physical properties.

Eight-node and six-node solid elements are used to model the different parts of the structure. These elements have six degrees of freedom at each node – translations and rotations in the nodal x, y, and z directions. The geometry and node locations for these element types are shown in Figure 3-8.

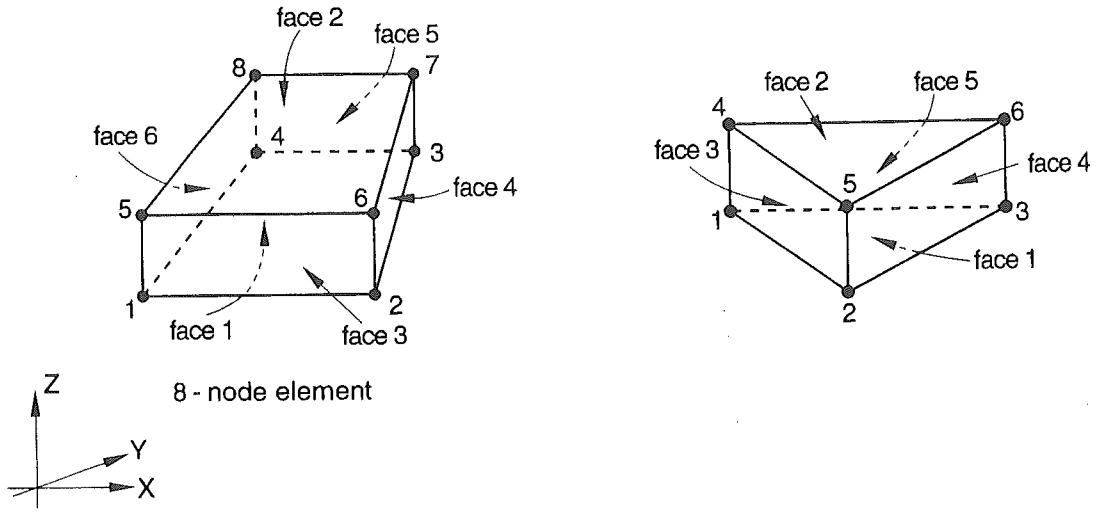

Figure 3-8. Node and face numbering of three-dimensional elements.

3.1.2. Geometry of the model

The first step of the modeling process is to divide the model into a number of small elements so that, after loading, stresses and strains can be calculated at the integration points of these small elements. Therefore, one of the most significant problems is to find the best density of the mesh for the model to have precise results and reproduce accurately the behavior of the bridge. On the other hand, a very large number of nodes and elements make the computations too complicated.

Girders

The girders are modeled using three-dimensional elements. The geometry of the concrete beams with varying dimensions (Figure 3-8), was solved by dividing the section into small elements and using tetrahedral elements to model the transition.

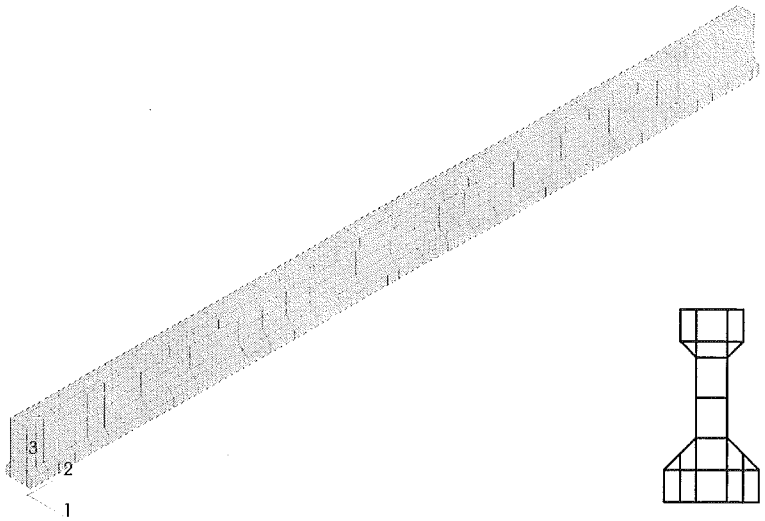

Figure 3-9. Finite element model of a single girder.

Longitudinally, the girders are divided into 37 elements, providing sufficient accuracy. As shown in Figure 3-9, the dimension of elements is not constant along the span. The elements are smaller when close to the support, to provide a more accurate model of the support conditions, and to account for the presence of the diaphragms (at the midspan and the beam ends).

Slab

The investigation of the slab behavior is the main purpose of this project. Therefore, the most accurate results should be obtained for this part of structure. This requirement implies the need for a fine element mesh in this part of the model. Four layers of elements represent the thickness of the slab; this allows for an accurate calculation of stress levels within the slab. Longitudinally, the element length is the same as that of the girders in order to ensure continuity. Transversally, the slab is divided into six elements between each girder.

Diaphragms

There are three diaphragms within the span; they are situated at the midspan and over the supports. Like the other parts of the bridge, they are modeled using three-dimensional elements (Figure 3-10).

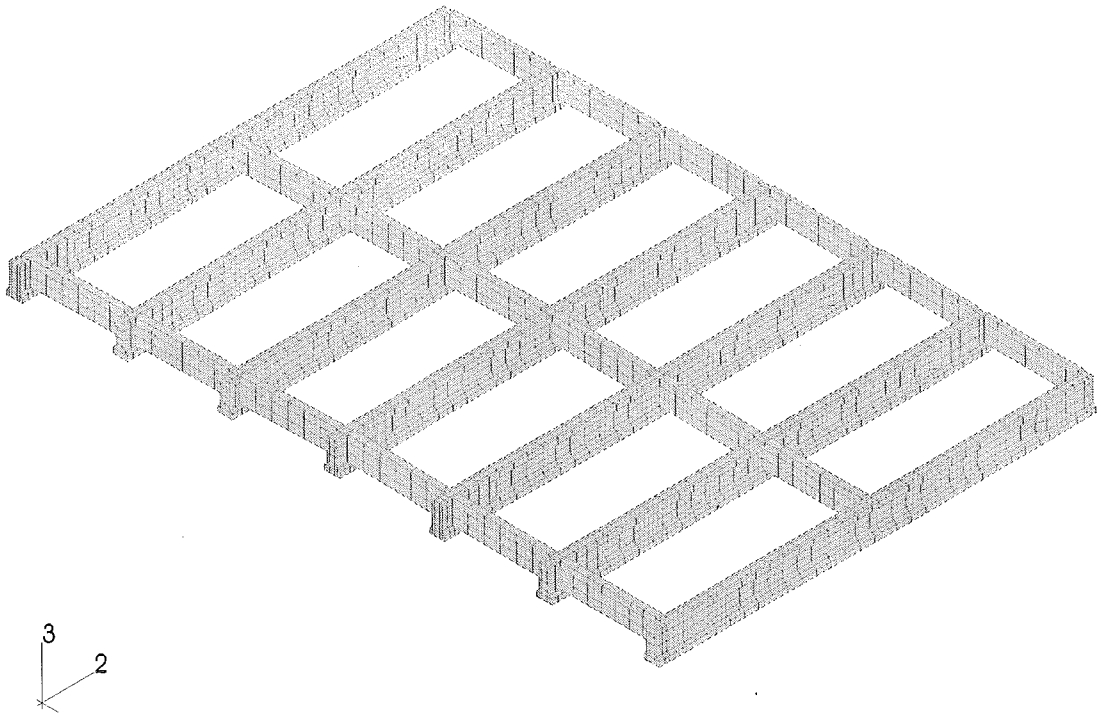

Figure 3-10. Diaphragms modeling.

Non-structural members

The bridge considered in this study includes a sidewalk and two Type 4 barriers that are connected with a concrete slab using reinforcement. Therefore, their contribution to the bridge stiffness cannot be neglected. The barriers increase the stiffness of the exterior girders. The sidewalk and barriers are modeled using solid elements (Figure 3-11).

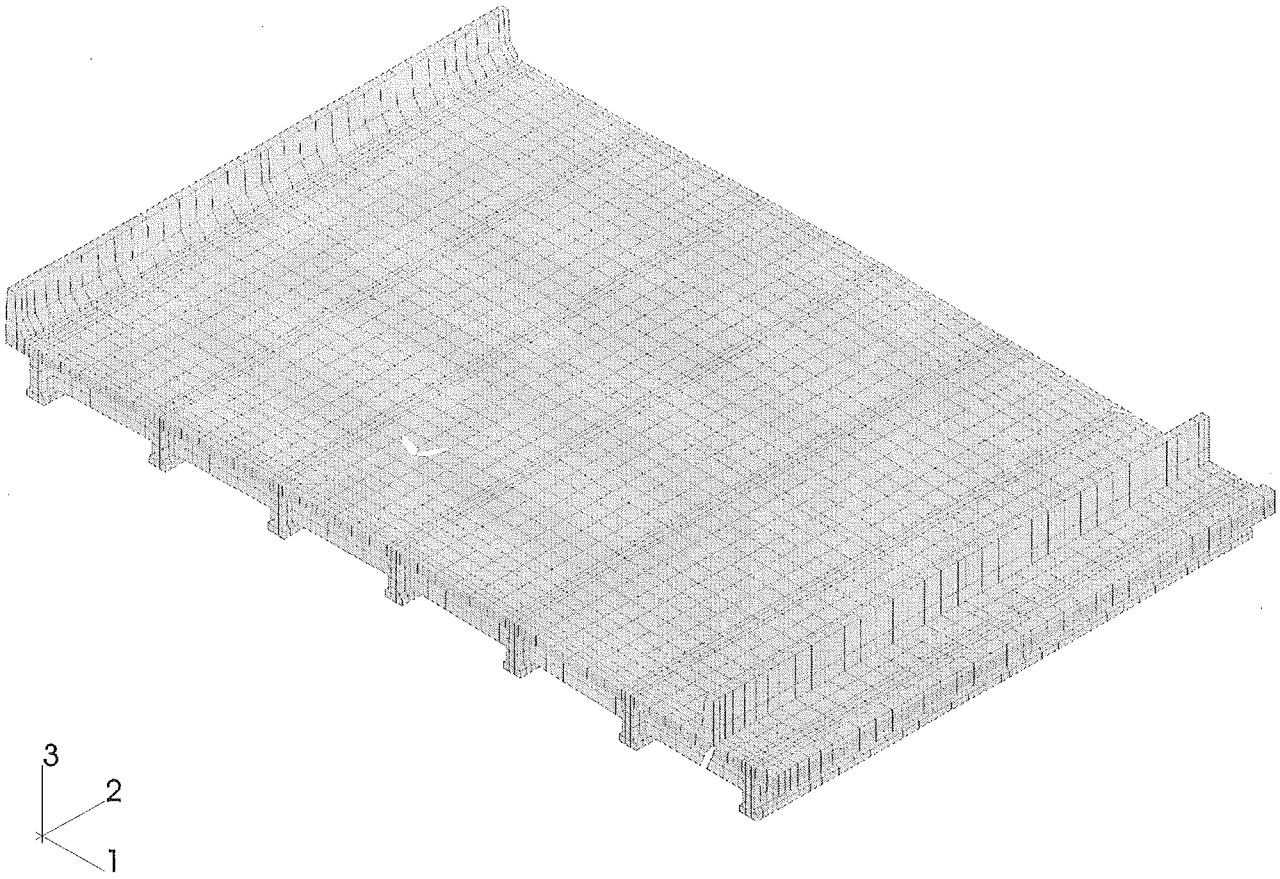

Figure 3-11. Model of bridge superstructure.

Finally, the whole bridge superstructure model is composed of 15,955 elements, which corresponds to 20,994 nodes and 62,982 variables (degrees of freedom and any Lagrange multiplier variables).

3.1.3. Prestressing and reinforcement modelling

Reinforcement

In ABAQUS, reinforcement in concrete structures is typically provided by means of rebars, which are one-dimensional elements (rods). Rebars are defined with the *REBAR option. They are superposed on the mesh of solid elements used to model the concrete but they do not contribute to the mass of the model. They can be defined as individual reinforcing bars, or layers of uniformly spaced reinforcing bars. Stresses, strains and other results are meaningful only in the rebar direction. The concrete behavior is considered independently of the rebar.

Reinforcement is modeled as layers of bars (Figure 3-12). Such layers are treated as a smeared layer with a constant thickness equal to the area of each reinforcing bar divided by the reinforcing bar spacing.

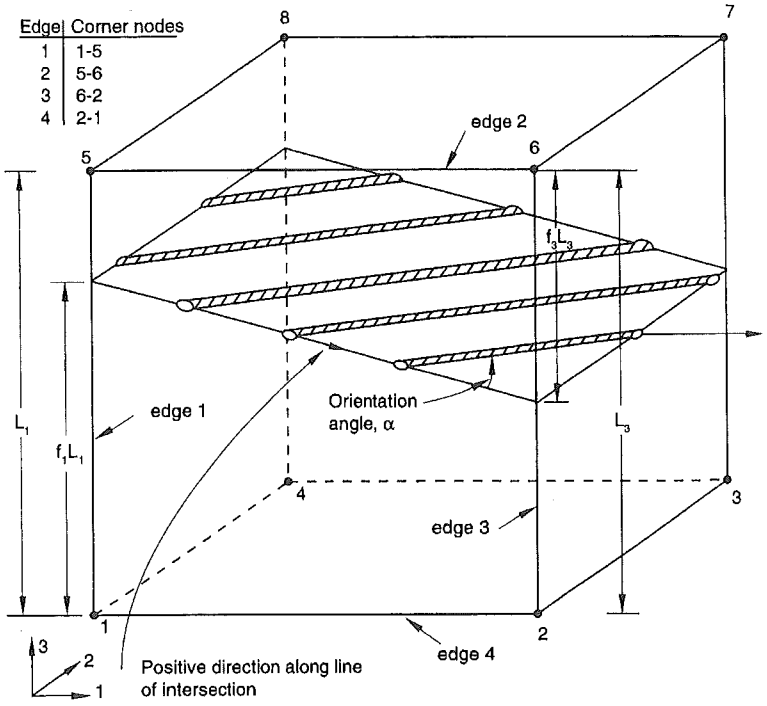

Figure 3-12. Rebar layer definition in a three-dimensional element.

The model includes rebars in the slab and in the concrete girders. The characteristics of this reinforcement are taken from the bridge drawings.

The slab has four main layers of reinforcement as shown in Figure 3-13. The girders include transverse stirrups, that make the connection between slab and beams, and longitudinal rebars. An elevation of a typical modeled beam is given in Figure 3-13.

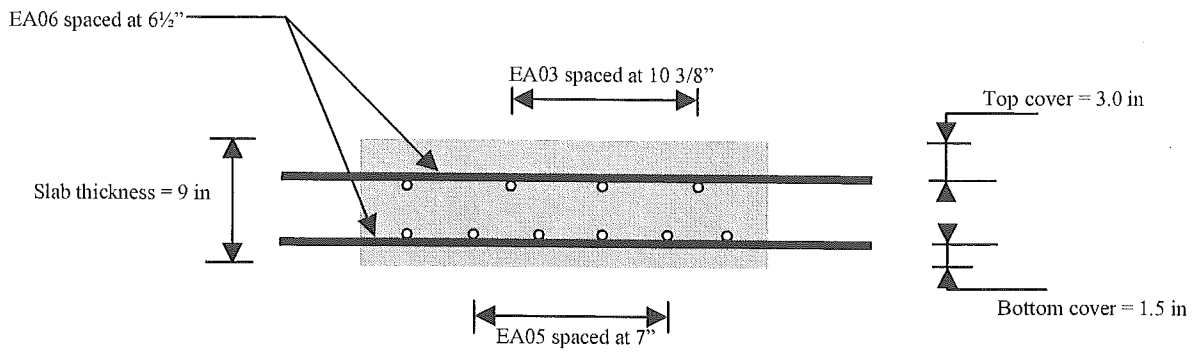

Figure 3-13. Slab reinforcement.

Prestressing

In ABAQUS, modeling of the prestressing tendons can be done using the same procedure as for modeling the reinforcement. Prestressing tendons are one-dimensional elements, with a prestress defined using the *INITIAL CONDITIONS option.

The bridge girders are composed of both straight and curved tendons, which are defined as four layers of rebars in each beam, as shown in Figure 3-14.

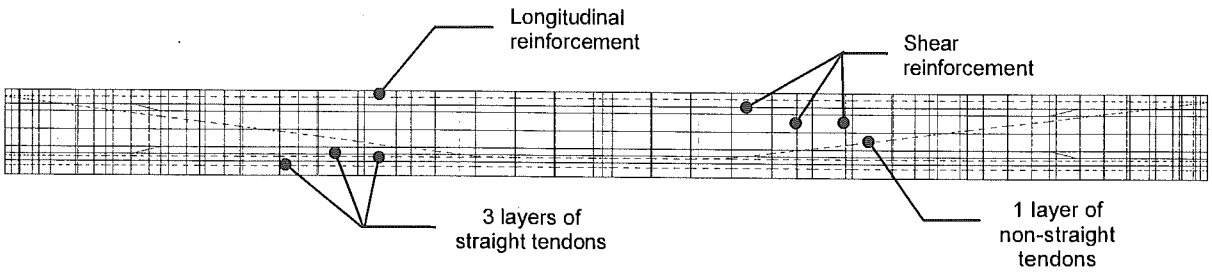

Figure 3-14. Rebar modeling in the girder.

- Determination of the input prestressing:

The original bridge plans provided by MDOT, give value of the prestressing force initially applied to the tendons: 31,000 lb each, that corresponds to a total initial force

$$F_i = 18 \times 31{,}000 = 558{,}000 \text{ lb.}$$

The modeled bridge is assumed to be in a service state. It means that prestress losses have already occurred in the tendons. So, the effective stress that is the input in the model must take into account the loss of the prestressing force. The total loss is obtained by

estimating the prestress losses that occur after the initial state, and subtracting them from the initial prestressing force. Prestress losses are divided into short-term and long-term, time dependent losses, as developed in the following calculations.

- Initial prestress losses (due to elastic shortening) :

$$\Delta f_{pES} = \frac{E_p}{E_{ci}} f_{cgp}$$

where E_p = 28 500 ksi

E_{ci} = 4 112 ksi

f_{cpg} = sum of concrete stresses at the center of gravity of prestressing tendons due to the prestressing force at transfer, F_i ,and the self-weight of the girder at the section of the maximum moment.

$$f_{cgp} = -\frac{F_i}{A_c} - \frac{F_i.e^2}{I_G} + \frac{M_{Gird}.e}{I_G}$$

$$f_{cgp} = -\frac{558}{369} - \frac{558 \times 10.27^2}{50980} + \frac{1074 \times 10.27}{50980} = -2.45 \text{ ksi}$$

Minus sign indicates the elastic shortening of concrete. This shortening results in a positive prestress loss.

$$\Delta f_{pES} = \frac{28500}{4112} \times 2.45 = 16.98 \text{ ksi}$$

- Time-dependent losses:

An approximate lump sum estimates losses resulting from creep and shrinkage of concrete and relaxation of steel in prestressed members and can be taken as specified in the AASHTO LRFD Bridge design specifications [A5.9.5.3]. For strands with f_{pu} = 270 ksi, the average time dependent losses are:

$$\text{average} = 33.0\left[1.0 - 0.15\frac{f_c' - 6.0}{6.0}\right] + 6.0PPR$$

where f_c' = 5.5 ksi and PPR = 1.0 (partial prestress ratio)

average = 39.41 ksi

For low-relaxation strands, this value may be reduced by 6.0 ksi for I-girders.

Total loss of prestress $\Delta f_{pT} = 39.41 - 6.0 + 16.98 = 50.39$ ksi

Therefore, the stress in tendons at service limit state is equal to:

$$f_{pf} = 0.74.f_{pu} - \Delta f_{pT} = 0.74 \times 270 - 50.39 = 149.41 \text{ ksi}$$

which corresponds to a final prestressing force:

$$F_f = f_{pf}.A_{ps} = 149.41 \times 18 \times 0.153 = 411.475 \text{ kips}$$

where f_{pf} is the value of the stress that will be used in the input file of the finite element model.

Materials

Two main materials that are used in the bridge deck model are concrete and steel. They are assumed to have an elastic linear behavior, which is the simplest form of elasticity available in ABAQUS. In this study, the linear elastic model defines an isotropic material behavior and is valid for small elastic strains.

The required parameters for the analysis include Young's modulus of elasticity, E, and the Poisson's ratio, ν. The density of materials is also defined in the input file. ABAQUS uses this value to calculate the gravity loading (i.e. self-weight) of elements. A summary of the input properties is provided in Table 3-1.

Table 3-1. Input properties of materials.

	Young's modulus E (ksi)	Poisson's ratio ν	Density γ (lb/in^3)
Concrete 1 (Girders)	4496	0.2	0.0868
Concrete 2 (Slab)	3395		
Steel 1 (Prestressing)	28500	0.3	0.2815
Steel 2 (reinforcement)	29000		

Boundary conditions

Boundary conditions can be applied to any of the displacements or rotation degrees of freedom. In the preliminary analysis, the span was assumed to be simply supported (Figure 3-15). Then, various support conditions were considered with the support constraints modeled using field test data.

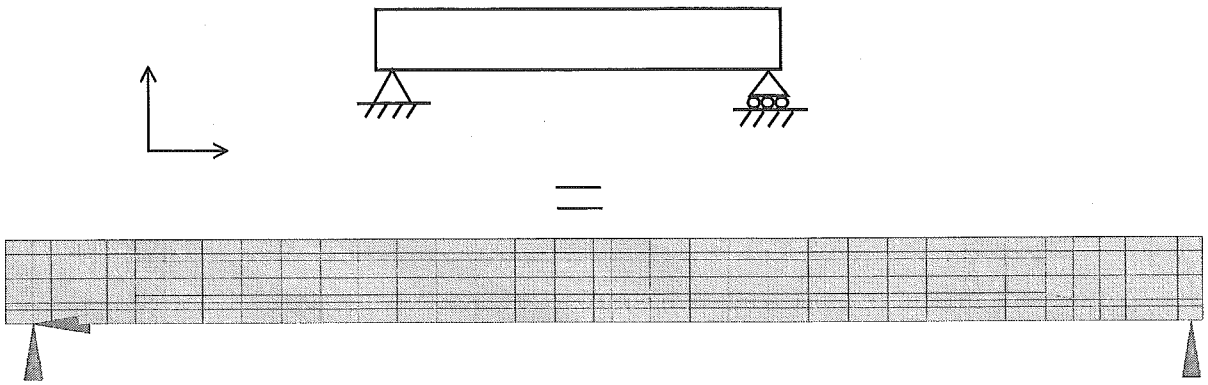

Figure 3-15. Support conditions.

3.1.4. Steps of construction in the finite element model

Stress distribution in slab-on-girder bridge decks is strongly influenced by the construction process. First, the loads are carried by the non-composite girders. Then, a composite section carries the deck slab and live load.

- **Step 1 : Erection of girders**

  After the precast girders are erected, there are two load components, including the self-weight of the girders, and the prestressing force. These loads are carried by the girder section only (non-composite). Due to the eccentricity of the prestressing force, there is tension at the top fibers of the girder, (Figure 3-16) and this results in an upward deflection (camber). In Figures 3.16 and 3.17, tension is defined as positive and stresses are shown in psi.

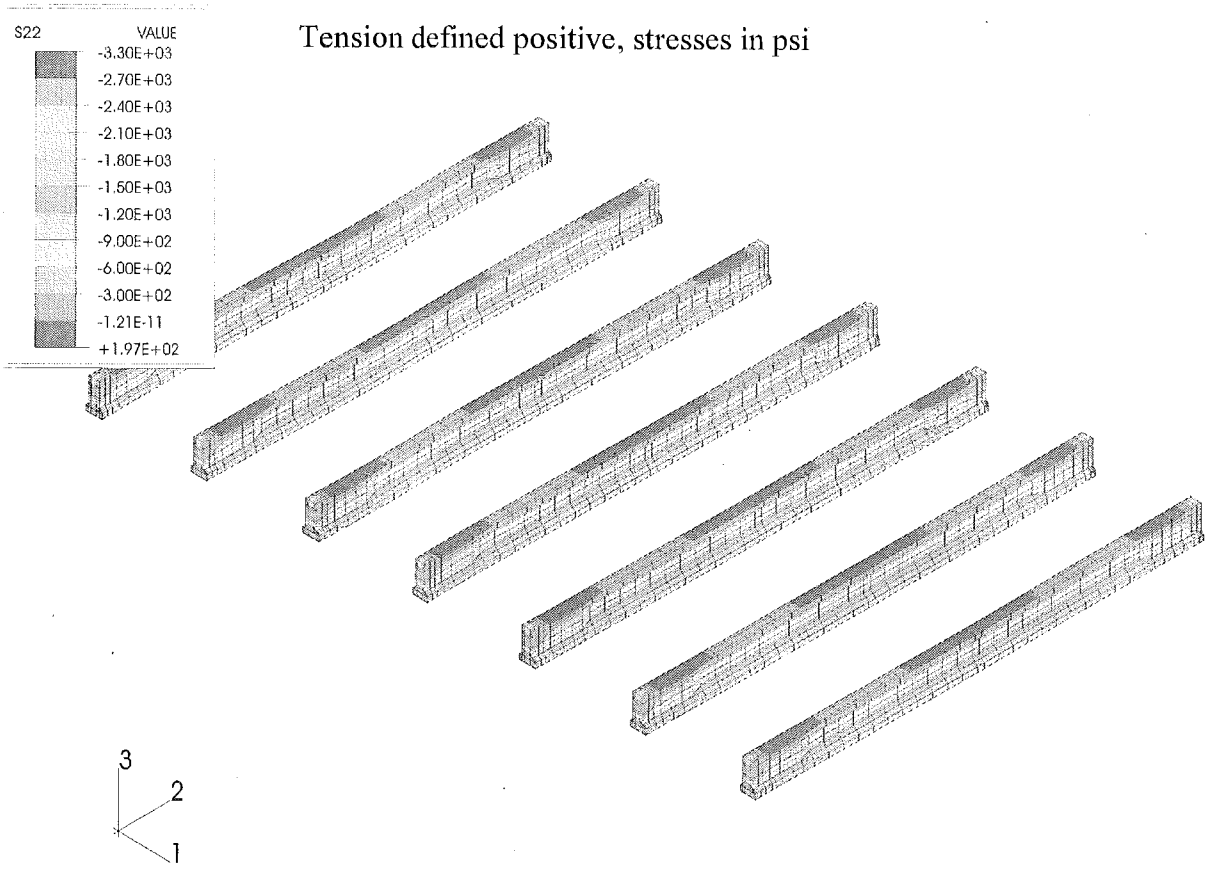

Figure 3-16. Stress distribution in girders at release.

- **<u>Step 2</u> : Casting of diaphragms and slab**

  In the next step, the diaphragms are cast and the deck slab is placed, but the concrete is not hardened yet. The self-weight is supported by the non-composite girders.

- **<u>Step 3</u> : Hardening of concrete slab and casting of superstructure components**

  The concrete in the slab hardens, and all superstructure elements (barriers) are added to the composite section (girders + slab). As it can be observed in Figure 3-17, there is almost no stress in the concrete slab in this stage.

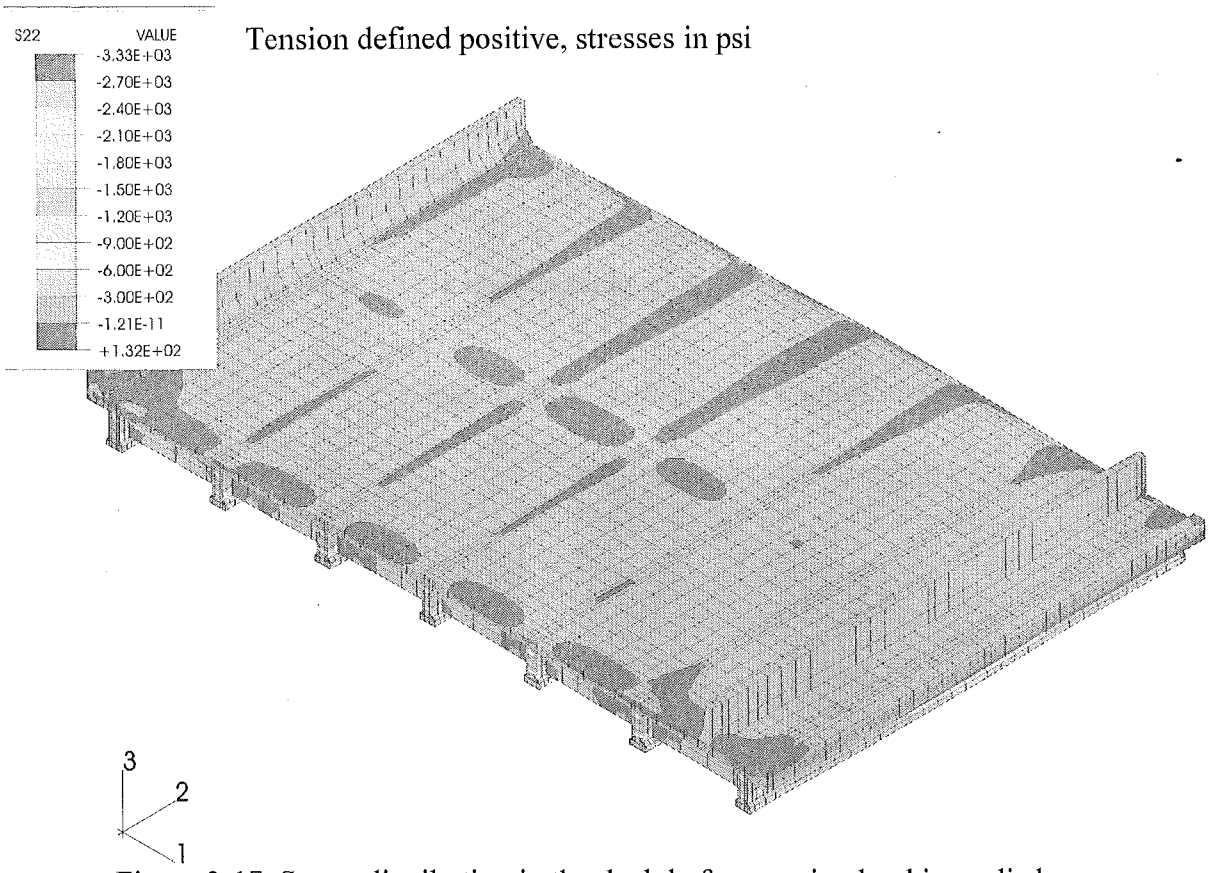

Figure 3-17. Stress distribution in the deck before service load is applied.

3.2. Description of the field test

The field load test was performed on the selected span and the behavior was modeled using finite element method. An 11-axle truck was used as the load acting on the bridge. The truck was moving at a crawling speed over the bridge in seven different transversal positions (three traffic lanes). The measurements were taken on all girders (seven), at the midspan, and close to the support, at the lower flange of the I-beams.

The test data was used to calibrate the supporting conditions for the girders in the FEM model of the bridge superstructure.

3.2.1. Scope of testing

The following tests were performed on the bridge:

- Visual inspection of the bridge.
- Strain measurements on the East span

Instrumentation and Data Acquisition

The strain transducers were attached to the following parts of the bridge:

- lower flanges of the girders, close to support (1 ft from the support) (Figure 3-18).
- and lower flanges of the girders at the midspan.

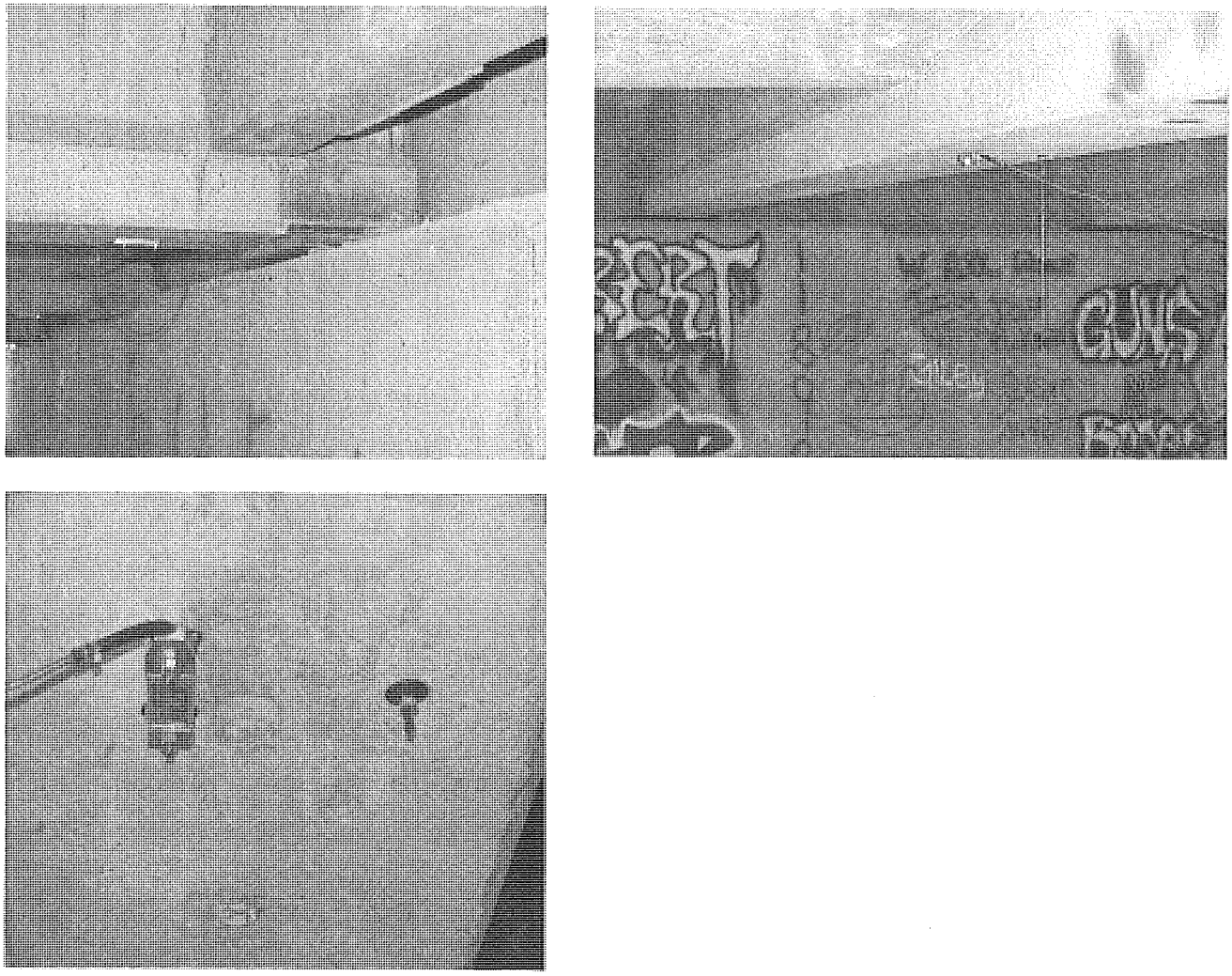

Figure 3-18. Locations of the removable strain transducers.

Strain transducers were connected to the BDI data acquisition system through the intermediate connection boxes. The data acquisition mode is controlled from the external PC notebook computer, and acquired data is processed and directly saved in the PC's hard drive.

Test Load

The load was applied in form of an 11-axle truck with axle loads and spacing shown in Figure 3-19. The measurements were taken under each passage of the test truck. When the truck was passing on the bridge, the maximum values were recorded, first at the support and then at the midspan. The actual axle weights of the truck were measured prior to the test using the State Truck Weigh Station scale. The truck was driven over the bridge at a crawling speed.

The truck has a gross vehicle weight of 142.9 kips, with a wheelbase of 58'-7". The truck configuration is shown in Figure 3-19.

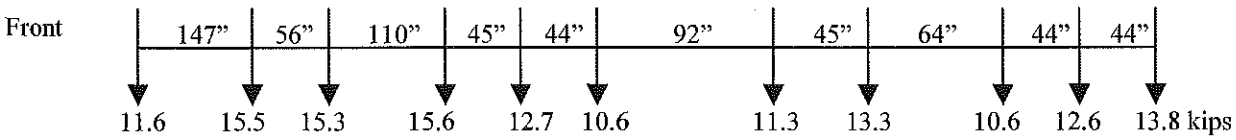

Figure 3-19. Truck configuration.

Location of Strain Transducers

Strain transducers were installed on the bottom flanges of the girders, close to the support, and at the midspan in the East span of the bridge. Figure 3-20 shows the cross-section of the tested span. Overall, 14 locations in the tested span were selected for the strain measurement. Gages No.1 to 7 were installed close to the support (S1 to S7 in Figure 3-21). Gages No.8 to 14 were installed at the midspan.

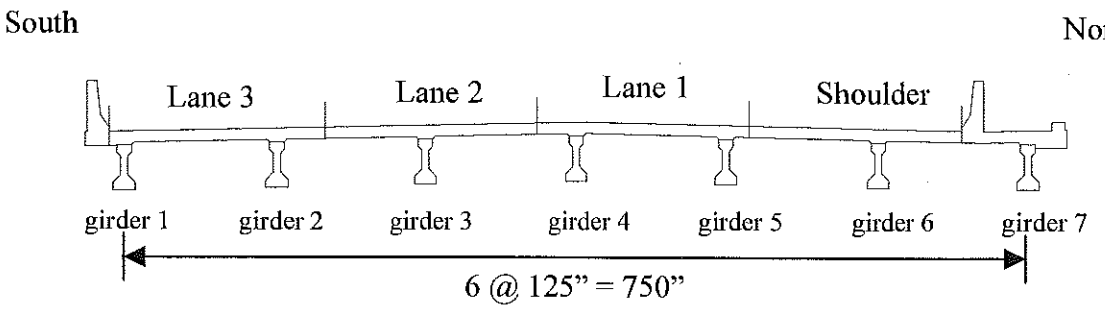

Figure 3-20. Cross section of the bridge superstructure.

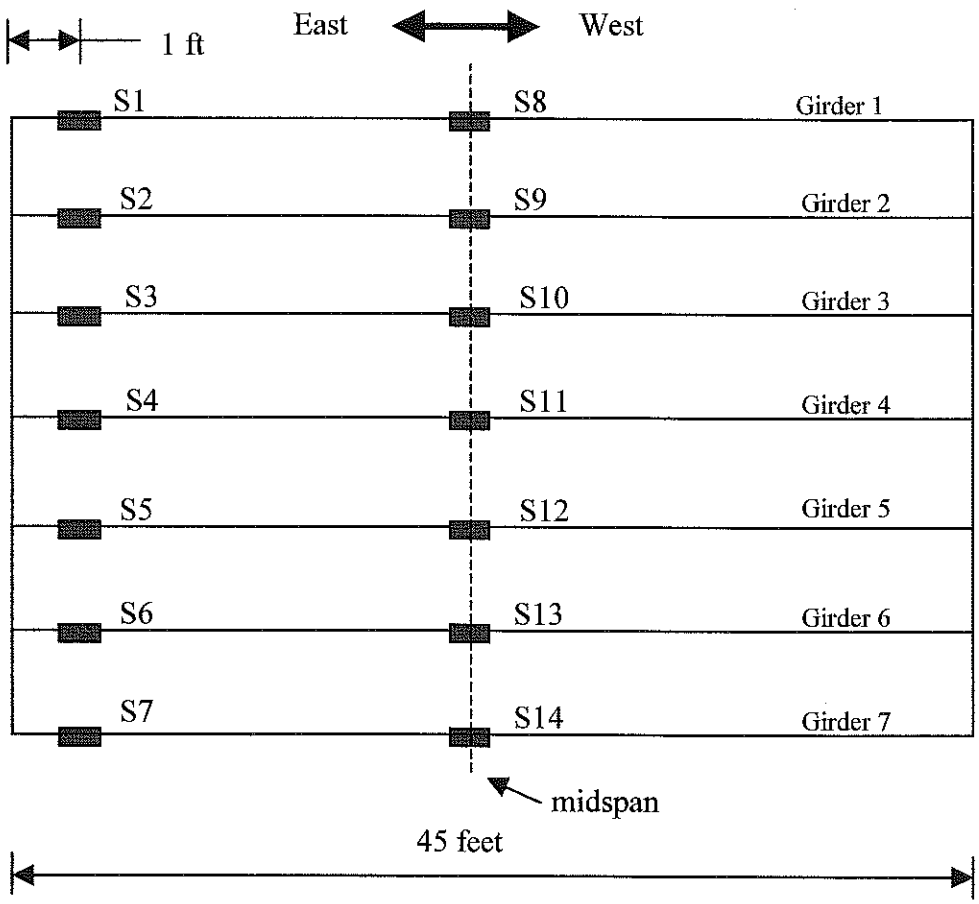

Figure 3-21. Location of strain transducers.

Loading Cases

A total of 10 loading cases were considered, as shown in Table 3-2. For all the runs, the truck was driven at a crawling speed over the bridge (from East to West) in different transversal positions. Runs 9 and 10 were a repetition of runs 6 and 7.

Table 3-2. Test Load Runs.

Run #	Lane	Position	Truck Speed
1	Shoulder	Center	Crawling
2	Lane 1	Center	Crawling
3	Lane 2	Center	Crawling
4	Lane 3	Center	Crawling
5	Shoulder-Lane 1	Center	Crawling
6	Lane 1-Lane2	Center	Crawling
7	Lane 2-Lane 3	Center	Crawling
8	Lane 3	Close to curb	Crawling
9	Lane1-Lane 2	Center	Crawling
10	Lane 2-Lane 3	Center	Crawling

3.3. Test results

The measurements at the midspan for runs 1, 2, 3 and 4 are presented in Figure 3-22, and in Figure 3-24 for runs 5, 6, 7 and 8. The measurements close to support are presented in Figure 3-23 for runs 1, 2, 3 and 4, and in Figure 3-25 for runs 5, 6, 7 and 8.

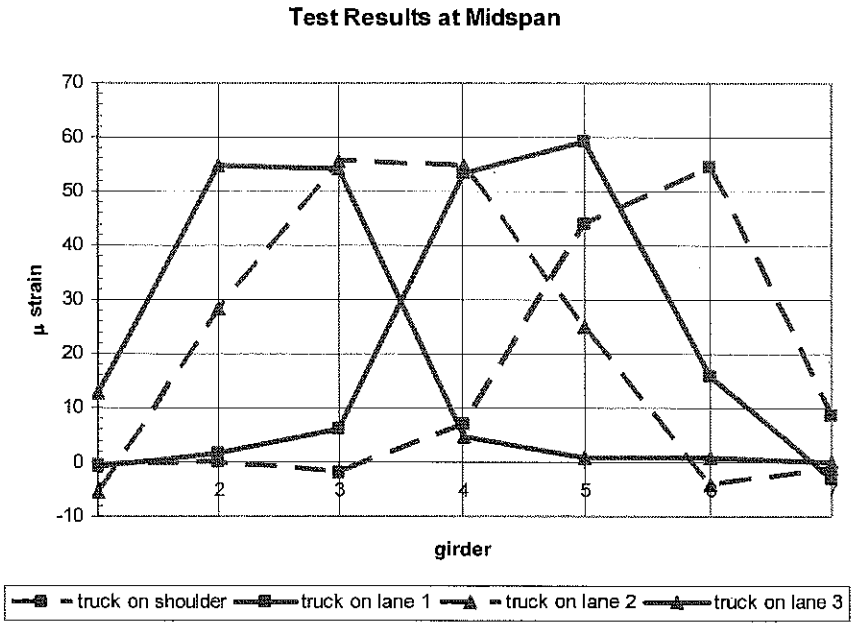

Figure 3-22. Results at the midspan for runs 1, 2, 3, and 4.

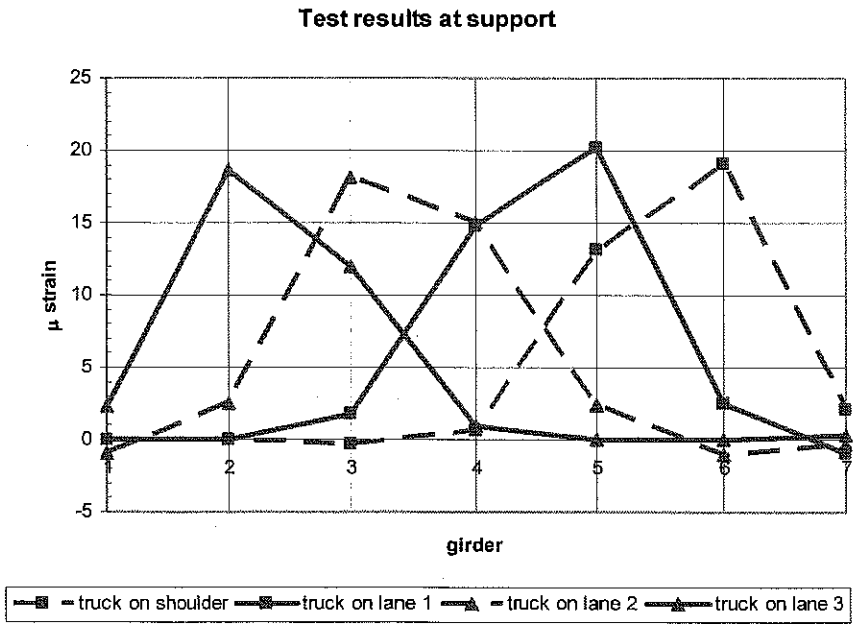

Figure 3-23. Results at the support for runs 1, 2, 3 and 4.

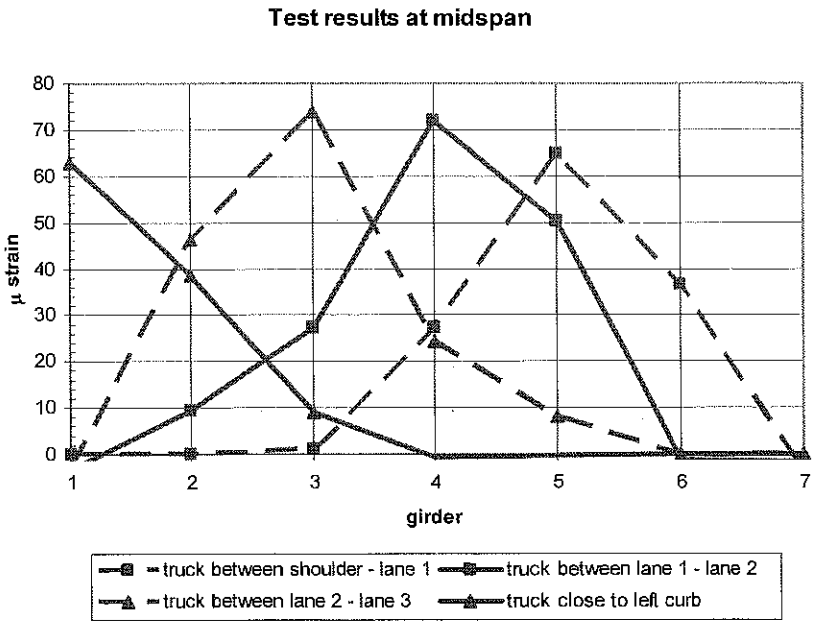

Figure 3-24. Results at the midspan for runs 5, 6, 7, and 8.

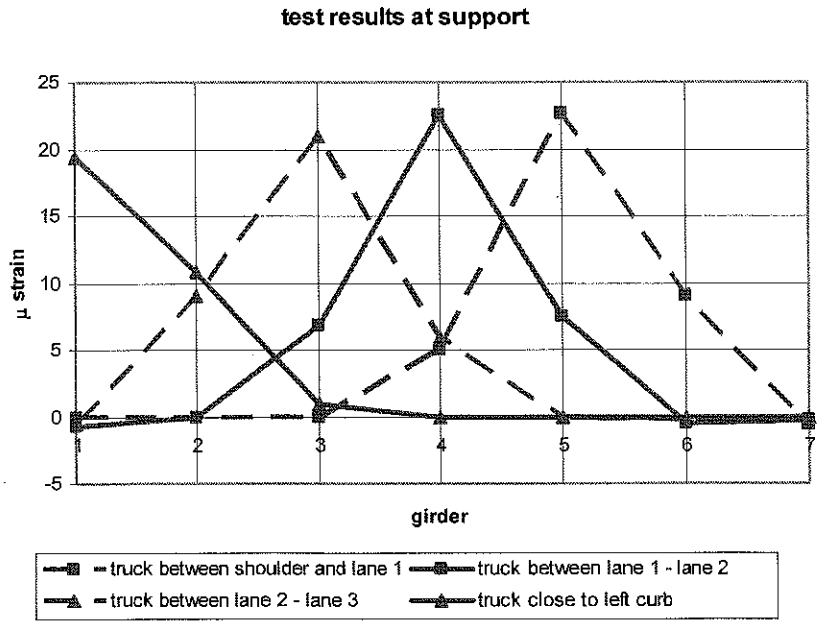

Figure 3-25. Results at the support for runs 5, 6, 7, and 8.

For all runs, the maximum strain reading at the midspan was around 60-70 με. The distribution of strain was strongly non-uniform, with only two or three girders resisting most of the load. This can be explained by a larger spacing between the girders (10"-5"), and a considerable stiffness of the beams. This observation also applies to runs 5, 6, 7 and

8 with the truck positioned directly over one of the seven girders. The strain differences between two adjacent girders were up to 40 με.

The same observation applies to the strains measured close to the support. These strain values were positive. This indicates that the girders behave as simply supported with no partial fixity at supports.

3.4. Calibration procedure

The calibration procedure for the finite element model of the deck supported on prestressed concrete girders is based similarly to the model of the deck supported on steel girders, on the data recorded during the field test. Two supporting conditions for girders were assumed in the finite element model: hinge – roller, and hinge – hinge. Strains at the bottom flanges of the girders were calculated using the finite element model for these two support options, and compared with the measured test results. The comparisons for all loading positions (test runs) are presented in Figures 3-26 to 3-41.

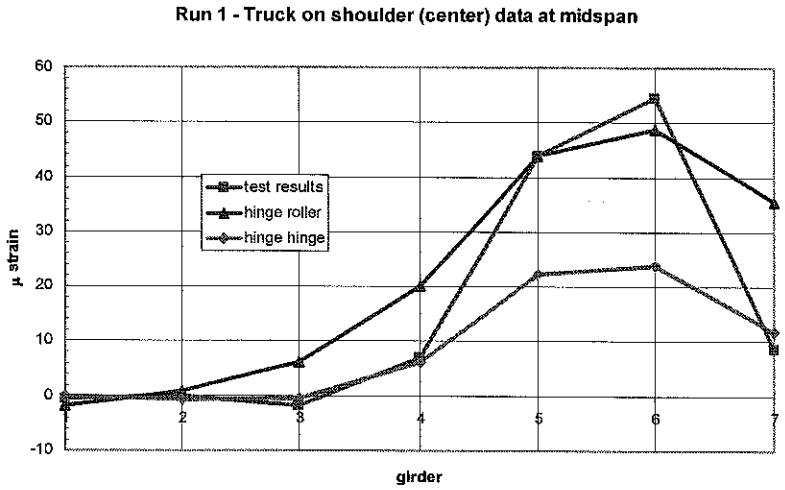

Figure 3-26. Comparison of strains calculated for two supporting options in FE model and strains measured during the test (truck located at the center of the shoulder, at the midspan).

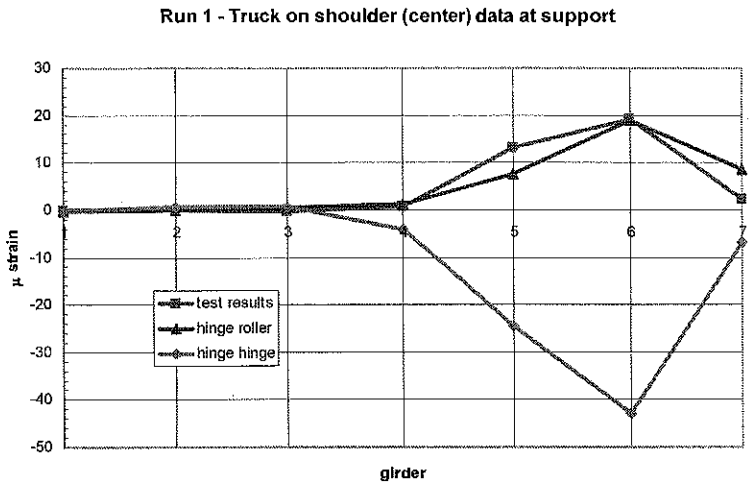

Figure 3-27. Comparison of strains calculated for two supporting options in FE model and strains measured during the test (truck located at the center of the shoulder, close to support).

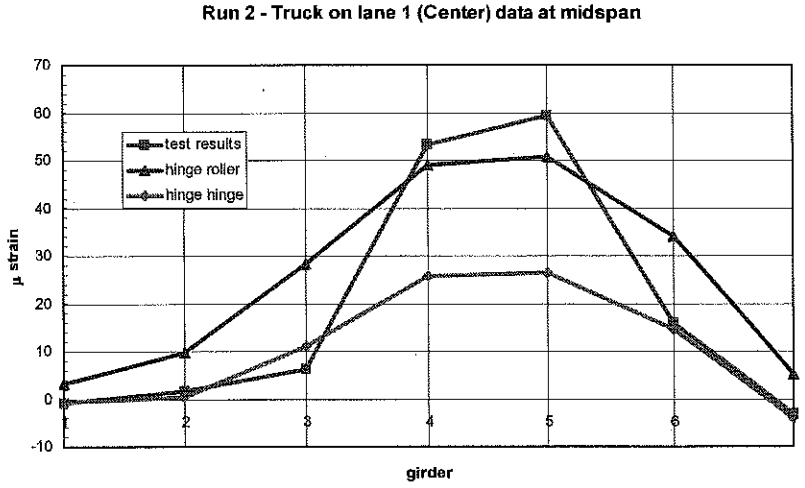

Figure 3-28. Comparison of strains calculated for two supporting options in FE model and strains measured during the test (truck located at the center of the 1st lane, at the midspan).

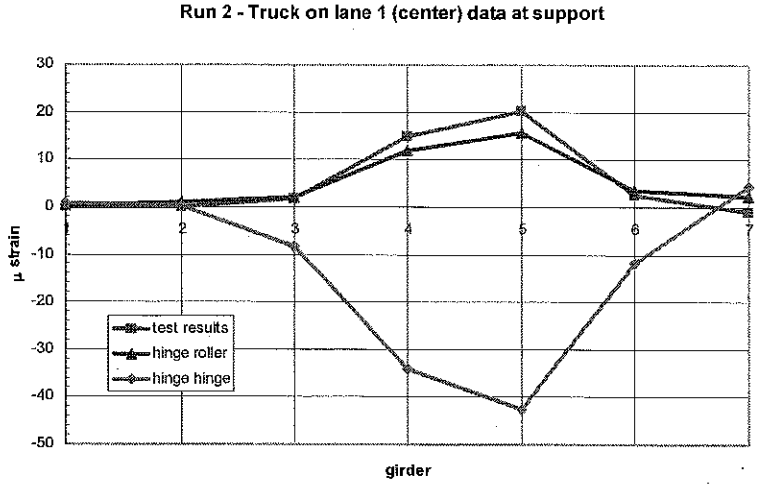

Figure 3-29. Comparison of strains calculated for two supporting options in FE model and strains measured during the test (truck located at the center of the 1st lane, close to support).

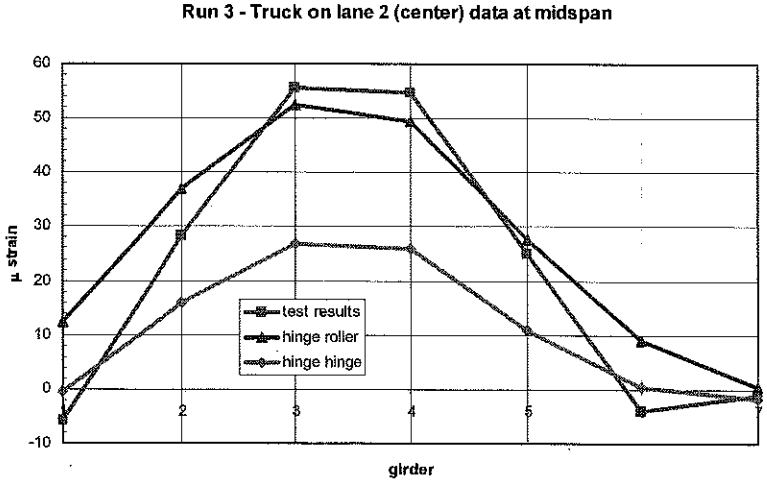

Figure 3-30. Comparison of strains calculated for two supporting options in FE model and strains measured during the test (truck located at the center of the 2nd lane, at the midspan).

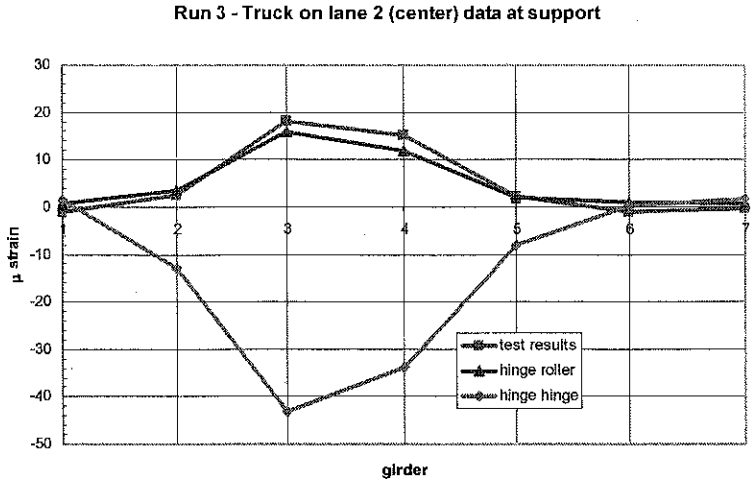

Figure 3-31. Comparison of strains calculated for two supporting options in FE model and strains measured during the test (truck located at the center of the 2nd lane, close to support).

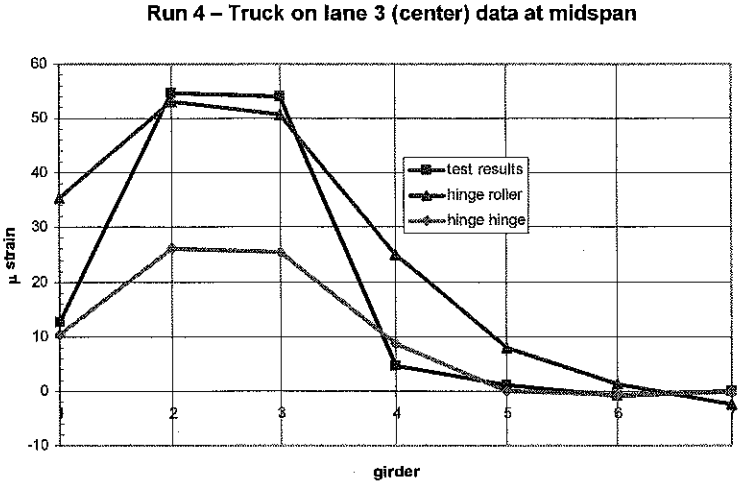

Figure 3-32. Comparison of strains calculated for two supporting options in FE model and strains measured during the test (truck located at the center of the 3rd lane, at the midspan).

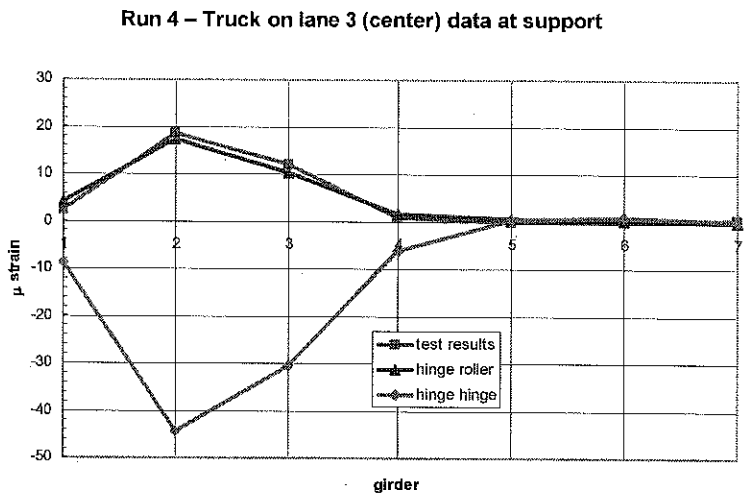

Figure 3-33. Comparison of strains calculated for two supporting options in FE model and strains measured during the test (truck located at the center of the 3rd lane, close to support).

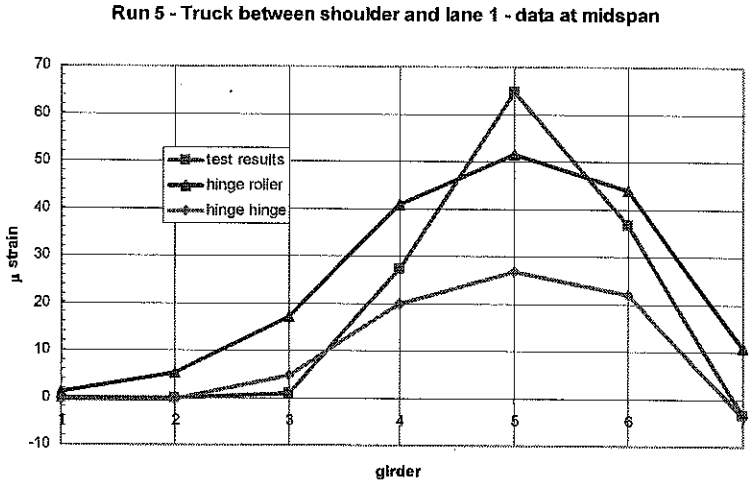

Figure 3-34. Comparison of strains calculated for two supporting options in FE model and strains measured during the test (truck located between shoulder and the 1st lane, at the midspan).

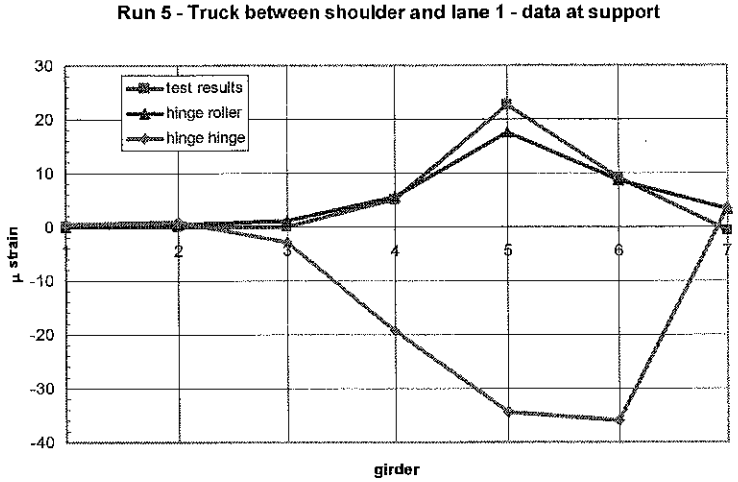

Figure 3-35. Comparison of strains calculated for two supporting options in FE model and strains measured during the test (truck located between shoulder and the 1st lane, close to support).

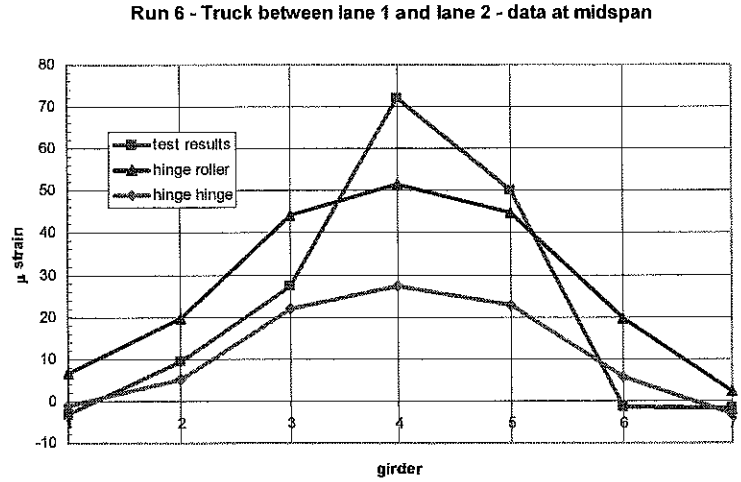

Figure 3-36. Comparison of strains calculated for two supporting options in FE model and strains measured during the test (truck located between the 1st and the 2nd lane, at the midspan).

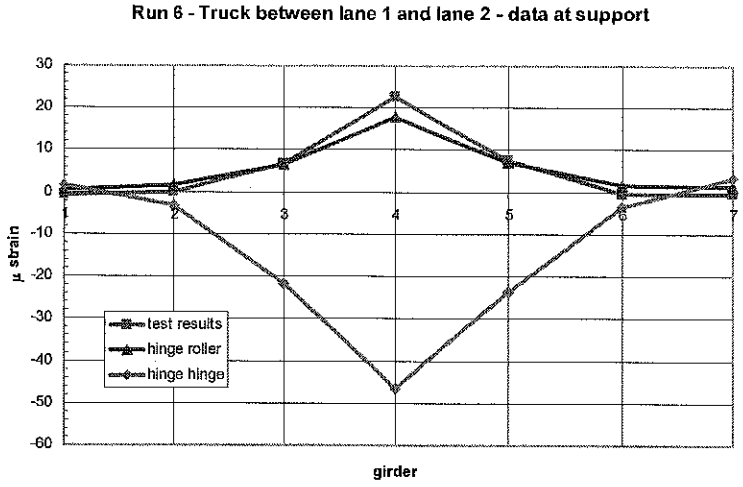

Figure 3-37. Comparison of strains calculated for two supporting options in FE model and strains measured during the test (truck located between the 1st and the 2nd lane, close to support).

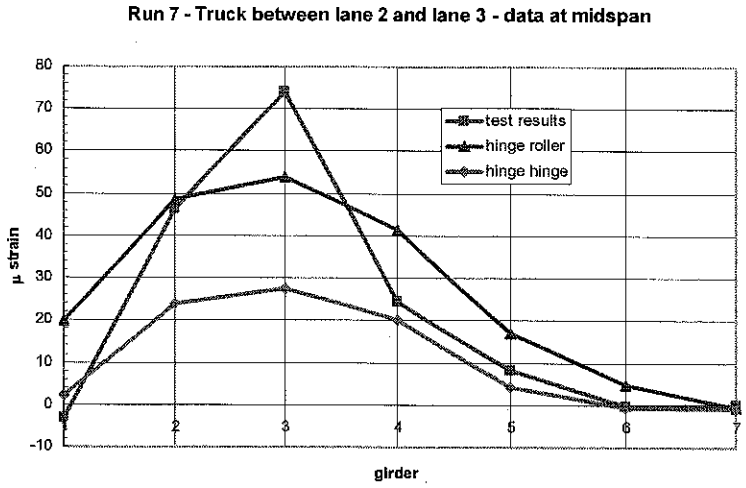

Figure 3-38. Comparison of strains calculated for two supporting options in FE model and strains measured during the test (truck located between the 2nd and the 3rd lane, at the midspan).

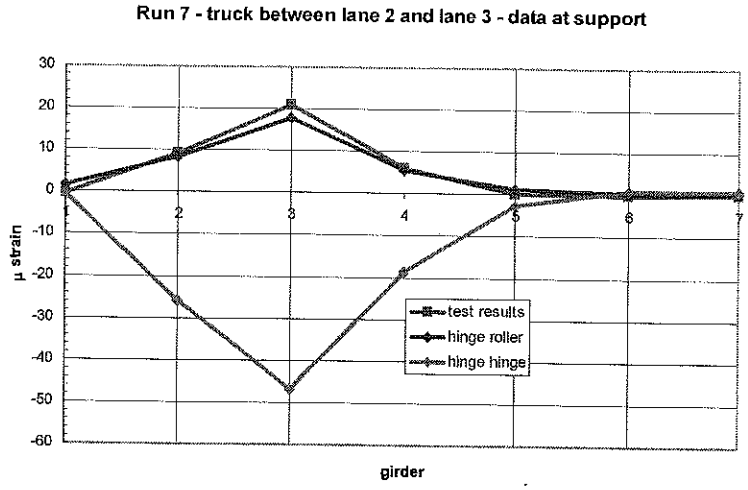

Figure 3-39. Comparison of strains calculated for two supporting options in FE model and strains measured during the test (truck located between the 2nd and the 3rd lane, close to support).

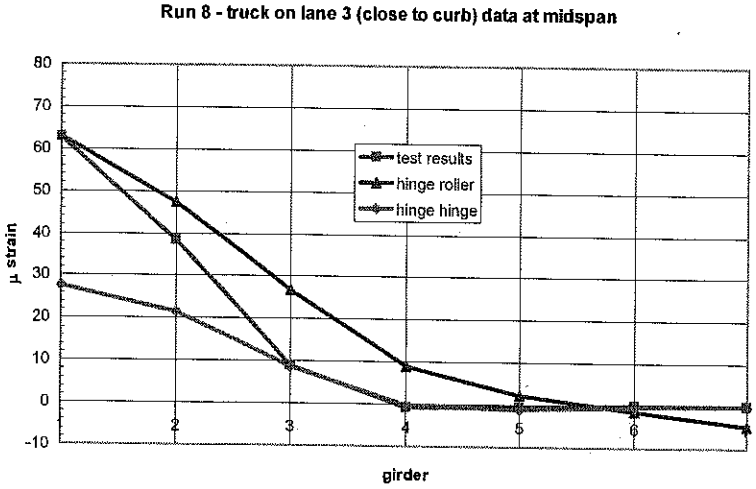

Figure 3-40. Comparison of strains calculated for two supporting options in FE model and strains measured during the test (truck located close to curb in the 3rd lane, at the midspan).

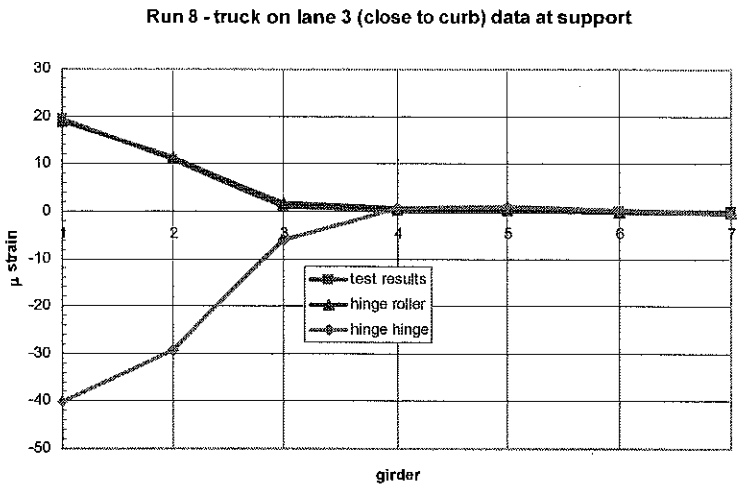

Figure 3-41. Comparison of strains calculated for two supporting options in FE model and strains measured during the test (truck located close to curb in the 3rd lane, close to support).

The comparison of strains, calculated using two options of supporting conditions in the finite element model and measured values, clearly shows that all measured values are closer to the hinge – roller option. This trend is especially visible for girders that are directly under the load. Such a behavior indicates that there is no need for support constraints in the finite element model. In conclusion, the support condition analysis shows that there are no springs added at the end of the prestressed concrete girders in the finite element model.

4. STRESS ANALYSIS OF THE DECK BASED ON THE FINITE ELEMENT MODELS

A numerical analysis of the selected bridges using the FEM models was performed for concrete decks supported on steel and prestressed concrete girders. A calibration of the developed finite element models was presented in the previous chapters. The first analyzed bridge is a composite structure with a concrete deck supported on steel girders. The second bridge is also a composite structure with a concrete deck supported on prestressed concrete girders. Several construction stages (prestressed girders) and loading cases were considered using finite element models to evaluate the extreme stresses in the deck.

4.1. Stress values in the deck supported on steel girders

A numerical analysis is performed based on the calibrated finite element model prepared for the concrete deck supported on steel girders with spans of 10 ft 3in. Empirical reinforcement is assumed in the deck. Various truck positions were considered. For a single truck, the same positions as those in the field tests discussed in Chapter 2 were used. On the other hand, two trucks were used as a live load in the numerical models in order to obtain the extreme, possible values for stress in the deck. All results from the finite element method analysis for the deck supported on steel girders are presented in Appendix A.

Representative results are presented below. They include the maximum values, obtained from the extreme cases of live load (for transverse and longitudinal positions of the 11-axle truck used during the test; see Figure 2-6), dead load, and restrained shrinkage. To calculate the restrained shrinkage, the slab was subjected to contraction strain of 2.1×10^{-4} that represents free shrinkage after 3 months (see Figure 6-2). The results are presented in Figures 4-1 to 4-24. The numerical shrinkage analysis was performed to determine the distribution of the restrained shrinkage stress in the deck. Tension stress is defined as positive, and the stresses are given in ksi.

Dead load

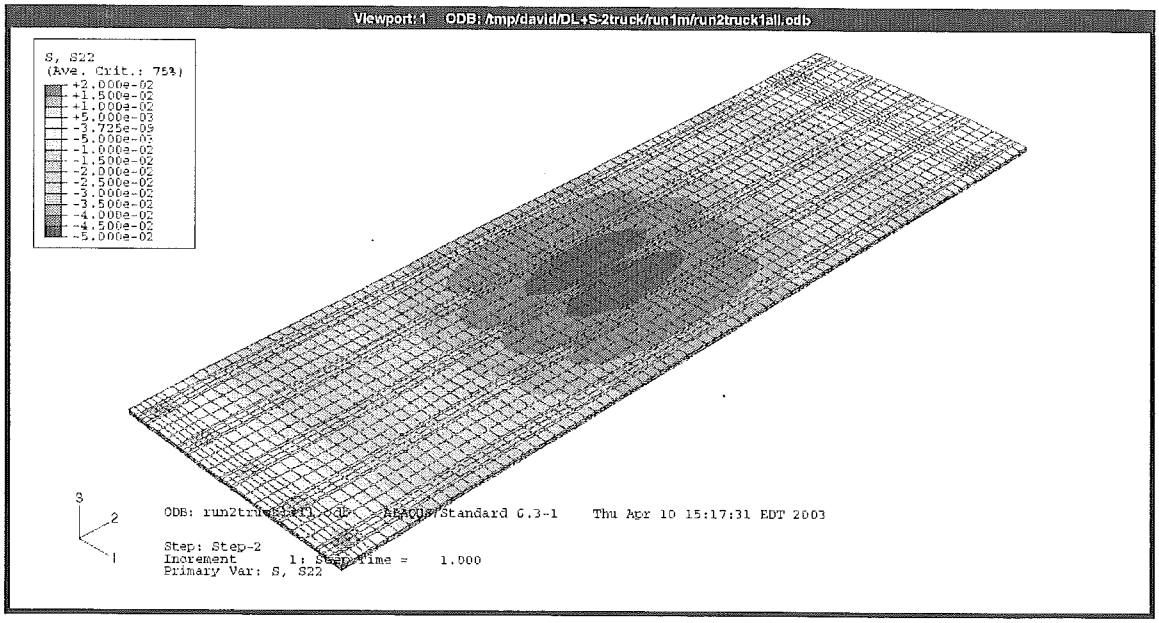

Figure 4-1. Longitudinal stress due to dead load – top surface of the deck

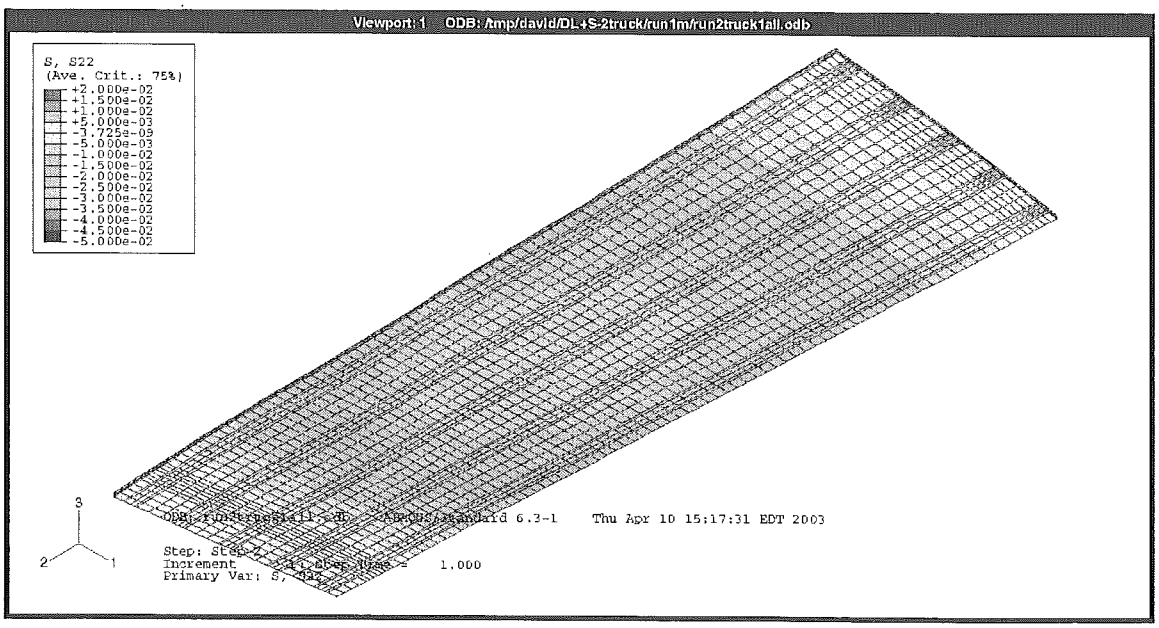

Figure 4-2. Longitudinal stress due to dead load – bottom surface of the deck

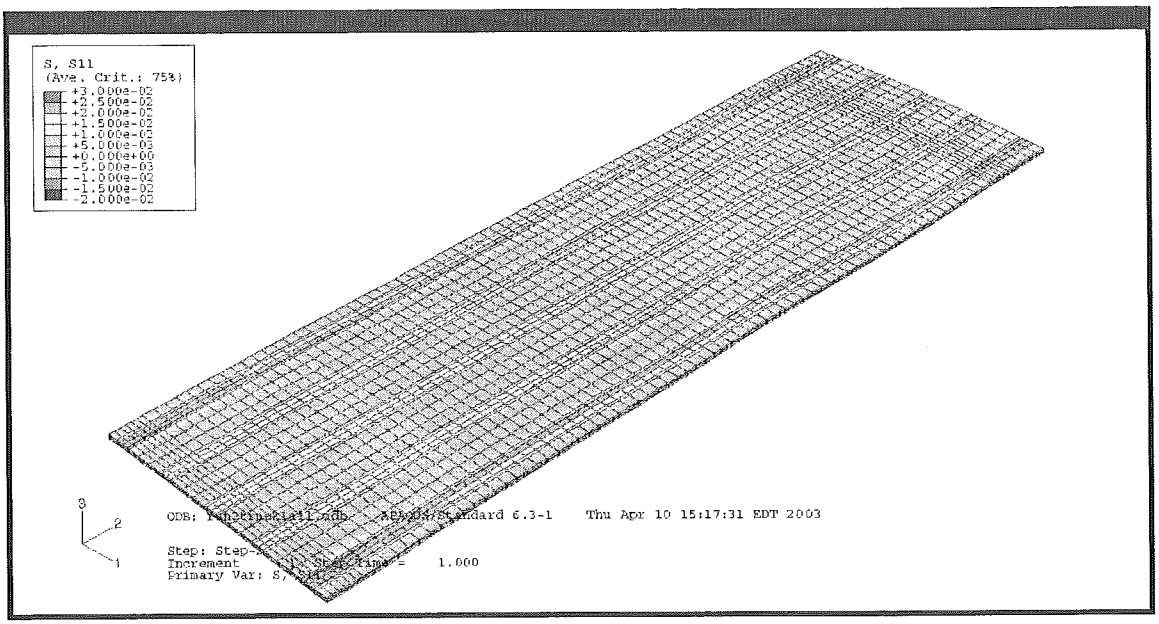

Figure 4-3. Transversal stress due to dead load – top surface of the deck

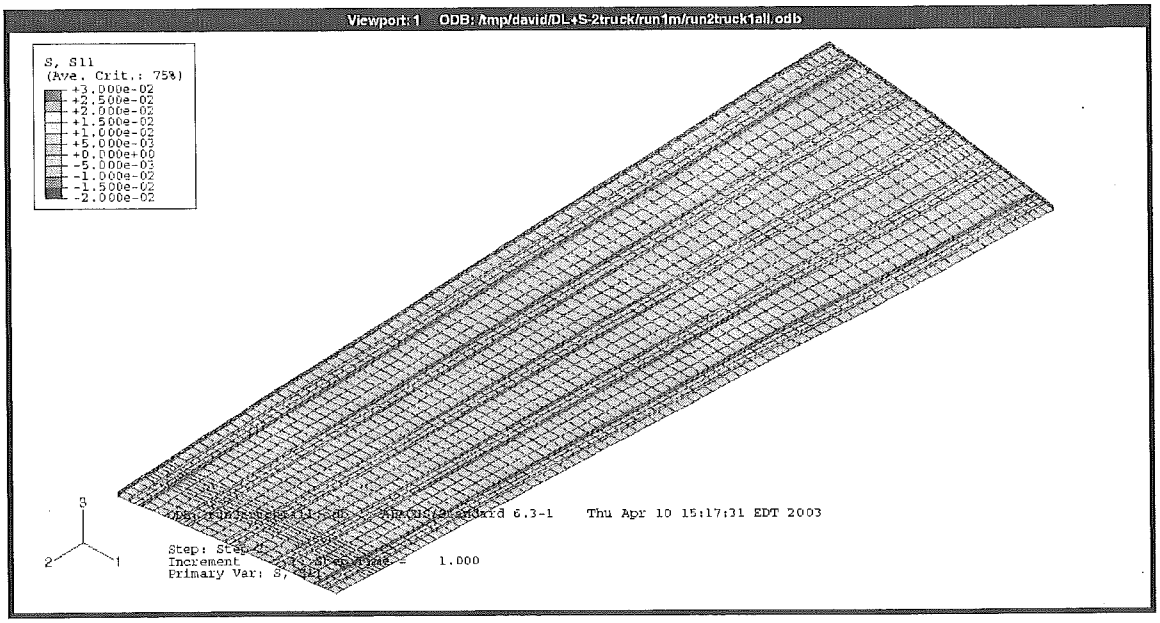

Figure 4-4. Transversal stress due to dead load – bottom surface of the deck

Dead load + Shrinkage

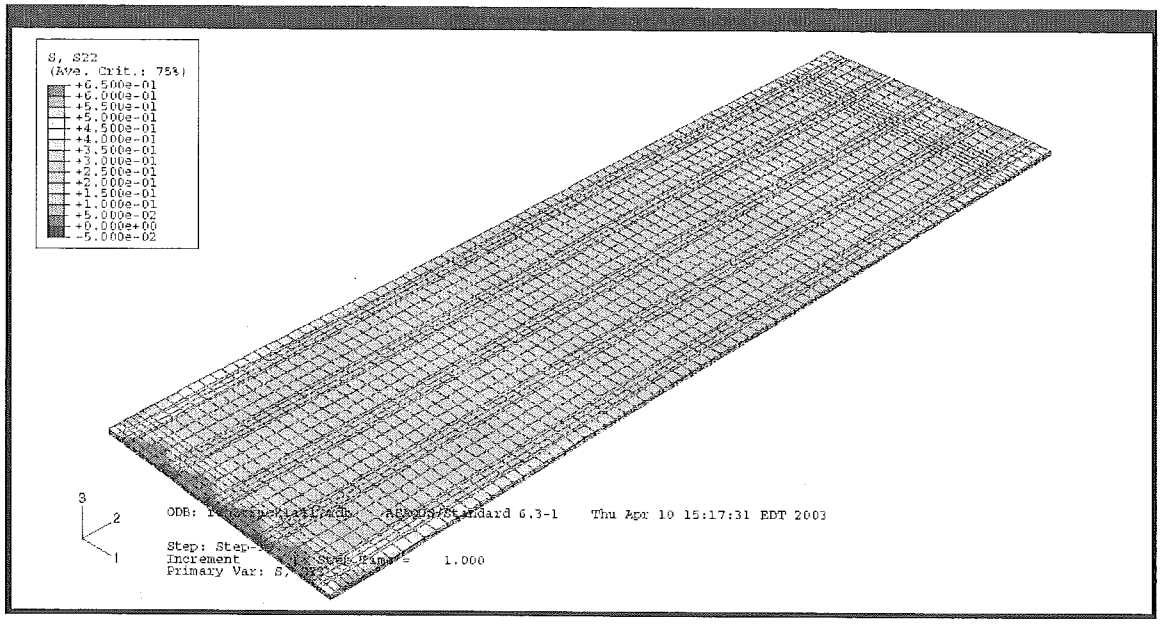

Figure 4-5. Longitudinal stress due to dead load and shrinkage – top surface of the deck

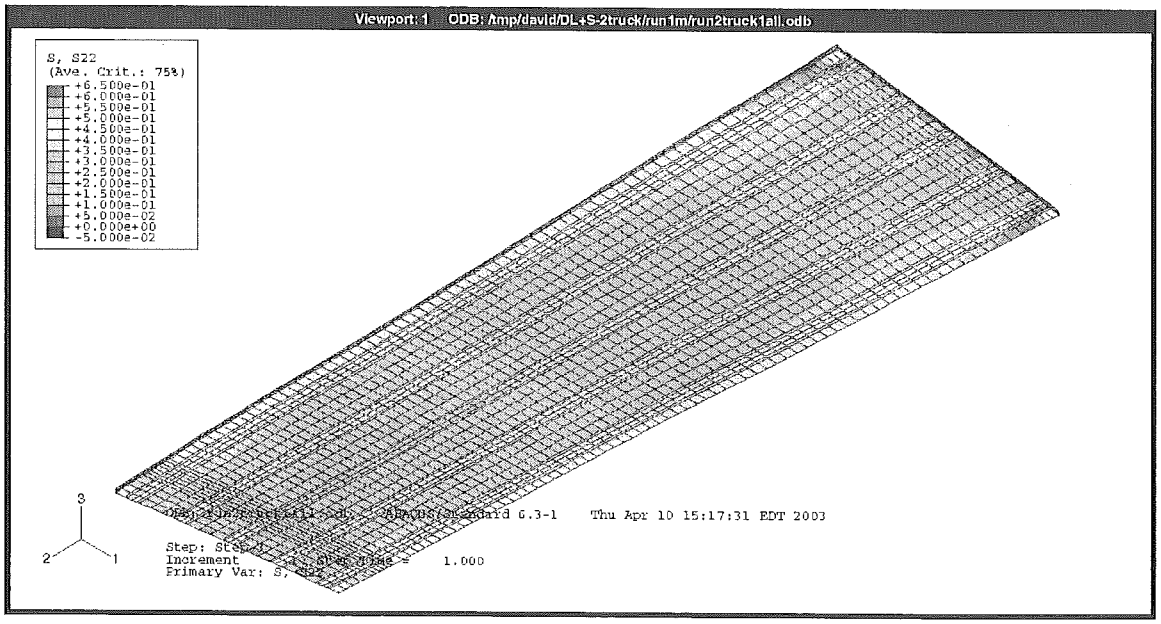

Figure 4-6. Longitudinal stress due to dead load and shrinkage – bottom surface of the deck

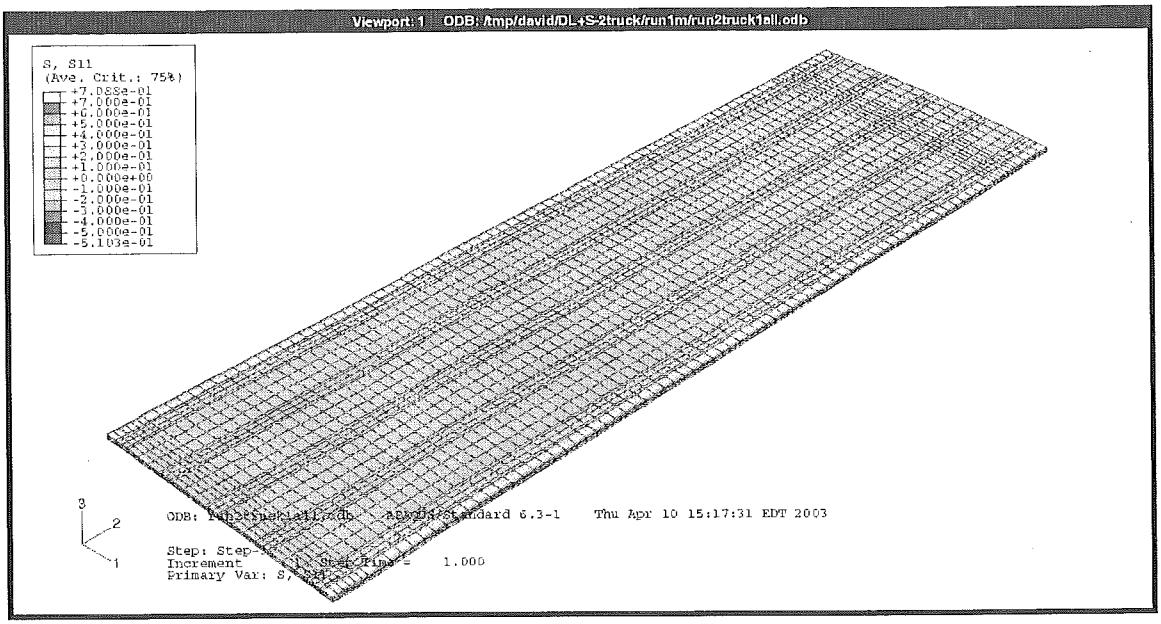

Figure 4-7. Transversal stress due to dead load and shrinkage – top surface of the deck

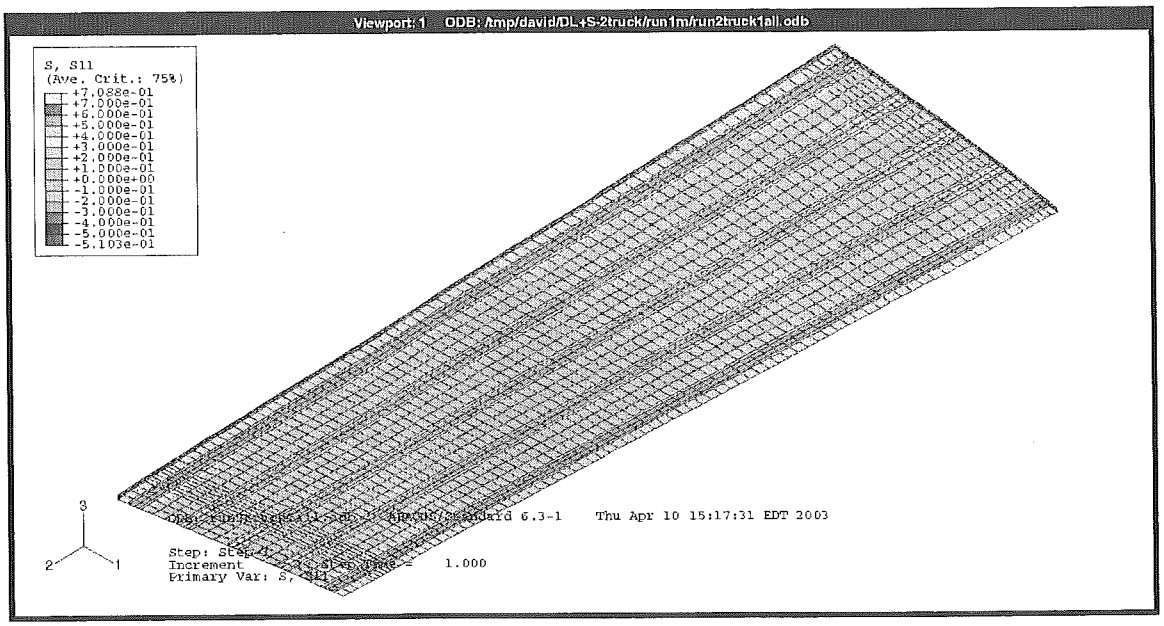

Figure 4-8. Transversal stress due to dead load and shrinkage – bottom surface of the deck

Dead load + shrinkage + 2 trucks (maximum at midspan), load option 1

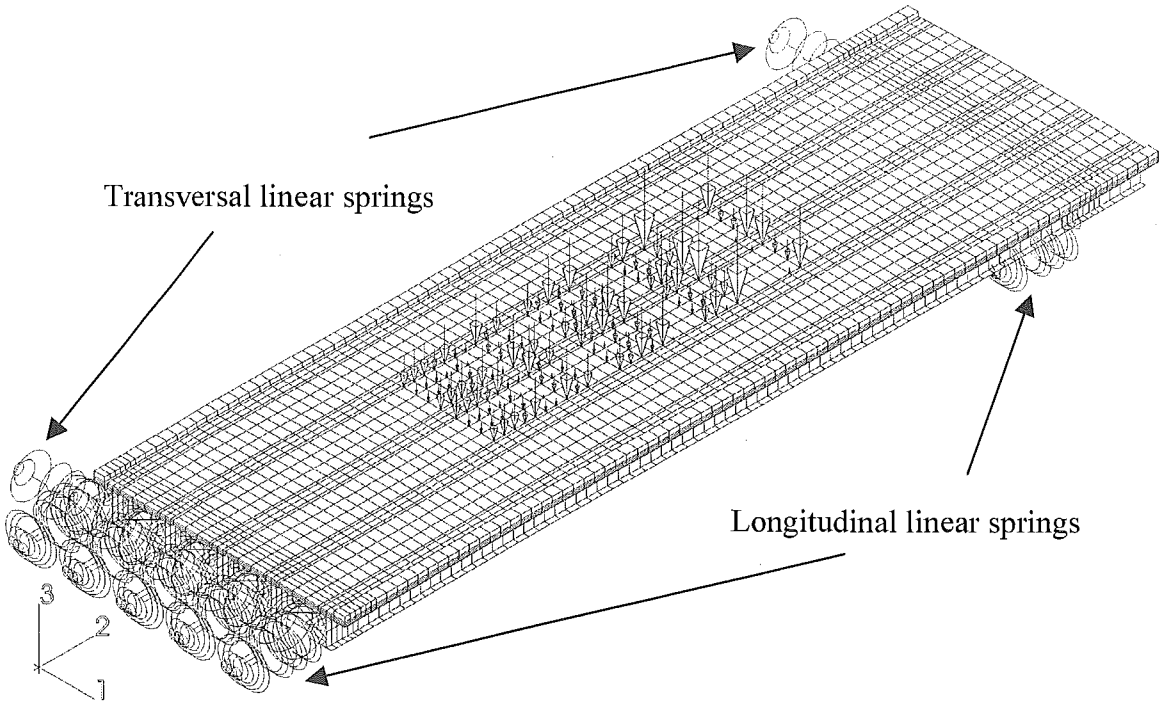

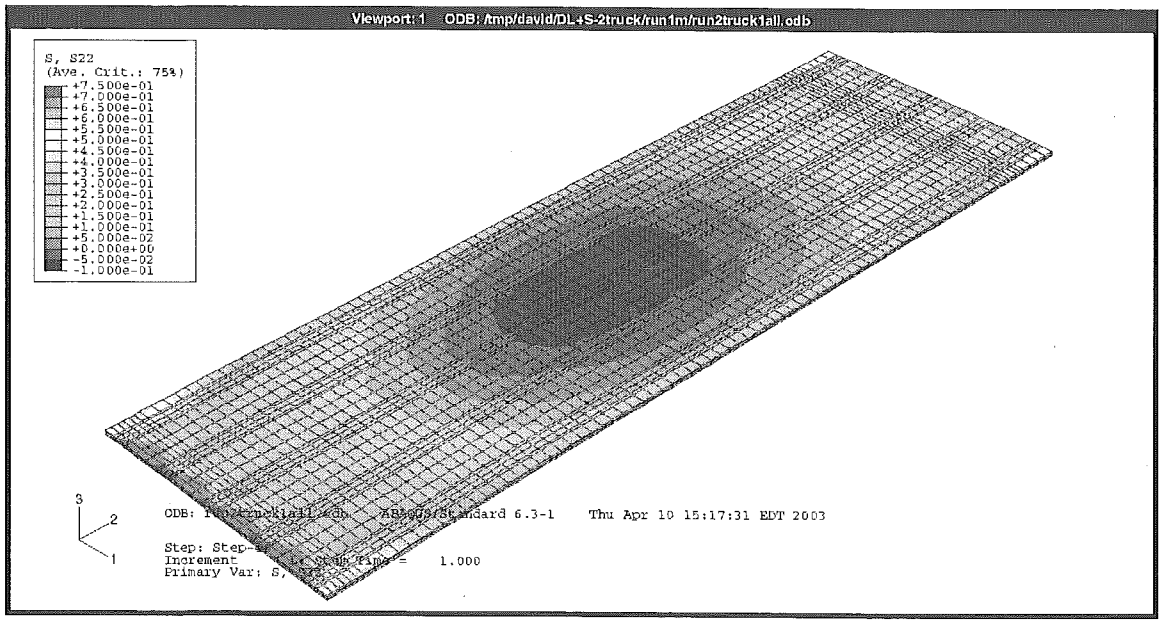

Figure 4-9. Longitudinal stress due to dead load, shrinkage and live load – top surface of the deck

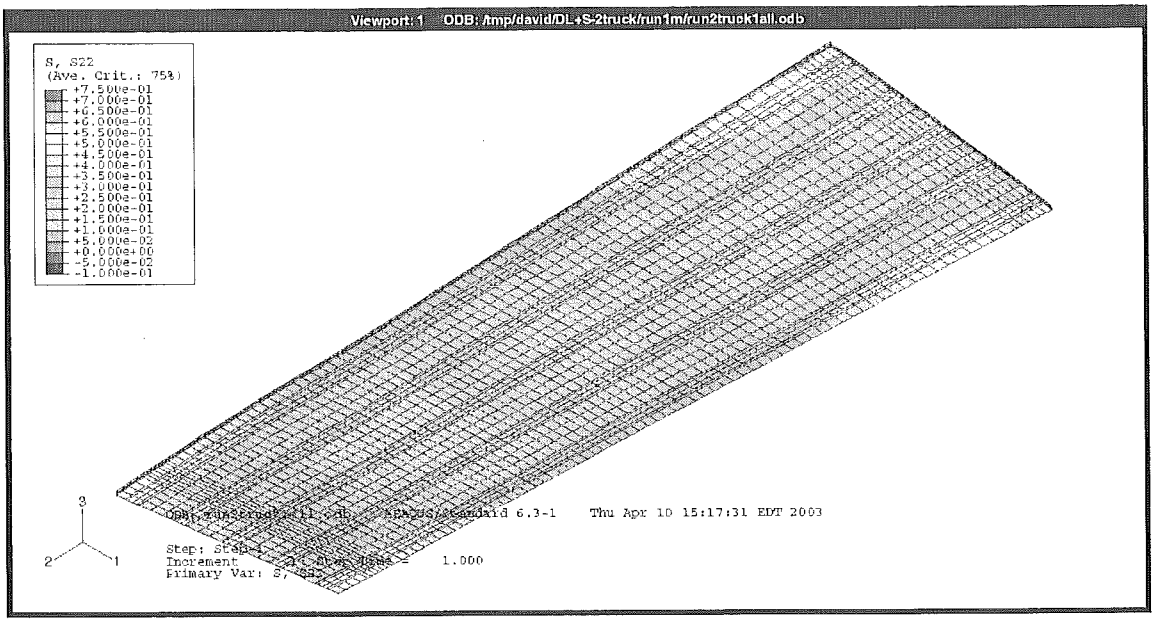

Figure 4-10. Longitudinal stress due to dead load, shrinkage and live load – bottom surface of the deck

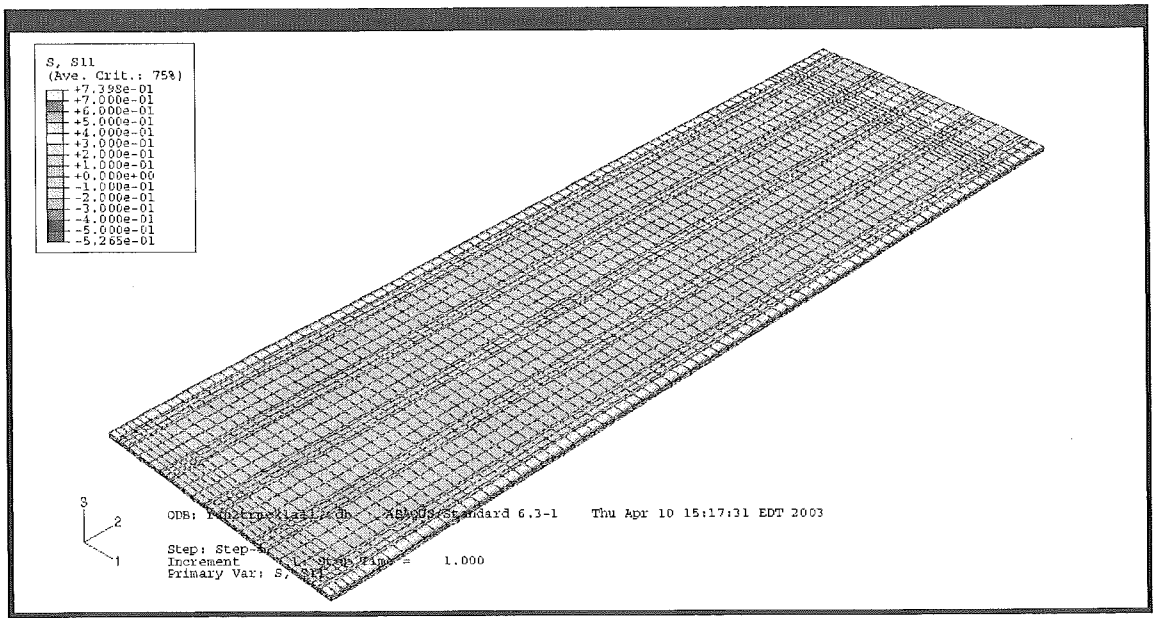

Figure 4-11. Transversal stress due to dead load, shrinkage and live load – top surface of the deck

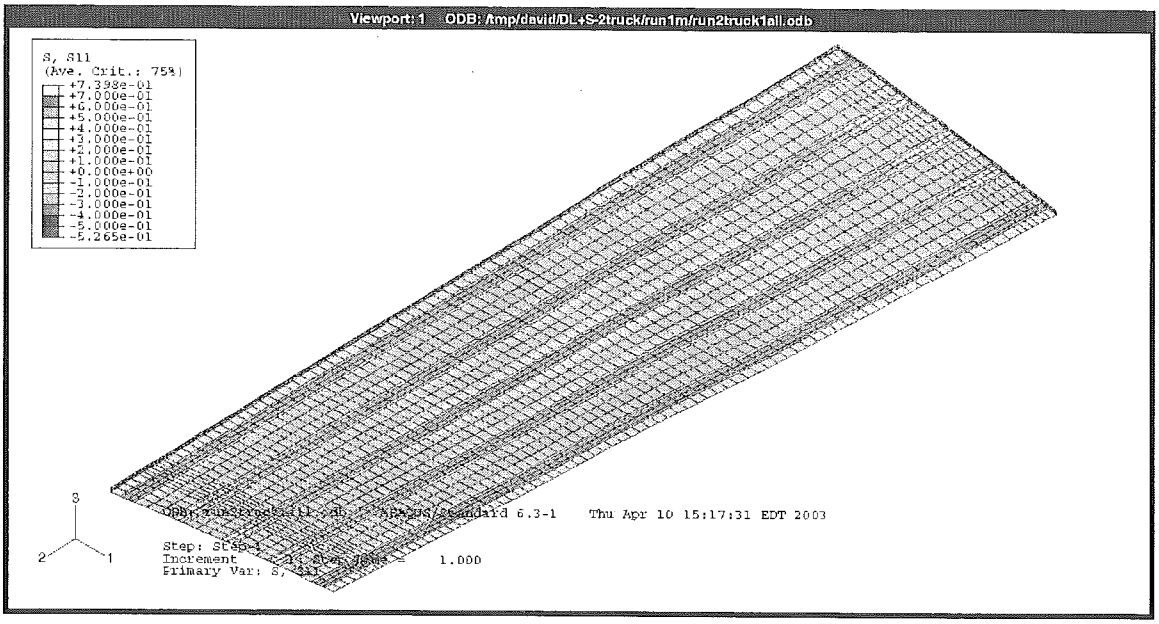

Figure 4-12. Transversal stress due to dead load, shrinkage and live load – bottom surface of the deck

Dead load + shrinkage + 2 trucks (maximum close to support) load option 1

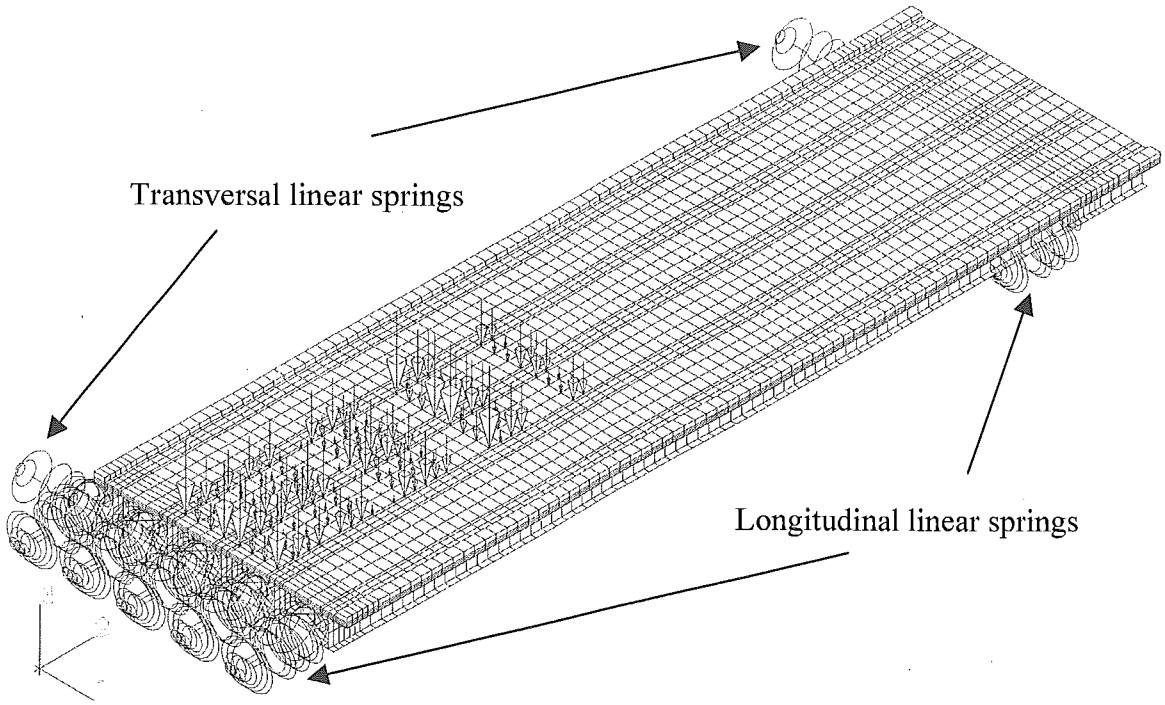

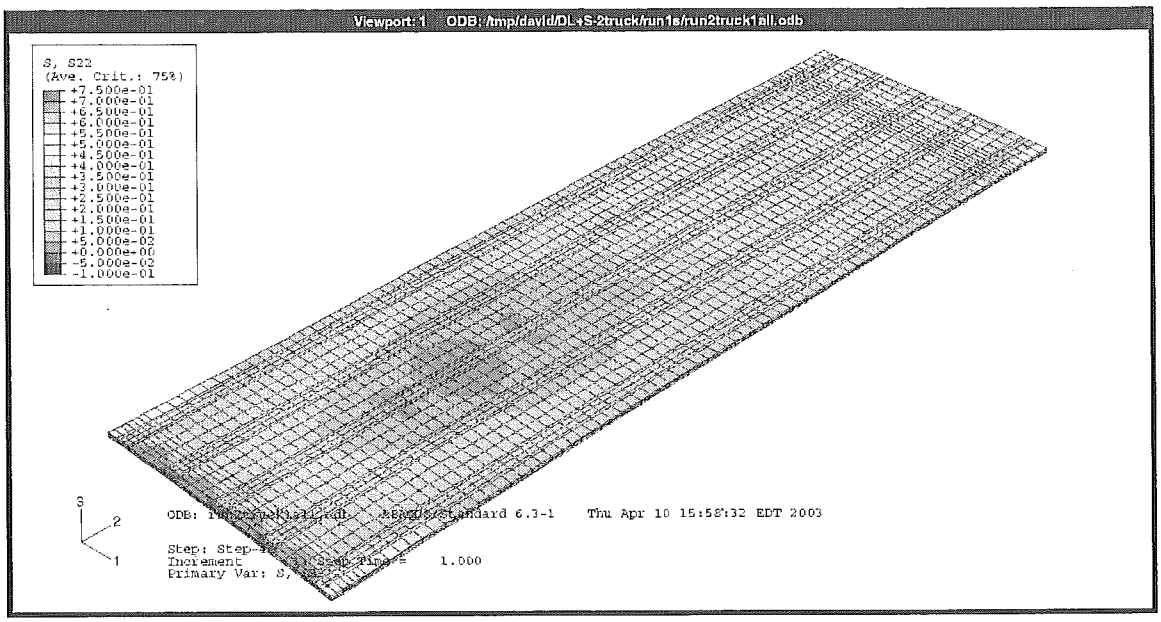

Figure 4-13. Longitudinal stress due to dead load, shrinkage and live load – top surface of the deck

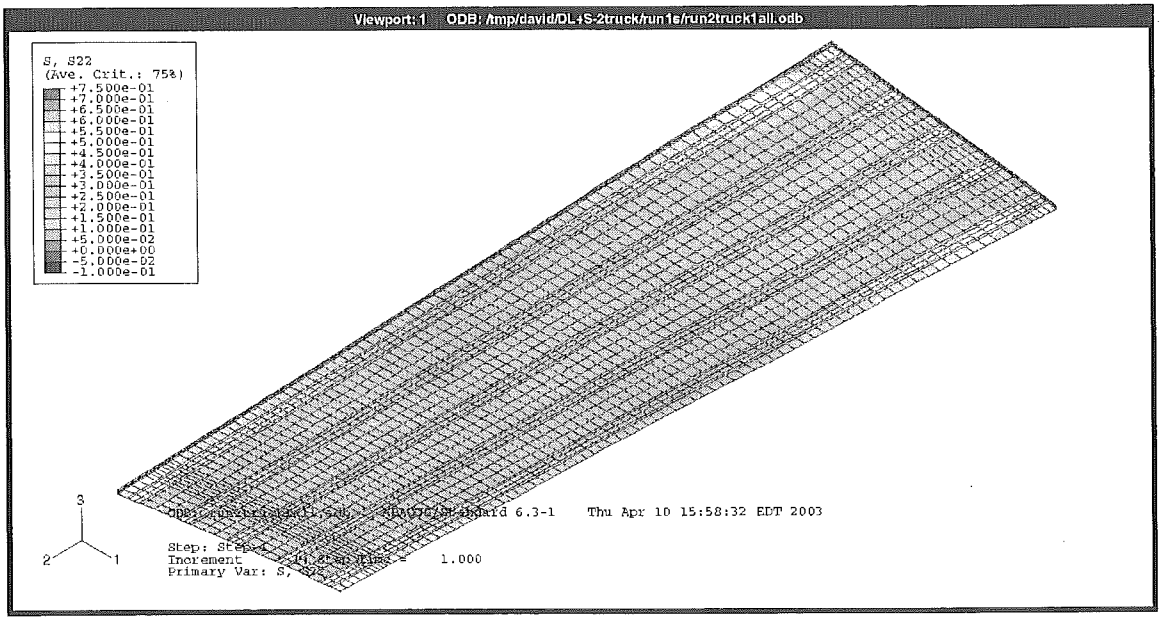

Figure 4-14. Longitudinal stress due to dead load, shrinkage and live load – bottom surface of the deck

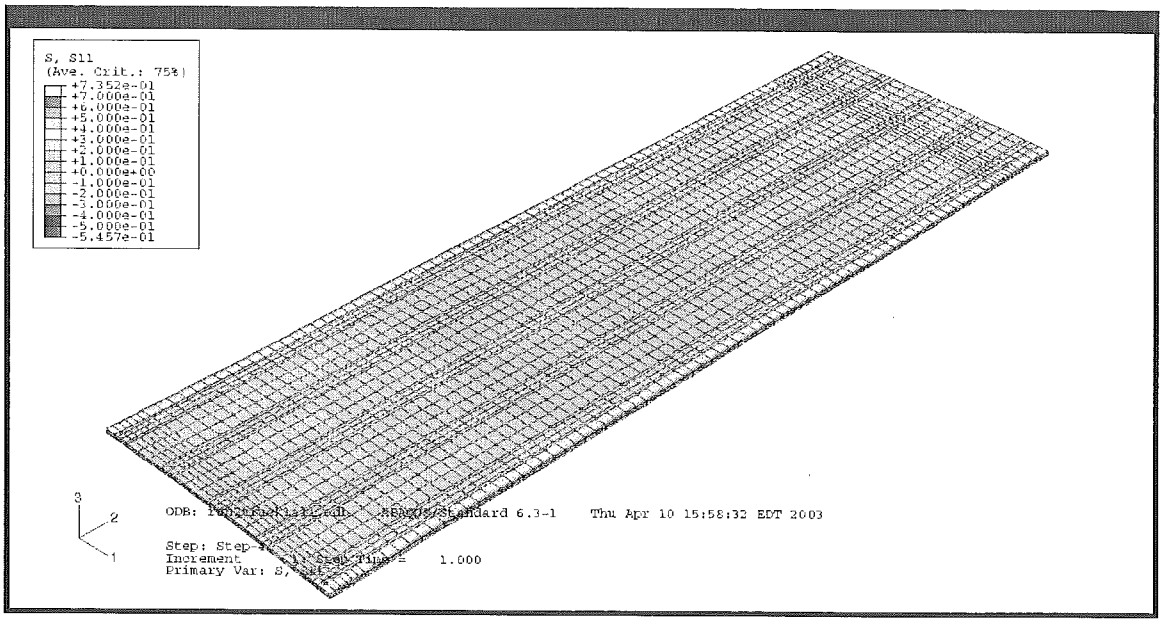

Figure 4-15. Transversal stress due to dead load, shrinkage and live load – top surface of the deck

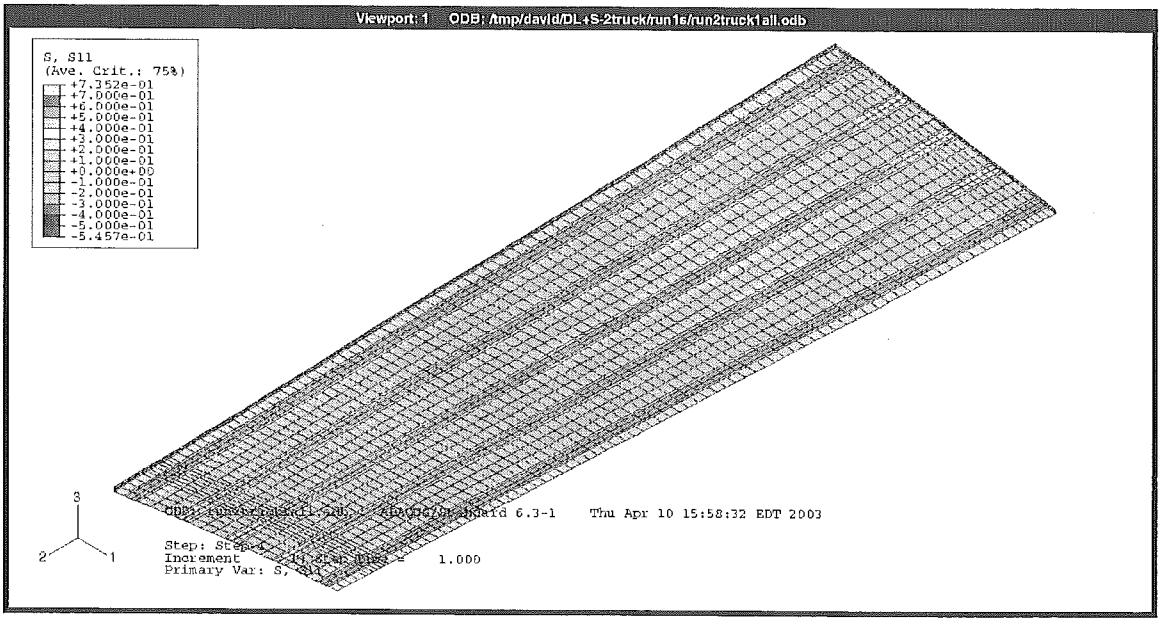

Figure 4-16. Transversal stress due to dead load, shrinkage and live load – bottom surface of the deck

Dead load + shrinkage + 2 trucks (maximum at midspan) load option 2

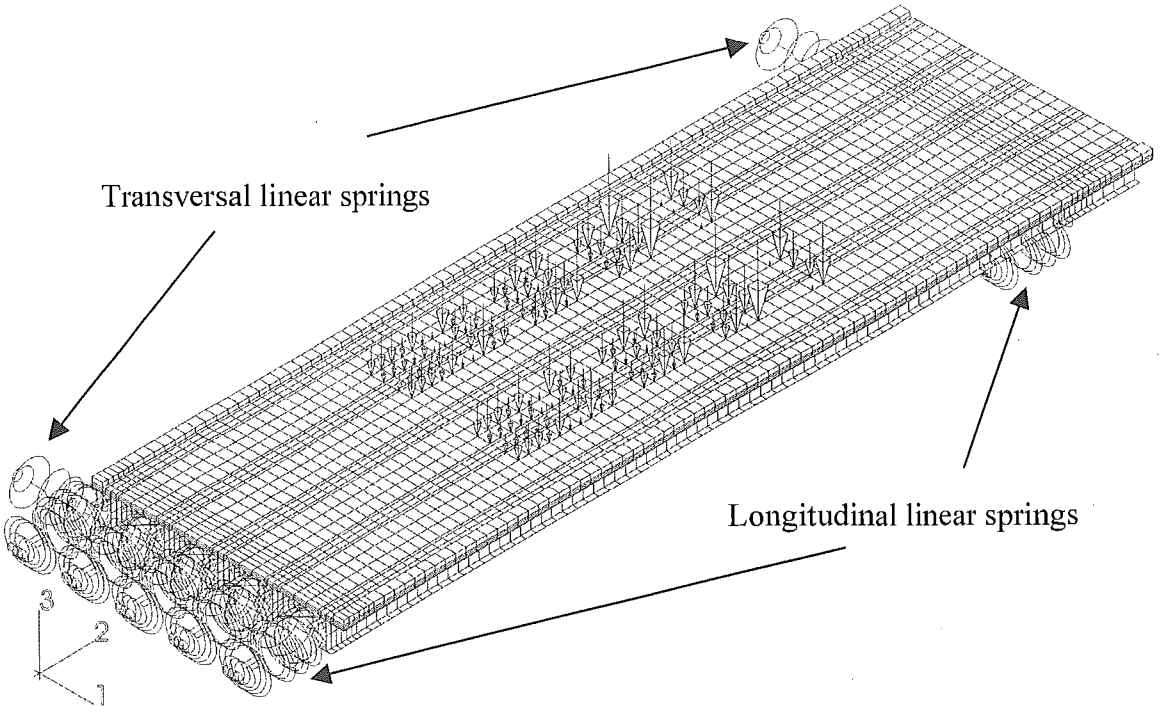

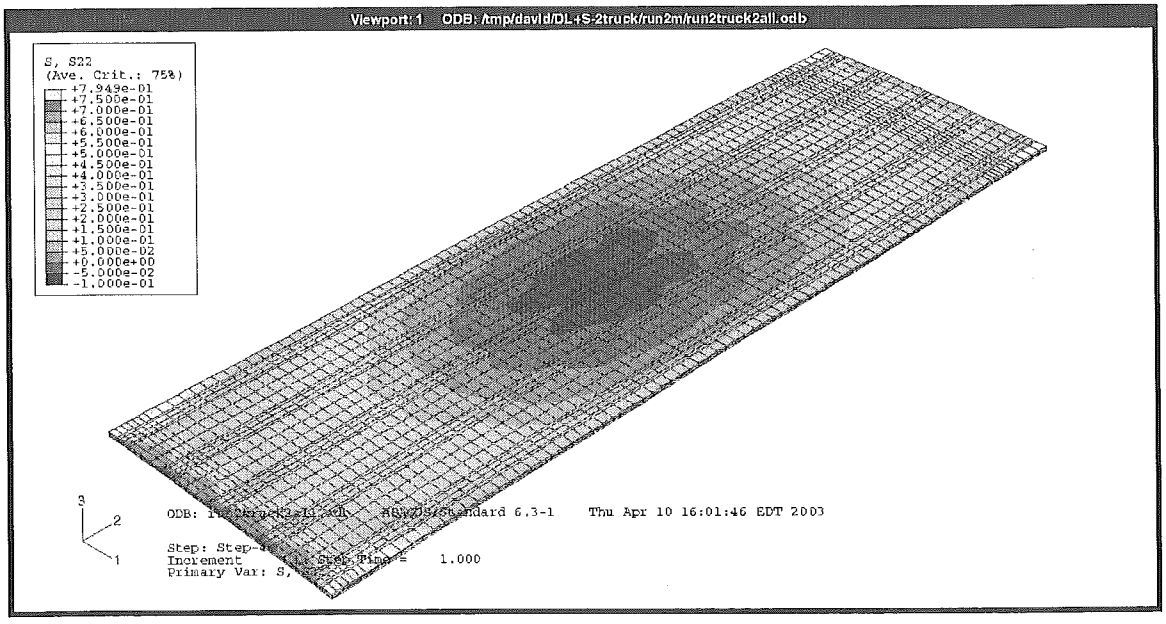

Figure 4-17. Longitudinal stress due to dead load, shrinkage and live load – top surface of the deck

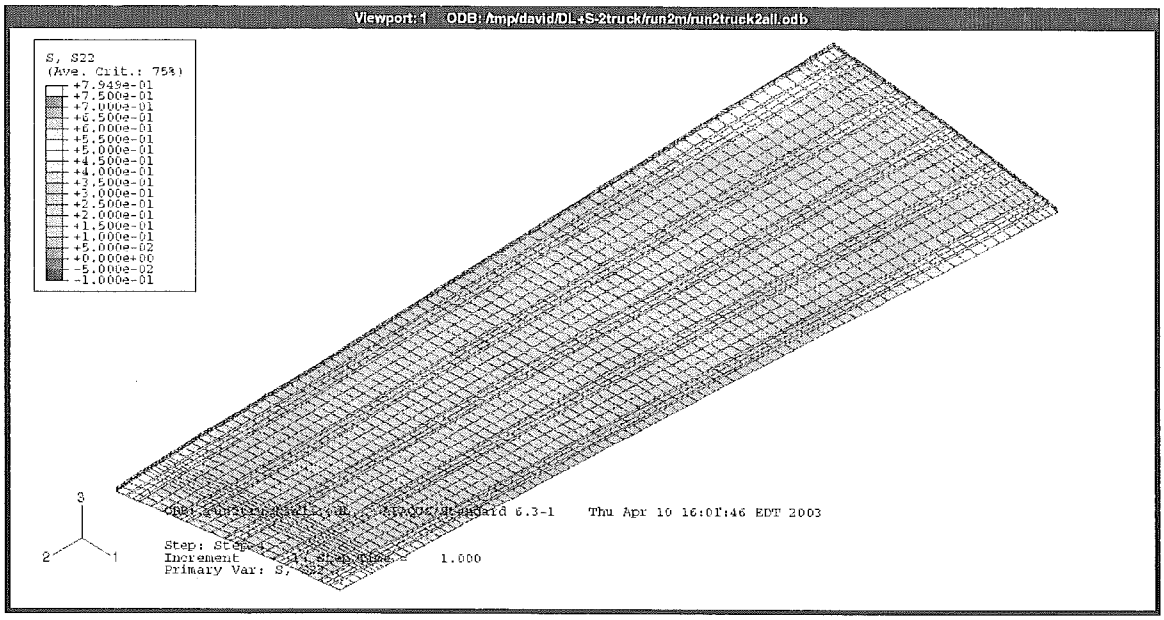

Figure 4-18. Longitudinal stress due to dead load, shrinkage and live load – bottom surface of the deck

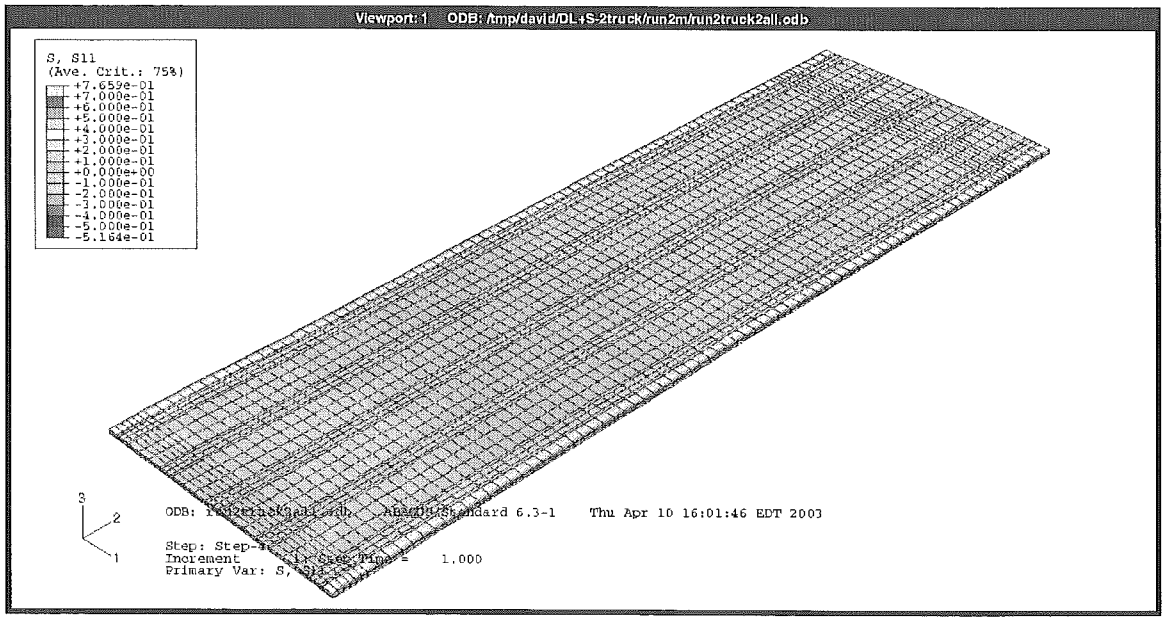

Figure 4-19. Transversal stress due to dead load, shrinkage and live load – top surface of the deck

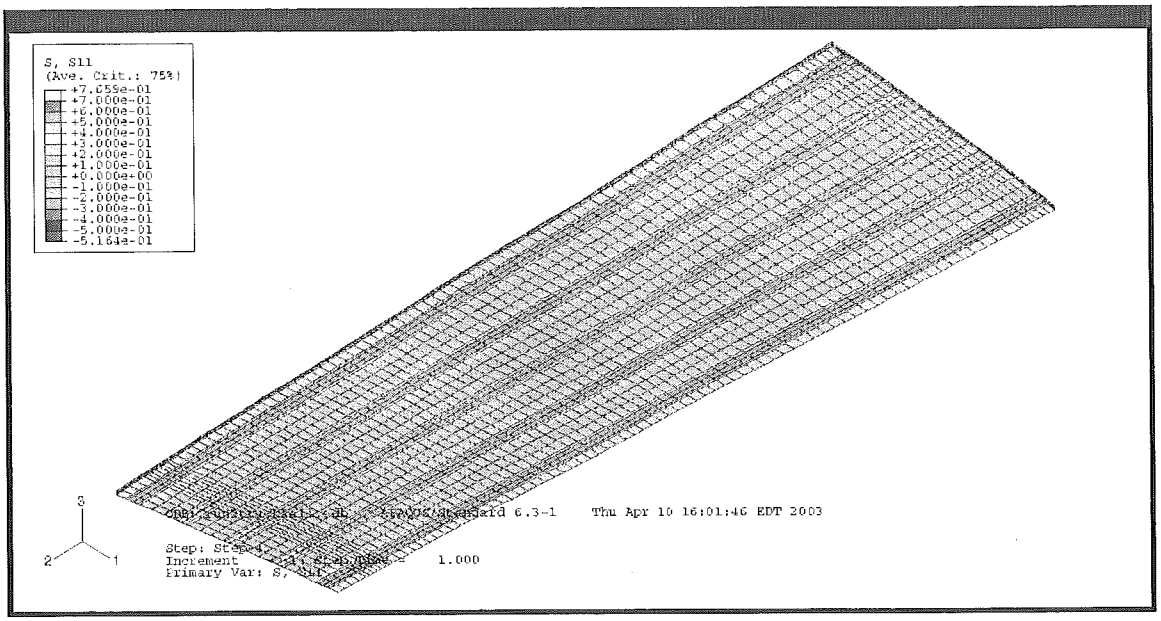

Figure 4-20. Transversal stress due to dead load, shrinkage and live load – bottom surface of the deck

Dead load + shrinkage + 2 trucks (maximum close to support) load option 2

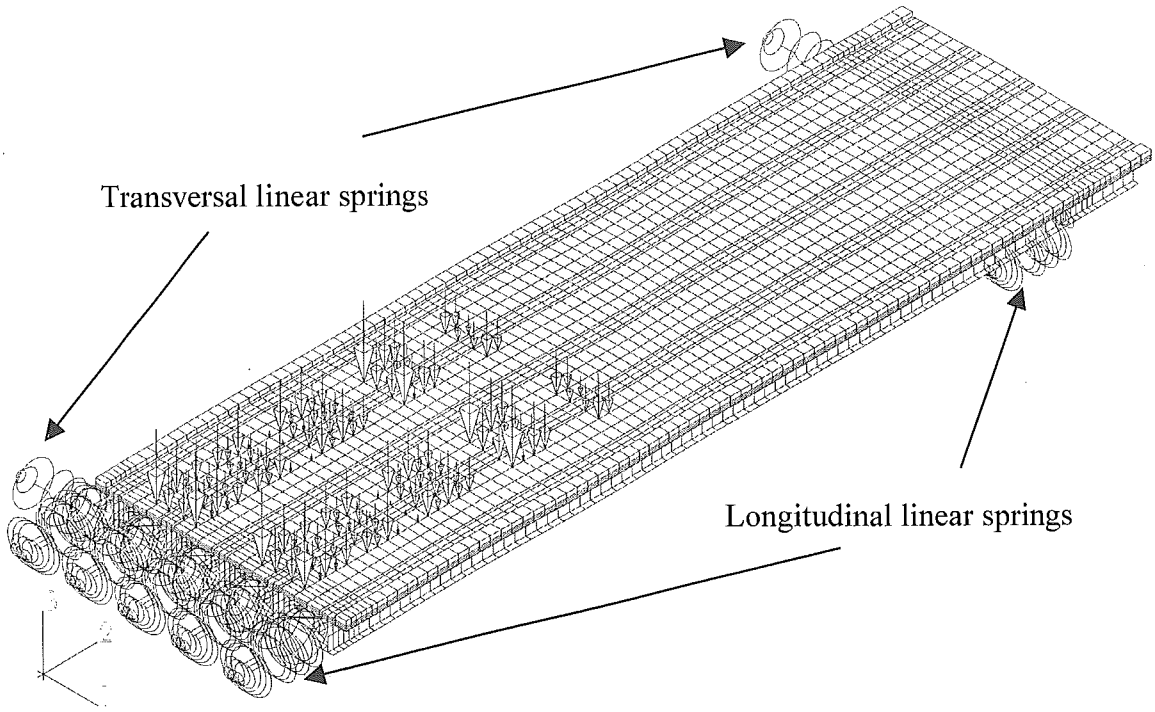

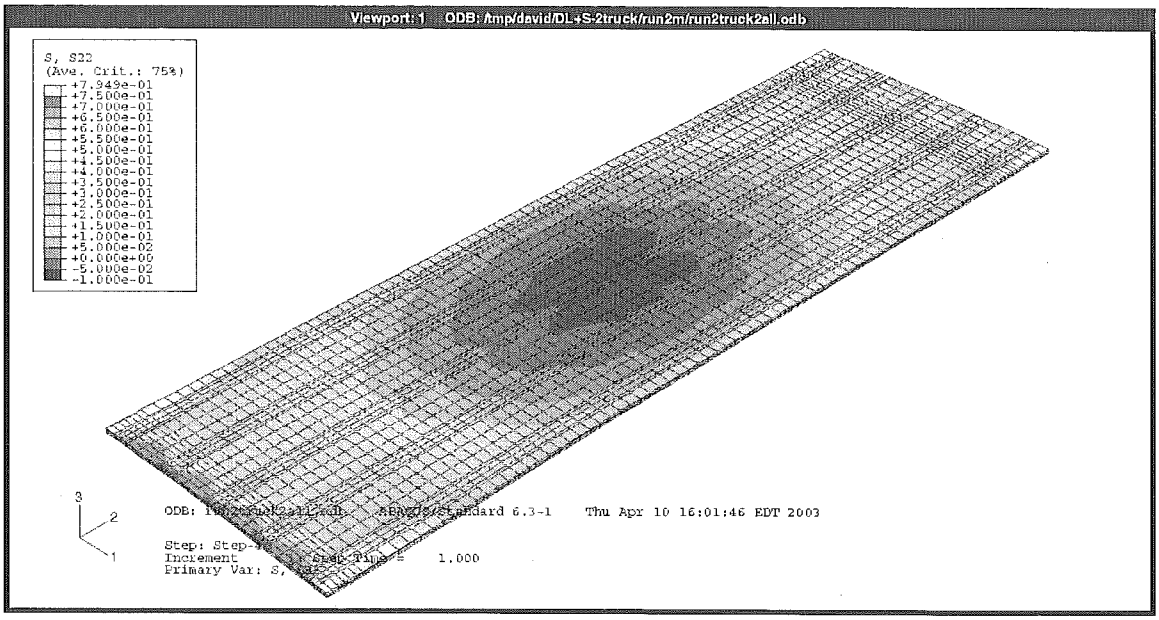

Figure 4-21. Longitudinal stress due to dead load, shrinkage and live load – top surface of the deck

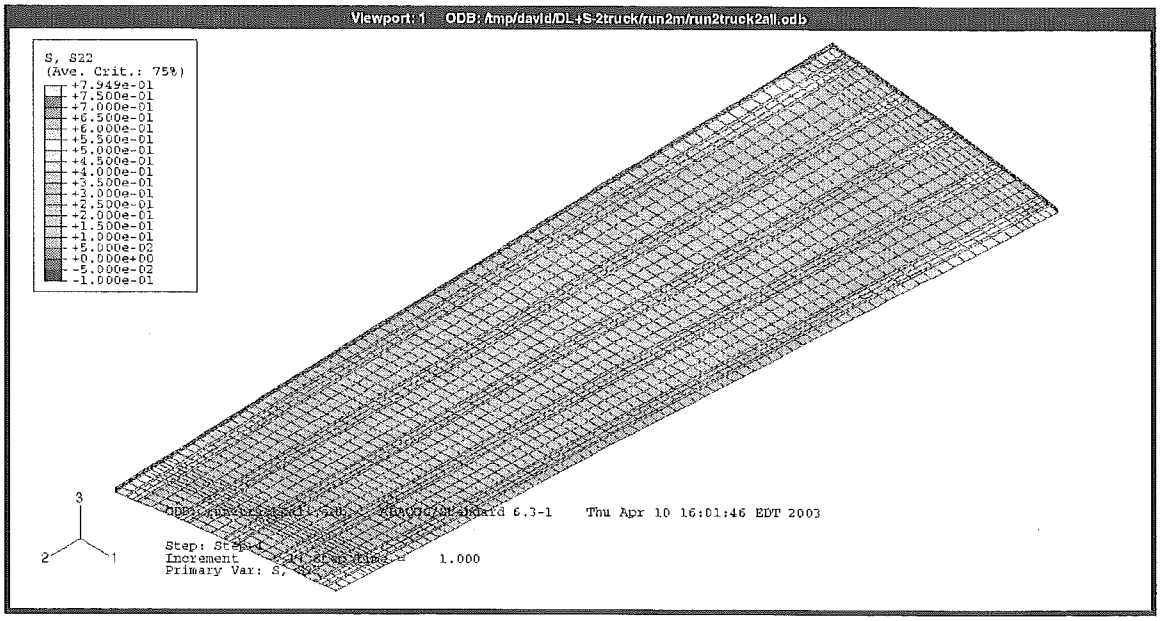

Figure 4-22. Longitudinal stress due to dead load, shrinkage and live load – bottom surface of the deck

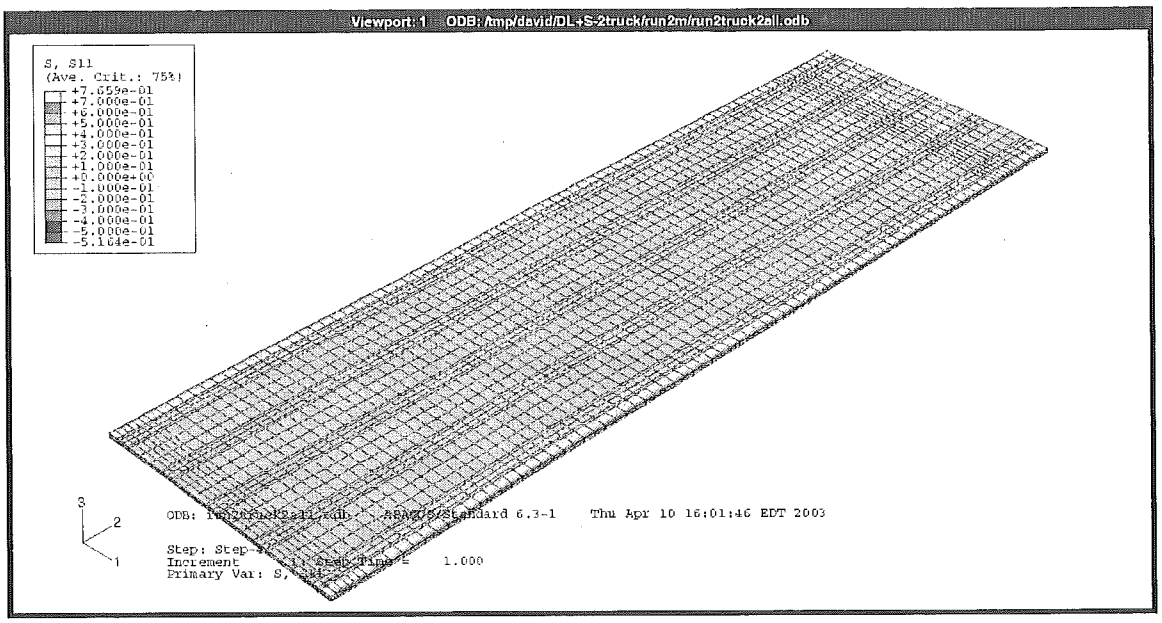

Figure 4-23. Transversal stress due to dead load, shrinkage and live load – top surface of the deck

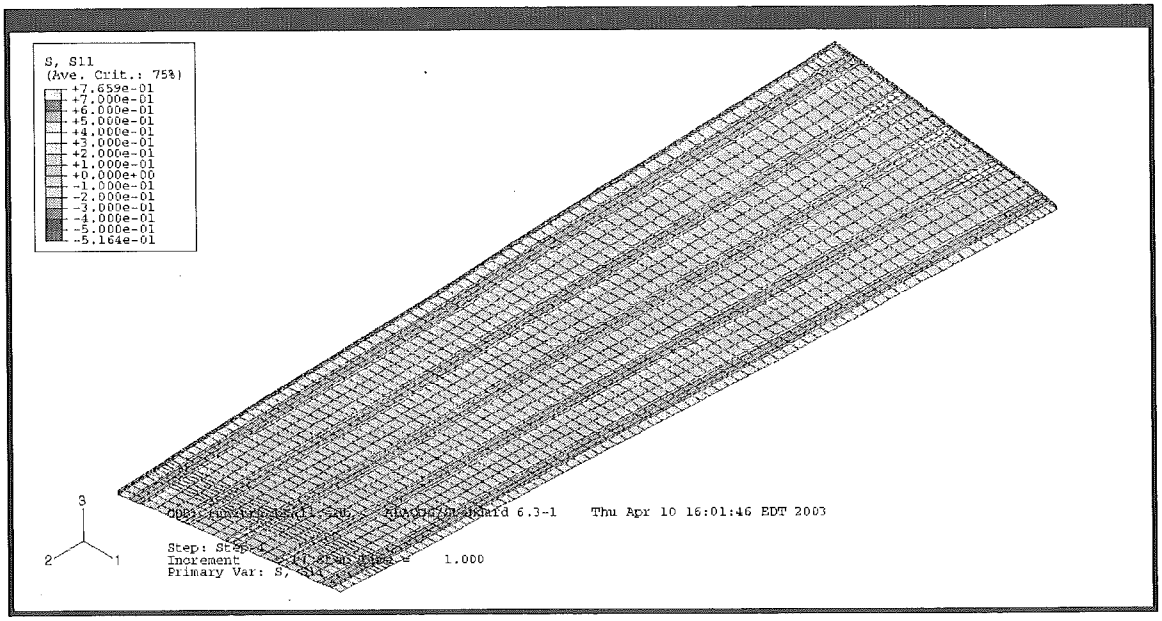

Figure 4-24. Transversal stress due to dead load, shrinkage and live load – bottom surface of the deck

4.2. Stress values in the deck slab supported on prestressed concrete girders

The finite element model of a concrete deck slab supported on prestressed concrete girders was used to calculate the stress distribution in the deck. Calibration of the FEM

model is presented in Chapter 3. The isotropic deck is composite with the AASHTO Type II girders, spaced at 10 ft 5 in. The thickness of the deck is equal to 9 in, and empirical reinforcement is assumed in the section. 11-axle trucks (presented in Figures 2-6 and 3-18) are used as live load in the numerical calculations. Because the modeled bridge carries three lanes and it has a wide shoulder, two and three trucks were used as live load to obtain the maximum possible stress (in the field tests only one truck was used as live load). Several loading options were considered in this study. In the first case, one 11-axle truck is used as the live load acting on the bridge. In the second case, two identical 11-axle trucks are used as a load. The weight and axle configuration of the trucks is the same as for the truck used during the field test. In the third loading case, three trucks were used as a load (no reduction coefficient due to the coincidence of loading was applied). Transversally, truck was positioned on the deck in the same manner as during the test (center of lane, close to curb and in the middle between two lanes). When two trucks were used as the load, several transverse positions were considered in order to cover the considered loading options. Three trucks were positioned transversally in the middle of the deck, to obtain the maximum load effect. Longitudinally, in all loading cases (one, two, or three trucks), the trucks were positioned to obtain the maximum stress at the midspan and close to the support. Stresses calculated for all loading options are presented in Appendix B. The positions of the load for each loading option are also presented in Appendix B.

Representative results with a maximum stress in the deck, calculated using the finite element model for a concrete deck supported on prestressed concrete girders, are presented in Figures 4-25 to 4-32, 4-34 to 4-37, 4-39 to 4-42, 4-44 to 4-47, 4-49 to 4-52, 4-54 to 4-57 and 4-59 to 4-62. Tension is defined as positive and the values of stresses are in ksi. The positions of the live load are shown in Figures 4-33, 4-38, 4-43, 4-48, 4-53 and 4-58. The results of the shrinkage analysis (described on page 81) are also presented in this chapter. Stresses caused by a restrained shrinkage are added to the stresses caused by the dead load and live loads. The numerical analysis of the restrained shrinkage is treated as a quantitive analysis, giving the distribution of shrinkage stresses in the deck.

Dead load

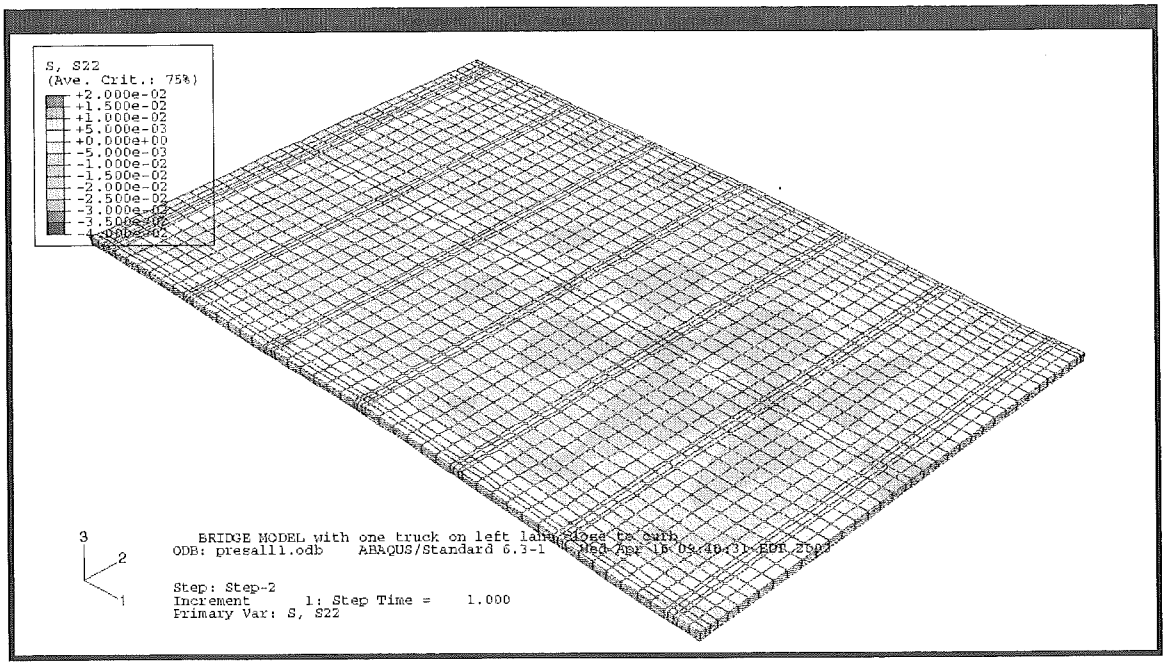

Figure 4-25. Longitudinal stress due to dead load – top surface of the deck

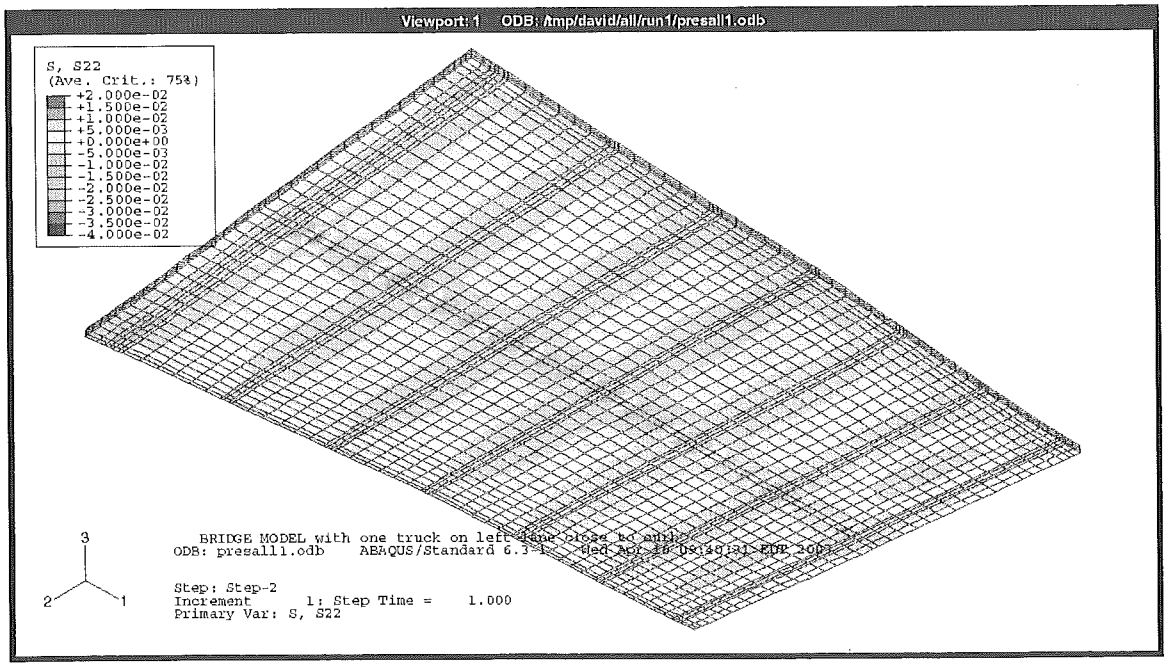

Figure 4-26. Longitudinal stress due to dead load – bottom surface of the deck

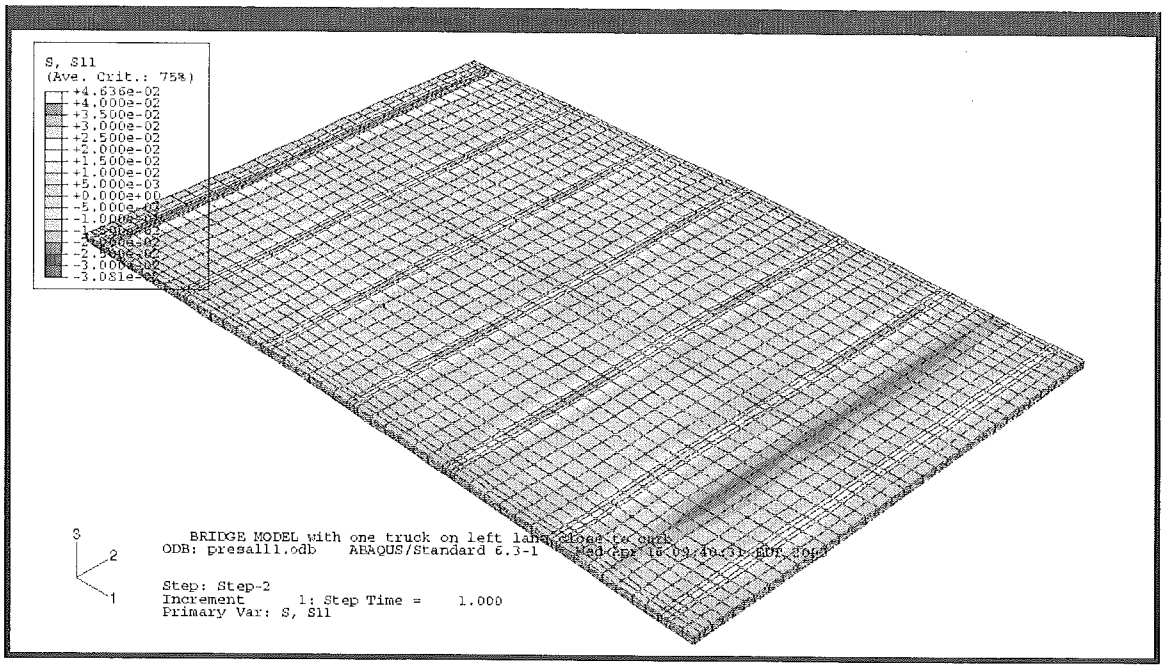

Figure 4-27. Transversal stress due to dead load – top surface of the deck

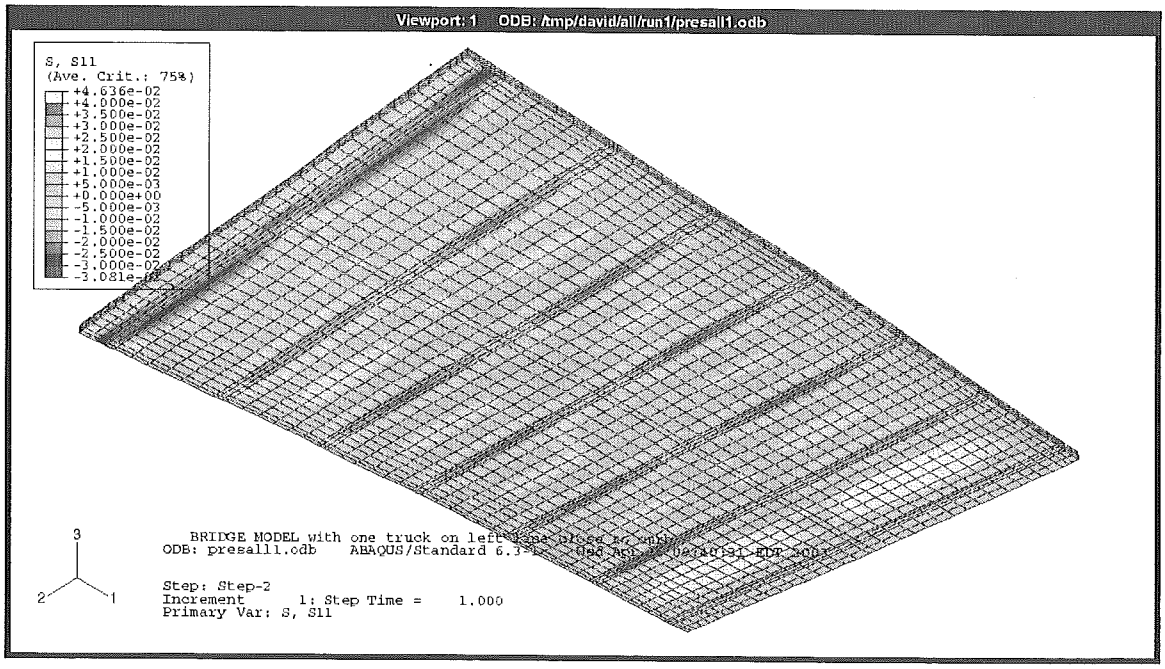

Figure 4-28. Transversal stress due to dead load – bottom surface of the deck

Dead load + Shrinkage

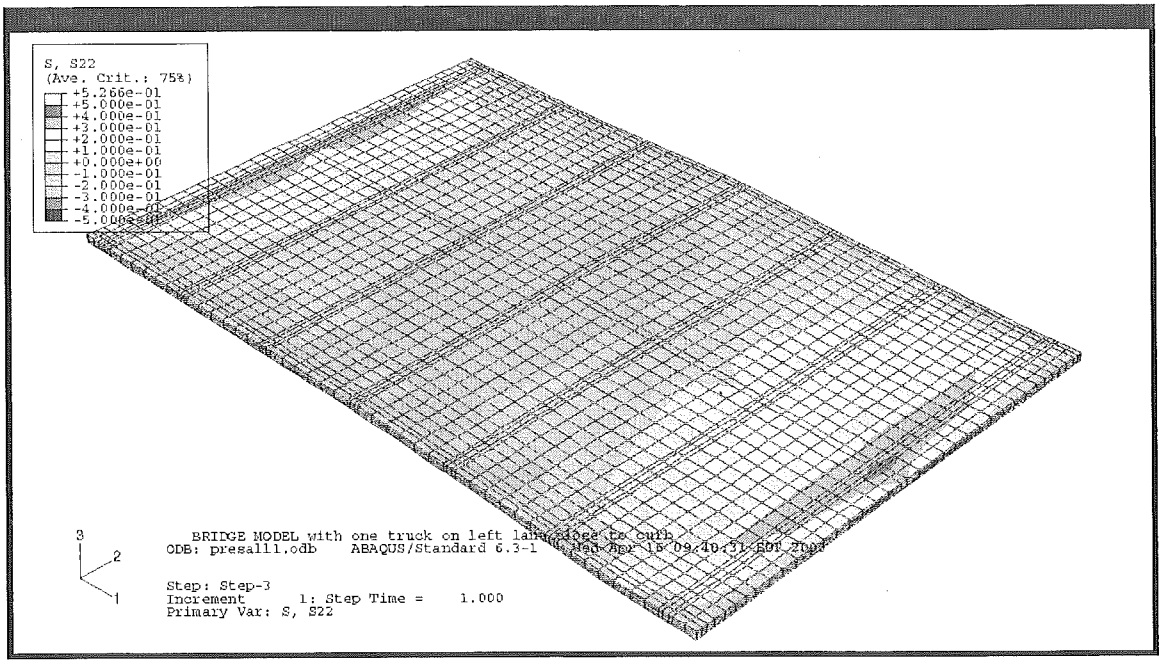

Figure 4-29. Longitudinal stress due to dead load and shrinkage – top surface of the deck

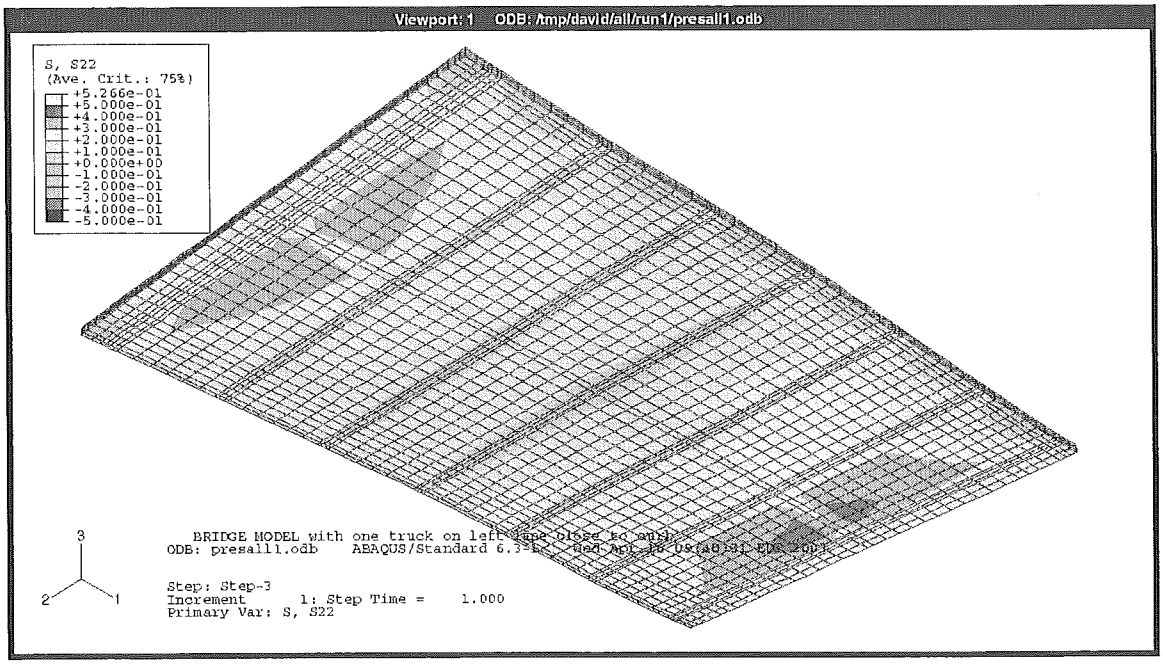

Figure 4-30. Longitudinal stress due to dead load and shrinkage – bottom surface of the deck

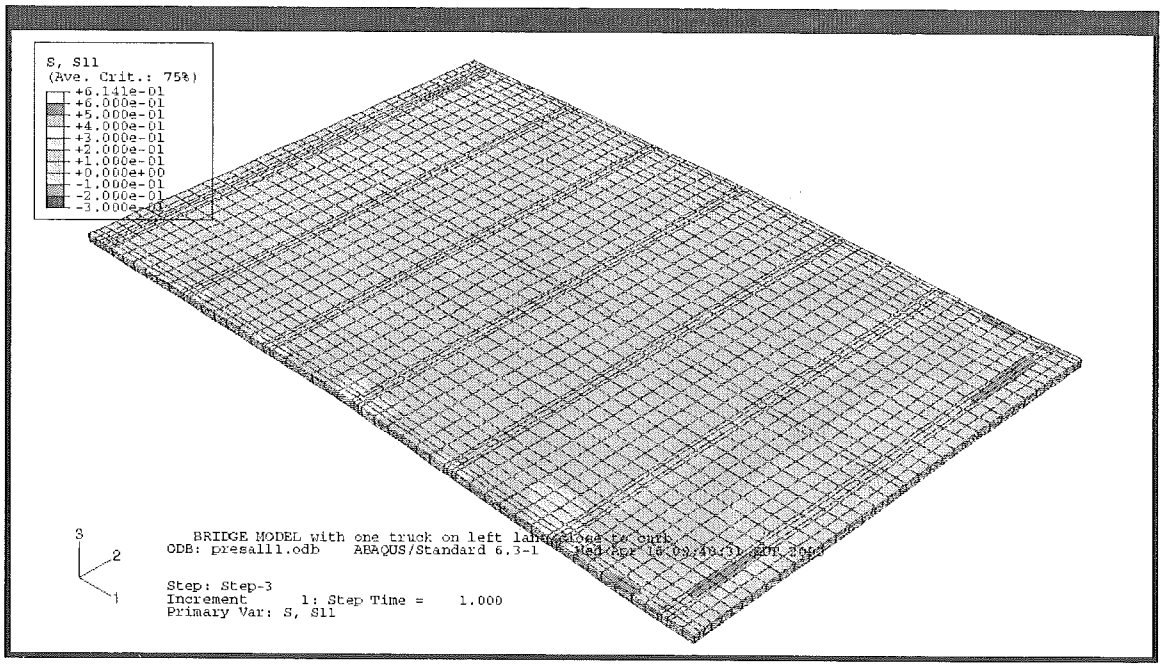

Figure 4-31.Transversal stress due to dead load and shrinkage – top surface of the deck

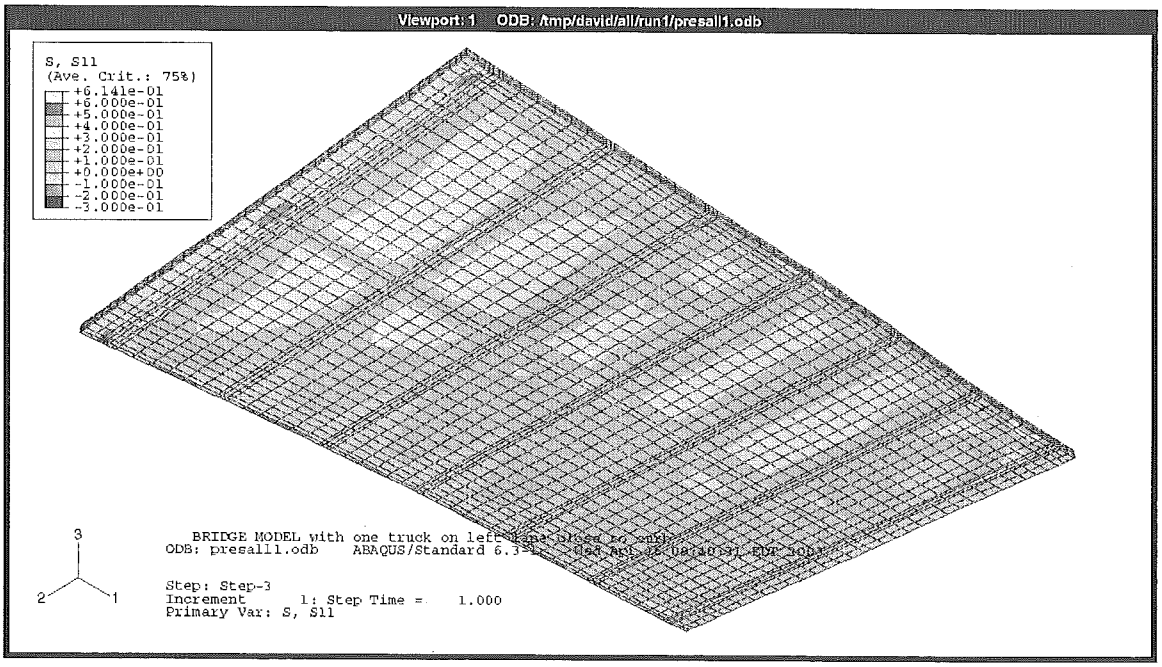

Figure 4-32. Transversal stress due to dead load and shrinkage – bottom surface of the deck

Dead load + shrinkage + 3 trucks (maximum at midspan) position 1

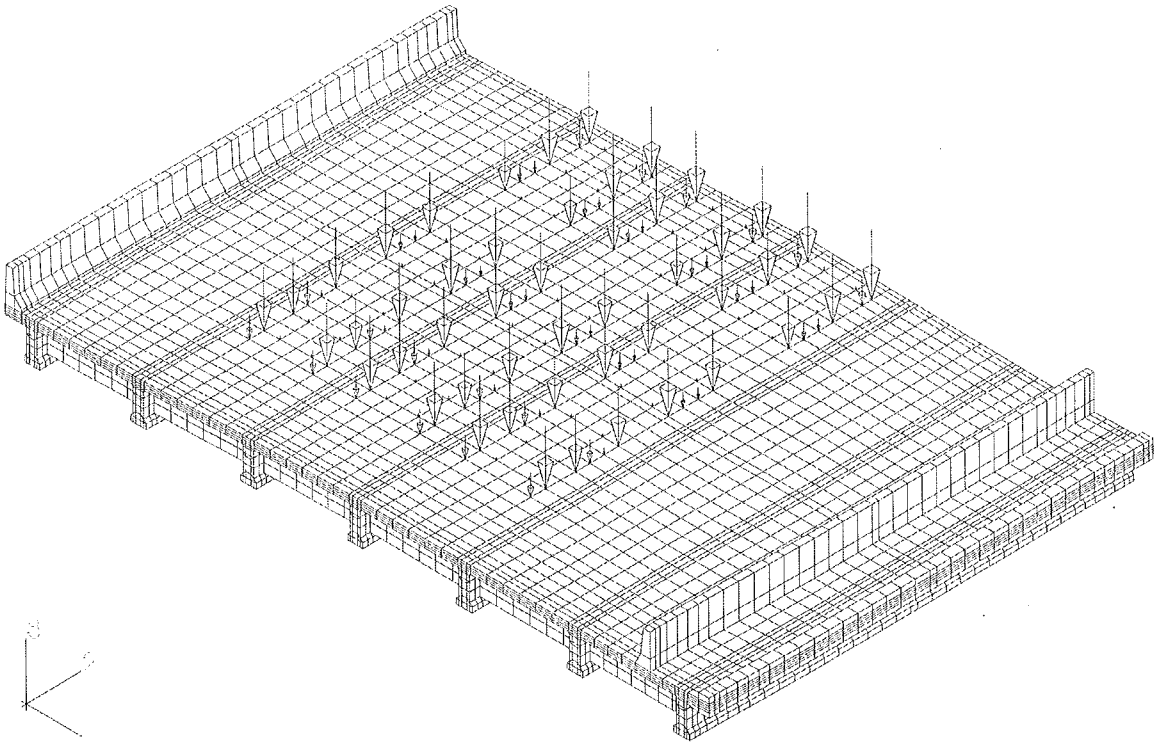

Figure 4-33. Position 1 of the live load (maximum at the midspan)

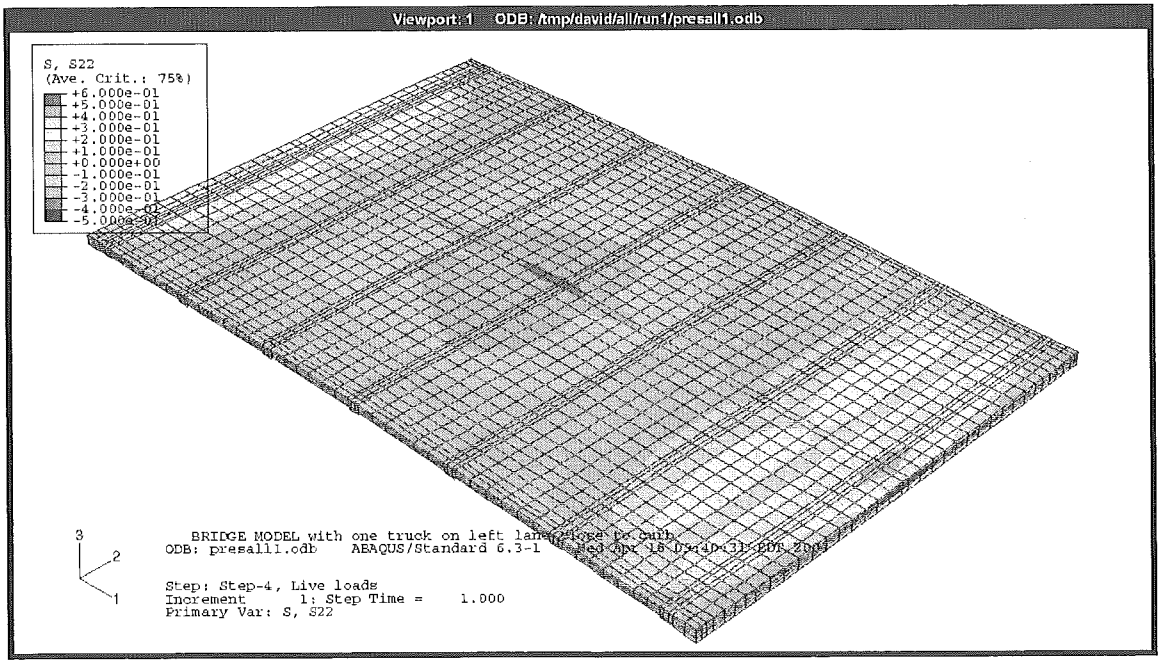

Figure 4-34. Longitudinal stress due to dead load, shrinkage and live load – top surface of the deck

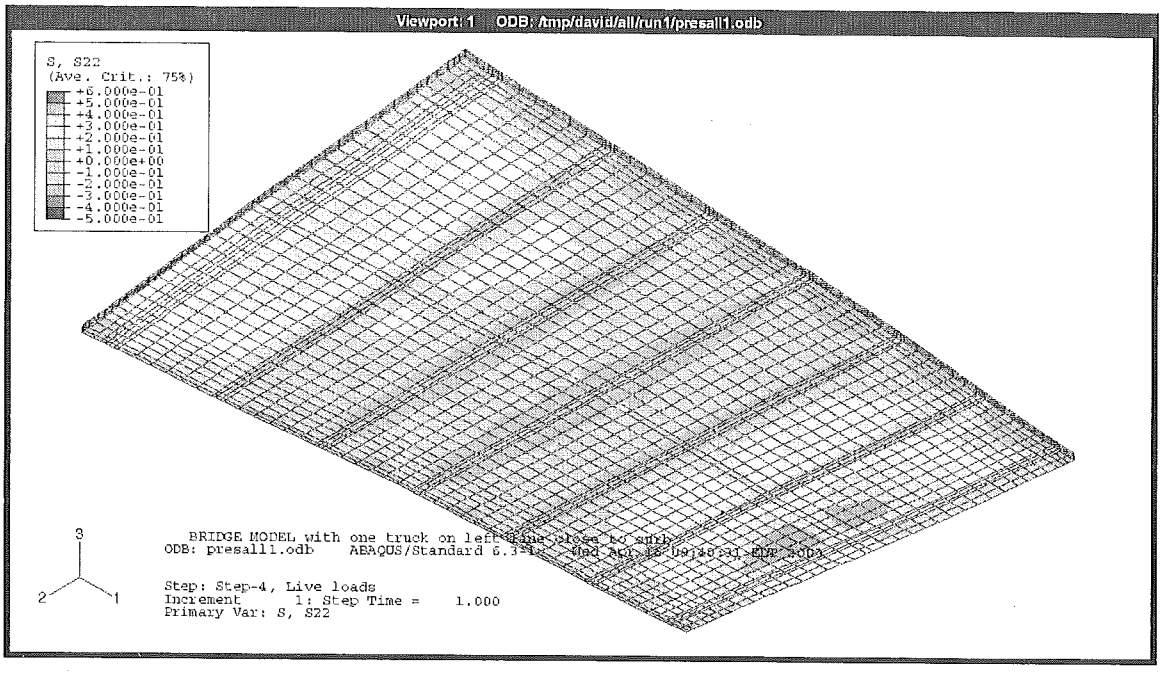

Figure 4-35. Longitudinal stress due to dead load, shrinkage and live load – bottom surface of the deck

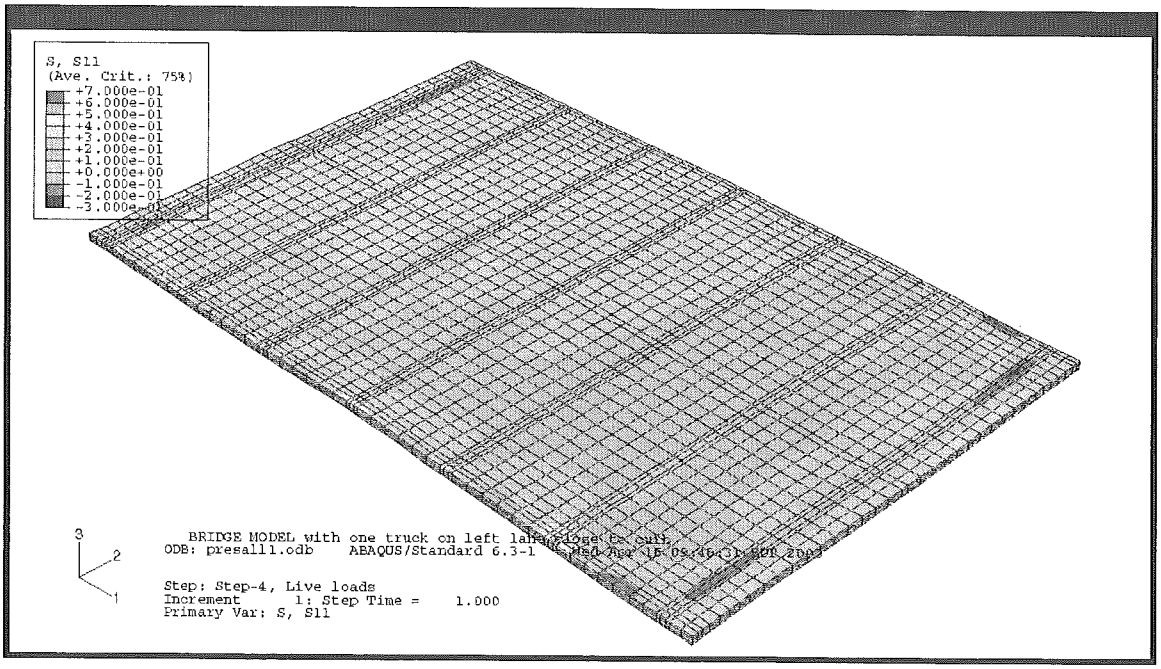

Figure 4-36. Transversal stress due to dead load, shrinkage and live load – top surface of the deck

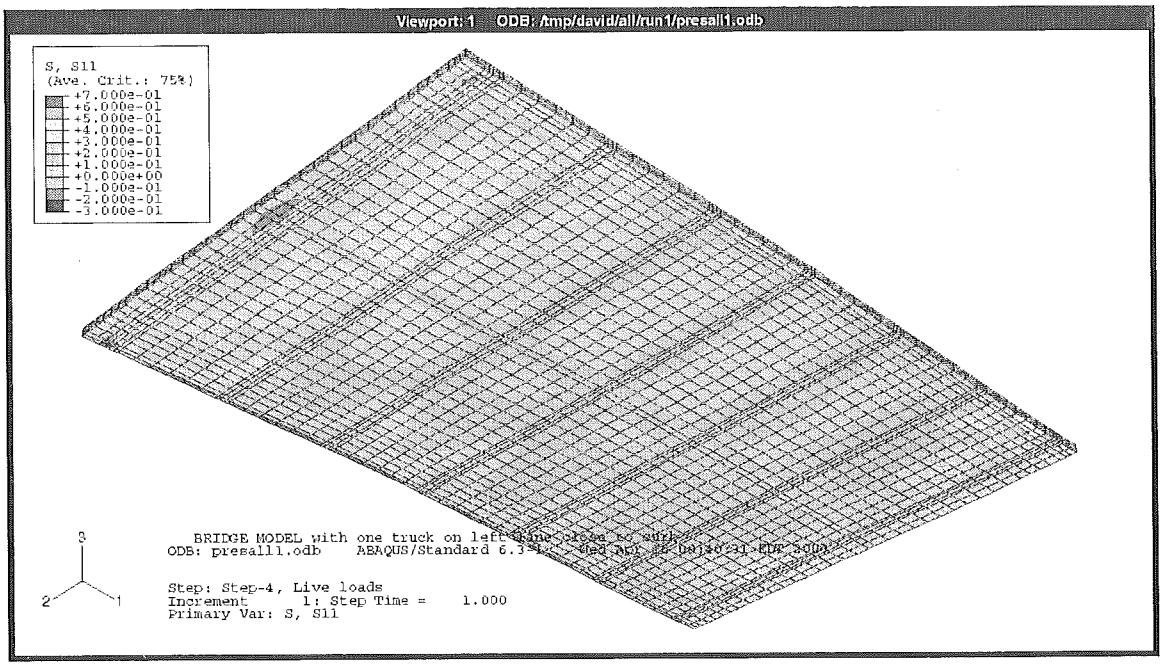

Figure 4-37. Transversal stress due to dead load, shrinkage and live load – bottom surface of the deck

Dead load + shrinkage + 3 trucks (maximum closeness to support) position 1

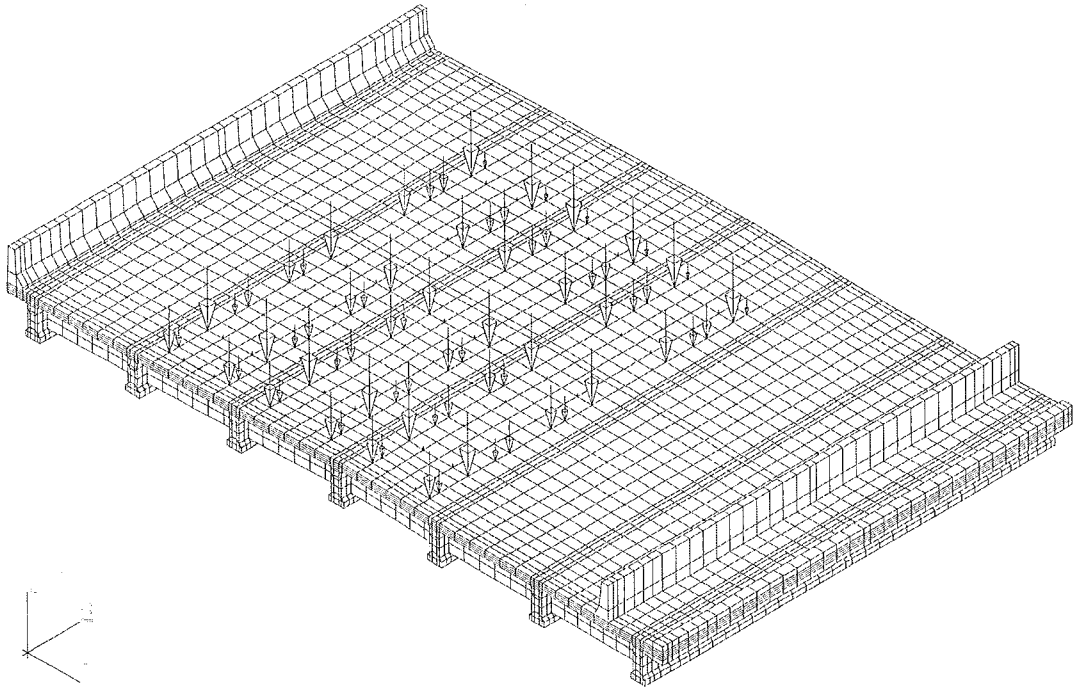

Figure 4-38. Position 1 of the live load (maximum closeness to support)

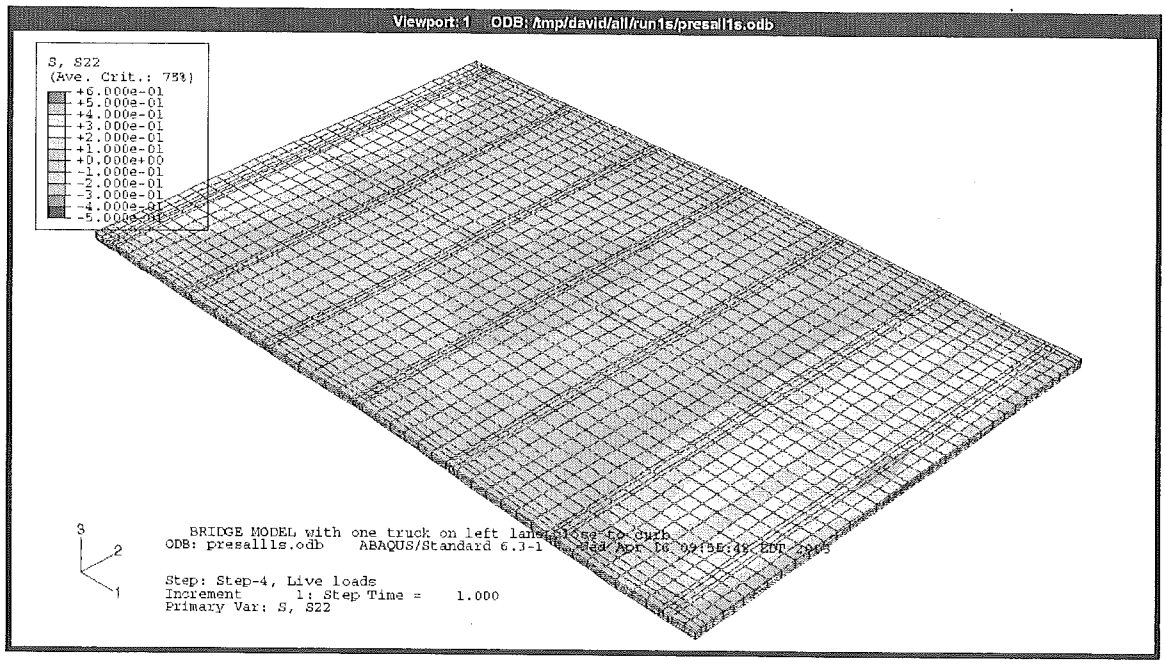

Figure 4-39. Longitudinal stress due to dead load, shrinkage and live load – top surface of the deck

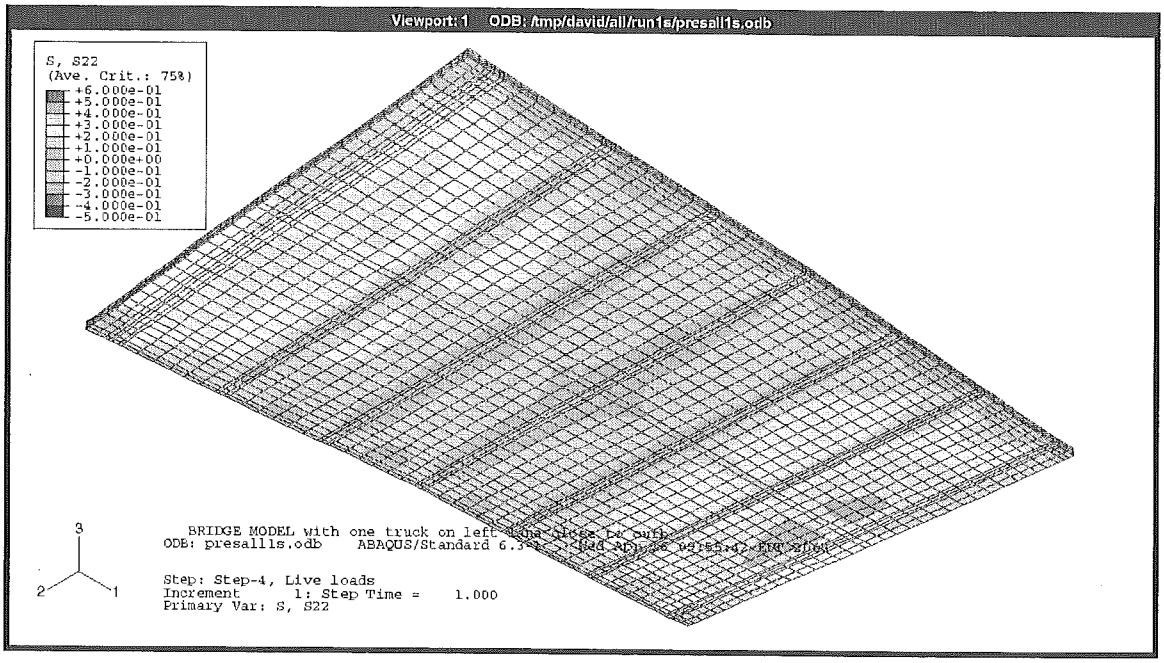

Figure 4-40. Longitudinal stress due to dead load, shrinkage and live load – bottom surface of the deck

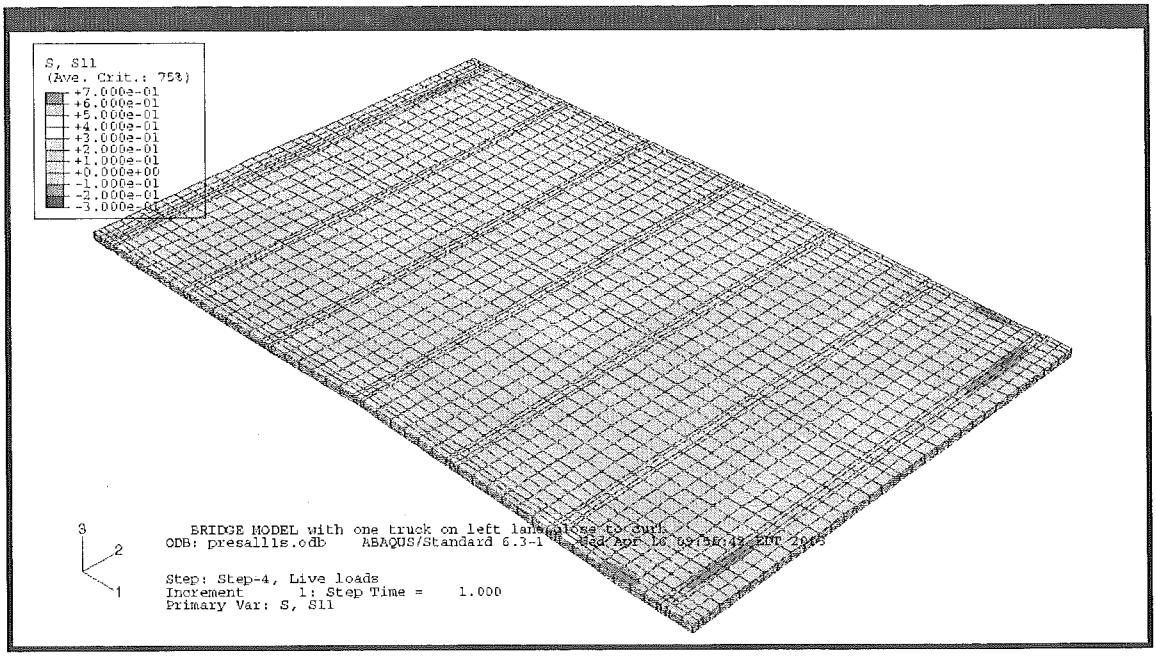

Figure 4-41. Transversal stress due to dead load, shrinkage and live load – top surface of the deck

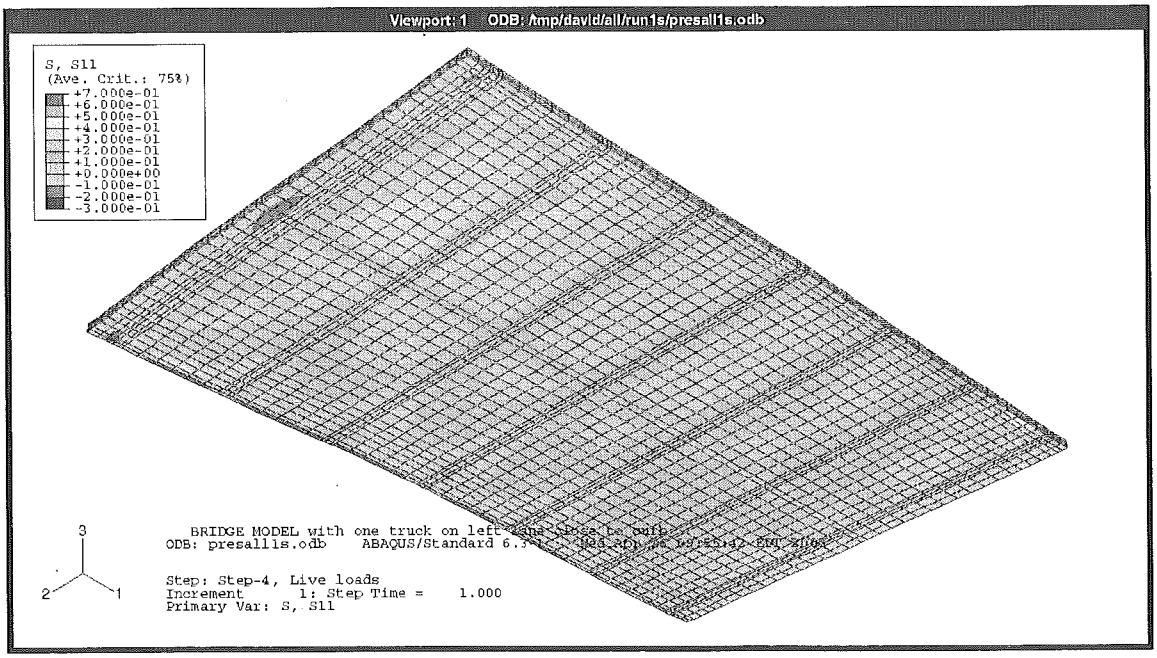

Figure 4-42. Transversal stress due to dead load, shrinkage and live load – bottom surface of the deck

Dead load + shrinkage + 2 trucks (maximum at midspan) position 2

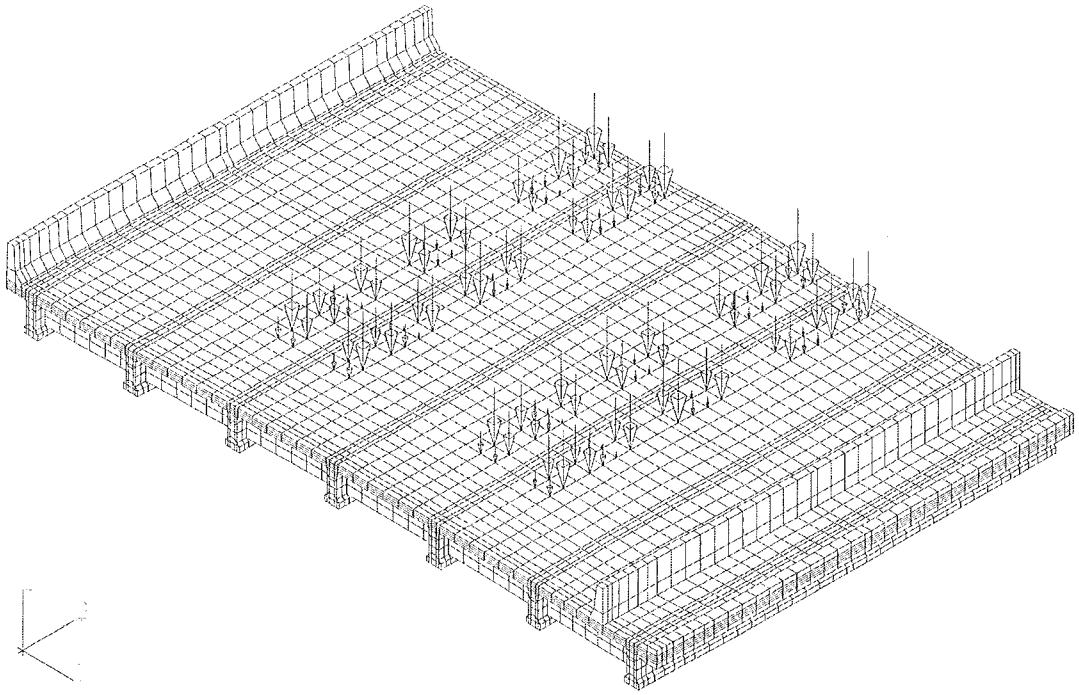

Figure 4-43. Position 2 of the live load (maximum at the midspan)

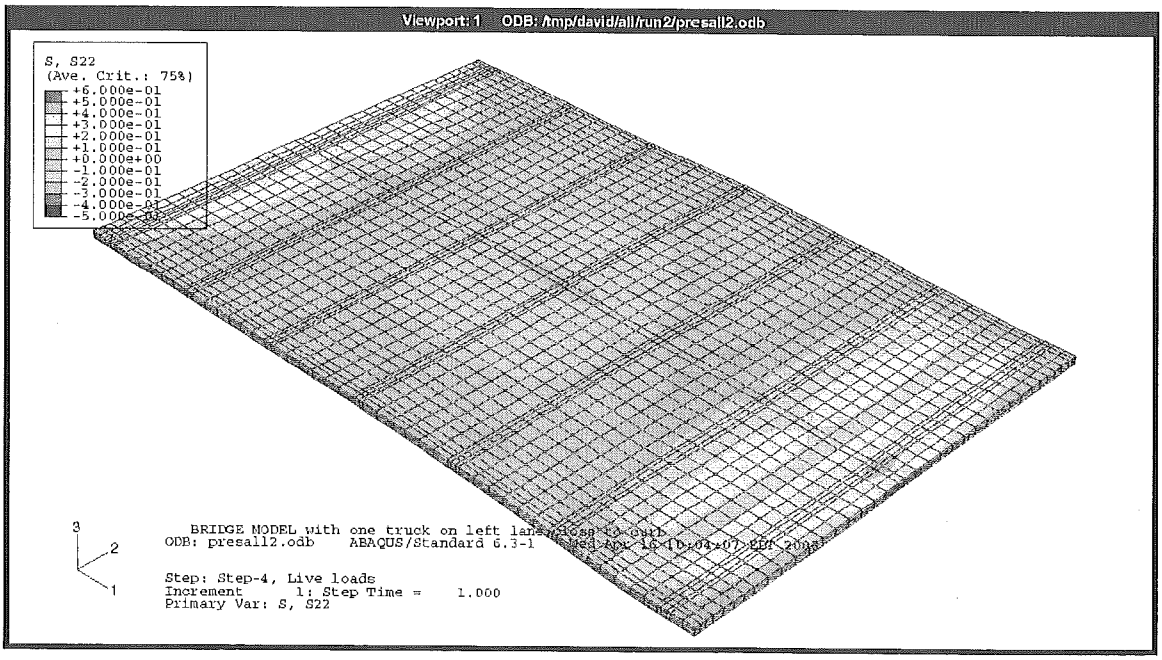

Figure 4-44. Longitudinal stress due to dead load, shrinkage and live load – top surface of the deck

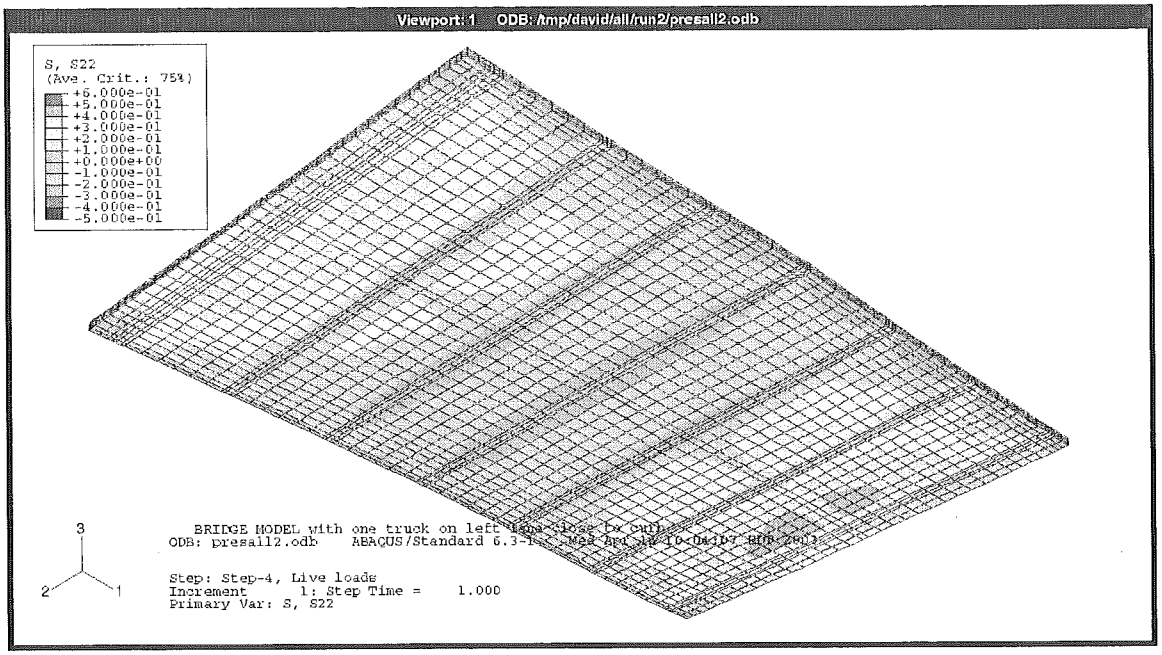

Figure 4-45. Longitudinal stress due to dead load, shrinkage and live load – bottom surface of the deck

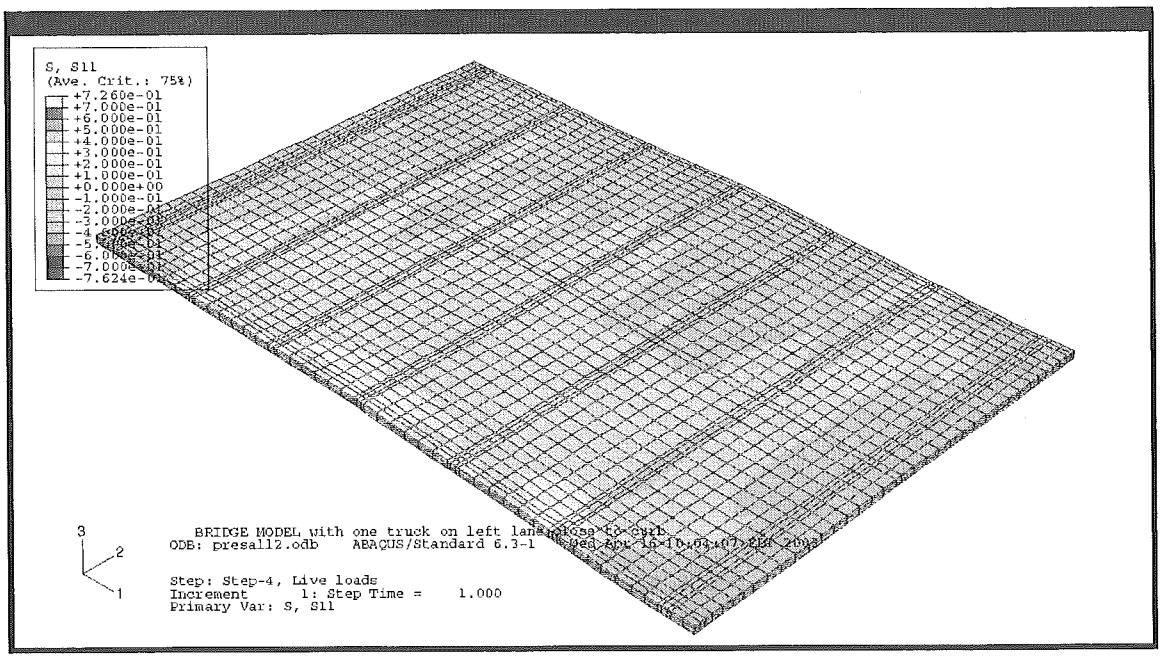

Figure 4-46. Transversal stress due to dead load, shrinkage and live load – top surface of the deck

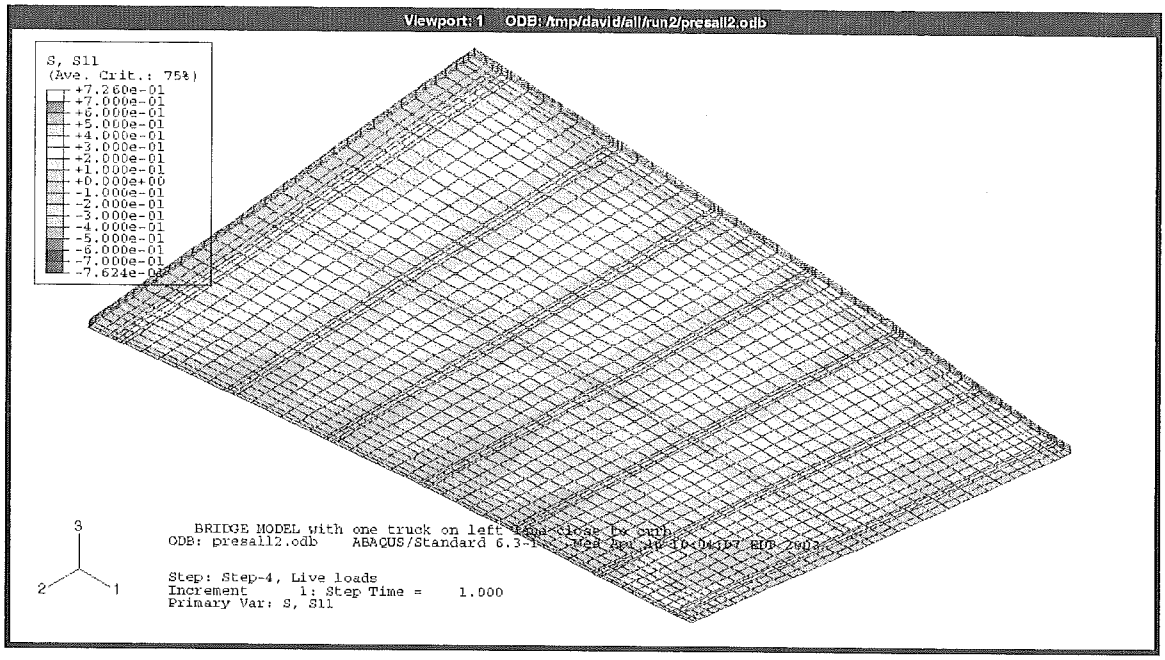

Figure 4-47. Transversal stress due to dead load, shrinkage and live load – bottom surface of the deck

Dead load + shrinkage + 2 trucks (maximum closeness to support) position 2

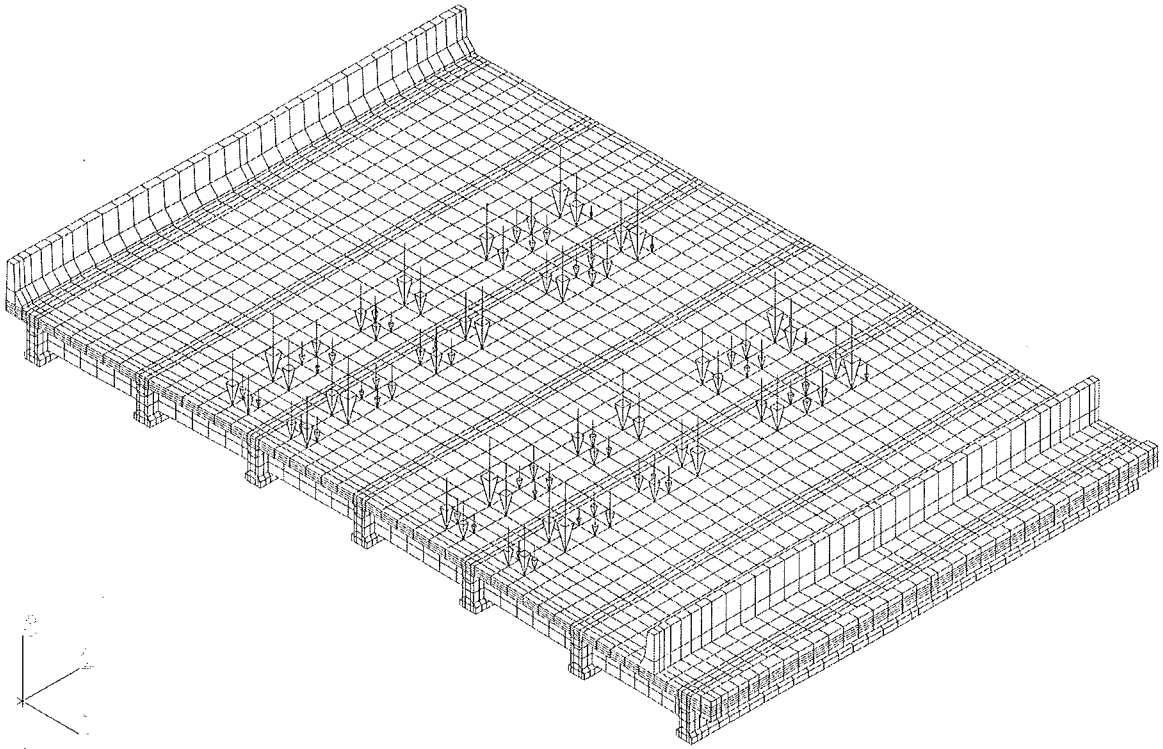

Figure 4-48. Position 2 of the live load (maximum closeness to support)

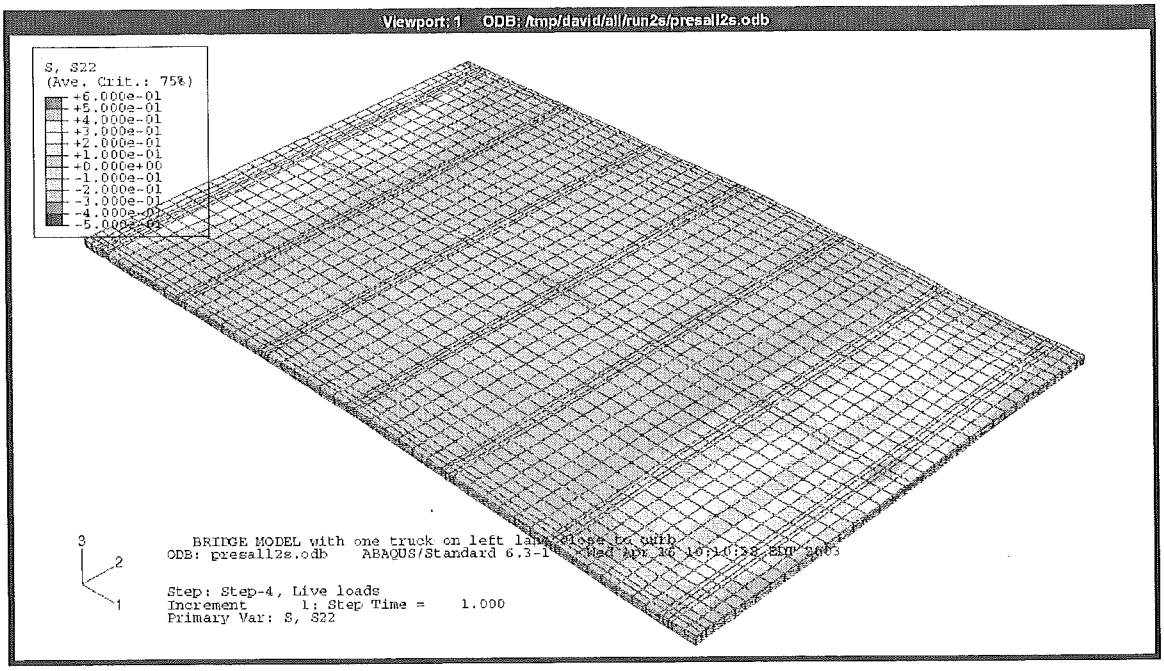

Figure 4-49. Longitudinal stress due to dead load, shrinkage and live load – top surface of the deck

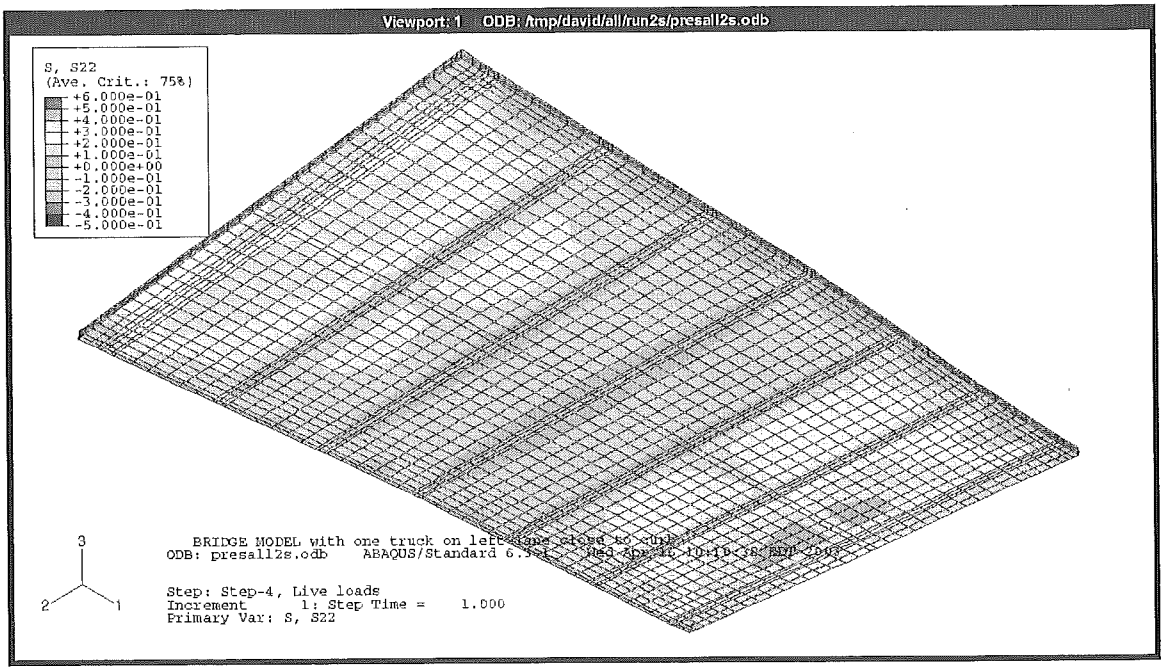

Figure 4-50. Longitudinal stress due to dead load, shrinkage and live load – bottom surface of the deck

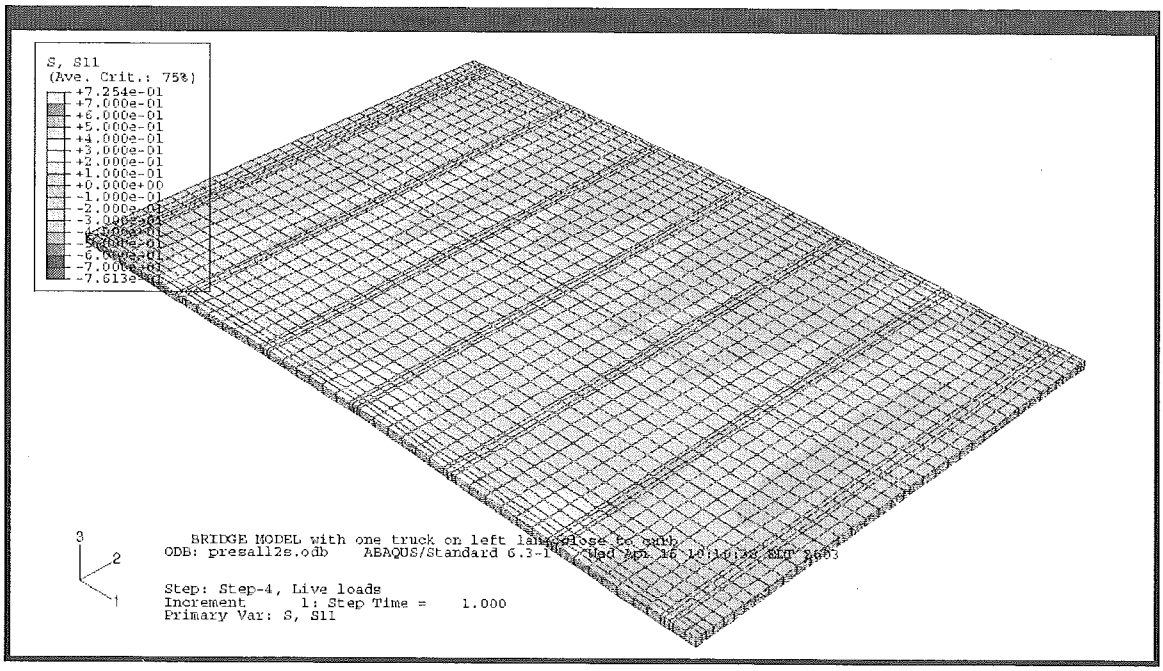

Figure 4-51. Transversal stress due to dead load, shrinkage and live load – top surface of the deck

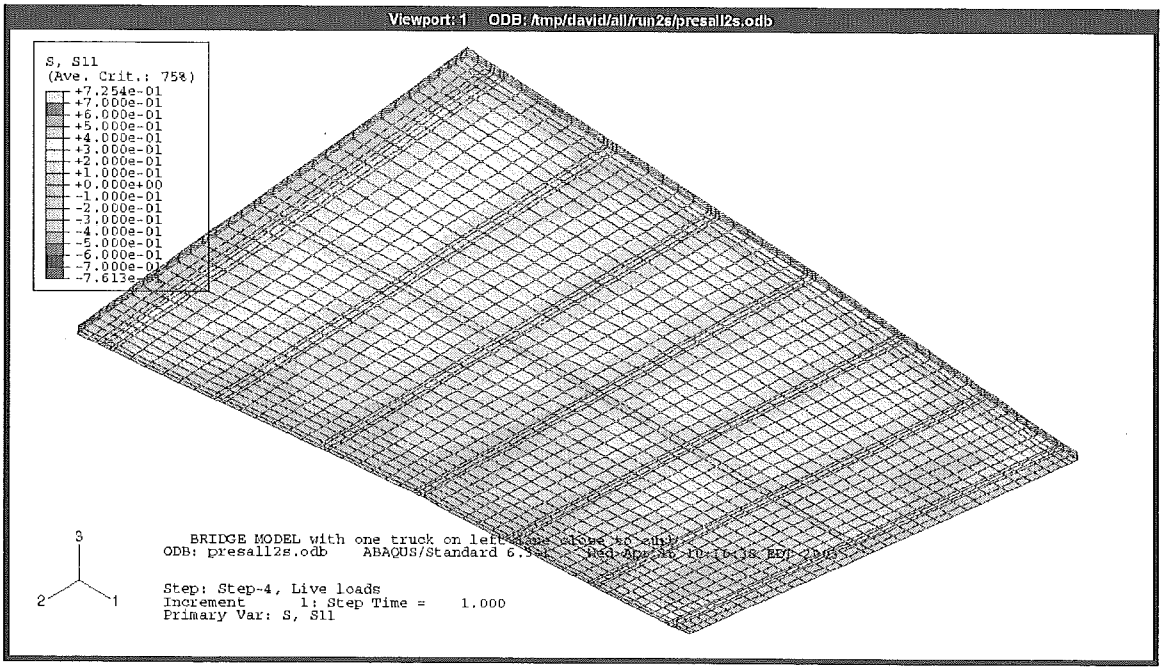

Figure 4-52. Transversal stress due to dead load, shrinkage and live load – bottom surface of the deck

Dead load + shrinkage + 2 trucks (maximum at midspan) position 3

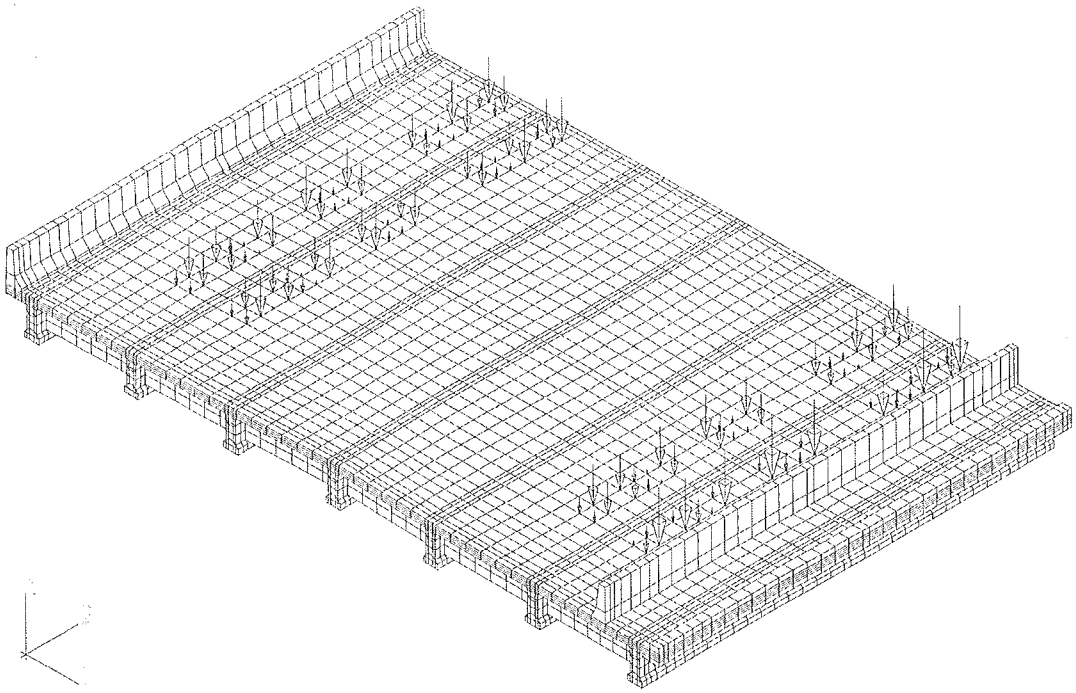

Figure 4-53. Position 3 of the live load (maximum at the midspan)

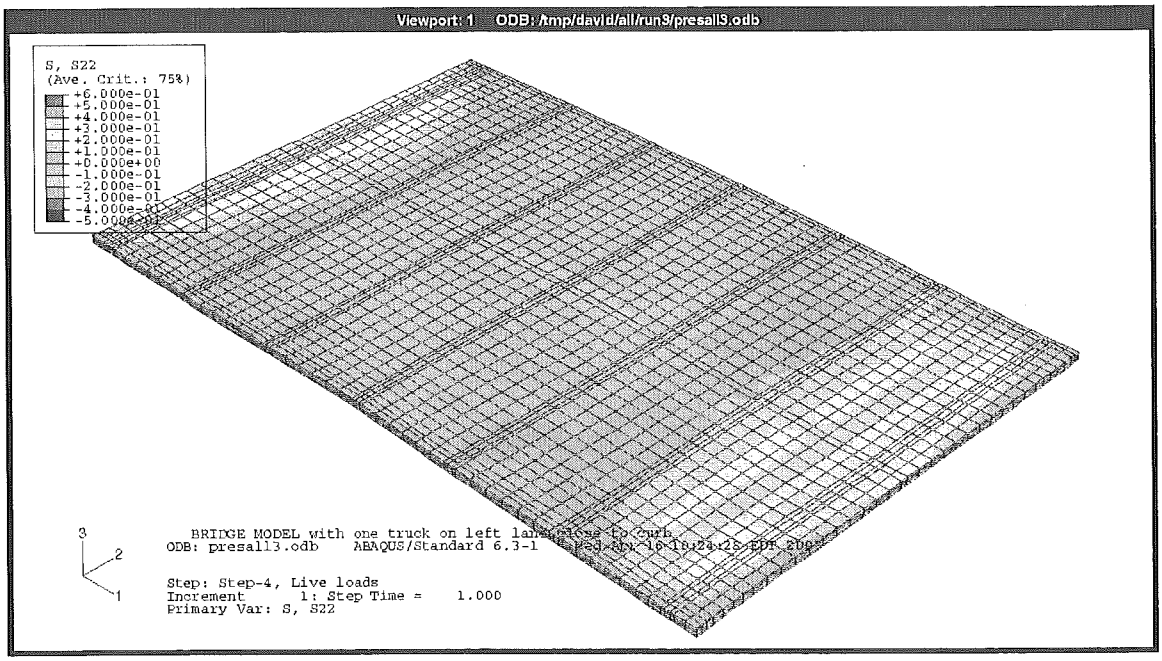

Figure 4-54. Longitudinal stress due to dead load, shrinkage and live load – top surface of the deck

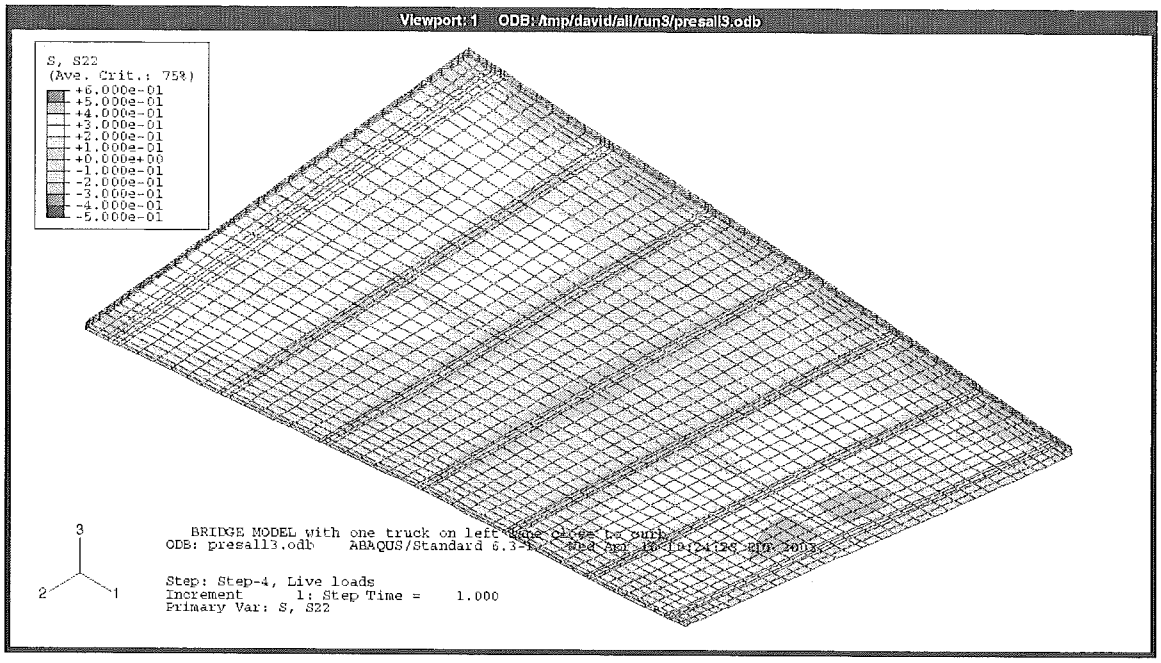

Figure 4-55. Longitudinal stress due to dead load, shrinkage and live load – bottom surface of the deck

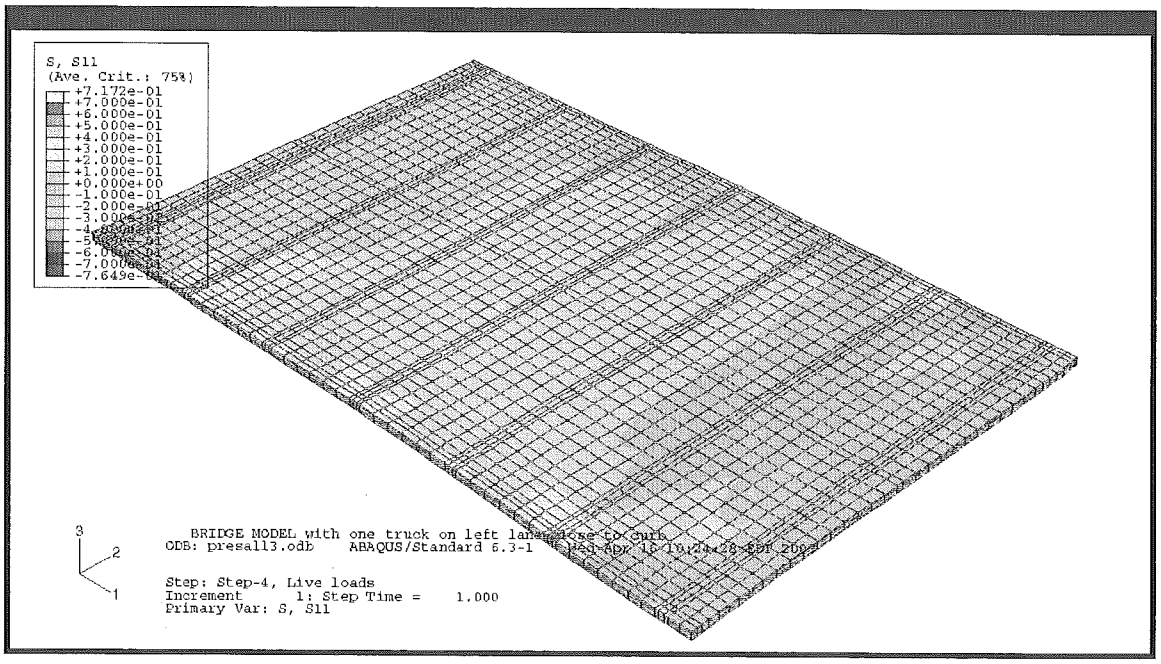

Figure 4-56. Transversal stress due to dead load, shrinkage and live load – top surface of the deck

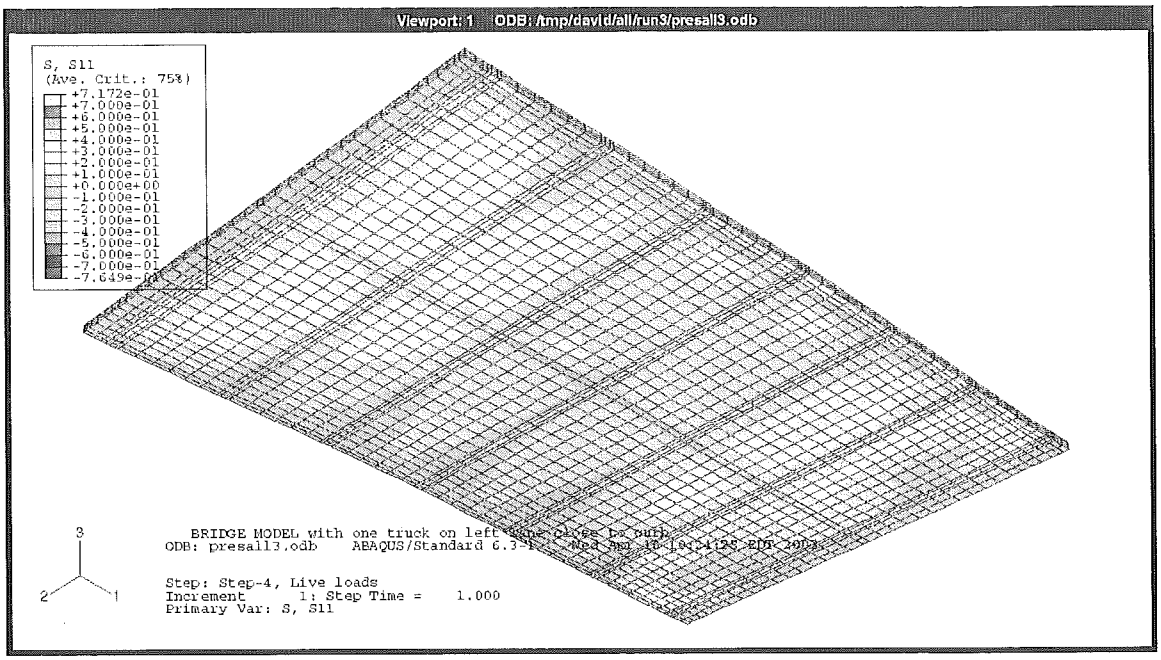

Figure 4-57. Transversal stress due to dead load, shrinkage and live load – bottom surface of the deck

Dead load + shrinkage + 2 trucks (maximum closeness to support) position 3

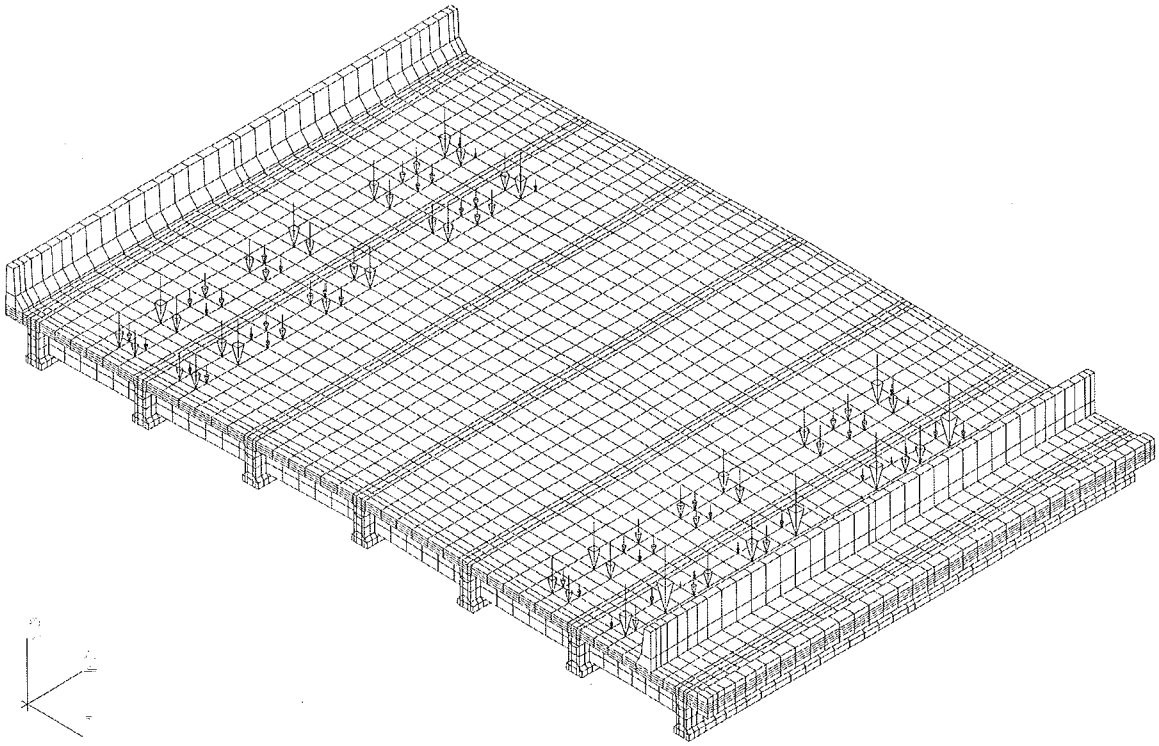

Figure 4-58. Position 3 of the live load (maximum closeness to support)

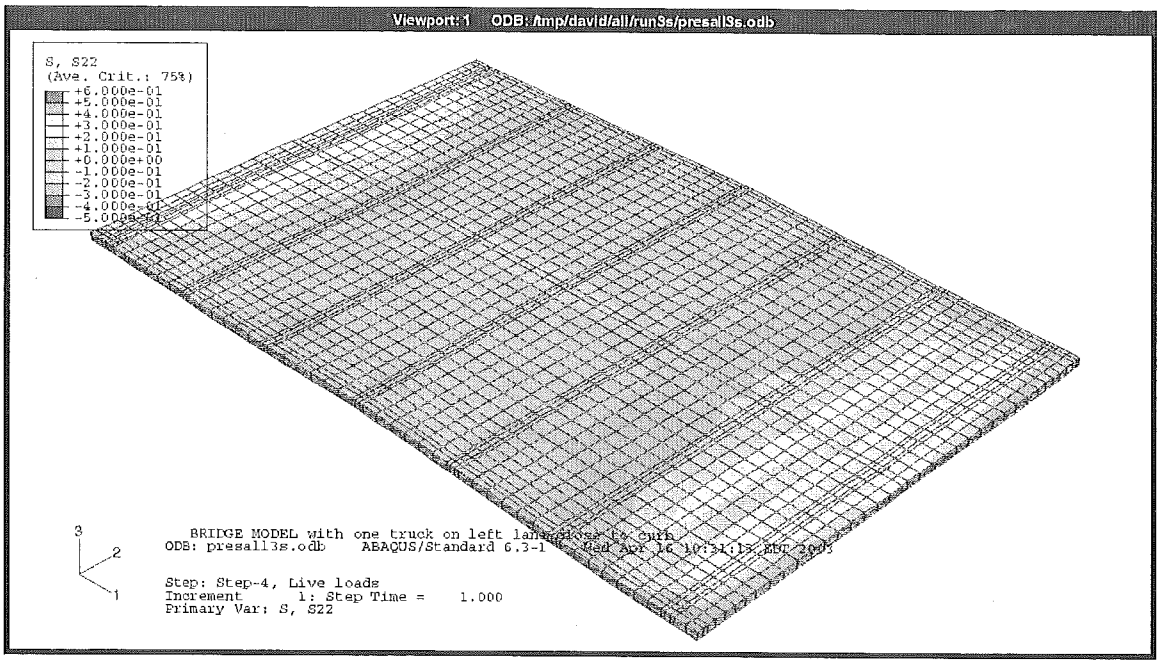

Figure 4-59. Longitudinal stress due to dead load, shrinkage and live load – top surface of the deck

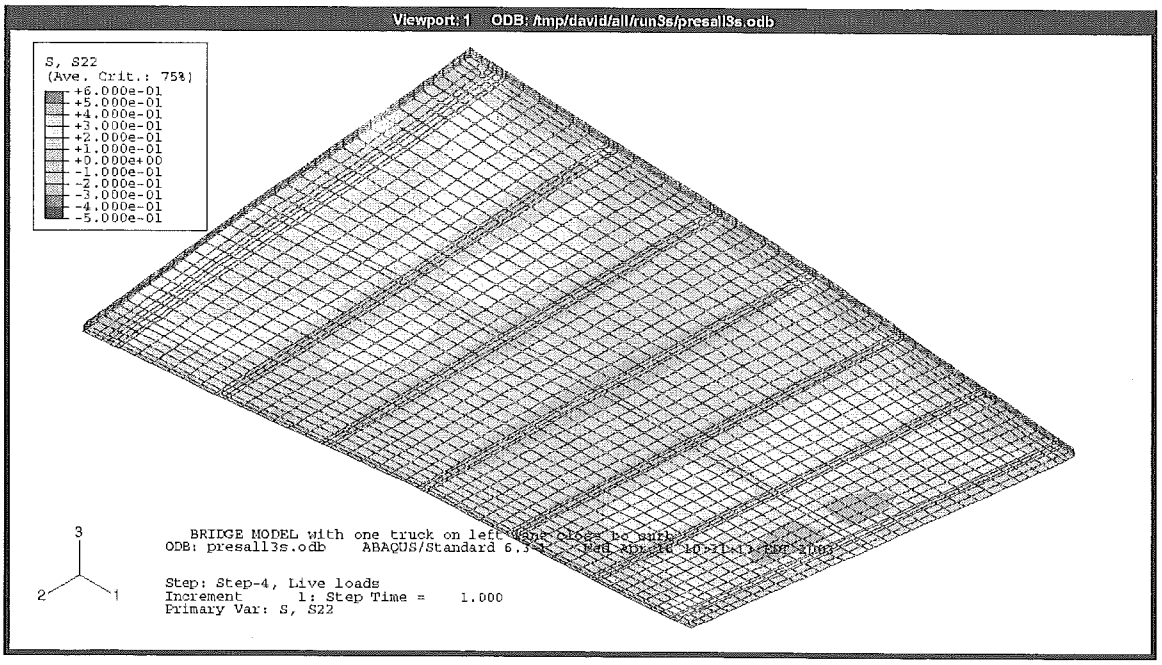

Figure 4-60. Longitudinal stress due to dead load, shrinkage and live load – bottom surface of the deck

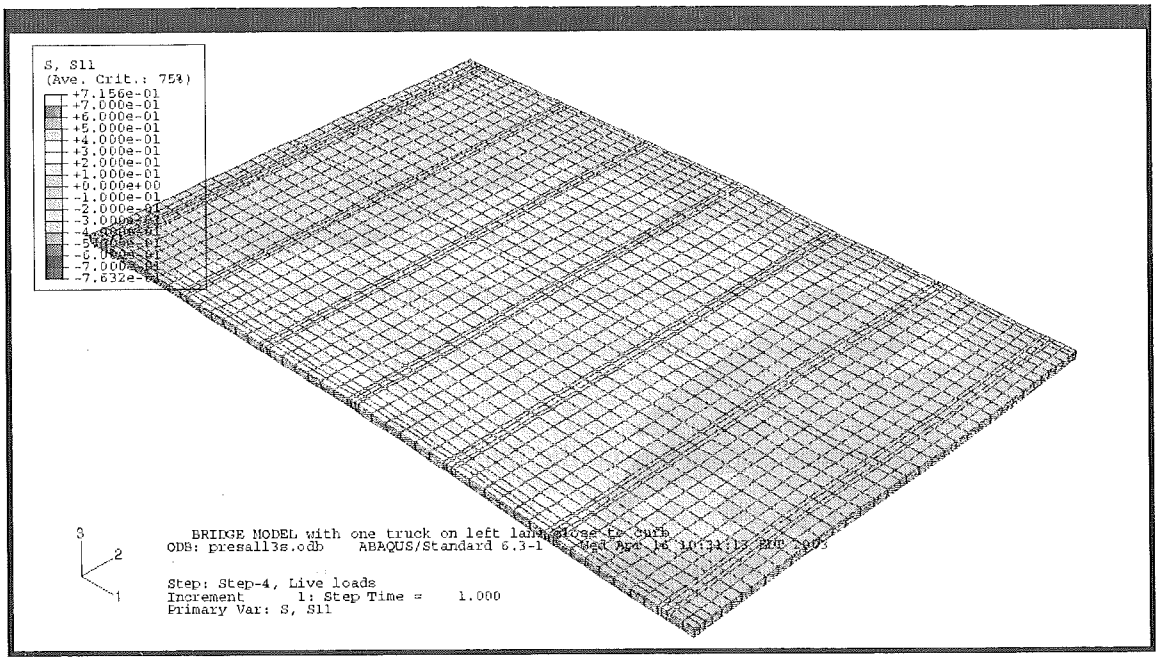

Figure 4-61. Transversal stress due to dead load, shrinkage and live load – top surface of the deck

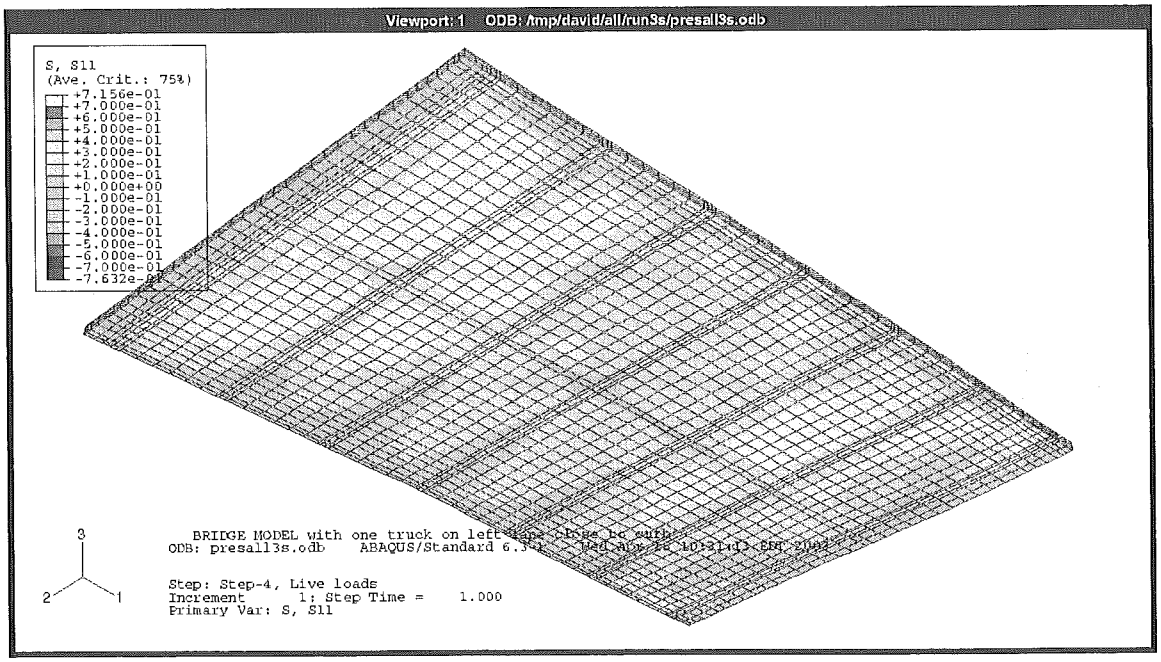

Figure 4-62. Transversal stress due to dead load, shrinkage and live load – bottom surface of the deck

5. CRACKING ANALYSIS OF THE DECK

A cracking analysis of the deck slab is performed based on the calculated maximum stresses. These stresses were determined using the calibrated finite element models of reinforced concrete decks supported on steel or prestressed concrete girders. The load options considered for all stress calculations are discussed in Chapter 4, depending on the deck type (supported on steel or prestressed concrete girders).

The maximum stress values obtained from the finite element analysis are listed below. The results are shown separately for the deck on steel girders and for the deck on prestressed concrete girders. The possibility of crack development is checked for the deck sections by subjecting them to extreme tension stresses. The empirical reinforcement is assumed in both types of decks (on steel girders and prestressed concrete girders). The transversal and longitudinal isotropic reinforcement in the upper and lower sections of the deck is used in the crack analysis. Stress due to dead and live loads is considered in these calculations. Stresses caused by a restrained shrinkage are analyzed separately in Chapter 6.

5.1. Maximum stresses in the deck supported on steel girders

1) Under dead load only (compression is defined as negative, tension is defined as positive)

A small value of stress (compression at the top and tension at the bottom of deck) is caused by the self-weigh of the deck after the removal of the formwork. Additional load is due to concrete barriers.

S22: (longitudinal)

-50 psi (at the top)

20 psi (at the bottom)

S11: (transversal)

-20 psi (at the bottom over the girder)

30 psi (at the top over the girder)

2) Under shrinkage load only

S22: (longitudinal)

-50 psi (at the end)

632 psi (in the corner)

S11: (transversal)

-248 psi (along the top edge)

700 psi (along the bottom edge of the deck and at the bottom over the girder)

3) Under dead load and shrinkage

S22: (longitudinal)

-50 psi (at the end)

650 psi (in the corner top and bottom)

S11: (transversal)

-50 psi (along the top edge)

710 psi (along the bottom edge of the deck and at the bottom over the girder)

4) Under live load only (2 trucks)

S22: (longitudinal)

-315 psi (at the top under the truck – 2 trucks)

85 psi (at the end top and bottom)

S11: (transversal)

-257 psi (at the top under the truck – 2 trucks)

215 psi (at the bottom under the truck – 2 trucks, refer to table at the end of Appendix A)

5) Under dead load, shrinkage and live load (2 trucks)

S22: (longitudinal)

-100 psi (at the top under the truck)

800 psi (in the corner)

S11: (transversal)

-550 psi (at the top over the girder)

765 psi (along the edge of the deck and at the bottom over the girder)

5.2. Maximum stresses in the deck supported on prestressed concrete girders

1) Under dead load only (compression defined as negative, tension defined as positive)

Small values of stress (compression at the top and tension at the bottom of the deck) are caused by the self-weight of the deck after the removal of the formwork. Additional load is due to concrete barriers.

S22: (longitudinal)

-40 psi (at the top, connection diaphragm-girder)

20 psi (at the bottom, connection diaphragm-girder)

S11: (transversal)

-30 psi (at the bottom over girder)

50 psi (at the top over girder)

2) Under shrinkage load only

S22: (longitudinal)

-370 psi (at the bottom over the girder)

535 psi (at the top along the edge of the deck)

S11: (transversal)

-635 psi (at the bottom along the edge of the deck– under haunch)

580 psi (at the end over girder)

3) Under dead load and shrinkage

S22: (longitudinal)

-400 psi (at the end – at the bottom over the girder)

530 psi (along the edge of the deck top and bottom)

S11: (transversal)

-300 psi (at the bottom along the edge of the deck)

615 psi (at the end)

4) Under live load only (2-3 trucks)

S22: (longitudinal)

-250 psi (at the top under the truck – 3trucks)

65 psi (at the bottom in the middle section and along the edge of the deck)

S11: (transversal)

-120 psi (at the top under the truck – 3 trucks)

80 psi (at the bottom under the truck – 3 trucks)

5) Under dead load, shrinkage and live load (2-3 trucks)

S22: (longitudinal)

-500 psi (at the top under the truck – 3 trucks)

600 psi (at the edge of the deck)

S11: (transversal)

-760 psi (along the edge of the deck)

730 psi (at the end)

5.3. Cracking analysis based on the maximum tensile stress in the deck

The finite element models developed in Chapters 2 and 3 used for the stress analysis of the bridge decks were based on a linear-elastic stress-strain relationship for concrete and reinforcing steel. Linear FEM analysis can be considered as a qualitative and quantitative method of the deck behavior evaluation. When tension stresses approach modulus of rupture for concrete, the FEM linear model can produce local extreme stress values, because this model does not account for stress redistribution after cracking.

Results of the stress analysis based on the finite element models show that for decks supported on steel as well as prestressed concrete girders, the maximum tensile stress due to dead and live load is lower than the modulus of rupture for concrete (for $f_c' = 4{,}000$ psi, $f_r = 480$ psi) and this alone cannot cause cracking of the deck.

Tensile stresses caused by restrained shrinkage are significantly higher than the stresses caused by the dead load and live load combined, therefore, additional study of restrained shrinkage is required. Shrinkage stress values, obtained from a linear-elastic finite element analysis, that are higher than the modulus of rupture, indicate a crack initiation. However, the prediction of stress redistribution requires a nonlinear FEM analysis.

The main restraint for shrinkage in the deck is caused by girders in the longitudinal direction. In the transversal direction, shrinkage is restrained by the diaphragms. The analysis of restrained shrinkage was performed for composite section. Stresses caused by shrinkage in the longitudinal direction were calculated by considering the difference between stiffness of the girder and that of the supported deck. These stresses were used in the cracking analysis to find if the longitudinal reinforcement in the top and bottom of the deck, provided by empirical design method, is sufficient for resisting the restrained shrinkage stresses caused by the girders. In the transversal direction, shrinkage stresses were estimated as half of the shrinkage stresses in the longitudinal direction. This is due to a smaller stiffness of the diaphragms compared to girders, and also because the diaphragms spacing is usually larger than the girder spacing.

The analytical model for a restrained shrinkage in the longitudinal direction is presented in Chapter 6.

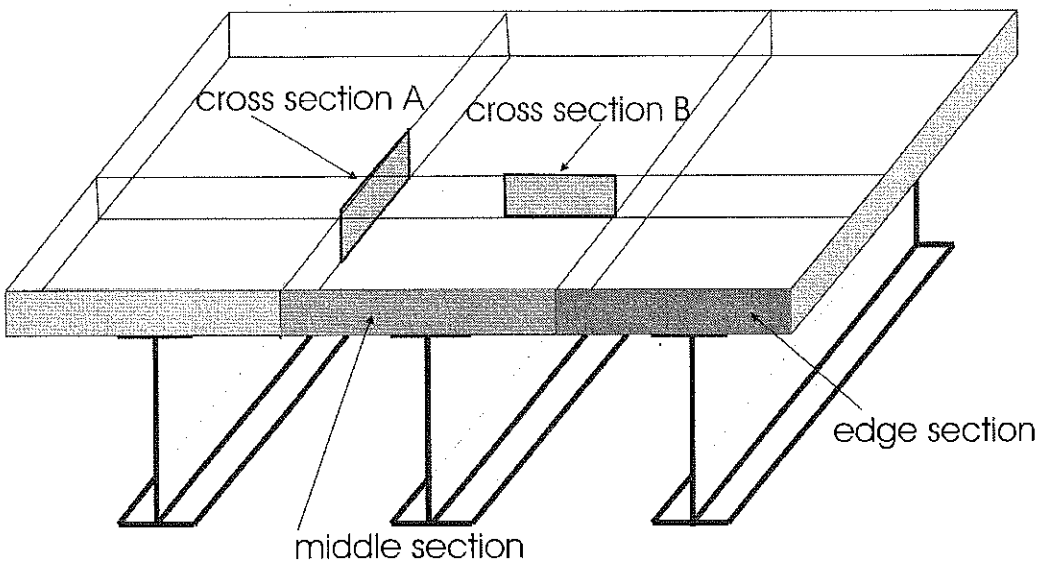

Figure 5-1. Cross sections considered in cracking analysis.

Figure 5-1 presents cross sections of the deck considered in cracking analysis. In general, two sections of the deck were considered: a middle section and an edge section (with overhang) accounting for the difference in longitudinal stresses caused by live load and restrained shrinkage. Cross section A refers to cracking analysis considering stresses acting in transverse direction (section 5.3). Cross section B refers to cracking analysis considering stresses acting in longitudinal direction (sections 6.3.2, 6.3.3 and 6.3.4).

Extreme longitudinal and transverse stresses based on FEM analysis are presented in Table 5-1. These values represent maximum stresses at the top and bottom of the deck in three sections: middle section, edge section and close to supports. For the close to support location only the higher value of stress in the middle section or edge section is listed in the Table.

Table 5-1. Extreme stresses in the deck based on FEM analysis

Section of deck	Localization of stress	Stress due to dead load (psi)		Max stress due to live load (psi)	
		Longitudinal	Transverse	Longitudinal	Transverse
Deck supported on steel girders					
Middle section at midspan	Top	0	0	-315	-257
	Bottom	0	0	-150	215
Edge section at midspan	Top	0	0	85	0
	Bottom	0	0	85	0
Close to support	Top	10	30	85	0
	Bottom	20	-20	85	0
Deck supported on prestressed concrete girders					
Middle section at midspan	Top	0	0	-250	-120
	Bottom	0	0	65	80
Edge section at midspan	Top	0	0	25	0
	Bottom	0	0	65	0
Close to support	Top	-40	50	25	0
	Bottom	20	-30	25	0

Cross section A of the deck supported on steel girders

Cracking analysis is carried out for stresses acting in the transverse direction. Combined stresses caused by dead load, live load and shrinkage acting in the deck cross section A are presented in Figure 5-2.

Stresses used in the analysis were calculated as follows:

Transverse stress due to dead load

Maximum transverse stresses in the deck caused by the dead load are located in cross sections over supports. The stress values are low; on the top, stress is equal to 30 psi in tension, and at the bottom stress is equal to 20 psi in compression (Table 5-1 and S11-max transversal stress due to dead load, p. 117). In the middle cross sections (between girders), these values are close to zero (Table 5-1, Figures 4-3, 4-4).

Transverse stress due to live load

Maximum transverse stresses in deck caused by the live load are located in the middle sections. Maximum tension in deck supported on steel girders is equal to 215 psi at the bottom, and at the same cross section stress on the top is equal to 257 psi in compression

(Table 5-1 and S11- max transversal stress due to live load, p.118). Compression top stress due to live load is not included in cracking analysis because it provides only temporary relief in tensile stress, but bottom tensile stress due to live load is included.

Transverse stress due to restrained shrinkage

Value of transverse stress in deck caused by restrained shrinkage was estimated based on analytical model developed in Chapter 6. Model accounts for restrained shrinkage in composite section. Value of restrained shrinkage stress in transverse direction was assumed to be a half of that calculated in longitudinal direction. For deck supported on steel girders, longitudinal restrained shrinkage stress is presented in Table 6-12. For girder of 60 in depth, stress on the top of the cross section is equal to 397 psi in tension, and at the bottom stress is equal to 504 psi in tension.

Total transverse stress at the bottom = 215 psi (live load) + 0 (dead load) + 504 psi/2 (shrinkage) = 467 psi (in tension)

Total transverse stress on the top = 0 (live load) + 0 (dead load) + 397 psi/2 (shrinkage) = 199 psi (in tension)

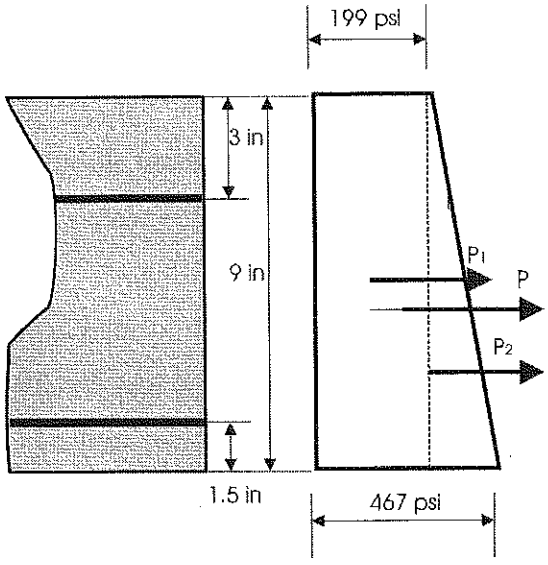

Figure 5-2. Total tensile stresses acting in the transverse direction of the deck (supported on steel girders).

$$\frac{0.467}{x} = \frac{0.199}{9-x} \Rightarrow x = 7.9in$$

$$P_1 = 0.467(7.9)12\frac{1}{2} = 22.14 kip/ft$$

$$P_2 = 0.199(9-7.9)12\frac{1}{2} = 1.31 kip/ft$$

$$P = 23.45 kip/ft$$

The resultant tensile force, P, acting in the deck section has to be balanced by the tensile force in the concrete section, F_t, as well as the force in the top transversal reinforcement, F_{As1}, and the bottom transversal reinforcement, F_{As2}. The assumed empirical reinforcement is: top bars 0.18 in^2/ft, and bottom bars 0.27 in^2/ft (transversally).

Tensile stress at the top and bottom of the deck section is smaller than the modulus of rupture f_r = 0.48 ksi (for concrete strength, f_c' = 4 ksi). Because of this, the whole concrete section can resist the tensile force F_t:

$$F_t = 0.480(9)12 = 51.84 kip/ft$$

This force is larger than the resultant tensile force due to the loads, so transversal empirical reinforcement is sufficient to carry the loads.

Cross section A of the deck supported on prestressed concrete girders

Combined stresses caused by dead load, live load and shrinkage acting in the section are presented in Figure 5-3. Stresses used in the analysis were calculated as follows:

Transverse stress due to dead load

Maximum transverse stresses due to dead load are located in cross sections over support. These stresses are equal to 50 psi in tension on the top, and 30 psi in compression at the bottom (Table 5-1 and S11- max transverse stress due to dead load, p.118). In the middle cross sections these stresses are close to zero (Table 5-1 and Figures 4-27, 4-28).

Transverse stress due to live load

Maximum transverse stresses in deck caused by the live load are located in the middle sections. Maximum tension in deck supported on prestressed concrete girders is equal to 80 psi at the bottom; in the same cross section, stress on the top is equal to 120 psi in compression (Table 5-1 and S11-max transverse stress due to live load, p.119). Compression top stress due to live load is not included in cracking analysis because it

provides only temporary relief in tensile stress, but bottom tensile stress due to live load is included.

Transverse stress due to restrained shrinkage

For deck supported on prestressed concrete girders, longitudinal restrained shrinkage stress is presented in Table 6-4. For AASHTO girder Type II (tested girders) with the depth of 36 in, stress on the top of the cross section is equal to 54 psi in compression, and at the bottom stress is equal to 246 psi in tension.

Total transverse stress on the top = 0 (live load) + 0 (dead load) – 54 psi/2 (shrinkage) = -27 psi (compression)

Total transverse stress at the bottom = 80 psi (live load) + 0 (dead load) + 246 psi/2 (shrinkage) = 203 psi (in tension)

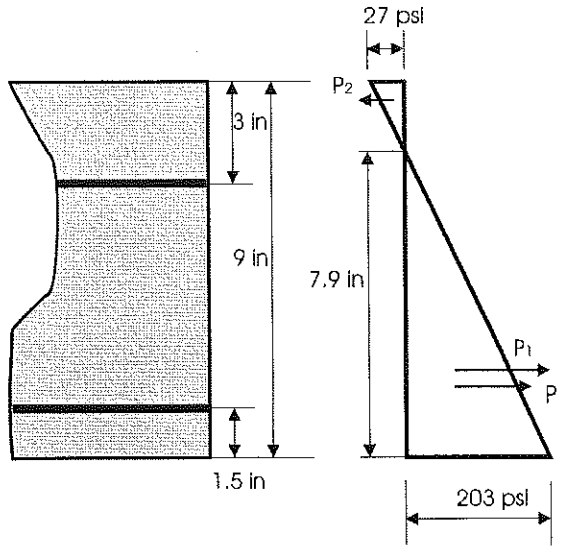

Figure 5-3. Total tensile stresses acting in the transverse direction of the deck (supported on prestressed concrete girders).

$$\frac{0.203}{x} = \frac{0.027}{9-x} \Rightarrow x = 7.9in$$

$$P_1 = 0.203(7.9)12\frac{1}{2} = 9.62 kip/ft$$

$$P_2 = 0.027(9-7.9)12\frac{1}{2} = 0.18 kip/ft$$

$$P = 9.8 kip/ft$$

Similarly as for the deck supported on steel girders, the tensile stresses at the top and the bottom of the deck section are smaller than the modulus of rupture f_r = 0.48 ksi (for concrete strength, f_c'=4 ksi). In fact, the tensile force resisted by concrete section, F_t = 51.84 kip/ft is enough to resist the resultant tensile force, P = 9.8 kip/ft. Transversal empirical reinforcement is enough to carry that load.

6. RESTRAINED SHRINKAGE ANALYSIS OF THE DECK

The shrinkage analysis was performed in two methods. First, a finite element model was developed to calculate accurate values of stresses due to shrinkage. Then, using the results FEM computations, a practical design procedure was formulated.

The finite element models developed for two types of decks (supported on steel girders and prestressed concrete girders) were used to estimate restrained shrinkage stress values and the most critical locations for these stresses. It was assumed that the deck is subjected to a temperature change resulting in stresses equivalent to shrinkage. The second approach allows for a more general analysis, including various stiffness for girders and concrete deck. Three types of prestressed concrete girders were considered, including AASHTO Type II, III and IV (with the depth of 36 in., 45 in. and 54 in. respectively), for girder spans from 40 ft to 80 ft, and eight types of steel girders (with different depth), with spans from 40 ft to 120 ft. Steel and prestressed concrete beam spacing considered in the analysis was equal to 10 ft.

6.1. Shrinkage analysis by the Finite Element Method (FEM)

The shrinkage analysis for concrete deck supported on steel and prestressed concrete girders was performed using the FEM models developed for these two types of bridge superstructures. The effect of shrinkage was modeled by applying a temperature change that results in an equivalent strain change. The strains and stresses due to shrinkage were considered at the top and at bottom of the slab. The obtained values indicate that there is a possibility of crack initiation due to shrinkage.

The slab was subjected to contraction strain of 2.1×10^{-4}. Figure 6-1 presents a typical behavior of concrete exposed to strain-control tension test. The tension stress value is divided by the modulus of rupture for concrete. Concrete exhibits a linear behavior up to $\varepsilon_{el} = 8.4 \times 10^{-5}$; and beyond this strain (peak on the graph), the relationship between stress and strain is nonlinear (post-critical behavior).

A typical relationship between shrinkage strain and time, shown in Figure 6-2 was used in the finite element method analysis. The strain value of 2×10^{-4} is reached after about 3

months. The scenario of shrinkage crack development is based on the FEM analysis of principal stress values and stress pattern in the deck. The fact that the tension stress is higher than the modulus of rupture for concrete indicates the crack initiation, and the direction of the principal stress shows the crack propagation. The sequence of developing shrinkage cracks in the deck due to increasing shrinkage strains is as follows:

(1) diagonal cracks close to the support occur first

(2) transversal cracks close to the diaphragms

(3) finally, major transversal cracks spaced at about 5 to 7 feet occur.

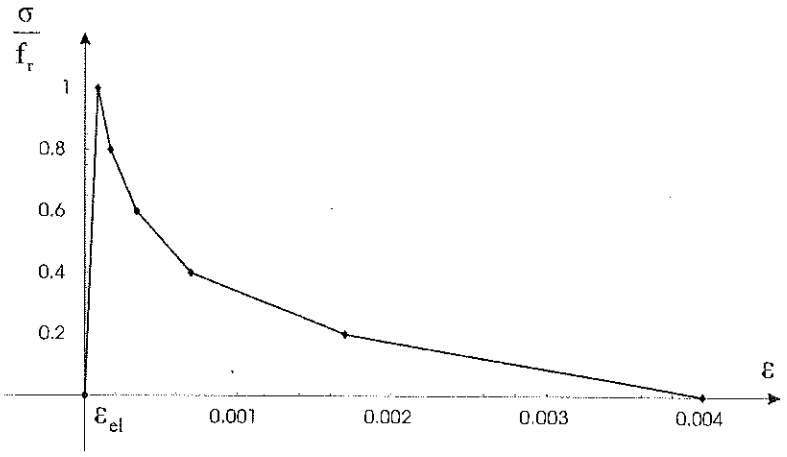

Figure 6-1. Typical concrete behavior in tension (strain-control test); elastic strain, $\varepsilon_{el} = 8.4 \times 10^{-5}$.

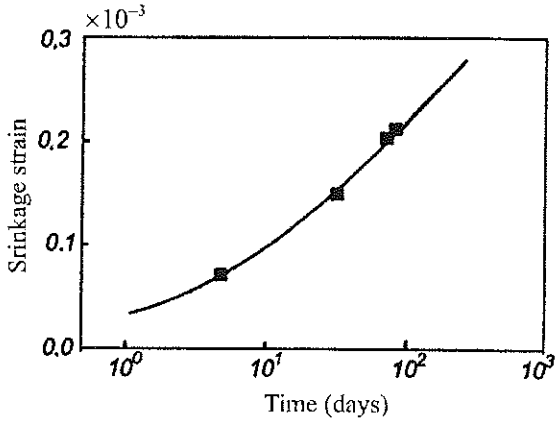

Figure 6-2. Typical shrinkage development as a function of time for the structural concrete; after McDonald (1972).

The resulting longitudinal and transversal stresses on the top and bottom of the deck caused by restrained shrinkage are presented in Appendix C. The extreme values of shrinkage stress are listed in Chapter 5.

Restrained shrinkage stresses in the deck are strongly affected by the type of material and stiffness of supporting girders. In newly constructed decks supported on prestressed concrete girders, only a fraction of the total shrinkage will develop in the deck, because concrete girders will be exposed to shrinkage at the same time as the deck. In fact, even though stiffness of concrete girders is larger than that of steel girders, the restriction caused by supporting concrete beams is smaller.

6.2. Practical longitudinal shrinkage analysis procedure

To account for various parameters influencing the restrained shrinkage in decks, there is a need to develop an analytical model for the calculation of shrinkage stresses in composite sections.

The distribution of stress and strain in a composite section due to restrained shrinkage is presented in Figure 6-3a. The analysis of the shrinkage effect in a composite girder section is performed for a general case with a vertical axis of symmetry. However, for simplicity, in Figure 6-3b, only rectangular cross-sections of the deck and girder are shown. Notation used in the analysis is shown in Figure 6-3b. The strains and stresses and their resultants are also shown. For non- rectangular cross-sections, the cross-section area and moment of inertia will have to be derived. In Figure 6-3b, c_D and c_G denote the center of gravity of the deck and girder, respectively.

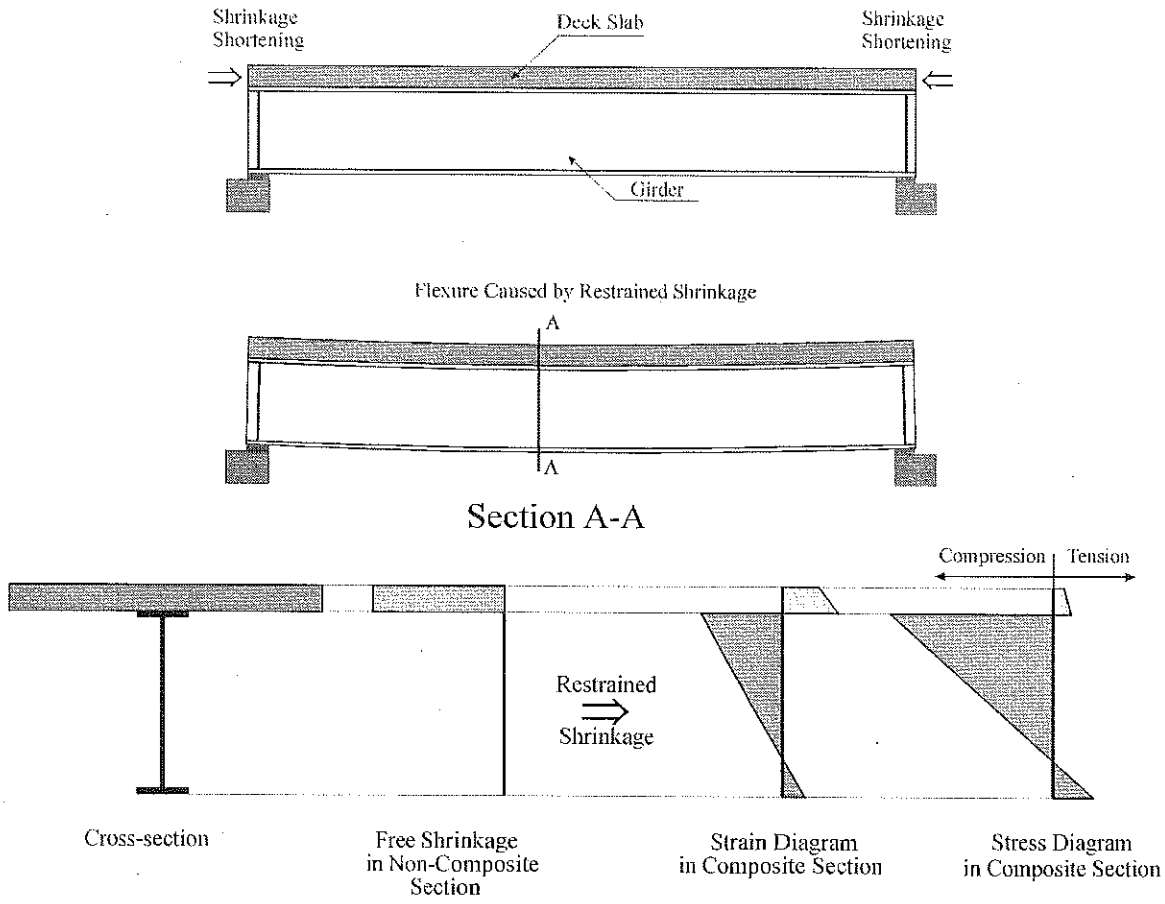

Figure 6-3a. Stress and strain in a composite section due to restrained shrinkage.

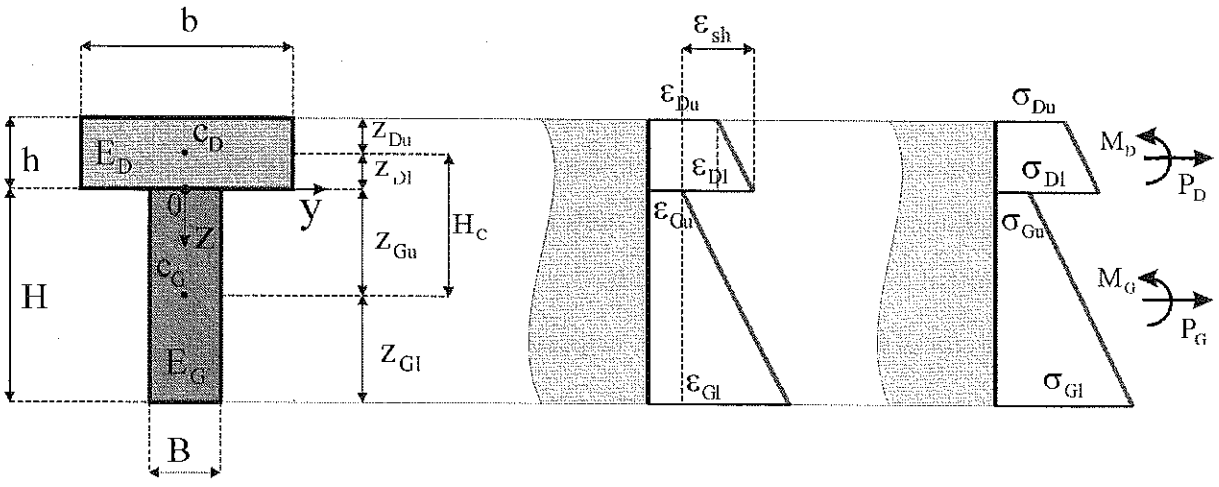

Figure 6-3b. Typical case of shrinkage strain and stress in a composite section.

Notation:

B	=	girder width
b	=	effective deck width
E_D	=	modulus of elasticity of the concrete in the deck
E_G	=	modulus of elasticity of the girder (concrete or steel)
H	=	depth of the girder
H_C	=	distance between gravity centers of the deck and girder
h	=	thickness of the deck
M_D	=	moment due to restrained shrinkage acting in the deck
M_G	=	moment due to restrained shrinkage acting in the girder
P_D	=	normal force due to restrained shrinkage acting in the deck
P_G	=	normal force due to restrained shrinkage acting in the girder
z_{Du}	=	distance from the top to the gravity center of the deck slab
z_{D1}	=	distance from the gravity center to the bottom of the deck slab
z_{Gu}	=	distance from the top to the gravity center of the girder
z_{G1}	=	distance from the gravity center to the bottom of the deck girder
ε_{Du}	=	strain at the top of the deck slab due to restrained shrinkage
ε_{D1}	=	strain at the bottom of the deck slab due to restrained shrinkage
ε_{Gu}	=	strain at the top of the girder due to restrained shrinkage
ε_{G1}	=	strain at the bottom of the girder due to restrained shrinkage
ε_{sh}	=	free shrinkage strain in the deck slab
σ_{Du}	=	stress at the top of the deck slab due to restrained shrinkage
σ_{D1}	=	stress at the bottom of the deck slab due to restrained shrinkage
σ_{Gu}	=	stress at the top of the girder due to restrained shrinkage
σ_{G1}	=	stress at the bottom of the girder due to restrained shrinkage

Basic equations

The relationships between the strains in the section and the depth of the slab and girder can be obtained using the strain diagram shown in Figure 6-3b.

$$\varepsilon_{Gu} + \varepsilon_{sh} = \varepsilon_{Dl}, \tag{6-1}$$

$$\frac{\varepsilon_{Dl} - \varepsilon_{Du}}{h} = \frac{\varepsilon_{Gl} - \varepsilon_{Gu}}{H}. \tag{6-2}$$

Using Hooke's law (linear elastic behavior of materials) the relationship between the stresses and strains in the upper and lower fibers of the deck and girder is derived,

$$\sigma_{Du} = E_D \varepsilon_{Du}, \tag{6-3}$$

$$\sigma_{Dl} = E_D \varepsilon_{Dl}, \tag{6-4}$$

$$\sigma_{Gu} = E_G \varepsilon_{Gu}, \tag{6-5}$$

$$\sigma_{Gl} = E_G \varepsilon_{Gl}. \tag{6-6}$$

Forces caused by shrinkage result in non-mechanical deformations in the bridge. In this case, self-equilibrated forces are induced in the bridge cross-section. The equilibrium equations can be formulated as follows,

$$P_D + P_G = 0, \tag{6-7}$$

$$M_D + M_G + P_G z_{Gu} - P_D z_{Dl} = 0, \tag{6-8}$$

where

$$P_D = \frac{A_D}{h}\left(\sigma_{Dl} z_{Du} + \sigma_{Du} z_{Dl}\right), \tag{6-9}$$

$$P_G = \frac{A_G}{H}\left(\sigma_{Gl} z_{Gu} + \sigma_{Gu} z_{Gl}\right), \tag{6-10}$$

$$M_D = \frac{I_D}{h}\left(\sigma_{Dl} - \sigma_{Du}\right), \tag{6-11}$$

$$M_G = \frac{I_G}{H}\left(\sigma_{Gl} - \sigma_{Gu}\right). \tag{6-12}$$

In the case of two rectangular cross-sections: $A_D = bh$, $A_G = BH$, $I_D = \frac{bh^3}{12}$, $I_G = \frac{BH^3}{12}$. For non-rectangular cross-sections, the formulas for the calculation of the areas and moments of inertia are different.

The newly introduced notation for a geometrical distance between the centers of gravity of the deck and girder sections and, accordingly, the notation for the stiffness for axial load and flexure of the deck and girder is as follows:

$$\begin{aligned} H_C &= z_{Dl} + z_{Gu}, \\ B_D &= E_D A_D, \\ B_G &= E_G A_G, \\ D_D &= E_D I_D, \\ D_G &= E_G I_G, \end{aligned} \tag{6-13}$$

Using equations (6-3) to (6-6) and (6-9) to (6-12), the solutions are found for Eq. (6-1), (6-2), (6-7) and (6-8),

$$\begin{aligned} P_D &= \frac{\varepsilon_{sh}}{\frac{1}{B_D}+\frac{1}{B_G}+\frac{H_C^2}{D_D+D_G}}, \\ M_D &= \frac{\varepsilon_{sh}}{\frac{H_C}{D_D}+\frac{1}{H_C}\left(1+\frac{D_G}{D_D}\right)\left(\frac{1}{B_D}+\frac{1}{B_G}\right)}, \\ P_G &= \frac{-\varepsilon_{sh}}{\frac{1}{B_D}+\frac{1}{B_G}+\frac{H_C^2}{D_D+D_G}}, \\ M_G &= \frac{\varepsilon_{sh}}{\frac{H_C}{D_G}+\frac{1}{H_C}\left(1+\frac{D_D}{D_G}\right)\left(\frac{1}{B_D}+\frac{1}{B_G}\right)}, \end{aligned} \tag{6-14}$$

or in rewritten form

$$\begin{aligned} P_D &= \frac{\varepsilon_{sh} B_D B_G (D_D + D_G)}{(B_D + B_G)(D_D + D_G) + H_C^2 B_D B_G}, \\ M_D &= \frac{\varepsilon_{sh} H_C B_D B_G D_D}{(B_D + B_G)(D_D + D_G) + H_C^2 B_D B_G}, \\ P_G &= \frac{-\varepsilon_{sh} B_D B_G (D_D + D_G)}{(B_D + B_G)(D_D + D_G) + H_C^2 B_D B_G}, \\ M_G &= \frac{\varepsilon_{sh} H_C B_D B_G D_G}{(B_D + B_G)(D_D + D_G) + H_C^2 B_D B_G}, \end{aligned} \tag{6-15}$$

Stresses in the upper and lower fibers can be calculated using the following formulas:

$$\sigma_{Du} = \frac{P_D}{A_D} - \frac{z_{Du} M_D}{I_D},$$
$$\sigma_{Dl} = \frac{P_D}{A_D} + \frac{z_{Dl} M_D}{I_D},$$
$$\sigma_{Gu} = \frac{P_G}{A_G} - \frac{z_{Gu} M_G}{I_G},$$
$$\sigma_{Gl} = \frac{P_G}{A_G} + \frac{z_{Gl} M_G}{I_G}. \qquad (6\text{-}16)$$

Strains in the upper and lower fibers can be calculated using the formulas in (6-3) to (6-6).

Stresses and strains in the deck slab caused by restrained shrinkage, calculated using the presented analytical model were decreased by 15 % due to uneven distribution along the cross section of the deck. This observation is based on the results obtained from the FEM model for restrained shrinkage.

6.2.1. Restrained shrinkage analysis of the reinforced concrete deck supported on AASHTO Girders (Type II, III and IV with the depth of 36 in, 45 in and 54 in respectively), spaced at 10 ft.

The analysis is performed using the analytical model for restrained shrinkage in a composite section, presented in Section 6.2. A constant deck thickness of 9 in and an empirical reinforcement are assumed. The maximum free shrinkage, ε_{sh} = 0.00035, is calculated for perfect curing conditions, humidity H = 70%, and the time of service being 30 years (according to AASHTO LRFD Code, Section 5.4.2.3.3).
In a case when perfect curing is not available, the code provision requires a 20% increase of the final shrinkage strain. The analysis for this increased shrinkage is also performed.

The maximum free shrinkage is assumed in the analysis for decks supported on steel girders. Because prestressed concrete girders are subjected to shrinkage from the moment when they are manufactured, only a fraction of the total shrinkage is applied to the deck. Depending on the age of the girders at the moment of pouring the slab, the part of total

shrinkage is applied to the deck as follows (base on shrinkage development diagram, Figure 6-4):

0.4 ε_{sh} - after 3 months from the date when a girder is manufactured
0.5 ε_{sh} - after 6 months from the date when a girder is manufactured
0.6 ε_{sh} - after 8 months from the date when a girder is manufactured
1.0 ε_{sh} – for the case of existing deck replacement

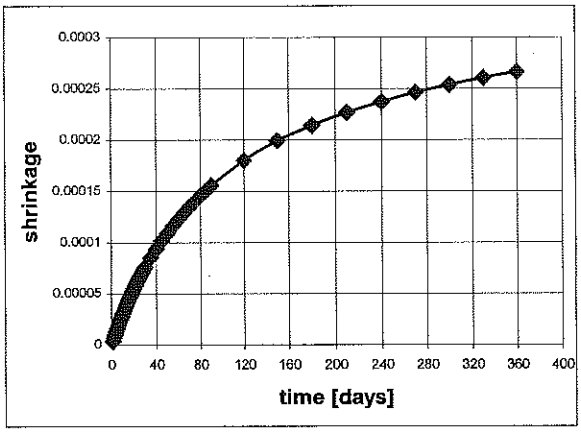

Figure 6-4. Shrinkage development diagram (AASHTO LRFD, Equation 5.4.2.3.3-1).

Three types of AASHTO Girders are investigated depending on the span length (40ft, 60ft and 80 ft).

The analytical model, developed to calculate restrained shrinkage in the composite section, accounts for the difference in the deck and girder stiffness, and the distance between the centers of gravity of the cross-sections of the deck and girder. Stresses caused by restrained shrinkage are calculated for the middle part of the deck (distance between girders is 10 ft). For the edge of the deck, there is a smaller difference between the deck and girder stiffness that causes higher shrinkage stresses. In this study, these shrinkage stresses are also calculated assuming a 3 ft overhang of the deck.

Tension stresses due to restrained shrinkage in the deck slab can be increased by unloading after the removal of the formwork and reduction of the deck weight due to the drying of concrete. Tables 6-1, 6-2, 6-5 and 6-6, contain the stress values in the deck

caused by restrained shrinkage (at the top, σ_{Du}, and bottom, σ_{D1}, of the deck). Tables 6-3 and 6-7 contain the stress after the removal of the formwork and reduction of weight due to the drying of concrete (at the top, σ_1, and bottom, σ_2, of the deck). The total stress at the top and bottom of the deck due to these two causes is presented in Table 6-4 for the middle part of the deck, and in Table 6-8 for the edge part of the deck. The weight of formwork is taken as 10 lb/ft^2 and a 5% weight loss of the deck slab due to the drying of concrete is assumed in calculations.

Table 6-1. Restrained shrinkage stress and strain in the middle of the deck supported on prestressed concrete girders, calculated after 30 years, assuming perfect curing conditions ($\varepsilon_{sh} = 0.00035$)

Shrinkage strain applied to deck	Span Length (ft)	Type of Girder	Top Stress σ_{Du} (ksi)	Bottom Stress σ_{D1} (ksi)	Top Strain ε_{Du}	Bottom Strain ε_{D1}
0.4 x ε_{sh}	40	Type II	-0.026	0.097	-6.71 x 10^{-6}	25.23 x 10^{-6}
0.4 x ε_{sh}	60	Type III	0.017	0.120	4.50x 10^{-6}	31.14 x 10^{-6}
0.4 x ε_{sh}	80	Type IV	0.070	0.151	18.16 x 10^{-6}	39.33 x 10^{-6}
0.5 x ε_{sh}	40	Type II	-0.032	0.122	-8.38 x 10^{-6}	31.54 x 10^{-6}
0.5 x ε_{sh}	60	Type III	0.021	0.1750	5.62 x 10^{-6}	38.92 x 10^{-6}
0.5 x ε_{sh}	80	Type IV	0.088	0.190	22.70 x 10^{-6}	49.16 x 10^{-6}
0.6 x ε_{sh}	40	Type II	-0.039	0.145	-10.06 x 10^{-6}	37.84 x 10^{-6}
0.6 x ε_{sh}	60	Type III	0.026	0.180	6.74 x 10^{-6}	46.71 x 10^{-6}
0.6 x ε_{sh}	80	Type IV	0.105	0.227	27.23 x 10^{-6}	58.99 x 10^{-6}
1.0 x ε_{sh}	40	Type II	-0.065	0.243	-16.77 x 10^{-6}	63.07 x 10^{-6}
1.0 x ε_{sh}	60	Type III	0.015	0.259	4.07 x 10^{-6}	67.32 x 10^{-6}
1.0 x ε_{sh}	80	Type IV	0.096	0.292	24.99 x 10^{-6}	75.79 x 10^{-6}

Note:
(-) sign means compression

Table 6-2. Restrained shrinkage stress and strain in the middle of the deck supported on prestressed concrete girders, calculated after 30 years, assuming imperfect curing conditions (ε_{sh} = 1.2 x 0.00035)

Shrinkage strain applied to deck	Span Length (ft)	Type of Girder	Top Stress σ_{Du} (ksi)	Bottom Stress σ_{D1} (ksi)	Top Strain ε_{Du}	Bottom Strain ε_{D1}
0.4 x ε_{sh}	40	Type II	-0.031	0.116	-8.05×10^{-6}	30.28×10^{-6}
0.4 x ε_{sh}	60	Type III	0.020	0.144	5.40×10^{-6}	37.37×10^{-6}
0.4 x ε_{sh}	80	Type IV	0.084	0.182	21.79×10^{-6}	47.19×10^{-6}
0.5 x ε_{sh}	40	Type II	-0.039	0.145	10.06×10^{-6}	37.84×10^{-6}
0.5 x ε_{sh}	60	Type III	0.026	0.180	6.74×10^{-6}	46.71×10^{-6}
0.5 x ε_{sh}	80	Type IV	0.105	0.227	27.23×10^{-6}	58.99×10^{-6}
0.6 x ε_{sh}	40	Type II	-0.047	0.175	-12.08×10^{-6}	45.41×10^{-6}
0.6 x ε_{sh}	60	Type III	0.031	0.216	8.09×10^{-6}	56.05×10^{-6}
0.6 x ε_{sh}	80	Type IV	0.126	0.272	32.68×10^{-6}	70.79×10^{-6}
1.0 x ε_{sh}	40	Type II	-0.077	0.292	-20.13×10^{-6}	75.65×10^{-6}
1.0 x ε_{sh}	60	Type III	0.018	0.311	4.88×10^{-6}	80.78×10^{-6}
1.0 x ε_{sh}	80	Type IV	0.115	0.350	29.99×10^{-6}	90.95×10^{-6}

Note:
(-) sign means compression

Table 6-3. Stresses in the middle of the deck supported on prestressed concrete girders unloaded after removal of the formwork and reduction of weight due to drying of concrete

Span Length (ft)	Type of Girder	Top Stress σ_1 (ksi)	Bottom Stress σ_2 (ksi)
40	Type II	0.011	0.003
60	Type III	0.017	0.007
80	Type IV	0.023	0.013

Table 6-4. Total stresses in the middle of the deck supported on prestressed concrete girders caused by restrained shrinkage increased due to unloading after the removal of the formwork and reduction of weight due to drying of concrete

Shrinkage strain applied to deck	Span Length (ft)	Type of Girder	ε_{sh} = 0.00035		ε_{sh} = 1.2 x 0.00035	
			Top Stress (ksi)	Bottom Stress (ksi)	Top Stress (ksi)	Bottom Stress (ksi)
0.4 x ε_{sh}	40	Type II	-0.015	0.100	-0.020	0.119
0.4 x ε_{sh}	60	Type III	0.034	0.127	0.037	0.151
0.4 x ε_{sh}	80	Type IV	0.093	0.164	0.107	0.195
0.5 x ε_{sh}	40	Type II	-0.021	0.125	-0.028	0.148
0.5 x ε_{sh}	60	Type III	0.038	0.182	0.043	0.187
0.5 x ε_{sh}	80	Type IV	0.111	0.203	0.128	0.240
0.6 x ε_{sh}	40	Type II	-0.028	0.148	-0.036	0.178
0.6 x ε_{sh}	60	Type III	0.043	0.187	0.048	0.223
0.6 x ε_{sh}	80	Type IV	0.128	0.240	0.149	0.285
1.0 x ε_{sh}	40	Type II	-0.054	0.246	-0.066	0.295
1.0 x ε_{sh}	60	Type III	0.032	0.266	0.035	0.318
1.0 x ε_{sh}	80	Type IV	0.119	0.305	0.138	0.363

Note:
(-) sign means compression

Table 6-5. Restrained shrinkage stress in the edge part of deck supported on prestressed concrete girders, calculated after 30 years, assuming perfect curing conditions (ε_{sh} = 0.00035)

Shrinkage strain applied to deck	Span Length (ft)	Type of Girder	Top Stress σ_{Du} (ksi)	Bottom Stress σ_{D1} (ksi)
0.4 x ε_{sh}	40	Type II	-0.004	0.114
0.4 x ε_{sh}	60	Type III	0.056	0.150
0.4 x ε_{sh}	80	Type IV	0.123	0.195
0.5 x ε_{sh}	40	Type II	-0.005	0.143
0.5 x ε_{sh}	60	Type III	0.070	0.187
0.5 x ε_{sh}	80	Type IV	0.154	0.242
0.6 x ε_{sh}	40	Type II	-0.007	0.171
0.6 x ε_{sh}	60	Type III	0.084	0.225
0.6 x ε_{sh}	80	Type IV	0.184	0.291
1.0 x ε_{sh}	40	Type II	-0.011	0.285
1.0 x ε_{sh}	60	Type III	0.048	0.285
1.0 x ε_{sh}	80	Type IV	0.138	0.326

Note:
(-) sign means compression

Table 6-6. Restrained shrinkage stress in the edge part of deck supported on prestressed concrete girders, calculated after 30 years, assuming imperfect curing conditions (ε_{sh} = 1.2 x 0.00035)

Shrinkage strain applied to deck	Span Length (ft)	Type of Girder	Top Stress σ_{Du} (ksi)	Bottom Stress σ_{Dl} (ksi)
0.4 x ε_{sh}	40	Type II	-0.005	0.137
0.4 x ε_{sh}	60	Type III	0.067	0.180
0.4 x ε_{sh}	80	Type IV	0.147	0.232
0.5 x ε_{sh}	40	Type II	-0.007	0.171
0.5 x ε_{sh}	60	Type III	0.084	0.225
0.5 x ε_{sh}	80	Type IV	0.184	0.291
0.6 x ε_{sh}	40	Type II	-0.008	0.181
0.6 x ε_{sh}	60	Type III	0.100	0.269
0.6 x ε_{sh}	80	Type IV	0.221	0.349
1.0 x ε_{sh}	40	Type II	-0.013	0.342
1.0 x ε_{sh}	60	Type III	0.058	0.342
1.0 x ε_{sh}	80	Type IV	0.166	0.391

Note:
(-) sign means compression

Table 6-7. Stresses in the edge part of deck supported on prestressed concrete girders unloaded after removal of the formwork and reduction of weight due to drying of concrete

Span Length (ft)	Type of Girder	Top Stress σ_1 (ksi)	Bottom Stress σ_2 (ksi)
40	Type II	0.019	0.010
60	Type III	0.025	0.013
80	Type IV	0.032	0.021

Table 6-8. Total stresses in the edge part of deck supported on prestressed concrete girders caused by restrained shrinkage, unloading after the removal of the formwork and reduction of weight due to drying of concrete

Shrinkage strain applied to deck	Span Length (ft)	Type of Girder	$\varepsilon_{sh} = 0.00035$		$\varepsilon_{sh} = 1.2 \times 0.00035$	
			Top Stress (ksi)	Bottom Stress (ksi)	Top Stress (ksi)	Bottom Stress (ksi)
0.4 x ε_{sh}	40	Type II	0.015	0.124	0.014	0.147
0.4 x ε_{sh}	60	Type III	0.081	0.163	0.092	0.193
0.4 x ε_{sh}	80	Type IV	0.155	0.216	0.179	0.253
0.5 x ε_{sh}	40	Type II	0.014	0.153	0.012	0.181
0.5 x ε_{sh}	60	Type III	0.095	0.200	0.109	0.238
0.5 x ε_{sh}	80	Type IV	0.186	0.263	0.216	0.312
0.6 x ε_{sh}	40	Type II	0.012	0.181	0.011	0.191
0.6 x ε_{sh}	60	Type III	0.109	0.238	0.125	0.282
0.6 x ε_{sh}	80	Type IV	0.216	0.312	0.253	0.370
1.0 x ε_{sh}	40	Type II	0.008	0.295	0.006	0.352
1.0 x ε_{sh}	60	Type III	0.073	0.298	0.083	0.355
1.0 x ε_{sh}	80	Type IV	0.170	0.347	0.198	0.412

Note:
(-) sign means compression

6.2.2. Restrained shrinkage analysis of the reinforced concrete deck supported on Steel I Girders spaced at 10 ft.

As for decks supported on prestressed concrete girders, the restrained shrinkage analysis is performed for decks supported on steel I girders. A constant deck thickness of 9 in and an empirical reinforcement are assumed. The maximum free shrinkage, $\varepsilon_{sh} = 0.00035$, is calculated for perfect curing conditions; humidity H = 70%, and the time of service is 30 years (according to AASHTO LRFD Code, Section 5.4.2.3.3).

In a case when perfect curing is not available, the code provision requires a 20% increase in the final shrinkage strain. The analysis for this increased shrinkage is also performed.

Steel girders with depths ranging from 24 in to 70 in are investigated depending on the span length. An increase of restrained shrinkage stresses after removal of the formwork and reduction of the deck slab weight due to the drying of concrete is also included in the analysis.

Tables 6-9, 6-10, 6-13 and 6-14, contain the stress level in the deck caused by restrained shrinkage (at the top, σ_{Du}, and the bottom, σ_{D1}, of the deck). Tables 6-11 and 6-15 contain the stress after the removal of the formwork and a reduction of weight due to the drying of concrete (at the top, σ_1, and the bottom, σ_2, of the deck). The total stress at the top and the bottom of the deck due to both causes is presented in Table 6-12 (for the middle part of the deck) and in Table 6-16 (for the edge part of the deck).

Table 6-9. Restrained shrinkage stress and strain in the middle of the deck supported on steel girders, calculated after 30 years, assuming perfect curing conditions ($\varepsilon_{sh} = 0.00035$)

Span Length (ft)	Depth of Girder (in)	Top Stress σ_{Du} (ksi)	Bottom Stress σ_{D1} (ksi)	Top Strain ε_{Du}	Bottom Strain ε_{D1}
40	24	-0.113	0.283	-21.30×10^{-6}	78.20×10^{-6}
45	27	-0.076	0.286	-15.43×10^{-6}	76.30×10^{-6}
50	30	-0.037	0.288	-5.66×10^{-6}	77.03×10^{-6}
55	33	0.003	0.296	2.82×10^{-6}	77.89×10^{-6}
60	36	0.043	0.308	15.64×10^{-6}	82.92×10^{-6}
80	48	0.197	0.378	51.20×10^{-6}	98.31×10^{-6}
100	60	0.340	0.467	88.25×10^{-6}	121.31×10^{-6}
120	70	0.445	0.541	115.63×10^{-6}	140.70×10^{-6}

Note:
(-) sign means compression
Shaded area indicates critical stress that exceeds modulus of rupture of concrete.

Table 6-10. Restrained shrinkage stress and strain in the middle of the deck supported on steel girders, calculated after 30 years, assuming imperfect curing conditions ($\varepsilon_{sh} = 1.2 \times 0.00035$)

Span Length (ft)	Depth of Girder (in)	Top Stress σ_{Du} (ksi)	Bottom Stress σ_{D1} (ksi)	Top Strain ε_{Du}	Bottom Strain ε_{D1}
40	24	-0.099	0.340	-25.56×10^{-6}	93.85×10^{-6}
45	27	-0.071	0.343	-18.51×10^{-6}	91.56×10^{-6}
50	30	-0.026	0.346	-6.79×10^{-6}	92.44×10^{-6}
55	33	0.004	0.355	3.38×10^{-6}	93.47×10^{-6}
60	36	0.052	0.370	18.77×10^{-6}	99.51×10^{-6}
80	48	0.236	0.454	61.44×10^{-6}	117.98×10^{-6}
100	60	0.407	0.560	105.89×10^{-6}	145.57×10^{-6}
120	70	0.534	0.650	138.75×10^{-6}	168.84×10^{-6}

Note: (-) sign means compression
Shaded area indicates critical stress that exceeds modulus of rupture of concrete.

Table 6-11. Stresses in the middle of the deck supported on steel girders unloaded after removal of the formwork and reduction of weight due to drying of concrete

Span Length (ft)	Depth of Girder (in)	Top Stress σ_1 (ksi)	Bottom Stress σ_2 (ksi)
40	24	0.053	-0.003
45	27	0.057	0.002
50	30	0.058	0.008
55	33	0.059	0.012
60	36	0.056	0.017
80	48	0.056	0.029
100	60	0.057	0.037
120	70	0.061	0.043

Note:
(-) sign means compression

Table 6-12. Total stresses in the middle of the deck supported on steel girders caused by restrained shrinkage, unloading after the removal of the formwork and reduction of weight due to drying of concrete

Span Length (ft)	Depth of Girder (in)	$\varepsilon_{sh} = 0.00035$		$\varepsilon_{sh} = 1.2 \times 0.00035$	
		Top Stress (ksi)	Bottom Stress (ksi)	Top Stress (ksi)	Bottom Stress (ksi)
40	24	-0.060	0.280	-0.046	0.337
45	27	-0.019	0.288	-0.014	0.345
50	30	0.021	0.296	0.032	0.354
55	33	0.062	0.308	0.063	0.367
60	36	0.099	0.325	0.108	0.387
80	48	0.253	0.407	0.292	0.483
100	60	0.397	0.504	0.464	0.597
120	70	0.506	0.584	0.595	0.693

Note:
(-) sign means compression
Shaded area indicates critical stress that exceeds modulus of rupture of concrete.

Table 6-13. Restrained shrinkage stress in the edge of deck supported on steel girders, calculated after 30 years, assuming perfect curing conditions (ε_{sh} = 0.00035)

Span Length (ft)	Depth of Girder (in)	Top Stress σ_{Du} (ksi)	Bottom Stress σ_{D1} (ksi)
40	24	-0.097	0.299
45	27	-0.053	0.303
50	30	-0.009	0.310
55	33	0.036	0.322
60	36	0.164	0.400
80	48	0.252	0.423
100	60	0.405	0.522
120	70	0.513	0.600

Note:
(-) sign means compression
Shaded area indicates critical stress that exceeds modulus of rupture of concrete.

Table 6-14. Restrained shrinkage stress in the edge of deck supported on steel girders, calculated after 30 years, assuming imperfect curing conditions (ε_{sh} = 1.2 x 0.00035)

Span Length (ft)	Depth of Girder (in)	Top Stress σ_{Du} (ksi)	Bottom Stress σ_{D1} (ksi)
40	24	-0.069	0.332
45	27	-0.031	0.350
50	30	0.036	0.372
55	33	0.043	0.387
60	36	0.197	0.479
80	48	0.302	0.508
100	60	0.486	0.626
120	70	0.616	0.720

Note:
(-) sign means compression

Shaded area indicates critical stress that exceeds modulus of rupture of concrete.

Table 6-15. Stresses in the edge of deck supported on steel girders unloaded after removal of the formwork and reduction of weight due to drying of concrete

Span Length (ft)	Depth of Girder (in)	Top Stress σ_1 (ksi)	Bottom Stress σ_2 (ksi)
40	24	0.051	0.001
45	27	0.070	0.005
50	30	0.076	0.020
55	33	0.075	0.026
60	36	0.074	0.031
80	48	0.074	0.045
100	60	0.076	0.053
120	70	0.083	0.062

Table 6-16. Total stresses in the edge of deck supported on steel girders caused by restrained shrinkage, unloading after removal of the formwork and reduction of weight due to drying of concrete

Span Length (ft)	Depth of Girder (in)	ε_{sh} = 0.00035		ε_{sh} = 1.2 x 0.00035	
		Top Stress (ksi)	Bottom Stress (ksi)	Top Stress (ksi)	Bottom Stress (ksi)
40	24	-0.046	0.300	-0.018	0.333
45	27	0.017	0.308	0.039	0.355
50	30	0.067	0.330	0.112	0.392
55	33	0.111	0.348	0.118	0.413
60	36	0.238	0.431	0.271	0.510
80	48	0.357	0.468	0.376	0.553
100	60	0.481	0.575	0.562	0.679
120	70	0.596	0.662	0.699	0.782

Note:
(-) sign means compression
Shaded area indicates critical stress that exceeds modulus of rupture of concrete.

The maximum stress values obtained from analytical model for restrained shrinkage in composite sections are comparable with the maximum shrinkage stresses obtained from the finite element models.

6.3. Cracking analysis of the concrete deck cross section

A cracking analysis of the reinforced concrete deck sections subjected to tensile stresses is performed separately for decks supported on prestressed concrete girders and on steel girders. Tensile stresses are caused by restrained shrinkage and they can be increased due to unloading after formwork removal and a reduction of weight due to the drying of concrete. In all considered cases, a constant deck thickness of 9 in. and an empirical reinforcement are assumed.

From stresses presented in Tables 6-12 and 6-16, it can be seen that transversal cracks can occur in the middle part of the deck, and at the edge part of the deck. These maximum tensile stresses will occur in sections with deeper steel girders. Higher tensile stresses can develop in a deck that is not perfectly cured after construction. However, even in a perfectly cured deck, shrinkage cracks can develop in sections with a substantial difference in stiffness between the deck slab and girder. This is even more visible at the edges of the deck because stiffness of the overhanging portion of the deck is smaller compared to an interior portion of the deck slab.

Examples of shrinkage cracks at the top and bottom of reinforced concrete decks are presented in Figures 6-4 to 6-10.

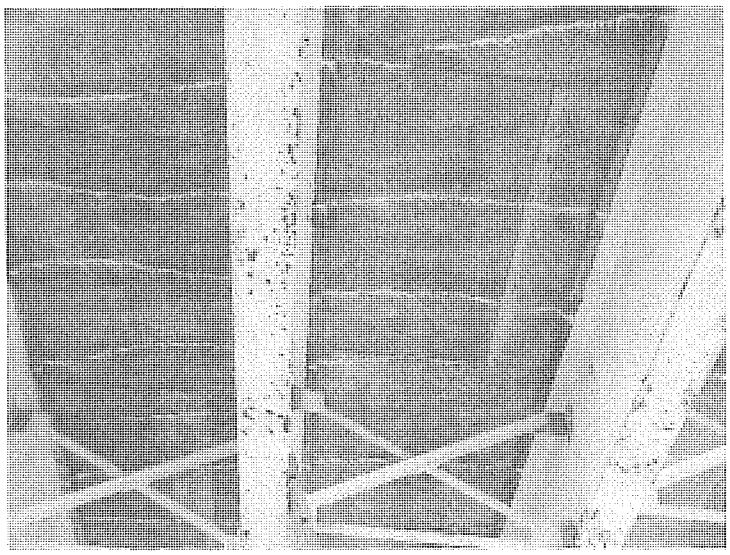

Figure 6-4. Transversal shrinkage cracks at the bottom of deck.

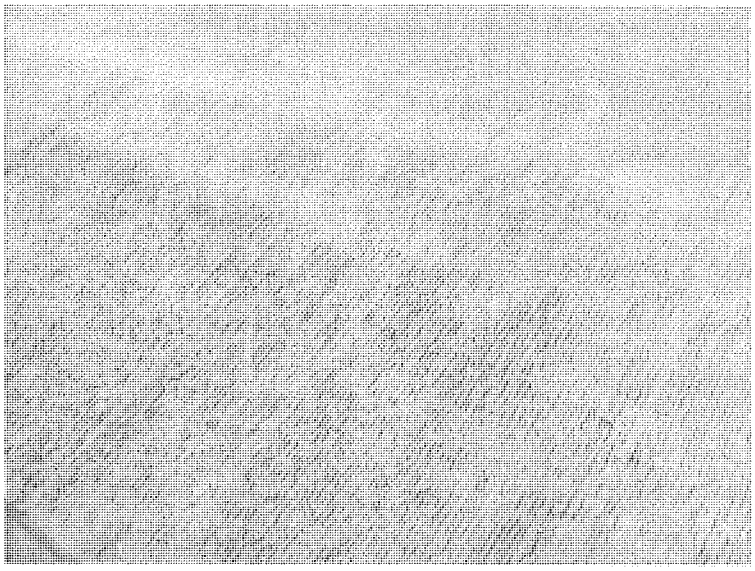

Figure 6-5. Transversal shrinkage cracks at the top of deck.

Figure 6-6. Transversal shrinkage crack at the bottom edge of deck.

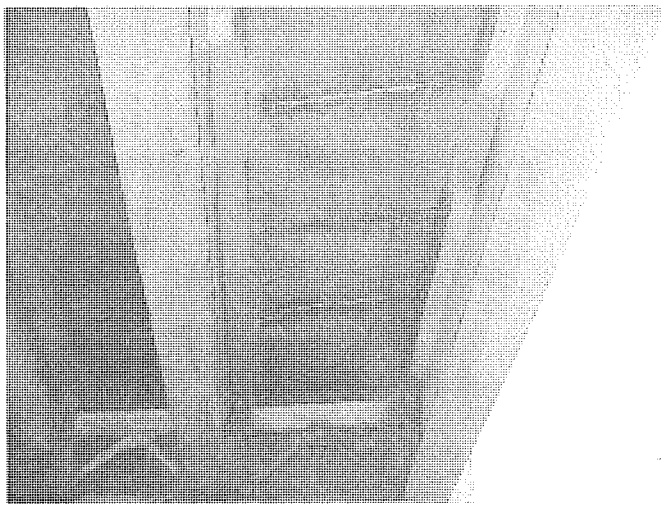

Figure 6-7. Transversal shrinkage cracks at the bottom edge of deck.

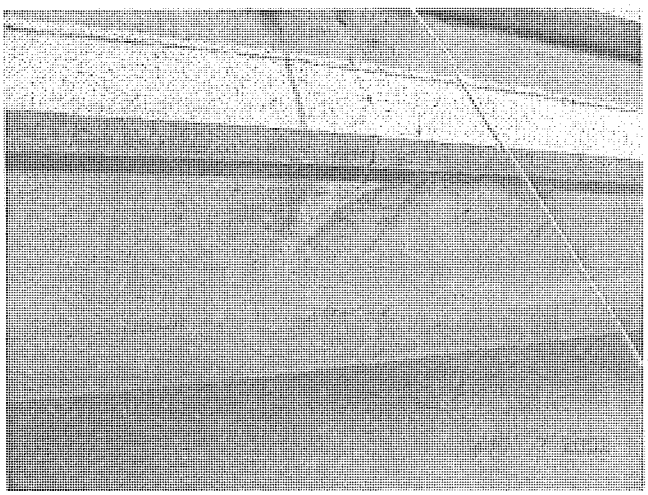

Figure 6-8. Transversal shrinkage cracks at the bottom edge of deck.

Figure 6-9. Corner shrinkage crack at the bottom of deck.

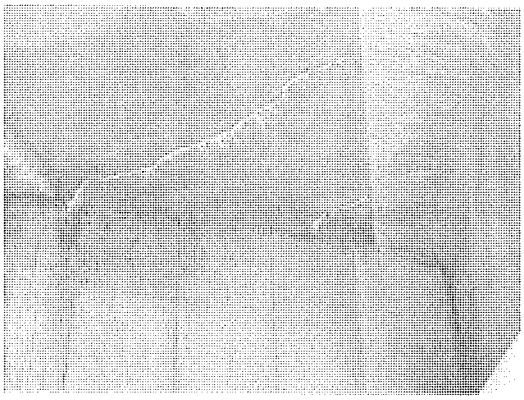

Figure 6-10. Corner shrinkage crack at the bottom of the deck.

6.3.1. Cracking analysis of decks supported on prestressed concrete girders, for the cross section B located in the middle section of deck (Figure 5-1).

According to the calculations shown in Table 6-4, there is no danger of cracking in the middle cross sections of the deck, due to restrained shrinkage, unloading after formwork removal, and a reduction of weight due to the drying of concrete in the slab. Longitudinal stress due to dead load is close to zero and can be neglected. Maximum longitudinal stress located in the middle sections of the deck due to live load is equal to 250 psi in compression on the top, and 65 psi in tension at the bottom (Table 5-1 and S22 - max longitudinal stress due to live load, p. 117). Compression top stress due to live load is not included in cracking analysis because it provides only temporary relief in tensile stress, but bottom tensile stress due to live load is included. Live load longitudinal stress added to maximum stress calculated in Table 6-4 (AASHTO girder Type IV, depth of 54 in.) results in tension stress on the top equal to 119 psi and tension stress equal to 370 psi at the bottom. These stresses will not cause cracking in the section. Restrained shrinkage stress is calculated assuming perfect curing conditions. Analysis is performed for girder spacing equal to 10 ft.

6.3.2. Cracking analysis of decks supported on prestressed concrete girders, for cross section B located in the edge section of deck (Figure 5-1).

A cracking analysis is performed for the cross sections located at the edge part of the deck, i.e. from the edge of the deck slab to the middle of the first slab span. Tensile stress

at the top and bottom of the deck cross section is calculated assuming perfect curing conditions, unloading after formwork removal and a reduction of deck weight due to the drying of concrete, shown in Table 6-8. In this example, a new deck is poured over existing (old) prestressed concrete girders (it is assumed that shrinkage in girders is completed). Longitudinal stress due to dead load is close to zero and is neglected (Table 5-1 and Figures 4-25, 4-26). Longitudinal stress due to live load is equal to 25 psi in tension on the top (close to support), and 65 psi in tension at the bottom of the deck (middle section), Table 5-1. Stresses calculated in Table 6-8 combined with stresses due to live load result in 195 psi in tension on the top, and 412 psi in tension at the bottom. These stresses will not caused cracking in the cross section. Analysis is performed for girder spacing equal to 10 ft.

As a result of the cracking analysis for a new deck supported on existing prestressed concrete girders (replacement), it is proposed as follows:

1. Always provide the best curing conditions and pour concrete slabs in an ambient humidity of 70% or more.
2. For the middle and edge sections of the slab supported on Type IV girders (depth 54 in), it is not necessary to increase longitudinal reinforcement.

For other cases (Type II girders -depth 36 in., Type III-depth 45in., and Type IV-depth 54 in.), when the deck is constructed on new prestressed girders, there is no need to increase the longitudinal empirical reinforcement. Over a part of the service life of the structure, shrinkage will develop in the deck and in girders simultaneously, which in fact causes smaller shrinkage stresses in the deck. In all cases, it is necessary to provide the best possible curing conditions.

6.3.3. Cracking analysis of decks supported on steel girders, for the cross section B located in the middle section of deck (Figure 5-1).

A cracking analysis is performed for the cross sections located in the middle of the deck (Figure 5-1); i.e. the effective concrete slab width is equal to the space between girders (10 ft). Analysis refers to stresses acting in the longitudinal direction of the deck.

Because of high restrained shrinkage stress in decks supported on deep steel girders (with depth of 48 in., 60 in., and 70 in.), it is proposed to use stay-in-place formwork to avoid additional tensile stress at the bottom of the deck caused by unloading after removal of formwork. Loss of self weigh of deck after drying of concrete results in small stresses that can be neglected. Longitudinal stress due to dead load is small. Due to flexibility of girders, longitudinal stress due to live load in the middle sections is in compression, because the neutral axis of the composite section is located in upper flange of girder. In parts of the deck close to supports (abutments), live load longitudinal stress is equal to 85 psi in tension on the top and the bottom of the cross section (Table 5-1).

Restrained shrinkage stress is calculated based on analytical model for composite section and is presented in Table 6-9. The slab supported on steel girders with a depth of 60 in. is presented in Figure 6-11. Tensile stress at the top and bottom of the deck cross section is calculated as follows:

Total longitudinal stress on the top = 0 (dead load) + 85 psi (live load) + 340 psi (shrinkage) = 425 psi (in tension)

Total longitudinal stress at the bottom = 0 (dead load) + 85 psi (live load) + 467 psi (shrinkage) = 552 psi

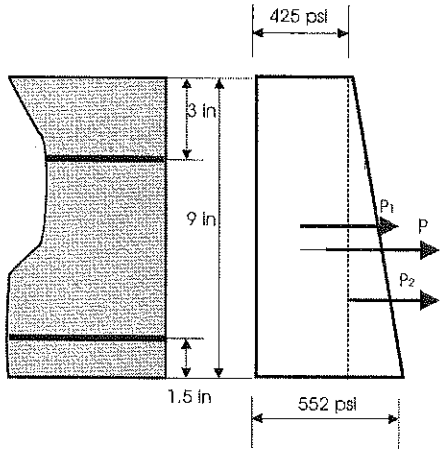

Figure 6-11. Stress diagram in deck cross section due to restrained shrinkage, dead and live load (middle section of the deck).

The resultant tensile force, P, acting in the section has to be balanced by the tensile force in concrete section, F_t, and the tensile forces in the top, F_{As1}, and the bottom, F_{As2}, longitudinal reinforcements.

Assumed empirical reinforcement: top bars 0.18 in^2/ft, and bottom bars 0.27 in^2/ft (longitudinally).

$$P_1 = 0.425(9)12 = 45.9kip$$

$$P_2 = (0.552 - 0.425)(9)12\frac{1}{2} = 6.9kip$$

$$P = 52.8kip$$

The tensile capacity of a section in an elastic range is calculated with the assumption of strain compatibility (Figure 6-12). Stresses in the section are calculated with respect to the moment/force ratio caused by shrinkage (Figure 6-11).

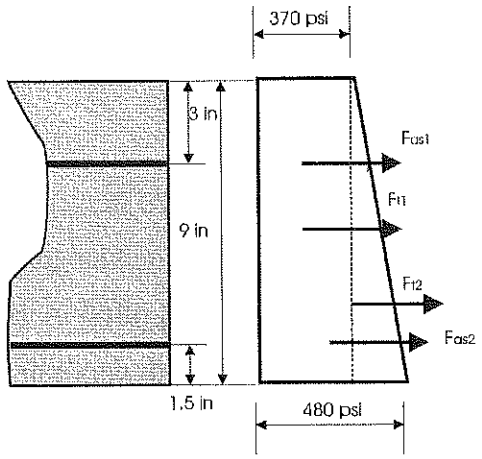

Figure 6-12. Tensile capacity of the section in the elastic range.

Tensile force, F_t, in concrete section is calculated as,

$$F_{t1} = 0.370(9)12 = 39.96kip/ft$$

$$F_{t2} = (0.480 - 0.370)(9)\times\frac{1}{2}\times 12 = 5.94kip/ft$$

$$F_t = F_{t1} + F_{t2} = 45.9kip/ft$$

Tensile forces, F_{As1} and F_{As2} in the top and bottom reinforcement are calculated with the assumption of strain compatibility,

$$\frac{(0.480-0.370)}{9}=\frac{(\sigma_{c1}-0.370)}{3}\Rightarrow \sigma_{c1}=0.407$$

$$\frac{(0.480-0.370)}{9}=\frac{(\sigma_{c2}-0.370)}{(9-1.5)}\Rightarrow \sigma_{c2}=0.462$$

$$\varepsilon_{As1}=\varepsilon_{c1}=\frac{0.407}{3850}=105.71\times10^{-6}$$

$$\varepsilon_{As2}=\varepsilon_{c2}=\frac{0.462}{3850}=120.0\times10^{-6}$$

$$\sigma_{As1}=\varepsilon_{As1}E_s=105.71\times10^{-6}\times29000=3.07ksi$$

$$\sigma_{As2}=\varepsilon_{As2}E_s=120.0\times10^{-6}\times29000=3.48ksi$$

$$F_{As1}=3.07(0.18)=0.552kip/ft$$

$$F_{As2}=3.48(0.27)=0.940kip/ft$$

$$F_l+F_{As1}+F_{As2}=45.9+0.552+0.940=47.39kip/ft<P=52.8kip/ft$$

Because of high value of resultant tensile force in the section it is proposed to increase thickness of the deck.

A slab supported on steel girders with a depth of 70 in. is presented in Figure 6-13. It is assumed that stress due to live load, in deck supported on girders with depth of 70 in. will be similar to that calculated for girders with depth of 60 in. (FEM model was developed for bridge superstructure supported on girders with depth of 60 in.). Live load stress is presented in Table 5-1, and restrained shrinkage stress is presented in Table 6-9. Tensile stress at the top and bottom of the deck cross section is calculated as follows:

Total longitudinal stress on the top = 0 (dead load) + 85 psi (live load) + 445 psi (shrinkage) = 530 psi (in tension)

Total longitudinal stress at the bottom = 0 (dead load) + 85 psi (live load) + 541 psi (shrinkage) = 626 psi

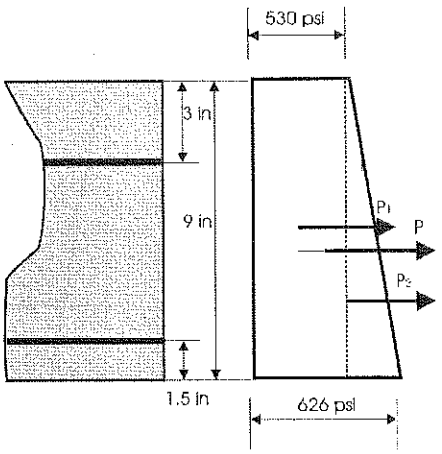

Figure 6-13. Stress diagram in deck cross section due to restrained shrinkage, dead load and live load (middle section of the deck).

The resultant tensile force, P, acting in the section, has to be balanced by tensile force in the concrete section, F_t, and tensile forces in the top, F_{As1}, and bottom, F_{As2}, longitudinal reinforcements.

Assumed empirical reinforcement: top bars 0.18 in^2/ft, and bottom bars 0.27 in^2/ft (longitudinally).

$$P_1 = 0.530(9)12 = 57.2kip$$

$$P_2 = (0.626 - 0.530)(9)12\frac{1}{2} = 5.2kip$$

$$P = 62.4kip$$

The tensile capacity of a section in an elastic range is calculated with the assumption of strain compatibility (Figure 6-14). Stresses in the section are calculated with respect to the moment/force ratio caused by shrinkage (Figure 6-13).

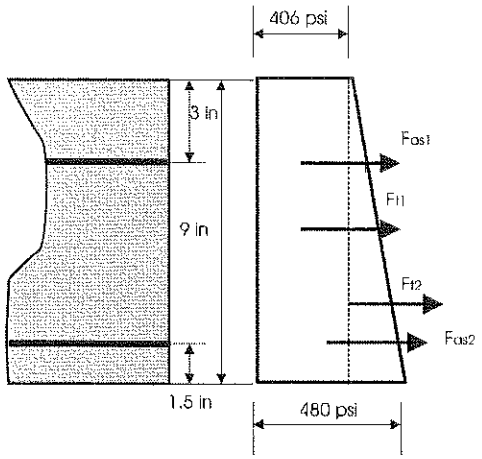

Figure 6-14. Tensile capacity of the section in the elastic range.

Tensile force, F_t, in concrete section is calculated as,

$$F_{t1} = 0.406(9)12 = 43.85 kip/ft$$

$$F_{t2} = (0.480 - 0.406)(9) \times \frac{1}{2} \times 12 = 4.00 kip/ft$$

$$F_t = F_{t1} + F_{t2} = 47.85 kip/ft$$

Tensile forces, F_{As1} and F_{As2} in the top and bottom reinforcement are calculated with the assumption of strain compatibility,

$$\frac{(0.480 - 0.406)}{9} = \frac{(\sigma_{c1} - 0.406)}{3} \Rightarrow \sigma_{c1} = 0.431$$

$$\frac{(0.480 - 0.406)}{9} = \frac{(\sigma_{c2} - 0.406)}{(9 - 1.5)} \Rightarrow \sigma_{c2} = 0.468$$

$$\varepsilon_{As1} = \varepsilon_{c1} = \frac{0.431}{3850} = 111.95 \times 10^{-6}$$

$$\varepsilon_{As2} = \varepsilon_{c2} = \frac{0.468}{3850} = 121.56 \times 10^{-6}$$

$$\sigma_{As1} = \varepsilon_{As1} E_s = 111.95 \times 10^{-6} \times 29000 = 3.25 ksi$$

$$\sigma_{As2} = \varepsilon_{As2} E_s = 121.56 \times 10^{-6} \times 29000 = 3.53 ksi$$

$$F_{As1} = 3.25(0.18) = 0.585 kip/ft$$

$$F_{As2} = 3.53(0.27) = 0.953 kip/ft$$

$$F_t + F_{As1} + F_{As2} = 47.85 + 0.585 + 0.953 = 49.39 kip/ft < P = 62.4 kip/ft$$

Because of high value of resultant tensile force in the section it is proposed to increase thickness of the deck.

6.3.4. Cracking analysis of decks supported on steel girders, for the cross section B located in the edge section of deck (Figure 5-1).

A cracking analysis is performed for the cross sections located in the edge section of the deck, i.e. from the edge of the deck to the middle of the first slab span. Because of high restrained shrinkage stress in decks supported on deep steel girders, it is proposed to use stay-in-place formwork to avoid additional tensile stress at the bottom of deck. Analysis starts with deck supported on 48 in. deep girders because restrained shrinkage stress at the edge of the deck combined with stress due to live load will increase modulus of rupture for concrete (480 psi). However, this analysis can be only an estimation, because FEM model was developed for bridge superstructure supported on girders with depth of 60 in. and it was assumed that stress due to live load, in deck supported on girders with depth of 48 in. will be similar to that calculated for girders with depth of 60 in.

Slab supported on steel girders with a depth of 48 in. is presented in Figure 6-15. Similarly as for middle sections, longitudinal stress due to dead load is close to zero. Live load results in longitudinal tension stresses at the top and bottom of cross section equal to 85 psi (Table 5-1). Restrained shrinkage stress calculated with the assumption of perfect curing conditions is presented in Table 6-13. Total tensile stress at the top and bottom of the deck cross section is calculated as follows:

Total longitudinal stress on the top = 0 (dead load) +85 psi (live load) + 252 psi (shrinkage) = 337 psi (in tension)
Total longitudinal stress at the bottom = 0 (dead load) + 85 psi (live load) + 423 psi (shrinkage) = 508 psi (in tension).

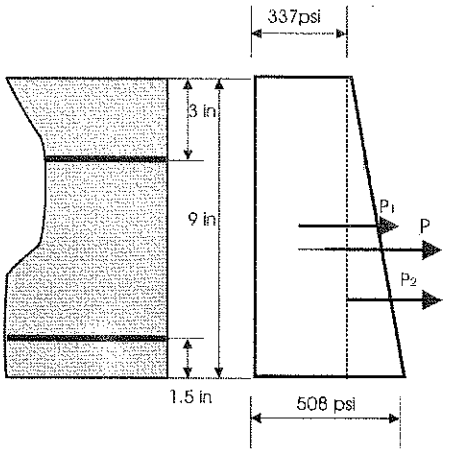

Figure 6-15. Stress diagram in deck cross section due to restrained shrinkage, dead load and live load (edge section of the deck).

The resultant tensile force, P, caused by the considered loads is equal to,

$$P_1 = 0.337(9)12 = 36.4kip/ft$$

$$(0.508-0.337)(9)12\frac{1}{2} = 9.23kip$$

$$P = 45.63kip$$

The tensile capacity of a section in an elastic range is calculated with the assumption of strain compatibility (Figure 6-16). Stresses in the section are calculated with respect to the moment/force ratio caused by shrinkage (Figure 6-15).

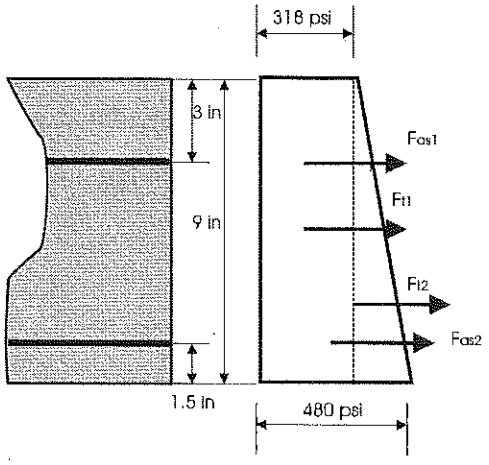

Figure 6-16. Tensile capacity of the section in the elastic range.

Tensile force, F_t, in concrete section is calculated as,

$$F_{t1} = 0.318(9)12 = 34.34 kip/ft$$

$$F_{t2} = (0.480 - 0.318)(9) \times \frac{1}{2} \times 12 = 8.75 kip/ft$$

$$F_t = F_{t1} + F_{t2} = 43.09 kip/ft$$

Tensile forces, F_{As1} and F_{As2} in the top and bottom reinforcement are calculated with the assumption of strain compatibility,

$$\frac{(0.480 - 0.318)}{9} = \frac{(\sigma_{c1} - 0.318)}{3} \Rightarrow \sigma_{c1} = 0.372$$

$$\frac{(0.480 - 0.318)}{9} = \frac{(\sigma_{c2} - 0.318)}{(9 - 1.5)} \Rightarrow \sigma_{c2} = 0.453$$

$$\varepsilon_{As1} = \varepsilon_{c1} = \frac{0.372}{3850} = 96.62 \times 10^{-6}$$

$$\varepsilon_{As2} = \varepsilon_{c2} = \frac{0.453}{3850} = 117.66 \times 10^{-6}$$

$$\sigma_{As1} = \varepsilon_{As1} E_s = 96.62 \times 10^{-6} \times 29000 = 2.80 ksi$$

$$\sigma_{As2} = \varepsilon_{As2} E_s = 117.66 \times 10^{-6} \times 29000 = 3.41 ksi$$

$$F_{As1} = 2.80(0.18) = 0.504 kip/ft$$

$$F_{As2} = 3.41(0.27) = 0.921 kip/ft$$

$$F_t + F_{As1} + F_{As2} = 43.09 + 0.504 + 0.921 = 44.51 kip/ft < P = 45.63 kip/ft$$

To increase tension capacity of the section is proposed to double the top and bottom longitudinal empirical reinforcement (2 x 0.18 in^2/ft at the top, and 2 x 0.27 in^2/ft at the bottom),

$$F_t + F_{As1} + F_{As2} = 43.09 + 2 \times 0.504 + 2 \times 0.921 = 45.94 kip/ft > P = 45.63 kip/ft$$

Calculation of restrained shrinkage for increased thickness of the deck slab

Table 6-17 presents values of restrained shrinkage stress calculated for an increased thickness of the deck slab supported on steel girders with a depth of 48 in., 60in. and 70

in. Stresses are calculated after 30 years with the assumption of very good curing conditions and an ambient humidity of 70%.

Table 6-17. Restrained shrinkage stress in the middle and edge cross sections of the deck supported on steel girders, calculated after 30 years, assuming perfect curing conditions ($\varepsilon_{sh} = 0.00035$)

Span Length (ft)	Depth of Girder (in)	Thickness of slab (in)	Top Stress σ_{Du} (ksi)	Bottom Stress σ_{Dl} (ksi)	Top Stress σ_{Du} (ksi)	Bottom Stress σ_{Dl} (ksi)
			Middle sections		Edge sections	
80	48	9.5	0.178	0.371	0.231	0.416
80	48	10.0	0.159	0.365	0.211	0.406
80	48	10.5	0.141	0.360	0.192	0.399
100	60	9.5	0.319	0.456	0.383	0.509
100	60	10.0	0.298	0.445	0.362	0.497
100	60	10.5	0.280	0.436	0.342	0.487
100	60	11.0	0.261	0.428	0.322	0.477
100	60	11.5	0.244	0.420	0.304	0.468
100	60	12.0	0.227	0.413	0.286	0.460
120	70	9.5	0.424	0.528	0.491	0.587
120	70	10.0	0.404	0.516	0.471	0.573
120	70	10.5	0.384	0.505	0.451	0.561
120	70	11.0	0.366	0.494	0.432	0.550
120	70	11.5	0.348	0.485	0.414	0.539
120	70	12.0	0.331	0.475	0.396	0.529

Shaded area indicates critical stress that exceeds modulus of rupture of concrete.

The slab supported on steel girders with a depth of 60 in. is presented in Figure 6-17. Tensile stress at the top and bottom of the cross section B located in the middle sections of the deck is calculated as follows (based on Table 6-17 for deck thickness of 11 in.):

Total longitudinal stress on the top = 0 (dead load) + 85 psi (live load) + 261 psi (shrinkage) = 346 psi (in tension)

Total longitudinal stress at the bottom = 0 (dead load) + 85 psi (live load) + 428 psi (shrinkage) = 513 psi

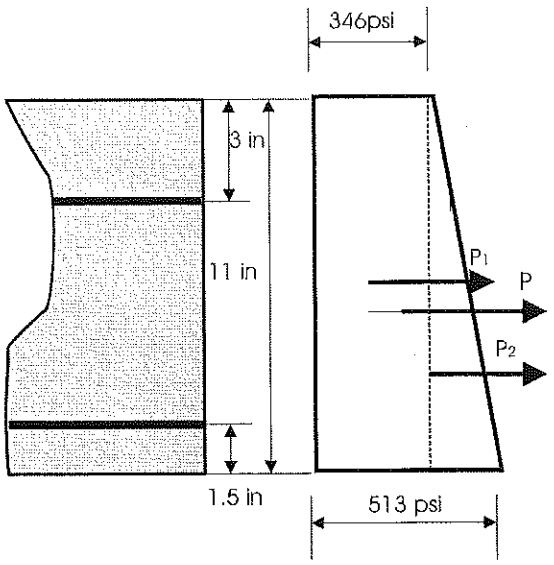

Figure 6-17. Stress diagram in deck cross section due to restrained shrinkage, dead and live load (middle section of the deck).

The resultant tensile force, P, acting in the section has to be balanced by the tensile force in concrete section, F_t, and the tensile forces in the top, F_{As1}, and the bottom, F_{As2}, longitudinal reinforcements.

Assumed empirical reinforcement: top bars 0.18 in^2/ft, and bottom bars 0.27 in^2/ft (longitudinally).

$$P_1 = 0.346(11)12 = 45.67 kip$$

$$P_2 = (0.513 - 0.346)(11)12\frac{1}{2} = 11.02 kip$$

$$P = 56.7 kip$$

The tensile capacity of the section in an elastic range is calculated with the assumption of strain compatibility (Figure 6-18). Stresses in the section are calculated with respect to the moment/force ratio caused by shrinkage (Figure 6-17).

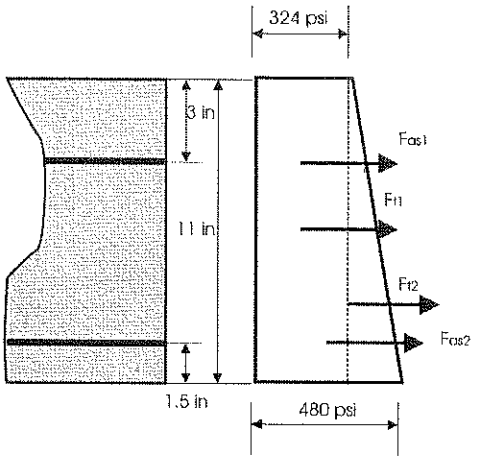

Figure 6-18. Tensile capacity of the section in the elastic range.

Tensile force, F_t, in concrete section is calculated as,

$$F_{t1} = 0.324(11)12 = 42.77 kip/ft$$

$$F_{t2} = (0.480 - 0.324)(11) \times \frac{1}{2} \times 12 = 10.30 kip/ft$$

$$F_t = F_{t1} + F_{t2} = 53.07 kip/ft$$

Tensile forces, F_{As1} and F_{As2} in the top and bottom reinforcement are calculated with the assumption of strain compatibility,

$$\frac{(0.480 - 0.324)}{11} = \frac{(\sigma_{c1} - 0.324)}{3} \Rightarrow \sigma_{c1} = 0.367$$

$$\frac{(0.480 - 0.324)}{11} = \frac{(\sigma_{c2} - 0.324)}{(11 - 1.5)} \Rightarrow \sigma_{c2} = 0.459$$

$$\varepsilon_{As1} = \varepsilon_{c1} = \frac{0.367}{3850} = 95.33 \times 10^{-6}$$

$$\varepsilon_{As2} = \varepsilon_{c2} = \frac{0.459}{3850} = 119.22 \times 10^{-6}$$

$$\sigma_{As1} = \varepsilon_{As1} E_s = 95.33 \times 10^{-6} \times 29000 = 2.76 ksi$$

$$\sigma_{As2} = \varepsilon_{As2} E_s = 119.22 \times 10^{-6} \times 29000 = 3.46 ksi$$

$$F_{As1} = 2.76(0.18) = 0.500 kip/ft$$

$$F_{As2} = 3.46(0.27) = 0.934 kip/ft$$

$$F_t + F_{As1} + F_{As2} = 53.07 + 0.500 + 0.934 = 54.5 kip/ft < P = 56.7 kip/ft$$

To increase tension capacity of the section, it is proposed to double longitudinal empirical reinforcement at the top and triple longitudinal empirical reinforcement at the bottom.

$$F_t + F_{As1} + F_{As2} = 53.07 + 2 \times 0.500 + 3 \times 0.934 = 56.9 kip/ft > P = 56.7 kip/ft$$

The slab supported on steel girders with a depth of 60 in. is presented in Figure 6-19 for the edge section. Tensile stress at the top and bottom of the cross section B (Figure 5-1) located in the edge sections of the deck is calculated as follows (based on Table 6-17 for deck thickness of 11 in.):

Total longitudinal stress on the top = 0 (dead load) + 85 psi (live load) + 322 psi (shrinkage) = 407 psi (in tension)

Total longitudinal stress at the bottom = 0 (dead load) + 85 psi (live load) + 477 psi (shrinkage) = 562 psi

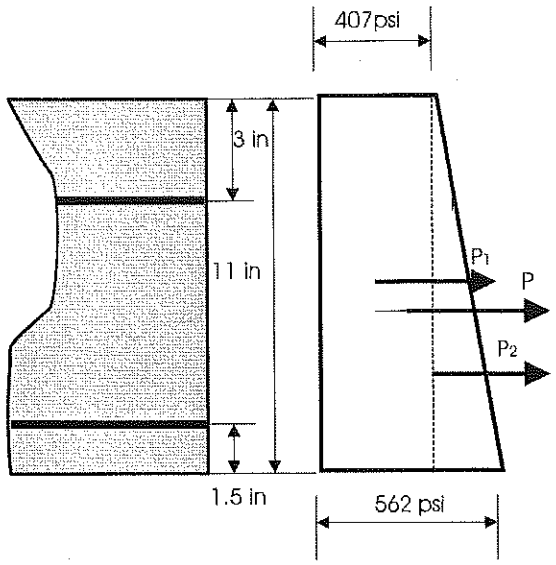

Figure 6-19. Stress diagram in deck cross section due to restrained shrinkage, dead and live load (edge section of the deck).

The resultant tensile force, P, acting in the section has to be balanced by the tensile force in concrete section, F_t, and the tensile forces in the top, F_{As1}, and the bottom, F_{As2}, longitudinal reinforcements.

Assumed empirical reinforcement: top bars 0.18 in^2/ft, and bottom bars 0.27 in^2/ft (longitudinally).

$$P_1 = 0.407(11)12 = 53.72kip$$

$$P_2 = (0.562 - 0.407)(11)12\frac{1}{2} = 10.23kip$$

$$P = 63.95kip$$

The tensile capacity of the section in an elastic range is calculated with the assumption of strain compatibility (Figure 6-20). Stresses in the section are calculated with respect to the moment/force ratio caused by shrinkage (Figure 6-19).

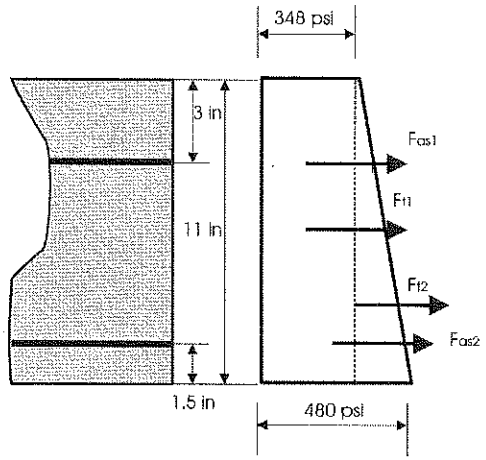

Figure 6-20. Tensile capacity of the section in the elastic range.

Tensile force, F_t, in concrete section is calculated as,

$$F_{t1} = 0.348(11)12 = 45.94kip/ft$$

$$F_{t2} = (0.480 - 0.348)(11)\times\frac{1}{2}\times 12 = 8.71kip/ft$$

$$F_t = F_{t1} + F_{t2} = 54.65kip/ft$$

Tensile forces, F_{As1} and F_{As2} in the top and bottom reinforcement are calculated with the assumption of strain compatibility,

$$\frac{(0.480-0.348)}{11} = \frac{(\sigma_{c1} - 0.348)}{3} \Rightarrow \sigma_{c1} = 0.384$$

$$\frac{(0.480-0.348)}{11} = \frac{(\sigma_{c2} - 0.348)}{(11-1.5)} \Rightarrow \sigma_{c2} = 0.462$$

$$\varepsilon_{As1} = \varepsilon_{c1} = \frac{0.384}{3850} = 99.74 \times 10^{-6}$$

$$\varepsilon_{As2} = \varepsilon_{c2} = \frac{0.462}{3850} = 120.0 \times 10^{-6}$$

$$\sigma_{As1} = \varepsilon_{As1} E_s = 99.74 \times 10^{-6} \times 29000 = 2.9 ksi$$

$$\sigma_{As2} = \varepsilon_{As2} E_s = 120.0 \times 10^{-6} \times 29000 = 3.48 ksi$$

$$F_{As1} = 2.9(0.18) = 0.522 kip/ft$$

$$F_{As2} = 3.48(0.27) = 0.940 kip/ft$$

$$F_t + F_{As1} + F_{As2} = 54.65 + 0.522 + 0.940 = 56.11 kip/ft < P = 63.95 kip/ft$$

To increase tension capacity of the section, it is proposed to increase area of longitudinal reinforcement. Four layers of bars #6 @ 6 in. (0.88 in^2/ft) can provide, together with tension capacity of the concrete cross section, the tension force to carry resultant force, P. The stress in four layers of longitudinal reinforcement is equal to:

$$\sigma_{As1} = 2.9 ksi$$

$$\sigma_{As2} = 3.09 ksi$$

$$\sigma_{As3} = 3.28 ksi$$

$$\sigma_{As4} = 3.48 ksi$$

$$F_t + F_{As1} + F_{As2} = 54.65 + (0.88)(2.9 + 3.09 + 3.28 + 3.48) = 65.87 kip/ft > P = 63.95 kip/ft$$

The slab supported on steel girders with a depth of 70 in. is presented in Figure 6-21. Tensile stress at the top and bottom of the cross section B (Figure 5-1) located in the middle sections of the deck is calculated as follows (based on Table 6-17 for deck thickness of 12 in.; stress due to live load is assumed the same as calculated for deck supported on girders with depth of 60 in.):

Total longitudinal stress on the top = 0 (dead load) + 85 psi (live load) + 331 psi (shrinkage) = 416 psi (in tension)

Total longitudinal stress at the bottom = 0 (dead load) + 85 psi (live load) + 475 psi (shrinkage) = 560 psi

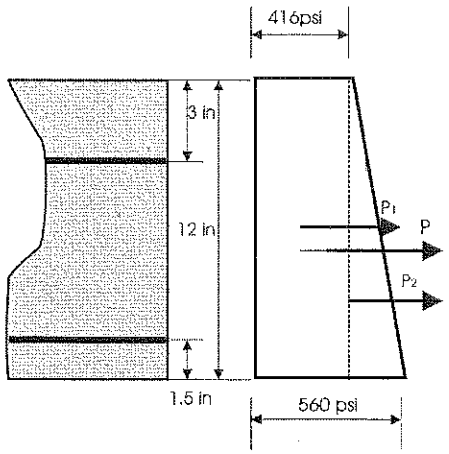

Figure 6-21. Stress diagram in deck cross section due to restrained shrinkage, dead and live load (middle section of the deck).

The resultant tensile force, P, acting in the section has to be balanced by the tensile force in concrete section, F_t, and the tensile forces in the top, F_{As1}, and the bottom, F_{As2}, longitudinal reinforcements.

Assumed empirical reinforcement: top bars 0.18 in^2/ft, and bottom bars 0.27 in^2/ft (longitudinally).

$$P_1 = 0.416(12)12 = 59.9 kip$$

$$P_2 = (0.560 - 0.416)(11)12\frac{1}{2} = 10.37 kip$$

$$P = 70.27 kip$$

The tensile capacity of the section in an elastic range is calculated with the assumption of strain compatibility (Figure 6-22). Stresses in the section are calculated with respect to the moment/force ratio caused by shrinkage (Figure 6-21).

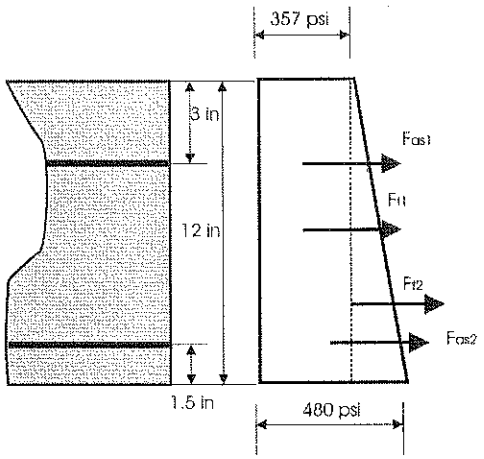

Figure 6-22. Tensile capacity of the section in the elastic range.

Tensile force, F_t, in concrete section is calculated as,

$$F_{t1} = 0.357(12)12 = 51.41 kip/ft$$

$$F_{t2} = (0.480 - 0.357)(12) \times \frac{1}{2} \times 12 = 8.86 kip/ft$$

$$F_t = F_{t1} + F_{t2} = 60.27 kip/ft$$

Tensile forces, F_{As1} and F_{As2} in the top and bottom reinforcement are calculated with the assumption of strain compatibility,

$$\frac{(0.480 - 0.357)}{12} = \frac{(\sigma_{c1} - 0.357)}{3} \Rightarrow \sigma_{c1} = 0.388$$

$$\frac{(0.480 - 0.357)}{12} = \frac{(\sigma_{c2} - 0.357)}{(12 - 1.5)} \Rightarrow \sigma_{c2} = 0.465$$

$$\varepsilon_{As1} = \varepsilon_{c1} = \frac{0.388}{3850} = 100.78 \times 10^{-6}$$

$$\varepsilon_{As2} = \varepsilon_{c2} = \frac{0.465}{3850} = 120.78 \times 10^{-6}$$

$$\sigma_{As1} = \varepsilon_{As1} E_s = 100.78 \times 10^{-6} \times 29000 = 2.9 ksi$$

$$\sigma_{As2} = \varepsilon_{As2} E_s = 120.78 \times 10^{-6} \times 29000 = 3.5 ksi$$

$$F_{As1} = 2.9(0.18) = 0.522 kip/ft$$

$$F_{As2} = 3.5(0.27) = 0.945 kip/ft$$

$$F_t + F_{As1} + F_{As2} = 60.27 + 0.522 + 0.945 = 61.74 kip/ft < P = 70.27 kip/ft$$

To increase tension capacity of the section, it is proposed to increase area of longitudinal reinforcement. Four layers of bars #6 @ 6 in. (0.88 in^2/ft) can provide, together with tension capacity of the concrete cross section, the tension force to carry resultant force, P. The stress in four layers of longitudinal reinforcement is equal to:

$\sigma_{As1} = 2.9ksi$

$\sigma_{As2} = 3.1ksi$

$\sigma_{As3} = 3.3ksi$

$\sigma_{As4} = 3.5ksi$

$$F_t + F_{As1} + F_{As2} = 60.27 + (0.88)(2.9 + 3.1 + 3.3 + 3.5) = 71.53kip/ft > P = 70.27kip/ft$$

The same amount of longitudinal reinforcement (#6 @ 6 in. in four layers) is proposed for edge sections of 12 in thick deck supported on steel girders with depth of 70 in.

As it is presented above, the resultant tensile force, P, caused by restrained shrinkage and the live load, can be much bigger than the tensile capacity of the cross section calculated in an elastic range. A viable way to decrease shrinkage cracks is to modify (increase) the empirical reinforcement. This approach is based on the behavior of concrete in tension, in presence of reinforcement. The model curve for concrete in tension is presented in Figure 6-1. The descending part of the curve (after reaching the modulus of rupture pick) can be modeled by adding more reinforcement to the cross section. This will not eliminate shrinkage cracking, but it will limit cracks number and decrease the crack opening because of stress redistribution in the cross section. Such approach will diminish corrosion development and the negative effect of freeze/thaw cycles.

As a result of the cracking analysis for a deck supported on steel girders, the following is proposed:

1. Always provide the best possible curing conditions and pour concrete slab in ambient humidity of 70% or more.
2. For decks supported on steel girders with depth of 48 in., 60 in. and 70 in., it is proposed to use stay-in-place formwork.

3. For the middle cross sections of a deck supported on girders with a depth of 60 in., it is proposed to increase the deck thickness to 11 in. and double top and bottom longitudinal empirical reinforcement.
4. For the middle cross sections of a deck supported on girders with a depth of 70 in., it is proposed to increase the thickness of the deck slab to 12 in., and use four layers of longitudinal reinforcement (#6 @ 6 in.)
5. For the edge cross sections of a deck supported on girders with a depth of 48 in, it is proposed to double top and bottom longitudinal empirical reinforcement, or increase the thickness of the deck slab. A slab thickness of 10.5 in. will prevent the occurrence of cracks caused by restrained shrinkage because the total tension stresses at the top and bottom of the deck are smaller than the modulus of rupture for concrete (Table 6-17).
6. For the edge cross sections of the slab supported on girders with depth of 60 in, it is proposed to increase the thickness of the deck slab to 11 in. and use four layers of longitudinal reinforcement (#6 @ 6 in.).
7. For the edge cross sections of the slab supported on girders with depth of 70 in, it is proposed to increase the thickness of the deck slab to 12 in. and also use four layers of reinforcement (the same as for middle sections).

7. PROCEDURE FOR LOAD RATING OF ISOTROPIC DECKS

The proposed procedure for the load rating of reinforced concrete isotropic bridge decks is based on punching shear capacity and bending moment capacity. Punching shear capacity is calculated as a nominal shear resistance for two-way slabs without shear reinforcement. Bending moment capacity is calculated for a cracked cross section.

7.1. Punching shear capacity

Punching shear capacity of the deck is calculated based on a nominal shear resistance, V_n, for two-way slabs, according to AASHTO LRFD Code (A5.13.3.6.3):

$$V_n = \left(0.063 + \frac{0.126}{\beta_c}\right)\sqrt{f_c'}\,b_o d_v \le 0.126\sqrt{f_c'}\,b_o d_v \qquad (7\text{-}1)$$

where:

V_n = nominal shear resistance for a cross section without shear reinforcement (kip)

β_c = ratio of long side to short side of the rectangle through which the concentrated load or reaction force is transmitted.

b_o = perimeter of the critical section at a distance $d_v/2$ from the perimeter of the load area (in).

f'_c = compressive strength of concrete (ksi).

d_v = effective shear depth (in) taken as the distance, measured perpendicular to the neutral axis, between the resultants of the tensile and compressive forces due to flexure; it need not to be taken to be less than the greater of $0.9d_e$ or $0.72h$ (in), where d_e is the effective depth of the deck and h is the full thickness of the deck .

The punching shear capacity is calculated for deck slabs on two tested bridges: one supported on steel girders and the other one on prestressed concrete girders, Figure 7-1.

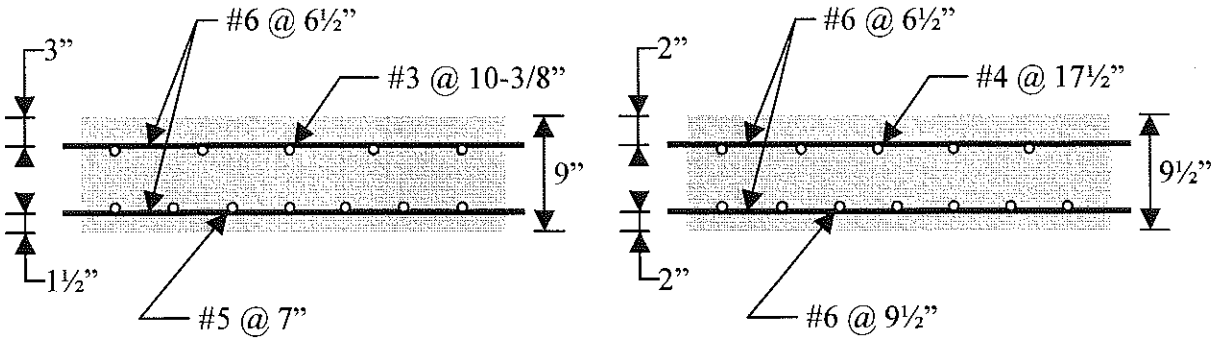

Deck reinforcement configuration for the prestressed girder bridge

Deck reinforcement configuration for the steel girder bridge

Figure 7-1. Transversal deck reinforcement configuration.

Computation of the effective shear depth, d_v

In order to compute d_v, the effective depth, d_e, of each deck slab configuration is calculated. The effective depth is the distance from the top compressed fiber to the centroid of the reinforcement; in this case, in order to be conservative, the centroid of the longitudinal rebars is taken into account.

For the prestressed girder deck configuration,

$$d_e = 9 - 1.5 - 6/8 - \frac{1}{2}(5/8) = 6.4375 \quad in$$

$$\left\{\begin{matrix} 0.9d_e = 5.79 & in \\ 0.72h = 6.48 & in \end{matrix}\right\} \rightarrow d_v = 6.48 \quad in$$

For the steel girder deck configuration,

$$d_e = 9.5 - 2 - 6/8 - \frac{1}{2}(6/8) = 6.375 \quad in$$

$$\left\{\begin{matrix} 0.9d_e = 5.74 & in \\ 0.72h = 6.84 & in \end{matrix}\right\} \rightarrow d_v = 6.84 \quad in$$

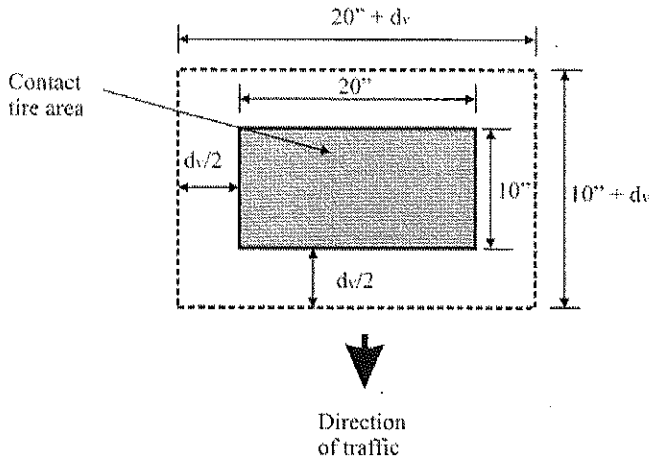

Figure 7-2. Critical section for punching shear in the deck.

Computation of the perimeter of the critical section

In AASHTO LRFD, the contact tire area (see Figure 7-2) is defined to be a rectangle of 10 in x 20 in (A3.6.1.2.5),

For the prestressed girder deck configuration,

$$b_o = 2\times(20+6.48)+2\times(10+6.48) = 85.92 \quad in$$
$$\beta_c = 2$$

For the steel girder deck configuration,

$$b_o = 2\times(20+6.84)+2\times(10+6.84) = 87.36 \quad in$$
$$\beta_c = 2$$

For both deck configurations, f'_c is taken equal to 4 ksi.

Computation of the nominal shear capacity

For the prestressed girder deck configuration,

$$V_n = \left(0.063+\frac{0.126}{2}\right)\sqrt{4}\times 85.92\times 6.48 = 140.3 \quad kip$$

For the steel girder deck configuration,

$$V_n = \left(0.063 + \frac{0.126}{2}\right)\sqrt{4} \times 87.36 \times 6.84 = 150.6 \quad kip$$

Computation of the Rating Factor

Rating Factor for the live load carrying capacity is defined as (according to AASHTO Manual for Condition Evaluation of Bridges, 1994, with 1995, 1996, 1998 and 2000 Interim Revisions),

$$RF = \frac{C - A_1 D}{A_2 L(1+I)} \tag{7-2}$$

where:

RF	=	rating factor for the live load carrying capacity
C	=	capacity of the member
D	=	dead load effect
L	=	live load effect
I	=	impact factor
A_1	=	dead load factor
A_2	=	live load factor

Equation 7-2 is a general formula proposed by AASHTO Bridge Manual to calculate rating factors for highway bridges corresponding to two rating levels: inventory rating level and operating rating level. The formula is used to calculate rating factors for primary structural elements of the bridge, such as girders or columns. This formula is adopted here to calculate rating factors for bridge deck slabs (not required by AASHTO Bridge Manual, A.6.7.2.1).

Dead load effect is estimated as:

$$D = \frac{20 \times 10}{12^2} \times \frac{9.5}{12} \times 0.150 = 0.16 kip$$

Live load effect is equal to:

$L = 16 kip$ (for the wheel load of HS20; lane load is not included)

Impact factor is taken as:

$I = 0.75$

The Dynamic Load Allowance of 75% is used as defined in AASHTO LRFD, Table 3.6.2.1-1 for deck joints.

The punching shear capacity is equal to:

$C = 0.85 \times 140.3 kip = 119.26 kip$ (for deck supported on prestressed concrete girders)
$C = 0.85 \times 150.6 kip = 128.0 kip$ (for deck supported on steel girders)

The load factors are as follows:

$A_1 = 1.3$
$A_2 = 2.17$ (for inventory level)
$A_2 = 1.3$ (for operating level)

Inventory rating factor

- For deck supported on prestressed concrete girders

$$RF = \frac{119.26 - 1.3 \times 0.16}{2.17 \times 16(1 + 0.75)} = 2.0$$

- For deck supported on steel girders

$$RF = \frac{128 - 1.3 \times 0.16}{2.17 \times 16(1 + 0.75)} = 2.1$$

Operating rating factor

- For deck supported on prestressed concrete girders

$$RF = \frac{119.26 - 1.3 \times 0.16}{1.3 \times 16(1 + 0.75)} = 3.3$$

- For deck supported on steel girders

$$RF = \frac{128 - 1.3 \times 0.16}{1.3 \times 16(1 + 0.75)} = 3.5$$

For comparison, in the Canadian Highway Bridge Design Code (CAN/CSA-S6-00), it is specified in article 14.13.1.2: "Where the concrete deck slab thickness is not less than 175 mm (6.9 IN), and the requirements for the empirical design method are satisfied, the deck slab shall be deemed to have adequate resistance for CL loadings (CL – truck load

for normal traffic)". The same statement is in the Ontario Highway Bridge Design Code (3rd Edition), but with a minimal deck slab thickness of 225 mm (8.9 IN)

7.2. Bending moment capacity

Bending moment capacity is calculated assuming the possibility of a cracked cross section of the deck. The relationships between the crack width, spacing between cracks, and the actual strain in the reinforcement is used in the model (CEB-FIP Model Code 1993). The bond characteristics of deformed bars and the repetitive nature of live loads are taken into account.

7.2.1. Average strain in the reinforcement

While a member is subjected to tensile stress, the first crack forms when the tensile stress of concrete (modulus of rupture, f_r) is reached at any section (at the weakest section). If the concrete cracks, the reinforcement has to take up all the tension previously carried by the concrete. This can cause a sudden increase of stress in the steel bar, leading to a differential movement between the reinforcement and the surrounding concrete. This will manifest itself in an increase of the crack width. Due to the bond between the steel and concrete, concrete resists the extension of the reinforcement. Because bond stresses are generated, the tensile force is transferred from the steel to the concrete. At a certain distance from the first crack, the compatibility of strains between steel and concrete is re-established and the section behaves as homogeneous (i.e. uncracked).

The element of length l, that is subjected to flexure (moment M) over the whole length, is replaced by a model element composed of two parts, Figure 7-3.

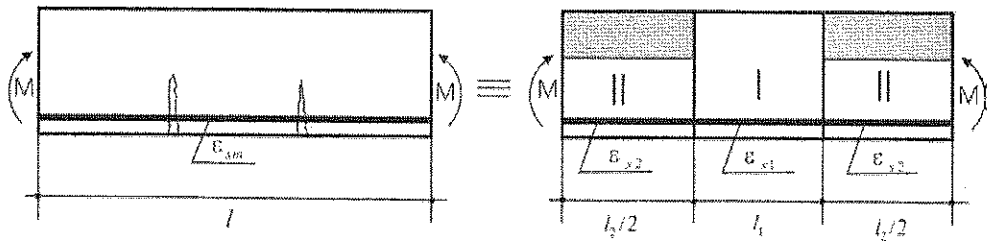

Figure 7-3. Calculation model for flexure.

Assumptions:

Part I - uncracked state.

Part II - a cracked section (only the reinforcement and concrete in compression are considered).

$$l_1 = (1-\xi)\times l$$
$$l_2 = \xi \times l \qquad (7\text{-}3)$$

where ξ is a distribution coefficient.

The average strain in tension reinforcement, ε_{sm}, is given by equation:

$$\varepsilon_{sm} = (1-\xi)\varepsilon_{s1} + \xi\varepsilon_{s2} \qquad (7\text{-}4)$$

where:

ε_{s1} = strain in the reinforcement calculated for an uncracked section (Part I)

ε_{s2} = strain in the reinforcement calculated for a cracked section (Part II).

The distribution coefficient, ξ, is given by,

$$\xi = 1-\beta_1\beta_2\left(\frac{\sigma_{sr}}{\sigma_{s2}}\right)^2 \qquad (7\text{-}5)$$
$$\xi = 0 \quad for \quad \sigma_{s2} < \sigma_{sr}$$

where:

$\beta_1 = 1/(2.5k_1)$ = coefficient characterizing the bond quality of the reinforcing bar;

$k_1 = 0.4$ for deformed bars

β_2 = coefficient representing the influence of the repeated loading; for large number of load cycles $\beta_2 = 0.5$

σ_{sr} = stress in the reinforcement calculated for a cracked section, where the maximum tensile stress in concrete is equal to the modulus of rupture for concrete

σ_{s2} = stress in the reinforcement at the cracked section under the combination of considered loads

In a case when cracking results from an external loading (live load) or from restrained shrinkage, the average crack width, w_m, for the established crack state is given by,

$$w_m = s_{rm} \times \varepsilon_{sm} \tag{7-6}$$

where:

w_m = average crack width

s_{rm} = average crack spacing

ε_{sm} = average strain in the reinforcement relative to the surrounding concrete.

Assuming the cracked section, from the equation 7-6, the average strain in the tensile reinforcement, ε_{sm}, can be calculated,

$$\varepsilon_{sm} = \frac{w_m}{s_{rm}} \tag{7-7}$$

From equation 7-4,

$$\xi = \frac{\varepsilon_{sm} - \varepsilon_{s1}}{\varepsilon_{s2} - \varepsilon_{s1}} \tag{7-8}$$

Introducing equation 7-8 into equation 7-5, and using Hook's law:

$$\frac{\varepsilon_{sm} - \varepsilon_{s1}}{\varepsilon_{s2} - \varepsilon_{s1}} = 1 - \beta_1 \beta_2 \frac{\sigma_{sr}^2}{E_s^2 \varepsilon_{s2}^2} \tag{7-9}$$

Assuming:

$$\varepsilon_{cr} = \frac{f_r}{E_c} \qquad and \qquad \varepsilon_{cr} = \varepsilon_{s1} = \frac{0.48}{3850} = 0.0001247$$

$$\sigma_{sr} = \varepsilon_{s1} E_s = 0.0001247(29000) = 3.62 ksi$$

$$\beta_1 = \frac{1}{2.5k_1} = \frac{1}{2.5 \times 0.4} = 1.0$$

$$\beta_2 = 0.50$$

Equation 7-9 is the third order parametric equation for ε_{s2} with w_m and s_m as known parameters,

$$\varepsilon_{s2}^3 - \varepsilon_{sm}\varepsilon_{s2}^2 - \beta_1\beta_2\left(\frac{\sigma_{sr}}{E_s}\right)^2 \varepsilon_{s2} + \beta_1\beta_2\left(\frac{\sigma_{sr}}{E_s}\right)^2 \varepsilon_{s1} = 0 \qquad (7\text{-}10)$$

$$\sigma_{s2} = \varepsilon_{s2} E_s$$

Equation 7-10 can be solved for selected crack widths: 0.0078 in., 0.0118 in., 0.0157 in. 0.0197 in., 0.0315 in., and spacing between cracks: 3 ft, 4 ft and 5 ft.

Having ε_{s2}, the tensile stress in reinforcement in the cracked section, σ_{s2}, can be obtained. This stress depends on the crack width and the distance between cracks. Based on that stress, the moment carrying capacity of the cracked section can be calculated. The ratio of the moment carrying capacity of the cracked section to the moment carrying capacity of the uncracked section provides the information about the load rating of the section.

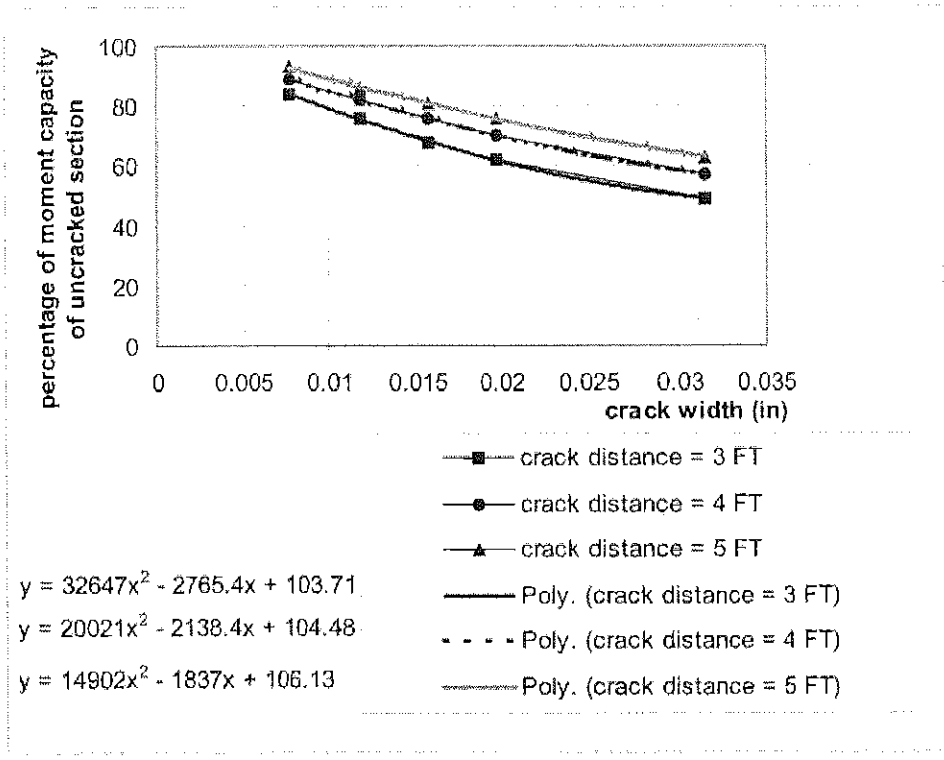

Figure 7-4. Load rating for cracked decks.

Figure 7-4 presents the ratio of moment carrying capacity for flexure, calculated for a cracked deck cross section, and the moment carrying capacity calculated for an uncracked cross section. Moment carrying capacity for a cracked cross section depends on the crack width and the distance between cracks. Each curve presents the percentage of the total flexural moment carrying capacity (calculated for an uncracked section), dependent on the average distance between cracks (3 ft, 4 ft and 5 ft). Figure 7-4 also provides the fitting curve equations for each curve. The χ variable is the width of the cracks (in.), the resulting Y is the remaining moment carrying capacity as a percentage of the full moment carrying capacity of the uncracked section.

The moment carrying capacity of the cracked section can be used as a nominal capacity to calculate the Inventory Rating, or Operating Rating Factors, according to AASHTO Manual for Condition Evaluation of Bridges.

8. SUMMARY AND GENERAL RECOMMENDATIONS

The stress analysis of reinforced concrete decks supported on steel or prestressed concrete girders was performed based on numerical calculations using the finite element models. The resulting stress distributed in longitudinal and transversal directions, on the top and bottom of the decks, was investigated. Three types of loads were considered: dead load, live load and restrained shrinkage. The live load (11-axle trucks) used in the finite element models was applied in various numbers and configurations to obtain the maximum possible stress.

In general, the cracking analysis of the deck's cross section has shown that the reinforcement determined using the empirical method is sufficient to resist stresses caused by a combined dead and live load. However, the restrained shrinkage analysis has shown that for some sections the empirical reinforcement is not enough to resist shrinkage stresses. In particular, this applies to composite sections with deeper steel girders. This conclusion also applies to newly constructed decks on existing prestressed concrete Type IV girders with depths of 54 in. (deck replacement). The most affected are the cross sections at the edge of the deck. For the considered structures, the constraints caused by girders resulted in longitudinal stresses higher than the modulus of rupture for a typical concrete used for bridge decks. This is a reason for transversal cracks on the top and bottom of the deck, often reported during bridge inspections.

The restrained shrinkage analysis was performed for isotropic decks that are 9 in. thick, supported on girders spaced at 10 ft. The obtained shrinkage stresses were calculated after 30 years of service, with an ambient humidity of 70% (typical for Michigan), and with two options of curing conditions: very good and average. The increase of tension stress in the deck after unloading caused by removal of the formwork and a reduction of weight due to the drying of concrete was also included in analysis. In this way, the total restrained shrinkage stress can be considered as an upper bound value.

In cases where the restrained shrinkage causes a tension force in a deck section larger that the elastic tension capacity of the section, in order to control cracking, it is proposed to

increase the empirical longitudinal reinforcement or to increase the thickness of the deck slab. The specific recommendations are separately listed after the cracking analysis of the decks supported on prestressed concrete girders (Section 6.3.2) and steel girders (Section 6.3.4).

The more general recommendations are as follows:

- Very good curing conditions are essential during the deck construction.
- In order to double the empirical reinforcement, it is proposed to specify the top layer of longitudinal reinforcement of #5 @ 10 in (0.37 in^2/ft) , and the bottom reinforcement of #5 @ 7 in (0.53 in^2/ft), as presented in Figure 8-1 for a middle cross section of the deck, and in Figure 8-2 for an edge cross section.
- The other option to double empirical longitudinal reinforcement is to place two layers of identical longitudinal reinforcement, two layers at the top and two layers at the bottom of the slab. The second layer of longitudinal reinforcement can be moved closer to the mid-depth of the deck cross section. These additional layers of longitudinal bars require transversal distribution reinforcement.
- The distribution reinforcement for additional layers of longitudinal bars is proposed as 0.11 in^2/ft.
- The cross section with four layers of longitudinal reinforcement is presented in Figure 8-3 for deck thickness of 11 in., and in Figure 8-4 for 12 in. thick deck.

The procedure for load rating of the decks is based on punching shear capacity and bending moment capacity of the deck. Rating factor in regard to punching shear is calculated based on nominal shear resistance of the cross section. The procedure for load rating factor in regard to bending moment is proposed in the form of curves and equations to estimate the remaining flexural moment capacity of the cracked deck, in comparison with an uncracked section. The procedure accounts for the width of the average crack and the average spacing between cracks.

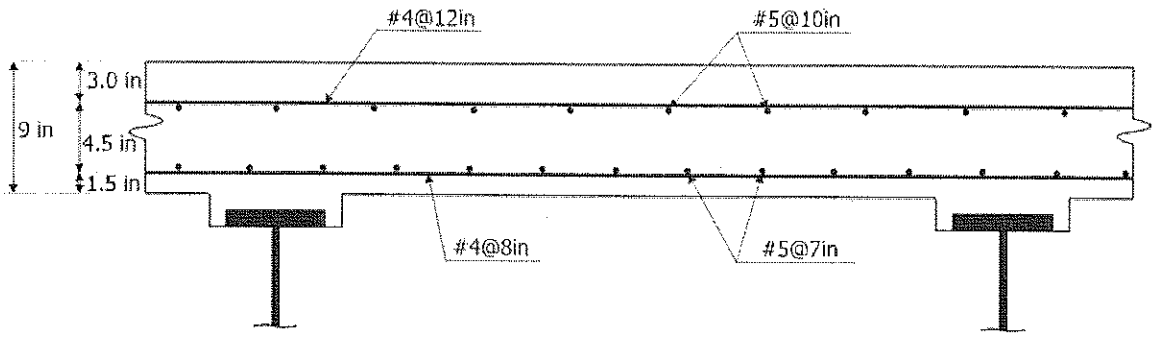

Figure 8-1. Middle cross section of the deck (doubled longitudinal empirical reinforcement).

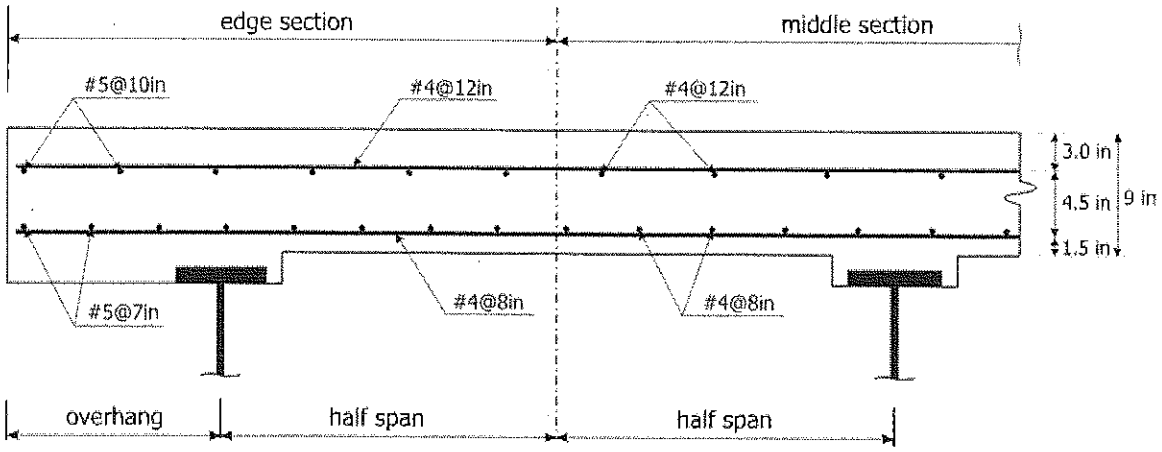

Figure 8-2. Edge cross section of the deck (doubled longitudinal empirical reinforcement).

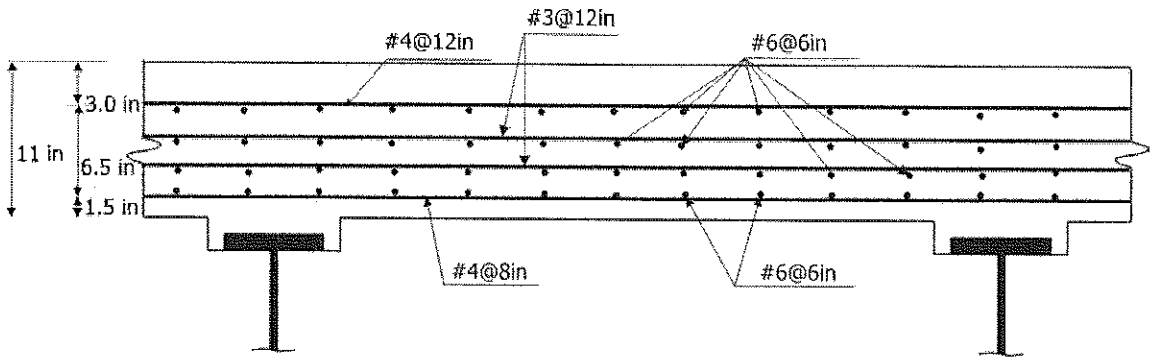

Figure 8-3. Middle cross section of the deck with thickness of 11 in. (four layers of reinforcement).

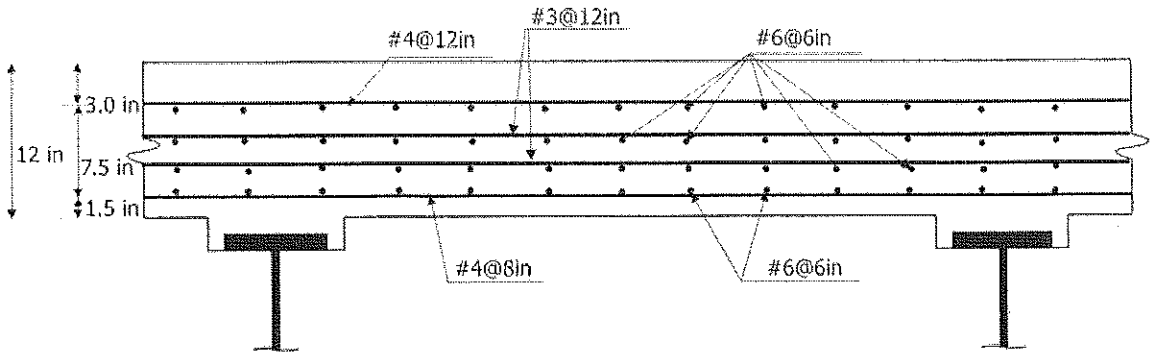

Figure 8-4. Middle cross section of the deck with thickness of 12 in. (four layers of reinforcement).

REFERENCES

1. AASHTO LRFD Bridge Design Specifications. US customary Units second edition 1998.

2. AASHTO Manual for Condition Evaluation of Bridges, second edition 1998 and 2000 Interim Revisions.

3. Barker, M., Puckett, Jay A., Design of Highway Bridges based on AASHTO LRFD Bridge Design Specifications. John Wiley & Sons, INC, 1997.

4. Beal, D. B., Load Capacity of Concrete Bridge Decks. Journal of the Structural Division, Proceedings of the American Society of Civil Engineers, Vol. 108, April 1982.

5. Brozzetti, J., Design Development of Steel-Concrete Composite Bridges in France. Journal of Constructional Steel Ressearch, 2000.

6. Cao, L., Shing, P., Simplified Analysis Method for Slab-on-Girder Highway Bridge Decks. Journal of Structural Engineering, January 1999.

7. Cao, L., Allen, J. H., Shing, P. B., Woodham, D., Behavior of RC Bridge Decks with Flexible Girders. Journal of Structural Engineering, January 1996.

8. CEB-FIP Model Code, Comite Euro – International Du Beton, Design Code, Thomas Telford 1993.

9. Fang, I.-K., Worley, J., Burns, N. H., Klingner, R. E., Behavior of Isotropic R/C Bridge decks on Steel Girders. Journal of Structural Engineering, October 1988.

10. Fang I-K, Lee J-H and Chen C-R, Behavior of partially restrained slabs under concentrated load, Department of Civil Engineering, National Cheng Kung University, Taiwan, Republic of China, ACI Structural Journal, Vol. 91, No. 2, March-April 1994.

11. Keogh D-L, and O'Brien E-J, Recommendation on the use of a 3-D grillage model for bridge deck analysis, Department of Civil, Structural and Environmental Engineering, Trinity College, Dublin, Ireland, Structural Engineering Review, Vol. 8, No. 4, pp.357-366.

12. Mabsout M-E, Tarhini K-M, Frederic G-R and Kesserwan A, Effect of multilanes on wheel load distribution in steel girder bridges, Department of Civil and Environmental Engineering, American University of Beirut, Lebanon, Journal of Bridge Engineering, Vol. 4, No. 2, May 1999.

13. McDonald, "An experimental study of multiaxial creep in concrete". Concrete for Nuclear Reactors, ACI SP-34, Detroit 1972, pp. 732-768.

14. Mohsen, A. Issa, Investigation of Cracking in Concrete Bridge Decks at Early Ages. Journal of Bridge Engineering, May 1999.

15. Mufti, A. A., Newhook, J. P., On the use of Steel Free Concrete Bridge decks in Continuous Span Bridges. Canadian Journal of Civil Engineer, March 1999.

16. Nowak A-S, Eamon C and Szerszen M-M, Bridge Engineering (Synthesis of planning, design, construction, maintenance, materials and research), Department of Civil and Environmental Engineering, University of Michigan, MDOT report, December 1998.

17. Nowak A-S and Kim S-J, Development of a Guide for Evaluation of existing Bridges, Part I and II, Department of Civil and Environmental Engineering, University of Michigan, MDOT Report, May 1998.

18. Riley, O., Heeding the Call for Better Bridge Decks: A Success Story, ACI Seminars on Repairing Concrete Bridges, Seminar Background Materials, SCM-27 (93), Second Edition.

19. Sargent, Dennis D., Ventura, Carlos E., Mufti, Aftab A., Bakht, Baidar, Testing of Steel-Free Bridge Decks. Concrete International, August 1999.

20. Schrader, E.K., Mistakes, Misconceptions, and Controversial Issues Concerning Concrete and Concrete Repairs, ACI Seminars on Repairing Concrete Bridges, Seminar Background Materials, SCM-27 (93), Second Edition.

21. Tarhini K-M, Experimental evaluation of wheel load distribution on steel I-girder bridges, Department of Civil Engineering, Valparaiso University, USA, 10th Conf. Eng. Mech. Boulder ASCE pp.593-596, 1995.

22. Tarhini K-M and Frederic G-R, Lateral load distribution in I-girder bridges, Department of Civil Engineering, Valparaiso University, USA, Computers & Structures, Vol. 54, No. 2, pp.351-354, 1995.

23. Tarhini K-M and Frederic G-R, Wheel load distribution in I-girder Highway bridges, Department of Civil Engineering, Valparaiso University, USA, Journal of Civil Engineering, Vol. 118, No. 5, 1992.